UNIVERSITY OF SOUTHAMPTON

Faculty of Engineering and the Environment
Fluid Structure Interactions Group

Coupled Dynamics of a Flapping Foil Wave Powered Vessel

by

James A. Bowker

A thesis submitted for the
degree of Doctor of Philosophy

June 24, 2018

UNIVERSITY OF SOUTHAMPTON

ABSTRACT

FACULTY OF ENGINEERING AND THE ENVIRONMENT
Fluid Structure Interactions Group

Doctor of Philosophy

COUPLED DYNAMICS OF A FLAPPING FOIL WAVE POWERED VESSEL

by James A. Bowker

Wave propelled vessels utilize submerged flapping foils to convert wave energy directly into propulsion. This works by coupling the response of foils operating in a wavy flow with the flapping motion driven by the wave-induced hull motions. For platforms that are solely propelled using this method the free running forward speed is dictated by the magnitude and frequency of the ambient wave energy. Submerged flapping foils also have the potential to recover wave energy for onboard power generation, and, in this way, a vessel could be both powered and propelled by the ambient wave energy. This thesis both numerically and experimentally investigates the coupled dynamic response of a wave powered vessel, which enables the prediction of the free running forward speed and an assessment of the potential for wave energy recovery.

A hybrid numerical model has been developed to capture the free running response of a flapping foil wave powered vessel, and this model has been validated by the experimental analysis. The hybrid method combines the frequency domain strip theory approach for solving the seakeeping response with a time domain solution for the response of a spring loaded flapping foil. The numerical model also evaluates the electromechanical conversion of wave energy by modelling the power generated by a permanent magnet tubular linear generator.

Free running wave propulsion experiments were performed in both regular head and following waves using a model with spring loaded flapping foils at the bow and stern over a range of wave frequencies. The experimental setup incorporated wave energy recovery in the form of electrical power by linking the flapping foils with a power take-off device, and a series of experiments were conducted for different wave heights and frequencies. In addition to validating the numerical model, the experimental results show a notable difference in the response of the forward and aft foils in head and following waves, and confirm numerical predictions that the optimal location of the foils is at or beyond the perpendiculars of the vessel. Furthermore, the experimental and numerical analysis demonstrate that it is possible to recover wave energy from the use of submerged foils.

Numerical simulations have been carried out to provide a more detailed insight into the effect on the coupled response of: foil size and location; flapping parameters; and seakeeping characteristics. In particular, it is shown that the wave-phasing parameter and the foil spring constant is of significant importance for the efficiency of wave propulsion. Lastly, the numerical analysis provides guidance for the design of flapping foil wave powered vessels, and highlights the importance of the wavelength to vessel length ratio.

Contents

List of Tables

List of Figures

UNIVERSITY OF Southampton

Academic Thesis: Declaration Of Authorship

I, James Andrew Bowker, declare that this thesis entitled 'Coupled Dynamics of a Flapping Foil Wave Powered Vessel' and the work presented in it are my own and has been generated by me as the result of my own original research.

I confirm that:

1. This work was done wholly or mainly while in candidature for a research degree at this University;
2. Where any part of this thesis has previously been submitted for a degree or any other qualification at this University or any other institution, this has been clearly stated;
3. Where I have consulted the published work of others, this is always clearly attributed;
4. Where I have quoted from the work of others, the source is always given. With the exception of such quotations, this thesis is entirely my own work;
5. I have acknowledged all main sources of help;
6. Where the thesis is based on work done by myself jointly with others, I have made clear exactly what was done by others and what I have contributed myself;
7. Either none of this work has been published before submission, or parts of this work have been published as: [please list references below]:

Bowker, J.A., Townsend, N.C., Tan, M. and Shenoi, R.A. (2016) Experimental analysis of submerged flapping foils; implications for autonomous surface vehicles (ASVs) At OCEANS'16 MTS/IEEE, United States. 01 Jan 2016. 10 pp.

Bowker, J.A., Townsend, N.C., Tan, M. and Shenoi, R.A. (2015) Experimental study of a wave energy scavenging system onboard autonomous surface vessels (ASVs) At OCEANS'15 MTS/IEEE Genova, Italy. 18 - 21 May 2015.

Signed: .....

Date: .....**24/6/18**.....

Acknowledgements

I would like to thank the University of Southampton for providing me this opportunity to pursue a PhD within the Fluid Structure Interactions Group. In particular, I would like to extend a thank you to my supervisors, Dr. Nick Townsend, Dr. Mingyi Tan and Prof. Ajit Shenoi: I have thoroughly enjoyed our countless discussions, and your enthusiastic guidance has been invaluable.

I would like to acknowledge the Lloyd's Register Foundation for supporting this research, and their continuous contribution to academic studies.

Thank you also to David Maclean (AutoNaut Ltd) for our discussions on wave propelled unmanned surface vehicles.

Abbreviations

3D	Three dimensional
AP	Aft perpendicular
AR	Aspect ratio
USV	Unmanned surface vehicle
AUV	Autonomous underwater vehicle
BEM	Boundary element method
CFD	Computational fluid dynamics
DC	Direct current
DWT	Dead weight tonnage
EEDI	Energy Efficiency Design Index
Exp	Experimental
FP	Forward perpendicular
Fwd	Forward
GUI	Graphical user interface
ITTC	International Towing Tank Committee
LCG	Longitudinal centre of gravity
LUT	Look up table
Num	Numerical
ODE	Ordinary differential equation
PMTLG	Permanent magnet tubular linear generator
Pos	Position
PTO	Power take-off
RANS	Reynolds-averaged Navier-Stokes
RAO	Response amplitude operator (seakeeping transfer function)
RMS	Root mean square
RSS	Root sum of squares
SEE	Standard error for estimation
Sim	Simulation
VCG	Vertical centre of gravity
WDPS	Wave devouring propulsion system

Nomenclature

A_{11}	Global surge added mass coefficient	$N/(m/s^2)$
A_{33}	Global heave added mass coefficient	$N/(m/s^2)$
A_{35}	Coupled heave global added mass coefficient	$N/(rad/s^2)$
A_{53}	Coupled pitch global added mass coefficient	$Nm/(m/s^2)$
A_{55}	Global pitch added moment of inertia coefficient	$Nm/(rad/s^2)$
A_{WP}	Waterplane area	m^2
AR	Foil aspect ratio	-
A_{APP}	Appendage wetted surface area	m^2
A_ξ	Hull section area	m^2
a	Foil pivot point	-
a_3	Sectional added mass coefficient	$N/(m/s^2)$
B	Vessel beam at amidships	m
B_{11}	Global surge damping coefficient	$N/(m/s)$
B_{33}	Global heave damping coefficient	$N/(m/s)$
B_{35}	Coupled heave global damping coefficient	$N/(rad/s)$
B_{53}	Coupled pitch global damping coefficient	$Nm/(m/s)$
B_{55}	Global pitch damping coefficient	$Nm/(m/s)$
b_3	Sectional damping coefficient	$N/(m/s)$
b_g	Centre of gravity of foil	m
b_ξ	Sectional beam	m
C'	Theodorsen's lift deficiency factor	-
C_{33}	Global heave restoring coefficient	N/m
C_{35}	Coupled heave global restoring coefficient	N/rad
C_{53}	Coupled pitch global restoring coefficient	Nm/m

C_{55}	Global pitch restoring coefficient	Nm/rad
C_D	Foil drag coefficient	-
C_{D_A}	Appendage drag coefficient	-
C_F	ITTC'57 skin friction coefficient	-
C_T	Thrust coefficient	-
c	Foil chord	m
c_f	Frictional damping constant in PTO	$N/(m/s)$
c_g	Wave celerity	m/s
c_z	Damping constant for hull-foil coupling	$N/(m/s)$
c_s	Foil support strut chord	m
D	Foil quasi-steady drag force	N
D_i	Foil induced drag	N
D_m	Inertial force of flapping foil in x-direction	N
d_f	Foil depth	m
d_ξ	Sectional draft	m
e_c	Induced emf constant	V
e_{ph}	Induced emf per phase	V
$F_{1,3,5}$	Vessel surge (1) force, heave (3) force and pitch (5) moment	N, N, Nm
F_L	Prandtl's lifting line force for an unsteady flapping foil	N
F_M	Electromagnetic force	N
F_x	Total force in x-direction acting on vessel	N
F_ζ	Wave-induced surge force	N
f	Wave frequency (Hz)	1/s
g	Gravitational acceleration	Nms^{-2}
H	Wave height	m
h	Wave or actively induced foil heave	m
h_a	Absolute heave of foil in energy recovery mode	m
h_e	Effective heave of foil relative to vessel	m
h_r	Foil relative heave with respect to ambient wavy flow	m
I_B	Total inertia of the vessel including foils	kgm^2
I	Electrical current	A
i	Complex number / Foil number	-
k	Wave number	-

k_f	ITTC'57 form factor	-
k_{red}	Reduced frequency	-
k_z	Spring constant for hull-foil coupling	N/m
k_θ	Foil pitch spring constant	Nm/rad
L	Waterline length	m
L_C	Hydrodynamic circulatory foil lift force	N
L_i	Internal inductance of electrical PTO device	$kgm^2s^{-2}A^{-2}$
L_{NC}	Hydrodynamic non-circulatory foil lift force	N
L_m	Inertial force of flapping foil in z-direction	N
L_z	Total resultant foil force in z-direction	N
M	Vessel displacement	kg
M_B	Total mass of the vessel including foils	kg
M_C	Hydrodynamic circulatory moment about foil pivot point	Nm
M_{NC}	Hydrodynamic moment about foil pivot point	Nm
M_m	Inertial moment about foil pivot point	Nm
M_{WP}	First moment of area acting about the transverse axis at the LCG	m^2
m_a	Foil added mass	kg
m_f	Foil mass	kg
n	Numerical step	-
$\bar{P}_z$	Average generated power	W
P_w	Wave power per m width of energy convertor (vessel beam)	W/m
R_{APP}	Added resistance due to appendages	N
R_{AW}	Added resistance due to waves	N
R_i	Internal resistance of electrical PTO device	Ω
R_L	Load resistor in PTO circuit	Ω
R_{SW}	Still water vessel resistance	N
R_T	Total resistance	N
St	Strouhal number	-
s	Foil span	m
s_ξ	Sectional area coefficient	-
T	Vessel draft	m
T_f	Flapping period of foil	s
T_w	Wave period	s

T_x	Total resultant foil force in x-direction	N
t	Time	s
t_s	Foil support strut thickness	m
U	Vessel forward speed	m/s
$\bar{U}$	Mean vessel forward speed	m/s
u_f	Relative flow speed in the x-direction at the foil location	m/s
u_w	Horizontal component of wave particle velocity	
V	Flow speed at foil	m/s
V_{ph}	Phase voltage at terminal	V
v_f	Relative flow speed in the z-direction at the foil location	m/s
v_w	Vertical component of wave particle velocity	m/s
w_p	Permanent magnet pole width	m
X_ξ	Sectional longitudinal distance from incident wave trough	m
x	Global x axis coordinate	-
x_B	Position of vessel LCG in x-direction	m
x_f	Foil longitudinal location relative to LCG	m
y	Global y axis coordinate	-
z	Global z axis coordinate	-
α_{dyn}	Dynamic angle of attack	rad
α_e	Effective angle of attack	rad
α_{qs}	Quasi steady angle of attack	rad
α_x	Angle of attack with respect to the x-axis	rad
β	Sum of vessel and foil pitch	rad
Δt	Time step	s
δ	Time dependent encountered angular position of vessel on wave	rad
δ_e	Electrical phase angle	rad
ϵ_f	Flapping phase between leading and trailing foil	deg
ϵ_{xx}	Experimental error	varies
ζ	Wave profile	m
ζ_{en}	Encountered wave profile	m
$\eta_{1,3,5}$	Vessel surge (1), heave (3) and pitch (5)	m, m, rad
η_g	Generator efficiency	-
η_r	Overall wave energy recovery efficiency	-

θ	Foil pitch	rad
λ	Wavelength	m
μ	Vessel heading	rad
μ_d	Empirical surge correction factor	-
ξ	Hull section longitudinal distance from LCG	m
ξ_f	Longitudinal distance between leading and trailing foil	m
ρ	Fluid density	kgm^{-3}
ϕ	Foil flapping phase (between foil heave and pitch)	rad
σ	Standard deviation	varies
$\varphi_{3,5}$	Global force (3) and moment (5) phase difference	rad
Ψ	Wave-phasing parameter	rad
ω	Wave frequency	rad/s
ω_e	Encountered wave frequency	rad/s
ω_z	Angular rotation frequency of pivot arm	rad/s

Chapter 1

Introduction

In ocean waves, there exists an inevitable transfer of wave energy to a floating object. The floating object effectively becomes energised by the ambient wave energy, but in most practical applications, such as ship propulsion, this additional energy acts to hinder the vessel. However, submerged flapping foils can exploit this energy for either propulsion or onboard power generation.

1.1 Background

For a ship transiting the oceans, motions are induced from incoming waves, and a considerable body of research has been devoted to understanding the seakeeping response. An important outcome from previous studies has been the identification of methods to mitigate the wave-induced response of a ship. In particular, foil appendages have been investigated for the purposes of ship stabilization as early as the 1930's with the installation of anti-roll fins on a Japanese cruise liner (Popular Mechanics, 1933).

It is also well established that the pitch motion of a vessel in a seaway is significantly reduced due to the presence of a flapping foil submerged at the bow (Naito and Isshiki, 2005). For a ship in a seaway, the reduction in hull motion is beneficial for several reasons; fuel savings, passenger comfort and structural integrity. Fuel savings can also be achieved with the generation of thrust from the interaction between the flapping foil and incoming waves, known as wave-augmented propulsion.

However, although this has been demonstrated, the technology is yet to be installed on commercial ships due to the difficulty of mounting a large appendage at the bow, which is only effective in waves.

In suitable wave conditions, the wave-induced flapping motion of submerged flapping foils combined with the incident wavy flow results in a time-average thrust force which can overcome the total resistance of the vessel. In this way, submerged flapping foils can act as the primary propulsor for vessels propelled by waves. This form of propulsion is currently impractical for commercial ships due to the aforementioned technical issues and the inconsistent availability of wave energy. However, these are not issues for small unmanned vessels, known as unmanned surface vehicles (USVs), and in this area wave propulsion has significant potential.

Figure 1.1 presents the cumulative number of publications relating to wave-induced flapping foil propulsion. An increase in this field of research is noted during the 1980s, which is mainly attributable to the research carried out on the principles of flapping foils for ship efficiency in waves, see Section 2.2.3. Since 2005, there has been an almost twofold increase in the research activity, which is mostly due to an increased interest in wave propelled USVs.

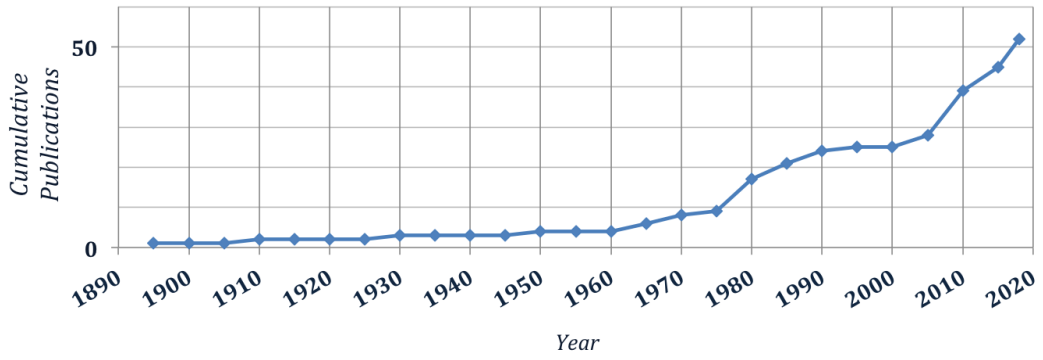

Figure 1.1: Cumulative publications on wave propulsion (based on the relevant citations referenced in this thesis)

Submerged flapping foils also offer a potential method for wave energy recovery by operating as point absorbers beneath the vessel. By working against the relative motion of the surface vehicle, the foils recover the wave-induced energy of the hull motions, which would otherwise be wasted. Depending on the damping or restoring force acting on the flapping foil from the power take-off system, the flapping foils could still generate propulsive thrust whilst recovering wave energy.

Submerged flapping foils could serve a dual purpose as mechanisms for both wave propulsion and energy recovery. The following section provides a description of the mechanisms for wave propulsion, and introduces a novel concept for wave energy recovery.

1.2 Wave powered vessels

1.2.1 Wave propulsion

There are fundamentally two mechanisms for submerged foil wave propulsion; heave-induced gliding and pitch-induced flapping, illustrated in Figure 1.2.

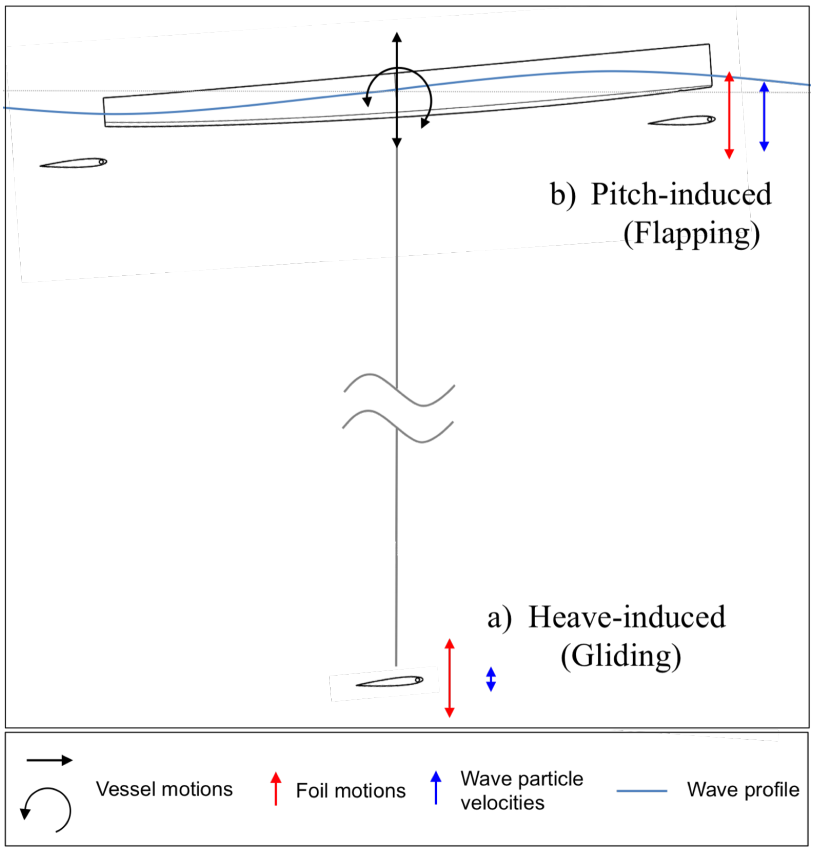

Figure 1.2: Heave and pitch-induced wave propulsion

The mechanism for heave-induced wave propulsion aims to induce a flow over submerged foils in the same way as an aerial glider with fixed wings. This method has been implemented for the

wave propulsion of a commercial USV called Wave Glider, developed by Liquid Robotics (Hine et al. 2009). The submerged foils are located at a significant depth beneath the waves to maximise the flow over foils. This is particularly important in low frequency waves where the vessel (or surface float) is assumed to contour the incoming waves, and the foil heave is in phase with the wave elevation. If the foils were located in the wavy flow near the surface, the summation of the local wavy flow and the foil heave would cause a significant reduction in the flow over the foils.

The pitch-induced method utilizes the vessel motions (pitch and heave) to drive the foils in a flapping motion. The induced flapping foil motions interact with the oscillating flow of the incoming wave to generate thrust. With the installation of one spring loaded foil mounted at the bow and another at the stern, the commercial USV called AutoNaut use pitch-driven method for wave propulsion.

The methods detailed in this thesis are based on the pitch-induced mechanism, but a similar analytical approach could be applied to the heave-induced method if required. A comparison of the two methods is conducted in Chapter 5.

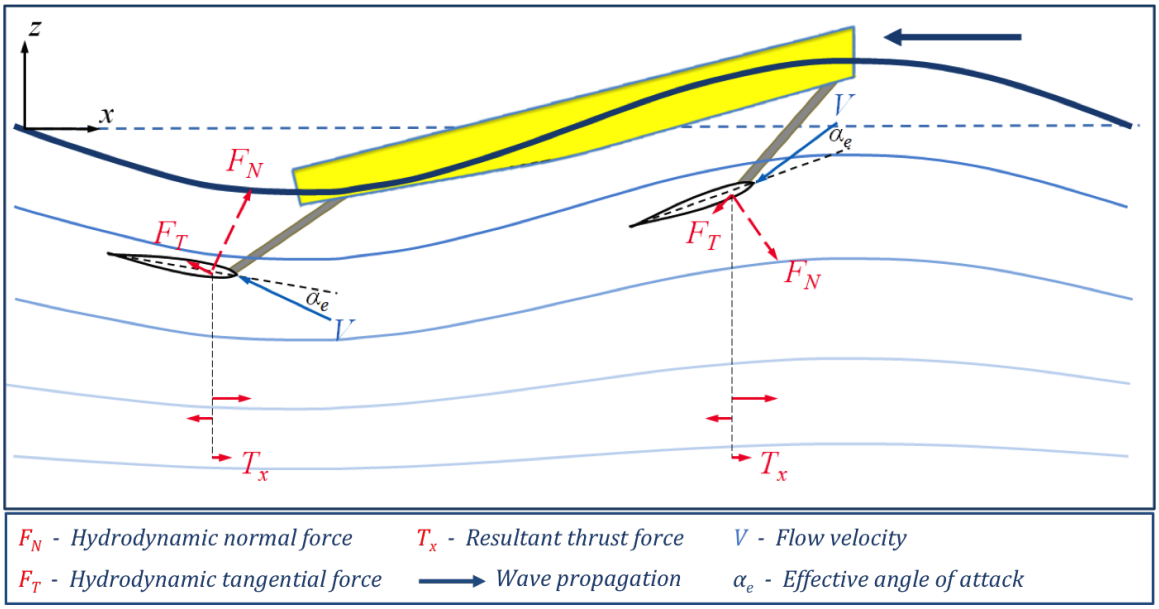

Figure 1.3: Schematic that illustrates the basic mechanisms for pitch-induced wave propulsion

For pitch-induced wave propulsion, the submerged flapping foils are fixed to the hull at the transom and the bow via a rigid arm, shown in Figure 1.3. The wave-induced vessel motion drives spring loaded submerged foils such that the foils are forced to flap at the frequency of the incoming

wave. The flapping motion of the foil results in an oscillating lift force which, when resolved in the x-direction, generates an average thrust force. Additionally, the submerged foils can generate thrust from the oscillating flow of the wave. The overall thrust force is, therefore, a combination of both the flapping foil response and the oscillating flow of the wave.

1.2.2 Wave energy recovery

Wave energy is recovered at the interface between the hull and the foil, illustrated in Figure 1.5. The wave-induced force that acts on a submerged foil is absorbed by a power take off (PTO) system, represented by a viscous damper in Figure 1.4. Wave energy is converted into kinetic energy in the form of relative motion between the hull and the foil, and this is then converted into useful onboard power. This relative motion also acts to reduce the wave-induced foil motion that is required for wave propulsion, and therefore energy recovery can also be used as a method for forward speed control.

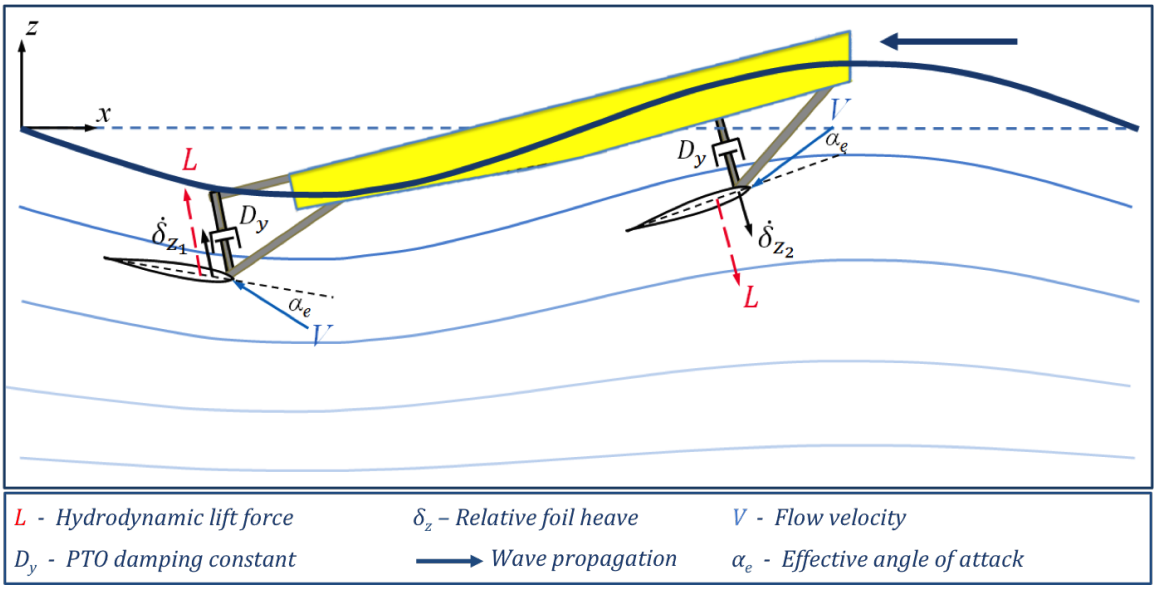

Figure 1.4: Schematic that illustrates the basic mechanisms for wave energy recovery

1.3 Research outline

1.3.1 Motivation

Whilst flapping foil wave propulsion has proven to be effective, the understanding of the free running response of a wave propelled vessel is limited, and the possibility of recovering wave energy has not been extensively investigated; a more comprehensive understanding of the coupled dynamics and response of such vessels is required. The work presented in this thesis is, therefore, focused on the wave-induced coupled response of a surface vehicle with submerged flapping foils with respect to wave propulsion and energy recovery. This research has the potential to enhance the capability of wave powered vessels such as USVs.

Although submerged flapping foils is most suitable for wave propelled USVs, the theory and conclusions of this thesis are equally applicable to all flapping foil wave powered vessels.

1.3.2 Aims and Objectives

The aim of this thesis is to investigate the coupled dynamics of flapping foil wave propulsion and energy recovery for wave powered vessels. In this case, the coupled dynamics refers to the cause and effect relationship between a vessel and submerged flapping foils in waves. The relationship is coupled due to the effect of the foils on the vessel and vice versa, and is dynamic due to the oscillating forces induced by an incoming wave.

To achieve this aim the following objectives have been set:

1. define the general dynamics of flapping foils and clarify the governing equations that influence the coupled response between a surface vehicle and submerged flapping foils;
2. develop a time-domain numerical model that can simulate both wave propulsion and energy recovery;
3. conduct experiments to validate the numerical model, to provide a proof of concept for wave energy recovery, and also to further investigate the physical response of the coupled dynamics;
4. analyse the coupled dynamics through numerical simulation

1.3.3 Research scope

The scope of this research encompasses the coupled response of a surface vehicle with submerged flapping foils in regular head and following waves for both wave propulsion and wave energy recovery. Both numerical and experimental analysis is conducted for the investigation of resultant forward speed and power generation over a range of wave frequencies. Figure 1.5 illustrates the kinematics associated with this research scope. The interface at which the flapping foil is mounted to the vessel can either be;

- fixed, which results in a total transfer of wave-induced energy from the hull to the foil for propulsion;
- or free, which results in a relative motion of the foil with respect to the hull and the ability to recover wave energy;
- or free, with an increased damping, which results in a combination of both wave propulsion and energy recovery.

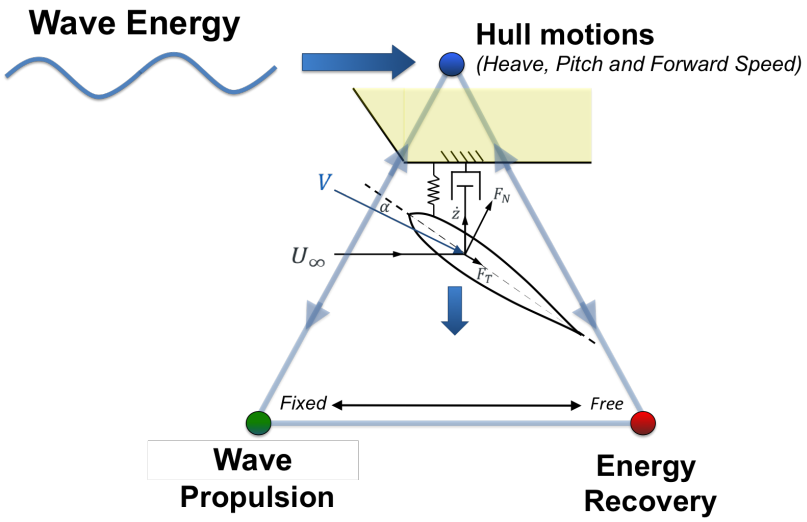

Figure 1.5: Schematic representing the research problem

1.3.4 Methodology

There are numerous theories at different levels of complexity that have been applied to capture the individual components of the coupled relationship. This research investigates the overall coupled dynamic response rather than the detailed analysis of each physical component. Linear theory is implemented for the numerical analysis, which assumes a harmonic response for both the vessel and foil motions. A numerical model is developed to combine the linear seakeeping and flapping foil theories for the prediction of both wave propulsion and energy recovery. To evaluate the validity of this method, a comparison with experiments is necessary.

To validate the numerical model, experiments are performed with a changing independent variable (e.g. wave frequency and/or amplitude) and a changing dependent variable (e.g. foil location). The experimental area of the research not only provides the basis for this validation, but also provides an additional insight into the coupled response and a proof of concept for wave energy recovery. Upon verification and validation, the model is then used to predict the coupled dynamic response over a range of parameters and to investigate the research scope in more detail.

The analysis, therefore, adopts the following conventional process; theory $\rightarrow$ numerical modelling $\rightarrow$ verification and validation $\rightarrow$ simulations.

1.4 Structure of the thesis

Chapter 2 provides a review of previous research including: flapping foil propulsion; wave-induced flapping foil propulsion; and recent concepts for wave energy recovery utilizing flapping foils.

Chapter 3 provides a theoretical overview of the coupled dynamics of a vessel with submerged flapping foils in regular waves. The free running response of a wave propelled vessel is considered, and the dynamic equations that define the responses are defined. Additionally, a simplified dynamic system is defined to describe the wave energy recovery response of submerged flapping foils. The methodology for numerically modelling the coupled response is described, and the numerical model is verified.

Chapter 4 presents an experimental analysis of wave propulsion and energy recovery, in head and following waves, for a vessel with submerged flapping foils mounted at the bow and stern. The

experiments enable validation of the numerical model.

Chapter 5 presents numerical simulations of the coupled response and highlights particular areas of interest. The simulations provide an analysis of wave propulsion and energy recovery over a range of parameters.

With reference to both the experimental and numerical analysis, Chapter 6 discusses key areas of interest relating the coupled response. Particular phenomena are explained and research outcomes are compared with the conclusions of previous academic studies.

Lastly, Chapter 7 summarizes the key outcomes and recommends areas for future research.

Chapter 2

Flapping foils in the maritime domain

This review of previous research has been subdivided into three key areas; flapping foil propulsion in a uniform flow, wave-induced flapping foil propulsion and wave energy recovery.

2.1 Flapping foil propulsion in a uniform flow

Knoller and Betz effect

In the early 20th century, Knoller and Betz independently identified the phenomenon of thrust generation by a harmonically heaving foil in a free stream flow, known as the Knoller-Betz effect (Knoller 1909, Betz 1912). A heaving foil in a uniform flow results in an effective angle of attack that generates an aerodynamic force normal to the angle of attack with both lift and thrust components. The Knoller-Betz effect was later validated by Katzmayr, who proved that a foil could generate thrust in an oscillating flow, assuming that this is the same effect as an oscillating foil in a uniform flow stream (Katzmayr 1922). The effect of generating thrust in a wavy flow, known as the Katzmayar effect, has been used to explain the high efficiency of flapping foil propulsion in nature (Zhu et al. 2002), and is also a key factor for wave propulsion (Wu 1972).

Unsteady foil theory

Garrick (1937) carried out a theoretical investigation of the thrust generated by an oscillating foil in a uniform flow by expanding upon the mathematics developed by Theodorsen (1935) concerning airfoil flutter and applying the general aerodynamic methods described by von Karman and Burgers (1935). To evaluate the aerodynamic forces experienced by an oscillating foil, Garrick developed a mathematical theory that assumes small amplitude oscillations at low frequencies.

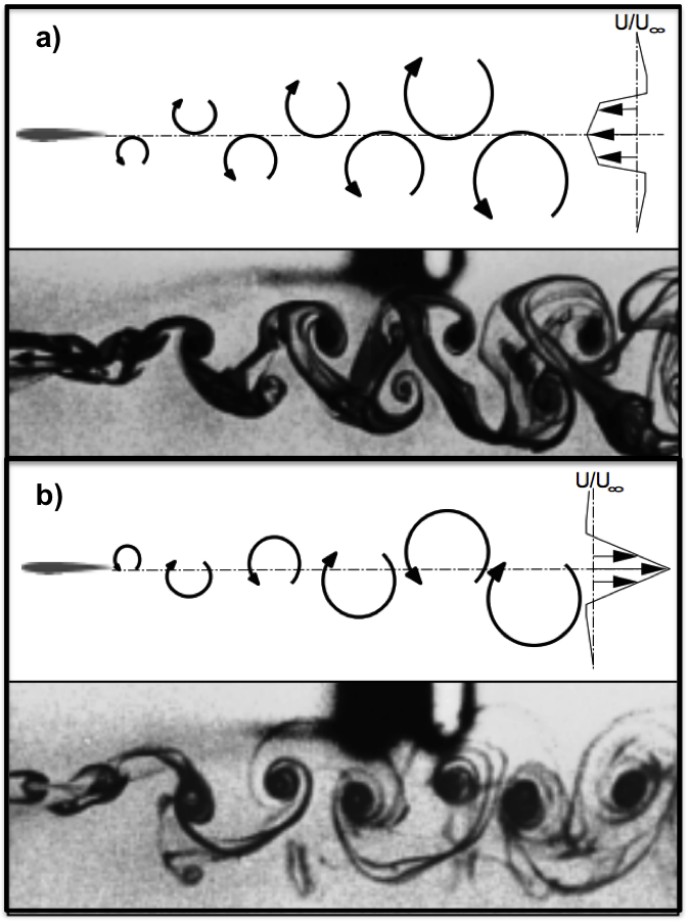

Figure 2.1: Wake profile for a) thrust generation and b) drag (Jones et al. 1996)

This linear theory, which Silverstein and Joyner (1939) validated by experiment, has since been applied by Lighthill to derive the dynamic processes of aquatic animal locomotion, which are discussed in more detail in Section 2.1.1. It has also provided a basis for the hydrodynamic analysis of flapping foil propulsion. Experiments by Harper et al. (1998). Jones et al. (1996) validated

the effectiveness of an unsteady panel code for capturing the wake profile of a purely heaving foil. This research also highlighted the importance of the wake dynamics on thrust generation, which is defined by reverse Von Karman street vortices, as shown in Figure 2.1 a). In comparison, a wake profile that is defined by Von Karman street vortices is indicative of drag, as shown in Figure 2.1 b).

Unsteady foil theory can be applied to multiple problems in engineering applications, and a large body of research has been undertaken in this field. Mathematical theories have evolved in complexity, and an increase in computational power has allowed fluid dynamicists to apply alternative and improved numerical techniques to evaluate the behaviour of flapping foils. Katz and Plotkin (1991) developed an unsteady panel method based on potential flow and the assumption that the flow is inviscid. More recently, improved computational capabilities have led to the application of Navier-Stokes solvers to evaluate the flow mechanisms over an oscillating airfoil, and simulate the corresponding wake. Ekaterinaris and Platzer (1997) first employed a Navier-Stokes solver to predict the unsteady characteristics of dynamic stall of an airfoil. Tuncer and Platzer (2000) further applied the method to analyse the unsteady flow fields over an oscillating NACA0012 airfoil. A comprehensive series of adaptations to these mathematical approaches have been made to evaluate different flapping foil problems, and to consider other fluid dynamic effects, such as three-dimensional and added mass effects. These research studies are focused primarily on the response of an ideal case with a flapping foil in a uniform flow.

2.1.1 Flapping foils in nature

An evolutionary drive to improve efficiency has made flapping foils the dominant mode of propulsion for marine organisms. This is achieved predominantly through the flexible muscular motion of their tail fin. Lighthill (1975) has completed a comprehensive study to address the biofluiddynamic behaviour associated with various modes of aquatic animal locomotion (Lighthill 1975). Particular emphasis has been on the hydromechanics of the carangiform mode of aquatic propulsion. This mode of propulsion, adopted by most cetaceans and fast fish such as marlin, generates thrust through the oscillation of the posterior half of the animal. Lighthill suggested that such forms of propulsion may be analysed in a similar way to the 'flapping' mode of bird and insect flight.

Lighthill further concludes that the oscillation of the caudal fin induces a 'reverse Von Karman vortex street' into the wake, which forms a net momentum change in the fluid, indicative of thrust.

Wu (1960) addressed this swimming characteristic by analysing the oscillation of a waving plate using a two-dimensional potential flow theory, and identified a net fluid momentum associated with the vortex wake as the key basic mechanism for thrust generation (Wu 1960). Triantafyllou et al (1991) experimentally demonstrated the dominance of wake dynamics on the thrust performance of an oscillating foil (Triantafyllou, Triantafyllou et al. 1991). The analysis was unable to replicate the efficiencies observed in nature, but it was later shown that aquatic animals recover energy at the tail fin by utilizing the Katzmayar effect and, therefore, increase the swimming efficiency (Zhu et al. 2002).

The wake dynamics can be described by the Strouhal number, which is the nondimensional ratio between the flapping frequency and amplitude, and the flow speed ($St = fh_0/U$). This ratio is important parameter for defining the regime of vortices shed in the wake. Taylor et al. (2003) shows that birds achieve maximum efficiency at Strouhal number of 0.25, and Triantafyllou et al. (1991) shows that this is achieved by marine animals for a range between 0.25 and 0.35.

2.1.2 Maritime propulsion

For open water propulsion, numerical studies (Yamaguchi and Bose 1994) and experimental studies (Anderson et al. 1998, Read et al. 2003) have demonstrated that actively driven flapping foils can achieve high efficiences, which for certain flapping characteristics are more efficient than conventional screw propellers.

Yamaguchi and Bose (1994) applied a linear theory for an oscillating foil propeller mounted at the stern of a 200,000 DWT tanker. Results showed that the flapping foil propulsor was theoretically 5% more efficient than an equivalent conventional screw propeller, but the authors concluded that significant work is required to develop a suitable drive mechanism (Yamaguchi and Bose 2014). Epps et al. (2016) have completed numerical simulations on tandem flapping foil propulsors, and have concluded that high efficiencies can be achieved with careful design consideration, such as inter-foil spacing. However, model ship experiments with a pair of flexible flapping foils only achieved a comparatively low propulsive efficiency of approximately 55% (Babu et al. (2014)).

Mannam et al. (2017) investigated the bollard pull and self propulsion of a vessel with two vertically aligned flapping foils close to the amidships. Their analysis was carried out over a range of Strouhal numbers and showed that the maximum efficiency of 73% was achieved at a Strouhal

number of 0.225 with a single flapping foil. However, at higher Strouhal numbers the efficiencies tend towards 55%, in agreement with the results of Babu et al. (2014). At lower Strouhal numbers, the efficiency decreases dramatically, which shows the importance of the Strouhal number on the propulsive performance. Thaweewat et al. (2018) have recently published a numerical study that investigated the difference between prescribed foil pitch and a spring loaded flapping foil for maritime propulsion. The results clearly show that a spring loaded foil has the advantage of passively adapting to an increase in flow speed, similar to that of variable pitch propeller. However, the efficiency values of approximately 80% are significantly greater than the efficiencies achieved in experimental studies.

2.1.3 Summary

Previous research has highlighted the effect of a flapping foil on the downstream wake, which is in the form of a reverse Von Karman wake for thrust generation. The exact profile of this wake governs the net momentum change of the fluid and, therefore, the propulsive efficiency. Improving the numerical modelling of the wake increases the accuracy of the numerical prediction of the propulsive performance. But the increased complexity of this approach is not considered necessary for analysing the coupled response of submerged flapping foils and a vessel in waves. However, it is evident from previous research that it is important to consider the effect of the wake on the thrust generation of a flapping foil. The linear theories of Theodorsen, which assume an inline wake, small harmonic amplitude motions and zero foil thickness, show remarkably good agreement with experimental and panel method numerical results for both pitching and heaving flapping motions (Jones et al. 1998, Jones 1997). Jones (1997) explains that the majority of highly nonlinear effects are due to a deformed wake at high Strouhal numbers ($St > 1$), but are higher than the expected Strouhal number for wave propulsion. Therefore, the linear theory remains a valid method for low Strouhal numbers and the basis linear theory of Theodorsen is considered sufficient for this research.

Aquatic animal flapping foil propulsion confirms the importance of the wake profile on the propulsive efficiency of flapping foils. The research shows that there is a narrow range of Strouhal numbers ($0.2 < St < 0.4$) adopted by aquatic animals for optimal propulsion. It is, therefore, necessary to consider the effect of this parameter for wave-induced propulsion.

Numerical predictions have shown that the efficiences of flapping foils for ship propulsion could be equivalent to or higher than conventional screw propellers, but this is yet to be experimentally demonstrated. Epps et al. (2016) showed that positive interactions between a forward and aft foil

could generate high efficiencies, which could be applicable for actively driven wave propelled USVs. This is beyond the scope of this research, but the experimental setup, described in Chapter 4, is capable of providing a test platform for actively driven flapping foil propulsion.

Previous research has also identified that a spring loaded passively pitching flapping foil is advantageous in comparison to an actively pitched flapping foil. The passive pitch refers to a pitch response that is invoked by the moment and lift forces acting on the foil and, therefore, the foil pitch amplitude and flapping phase is dependent on the free stream velocity and the flapping heave amplitude. In comparison a actively pitched foil applies a prescribed pitch amplitude and phase. Due to the ability to adapt to changes in the free stream flow (i.e. wavy flows), the passive method is particularly suitable for wave propulsion (Bockmann 2015).

2.2 Wave-induced flapping foil propulsion

2.2.1 Fundamentals of flapping foil propulsion in waves

Uniform flows theories have been adapted to analyse the performance of flapping foils in waves. Grue et al (1988) presented advances made in the mathematical theories of thrust generation by an oscillating foil moving in water waves. These theories follow on from the mathematical basis constructed by Lighthill (1969) and Wu (1960), and, more recently, the experimental and theoretical research carried out by Jakobsen and Isshiki respectively, in the early 1980s. Jakobsen (1981) performed various experiments to assess the feasibility of using foils to harness the energy of ocean waves for the propulsion of ships (Jakobsen 1981).

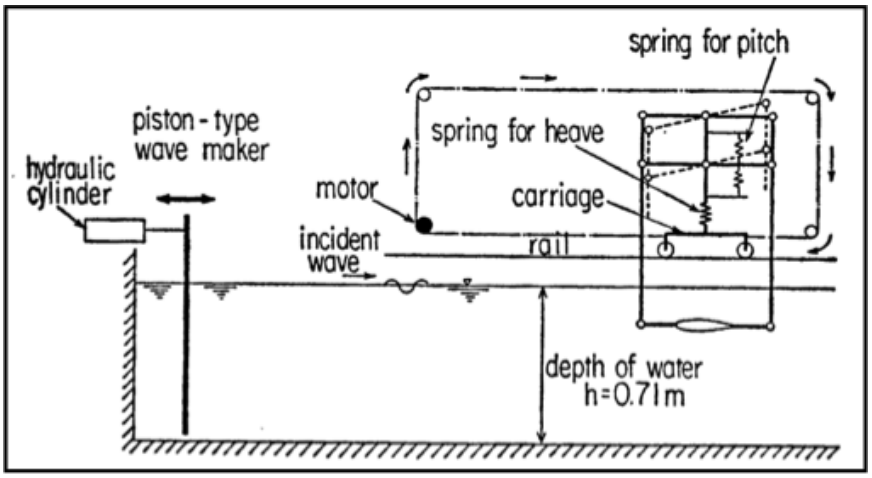

Figure 2.2: Experimental work of Isshiki on Wu's theory (Isshiki 1984)

Isshiki presented a theory that applies the formulae of Wu (Wu 1972) but also considers the presence of the free surface effect to compute the lift forces and moments acting upon a foil in waves (Isshiki 1982). Isshiki and Murakami (1984) performed various experiments, including the wave propelled foil experiment illustrated in Figure 2.2, which validated and supported theories proposed in their earlier work (Isshiki and Murakami 1983). Grue et al (1988) found reasonable agreement between their theory and the experiments of Isshiki and Murakami (1984) and Jakobsen (1981) with discrepancies at higher wave frequencies assumed to be due to non-linear effects. The advances in the classical theory of foils moving in waves may be considered to be the accumulation of work carried out by Theodorsen, Lighthill, Wu, Isshiki and Grue.

More recently, a Reynolds-averaged Navier-Stokes (RANS) CFD method has been implemented by De Silva and Yamaguchi (2012), who presented a fixed speed solution for wave-augmented propulsion. The results are in strong agreement with the experimental results of Isshiki and Murakami (1984), and show that the CFD method can accurately capture the thrust generation at higher wave frequencies. A key outcome from this analysis was the identification of the wave-phasing parameter, which De Silva and Yamaguchi defined as the phase difference between the foil heave and the local vertical velocity of the wave particles. In their study, the optimum wave-phasing parameter is found to be equal to $\pi/2$, which equates to the foil heave velocity being out of phase with the local vertical velocity of the wave.

Xu et al. (2017) applied a boundary element method to investigate the wave effects on a flapping foil. The numerical results showed that the phase difference between the wave and the foil heave is

in agreement with De Silva and Yamaguchi with regards to the optimal value of the wave-phasing parameter. Liu et al. (2016) carried out a study on the effect of wave-phasing on the propulsive performance of a flexible flapping foil, which also shows that the optimum wave-phasing parameter is equal to $\pi/2$.

2.2.2 Wave propulsion in nature

Wu (1972) observed the flight of certain seabirds over ocean waves, and noticed that these birds travelled long distances with minimal wing flapping motion, implying that energy could be absorbed from the surrounding wavy flow. Using the two-dimensional potential theory for flat plates, Wu investigated a hydrofoil oscillating in waves and showed that at a flapping frequency equivalent to the wave frequency a net mechanical power could be extracted from a wavy flow of large amplitude waves (Wu, 1972). This conclusion is supported by the numerical analysis of Xu et al. (2017).

Bose and Lien (1990) adapted Wu's theoretical approach to study the wave-augmented propulsion of cetaceans. They drew on common knowledge within the whaling industry that a dead whale could be propelled by waves to such an extent that if it was left floating unattended, whalers would remove the fluke of the whale to prevent losing the carcass. The approximate method adopted by Bose and Lien demonstrated the potential absorption of wave energy by cetacean flukes. It was estimated that a 14.5m immature fin whale is capable of propulsive power savings of approximately 30% at a depth of 2m, speed of 2.5ms^{-1}, regular wave frequency of 1.43rad s^{-1} and wave amplitude of 0.5m.

2.2.3 Wave-augmented maritime propulsion

Wave-augmented propulsion was first practically demonstrated almost 120 years ago through a series of full scale trials of a 13ft boat with flapping foils mounted at the bow and the stern (Linden 1895). Since then numerous efforts have been made to develop this initial invention and a historical summary of this is provided in Appendix A.

Konstantinov and Yakimov (1995) described a method to couple a submerged foil with the motions of a vessel in regular waves. The study provides a useful introduction to the kinematics of wave propulsion, and predicts thrust generation with respect to the wavelength to vessel length ratio for head and following waves. Naito and Isshiki (2005) published a comprehensive summary of

the various numerical and experimental studies on ship related flapping foil wave propulsion. The main conclusion of this summary was that, in suitable wave conditions, a bow mounted foil will act as an auxiliary propulsor, and will also reduce the motions of the ship. These conclusions have been supported by numerous experiments and numerical simulations of increasing complexity, and these are summarised in the following paragraphs.

Fixed speed experiments conducted by Bockmann (2015, 2016) investigated the thrust generation and motion reduction effect due to a fixed horizontal hydrofoil at the bow. The results show that a fixed hydrofoil is capable of generating thrust and counteracting ship motions in head waves, and that the combination of reduced ship motions and thrust generation significantly increases the propulsive efficiency (Bockmann and Steen 2013). Additionally, Huang et al. (2016) performed free running experiments with an actively pitching bow foil in waves, and results showed that the submerged flapping foil was capable of improving the vessel's propulsive efficiency by up to 19% (Huang et al. 2016).

Filippas and Belibassakis (2014) conducted a fixed speed numerical analysis using an unsteady boundary element method (BEM) incorporating free surface effects. The analysis provides an extensive comparison with alternative numerical methods. Filippas and Belibassakis (2014) predict that, under optimal conditions, flapping foil thrusters (oscillating hydrofoils with active pitch control) can augment ship propulsion by a maximum of 20% in regular head waves, which has been experimentally proven by Huang et al. (2016).

Belibassakis and Polities (2013) applied a non-linear 3D panel method, including a wake analysis, to solve the unsteady flow characteristics of horizontal and vertical flapping hydrofoils. Over a range of parameters, the results indicate significant thrust generation and reduced ship motions (Belibassakis and Politis 2013). The non-linear 3D panel method shows good agreement with a more simplified unsteady lifting line method, which indicates that the simplified method is a suitable method for low Strouhal number applications.

For fixed speed wave-augmentated propulsion, research by Belibassakis & Politis (2013) and Belibassakis & Filippas (2015) has shown that a spectral approach can be applied to predict the time domain thrust generation of a submerged foil in irregular waves. Based on the wave-induced vessel motions, both methods resolve the resultant foil heave in the frequency domain, which is in the form of a response amplitude operator (RAO) or transfer function. Using spectral analysis, the instantaneous foil heave is estimated for irregular waves, and the resultant forces are resolved in the

time domain using either an unsteady BEM model (Belibassakis & Filippas, 2015) or a nonlinear 3D panel method (Belibassakis & Politis, 2013). Feng et al. (2014) applied a frequency domain method to predict the effect in regular waves of a bow foil on the vessel motions, and added resistance due to waves. The resultant transfer functions were then used to predict the effect of a bow foil in an irregular sea state, and were combined with resistance and propulsion calculations to analyse the change in Energy Efficiency Design Index (EEDI) of a ship transiting the Pacific Ocean. However, the results show a minimal reduction in the EEDI ($< 1.4\%$) due to the presence of a submerged foil at the bow.

Bockmann (2014) has performed experiments to compare the thrust generation of an actively pitch controlled foil with the thrust generation of a spring-loaded foil. The results show that the spring-loaded foil is more efficient than the equivalent actively pitch controlled foil, which is in agreement with the numerical study of Thaweewat et al. (2018). An interesting new pitch control method has recently been investigated by Hao et al. (2017). This method involves using a float to adjust the angle of attack of the submerged foil.

2.2.4 Wave propelled vessels

Terao (1982) conducted a simplified free running experimental study with a surface float and submerged flapping foils in waves, which under certain conditions achieved self-propulsion. This research later developed into full scale trials of a 'wave devouring propulsion system' (WDPS) for a wave propelled catamaran. The WDPS technology has recently been applied onboard small USVs for the purposes of sea trials (Terao 2013, 2015), see Figure 2.3. The results of these trials proved the effectiveness of such a system for USVs.

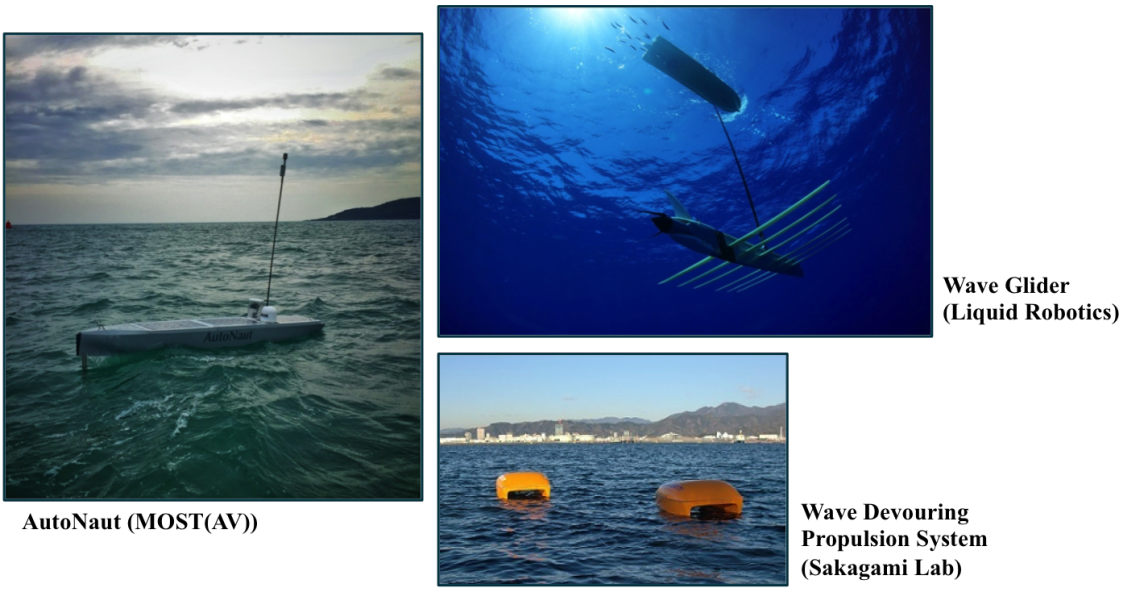

Figure 2.3: Current wave propelled USVs

In parallel with the work carried out by Terao, the wave glider ASV has been developed by Liquid Robotics. The Wave Glider, shown in Figure 2.3, is a commercial wave propelled ASV and there have been numerous publications that address the design, navigation and application of this vehicle (Hine et al. 2009, Manley & Wilcox 2010, Daniel et al. 2011). The Wave Glider operates a flapping foil propulsion system that is tethered to a surface float, and is designed to maximise the relative wave-induced heave motion by locating the foils at a significant depth.

The Wave Glider has recently completed a 7939 nautical mile journey over the course of more than a year (Liquid Robotics, Inc 2015). However, out of four Wave Glider USVs deployed in the Pacific, only two reached their destination with the remaining two encountering technical difficulties (Villareal and Wilson 2014). Ngo et al (2014) used the GPS trials data from the Wave Glider to perform regression analysis in order to predict the forward speed.

AutoNaut is the only other commercial wave propelled ASV. The AutoNaut ASV utilizes spring-loaded flapping foils at the bow and stern to transit the oceans for up to 3 months, and relies on solar energy combined with fuel cells to deliver power for onboard systems (MOST (AV) Ltd 2015). Although both USVs operate submerged flapping foils, but there is a significant difference in the wave-induced mechanism that drives the foils. The Wave Glider utilizes the wave-induced heave motion of a surface float, whilst the submerged foils of the AutoNaut ASV are driven by the

wave-induced pitch and heave motion of the surface vehicle.

The mathematical theory of wave propelled vehicles with submerged flapping foils remained undeveloped until the 1980's when Isshiki extended the previous theories on flapping foils in waves to incorporate a surface float. Isshiki (1984, 1994) implemented two numerical methods for solving the free running forward speed of a vehicle solely propelled by waves using submerged flapping foils. The initial method from Isshiki and Murakami (1984) assumes the forward speed and solves for thrust generated by a submerged foil in the frequency domain. The method then re-evaluates the forward speed by adjusting for the apparent thrust generated by the submerged flapping foils. However, Isshiki's initial method is a simplified model that does not consider hull motions and the consequent added resistance due to waves.

The second method implemented by Isshiki (1994) incorporates the motions of a surface vehicle and the added resistance due to waves. From experimental results, a gain coefficient is derived to represent the gain obtained from attaching a foil at the bow of a ship in head waves. This is then applied to classic ship theory resistance and propulsion calculations to compare the forward speed in waves with and without a submerged flapping foil.

Recent advances

Recent research has focused on the analysis of heave driven mechanisms for wave propulsion (Liu et al. 2016, Yu et al. 2016, Tian et al. 2016, Zhou et al. 2017). These numerical methods assume that the vessel contours the waves, and neglect the effect of the local wave particle velocities. Both assumptions are acceptable for a heave driven system, as the foils are submerged to a significant depth.

Liu et al. (2016) have completed numerical and experimental analysis to investigate the performance of tandem flapping foils for the heave driven Wave Glider application. The validated numerical model applies a turbulent CFD simulation that produces interesting results with regard to foil interaction and shed vortices. Yu et al. (2016) implemented a considerably lower order linear dynamic method to analyse the free running wave propulsion of a float with a submerged foil. The method provides a good explanation of the basic mechanics of a heave driven wave propelled system. Tian et al. (2016) have numerically modelled the dynamic relationship between the vessel and the submerged flapping foils, and this provides a more detailed explanation of the mechanisms for heave

driven wave propulsion. Zhou et al. (2017) present a numerical model that is capable of predicting the forward speed of a heave driven system. The numerical model is based upon the dynamics of a Wave Glider and uses Kane's method to solve the coupled dynamics of the surface vessel and submerged foils. Zhou et al. also conducted experiments, which show reasonable agreement with the numerical results. However, neither the numerical or experimental analysis considers the interaction of waves on the system, and only accounts for the wave-induced heave motion of the submerged foils by heaving the foils beneath the free surface at an equivalent amplitude to an incoming wave.

For pitch driven wave propulsion, the analysis is more complex as it is necessary to account for the wave-induced pitch of the vessel as well as the vessel heave response. Liu et al. (2011) have conducted a numerical study that investigates this mode of propulsion in regular waves. The vessel motions are solved in the frequency domain and coupled with the submerged foil motions via two springs. The hydrodynamic forces of the flapping foil are resolved using Wu's theory, and the results show that the location of the foil relative to the vessel is of key importance.

Xie et al (2017) have recently published a detailed CFD analysis of a tandem foil setup for a wave propelled unmanned catamaran. Although the analysis is detailed in terms of the resultant hydrodynamic forces, the analysis assumes the foil is not flapping (i.e does not pitch about its own axis), and also assumes that there is no physical interaction between the submerged foils and the catamaran motions (i.e the presence of the foils has no effect on the motions of the catamaran). The results do, however, show that the forward foil generates more thrust than the aft foil in head waves, which demonstrates the importance of foil location on the propulsive performance.

2.2.5 Summary

The previous research relating to a foil in waves with no surface vessel shows that the interaction of the foil with the local vertical velocity of the wave particles has a significant effect on the propulsive performance. The foil location will significantly change the phase difference between the foil and the local wave profile. This effect has not been investigated and is regarded as an important area of further research.

With regard to the previous research involving a surface vessel, the majority of the work has focused on fixed speed or free running experiments, and fixed speed theoretical models. Three fixed speed theories/methods exist for solving for the forward speed of a pitch driven wave propelled

vessel:

1. a theory based on a foil only scenario that assumes the forward speed then re-calculates the speed from the apparent thrust (Isshiki & Murakami 1984);

2. an empirical method specific to a particular hull shape (Isshiki 1994);

3. a resistance and propulsion approach implemented by Bockmann (2015) for a purely wind and wave propelled ship.

Whilst these methods provide a reasonable estimate of the forward speed, they do not capture the free running response of a wave propelled vessel. Although free running experiments and in-situ trials have been completed, a numerical model that is capable of solving for the forward speed of a pitch-driven free running wave propelled vessel, such as the AutoNaut ASV, does not exist.

Free running numerical models have been developed to predict the forward speed of a heave-driven wave propelled vessel, such as the Wave Glider ASV, but these involve a simplified approach to the vessel motions, and do not account for the interactions between an incident wave profile and the submerged foil (Yu et al. 2016, Zhou et al. 2017). Also, a regression method has been applied to solve for the forward speed of a heave driven system. However, this method relies on extensive data acquired on the forward speed and heading of an in-situ wave propelled boat (Ngo et al 2014).

For a pitch driven setup with foils located at the bow and stern, it has been shown that the forward foil generates more thrust than the aft foil. This has not been extensively investigated and further analysis is required to explain the differences between the response of the forward and aft foil.

Previous research has developed methods to evaluate the propulsive performance of a wave propelled vessel in irregular waves. However, these methods assume a fixed vessel speed, which simplifies the solution of the hydrodynamic forces acting on the foils. For a vessel solely propelled by waves, further work is required in this area in order to accurately predict the wave-induced forward speed in irregular, short crested waves and for different vessel headings.

Although there has been research on the optimal design of wave-augmented propulsion systems for ship efficiency in waves, there is no comprehensive guidance on the design of small unmanned pitch-driven wave propelled vessels. The ability to predict the performance of such vessels for a range of parameters would be a useful design tool.

2.3 Wave energy recovery utilizing flapping foils

2.3.1 Marine renewable energy recovery

Previous research on flapping foil power generation has focused primarily on energy extraction from uniform flows such as tides and currents. Young et al. (2014) present a comprehensive review of the fundamentals, kinematics, hydrodynamics and design of these flapping foil systems. The research area can be divided into three particular systems of oscillating foils; fully prescribed (prescribed heave and pitch), semi-passive (prescribed pitch and induced heave) and fully passive (both foil pitch and heave induced by the flow stream). Both prescribed methods rely on an active change in the foil pitch to induce the heave motion required to extract energy from the flow stream. Fully passive systems involve passive mechanisms at the end stops of the flapping foil heave stroke to reverse the pitch angle of the foil relative to the flow stream and induce heave in the opposite direction. Introducing a wavy flow into the system can also act to reverse the pitch of the submerged flapping foil and further extract energy from both waves and currents. Therefore, the fully passive method is of particular interest for extracting energy from wavy flows near the free surface.

The prospect of extracting energy from both waves and currents utilizing submerged flapping foils has recently been investigated by Belibasskis et al. (2015, 2016). The numerical analysis uses a time domain boundary element method to simulate the response of a semi-passive oscillating foil operating in shallow water of variable bathymetry, and includes considerations for the effect of the wavy free surface and the oscillating velocities due to the waves. The results show that the inclusion of wave energy significantly increases the power performance in comparison to solely a uniform flow, which suggests that submerged flapping foils can be utilized for the purposes of extracting wave energy. In addition, recent results from the same research highlights that optimum power extraction is attainable when the foil heave is out of phase with the incident wave profile (Fillipas et al. 2018), which is in agreement with the wave propulsion analysis conducted by De Silva and Yamaguchi (2012).

A novel area of this research is to investigate the combination of both wave energy recovery and wave propulsion utilizing submerged flappings, including the analysis of simultaneous thrust and power generation.

2.3.2 Unmanned marine vehicles

The concept of using submerged foils as a method of generating onboard power was recently published as a patent filed by the developers of the Wave Glider (Hine, 2013). More recently, research has been conducted to assess the potential of wave energy recovery onboard unmanned underwater vehicles (AUVs) utilizing the concept of a foil moving relative to a body in waves. Zhao et al. (2016) uses the principles of vibration energy harvesting to analyse the potential of energy recovery from the wave-induced vibrations of AUV wings when operating at the surface and a comprehensive design of the setup has been published by Sun et al. (2016). A similar concept modularizes the AUV wings so that they can rotate about a pivot point on the main body and, hence, perform work against an electromagnetic rotary generator, which is housed inside the AUV (Fenucci et al. 2016).

Whilst there are a few examples of research on recovering wave energy for onboard power generation on wave powered vessels, the topic is relatively unexplored and requires further investigation. Furthermore, the ability to control the forward speed of a wave powered vessel and recover wave energy simultaneously has not been investigated. This could prove to be a useful development for wave propelled USVs as current methods rely on following a circular pattern to keep station rather than holding a position whilst recovering wave energy.

2.4 Concluding remarks

The review of previous research has identified areas that have either not been investigated or merit more detailed investigation. Within the scope of this research the followings items are considered to be of significant importance, and are addressed in the remaining chapters:

Flapping foil propulsion

- the validity of using a simplified linear theory (Theodorsens) for evaluating the unsteady hydrodynamic forces acting on a foil in waves;
- the influence of the Strouhal number on the propulsive performance of the coupled system;

Wave-induced flapping foil propulsion

- the impact of the wave-phasing parameter on the coupled response, and the corresponding effect of the foil location;
- the difference between the response of a foil located at the bow and a foil at the stern for head and following waves;
- a method to predict the free running forward speed of a pitch-driven wave propelled vessel in regular and irregular waves;
- guidance for the design of wave powered vessels including the hull design, foil particulars and considerations for scaling;

Wave energy recovery utilizing flapping foils

- a proof of concept for wave energy recovery utilizing submerged flapping foils;
- a method to predict the wave energy recovery efficiency of a PTO device.
- a method to control the forward speed of a vessel that is solely propelled by waves

Chapter 3

Mathematical modelling of the coupled dynamics

This chapter firstly describes the equations that govern the motions of a vessel with submerged foils in waves (seakeeping theory), the dynamic response of spring loaded foils in waves (unsteady foil theory) and the wave energy recovery of flapping foils (vibration theory). These equations are then combined in a numerical algorithm that simulates the free running response of a wave propelled vessel and predicts the efficiency of a flapping foil wave energy recovery device. The numerical method applies the linear theories listed in Table 3.1.

Table 3.1: Summary of the physical components of the coupled dynamics and the corresponding theory

Physical component	**Corresponding theory**	**Description**
Water waves	Airy/linear wave theory	The wavy flow of the incident wave profile
Seakeeping	Strip theory	The vessel motion response and added resistance in waves
Unsteady foil	Theodorsen's theory	The flapping response of the foils
Vibration	Mass-spring-damper theory	Foil pitch response and relative foil heave for wave energy recovery

Whilst more detailed mathematical theories exist for the analysis of either seakeeping or unsteady foils, these add additional complexities which are not considered necessary for the scope of this research. The key focus is to capture the overall coupled dynamics rather than the detailed response of each component.

3.1 Frames of reference

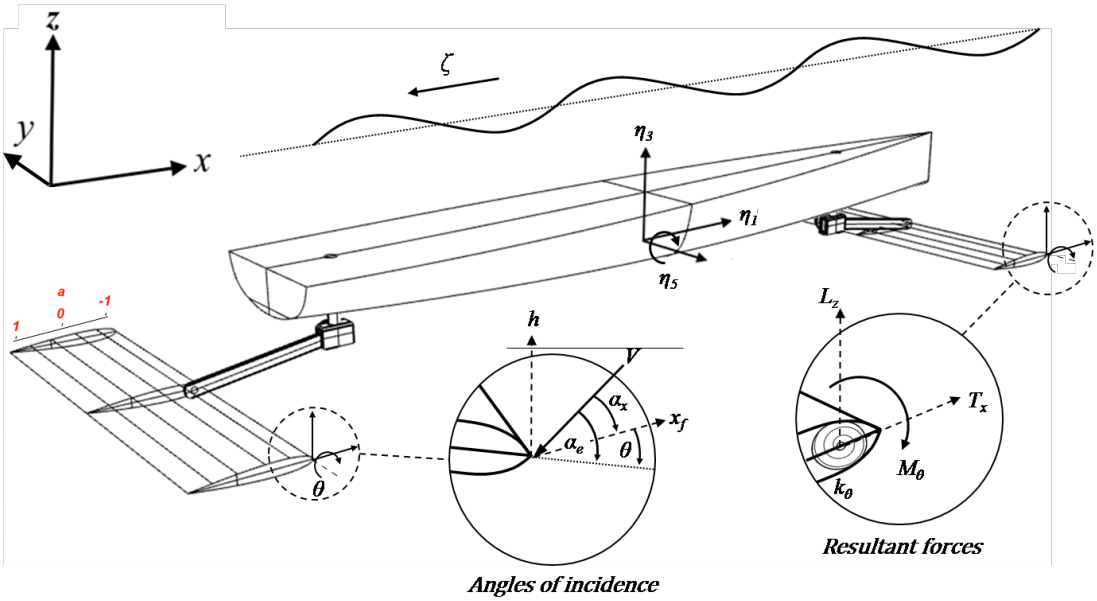

Figure 3.1: Global and local frames of reference

The origin of the global frame of reference is on the waterline ($z = 0$) and at the longitudinal centre of gravity (LCG) of the vessel at zero time ($x = 0$), see Figure 3.1. The vessel surge (η_1) and heave (η_3) are evaluated with respect to the inertial origin and the vessel pitch (η_5) is about the vessel's centre of rotation, which is the centre of the local frame of reference. On the same basis, the vessel induced foil heave (h) is evaluated in the inertial frame of reference as a remote location on the vessel at a depth below the waterline (d_f). The pitch of the foil (θ) is evaluated about the pivot point, a, and the pivot point is located along the foil chord (c), where a is 0 at the half-chord location, -1 at the leading edge and 1 at the trailing edge.

3.2 Theory

3.2.1 Linear wave theory

The wave elevation of a linear regular wave is given as the following sinusoidal function:

$$\zeta(t) = \zeta_0 \sin(kx \pm \omega t)$$

$$= \zeta_0 \sin \omega_e t \tag{3.1}$$

where ζ_0 is the wave amplitude ($\frac{H}{2}$), k is the wave number, ω is the wave frequency and ω_e is the encountered wave frequency (defined in Equation 3.62). The plus or minus is associated with the direction of the incident wave profile where a wave propagating in the negative x-direction is defined with a positive sign, and a wave propagating in the positive x-direction is defined with a negative sign.

3.2.2 Seakeeping

Numerous numerical methods have been developed to predict the seakeeping response of ships in waves. These methods are divided into frequency and time domain solutions, 2D and 3D, and methods of varying orders of complexity from linear to higher orders such as RANS CFD simulations. Figure 3.2 summarises the various numerical methods according to the degree of linearity. Linear methods are limited to small amplitude motions and nonlinear methods are required for ship motions in large waves. With the addition of further complexities such as submerged flapping foils and free running simulations, a fully nonlinear method would require significant computational power.

The more simplified methods divide the hydrodynamic forces into inertial, radiation, diffraction, Froude-Krylov (force from the undisturbed incident wave pressure field) and the hydrostatic restoring force. The difference between each of these methods is the solution of the forcing terms, which can be either solved in the frequency domain at various stations along the length of the vessel or solved with respect to a changing wetted surface, as depicted in Figure 3.2. The frequency domain approach is the basis of the strip method developed by Salvesen et al. (1970) and assumes a minimal change in hull shape between each station. The more exact approach utilizes panel methods to calculate the

Nonlinearity	Incident Wave	Disturbance Hydrodynamics	Froude-Krylov & Restoring Forces	Numerical Methods
Linear	Linear	Linear 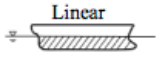	Linear 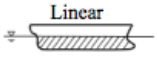	Strip, Wave Green Function, Rankine Panel, CFD
Weakly Nonlinear	Linear	Linear 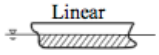	Nonlinear 	Strip, Impulse-Response-Function, Green Function, Rankine Panel
Weak Scatterer	Linear or Nonlinear	Linear w.r.t. incident wave (Nonlinear in conventional method) 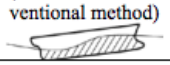	Nonlinear 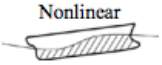	Rankine Panel
Fully Nonlinear	Nonlinear	Nonlinear 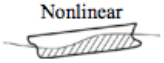	Nonlinear 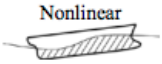	CFD

Figure 3.2: Comparison of linear and nonlinear seakeeping numerical methods (ITTC 2017)

instantaneous wave-induced pressure acting on the wetted surface of the hull and the instantaneous restoring force due to the local draft. This solution can then be combined with the frequency domain hydrodynamic coefficients to predict the seakeeping response for more complicated hull forms. Reisner et al. (2016) present a comprehensive comparison between the linear and nonlinear methods for predicting the seakeeping response of a ship with forward speed ($Fn < 0.2$) in waves. The numerical results show that there is only a marginal difference between the nonlinear and linear solutions for small amplitude motions, particularly for head wave conditions.

For the purposes of investigating the coupled response of a wave powered vessel, linear methods are implemented in the following sections with the assumption of small amplitude motions and are compared with experiments in the subsequent Chapter. More exact methods would be required for predicting the coupled response in larger waves, which may be more applicable for the analysis of USVs. However, the following methods form the basis of a numerical model that is capable of predicting the forward speed and energy recovery of wave powered surface vehicles. The incorporation of nonlinear effects is considered an area of future work to improve the numerical modelling in larger waves.

Strip theory

The following strip method is based upon the theories developed by Salvesen et al. (1970), and include coupled submerged foil forcing terms (abbreviated by F). The vessel heave (η_3) and pitch (η_5) motions are defined by ordinary differential equations (ODE) synonymous with a mass spring

damper system:

$$\underline{Heave}: \quad \overbrace{(M_B + A_{33})\ddot{\eta}_3}^{Inertial} + \overbrace{B_{33}\dot{\eta}_3}^{Damping} + \overbrace{C_{33}\eta_3}^{Restoring} + \overbrace{A_{35}\ddot{\eta}_5 + B_{35}\dot{\eta}_5 + C_{35}\eta_5}^{Coupled} = \overbrace{{F_3}^B + {F_{3_i}}^F}^{Forcing} \tag{3.2}$$

$$\underline{Pitch}: \quad \overbrace{(I_B + A_{55})\ddot{\eta}_5}^{Inertial} + \overbrace{B_{55}\dot{\eta}_5}^{Damping} + \overbrace{C_{55}\eta_5}^{Restoring} + \overbrace{A_{53}\ddot{\eta}_3 + B_{53}\dot{\eta}_3 + C_{53}\eta_3}^{Coupled} = \overbrace{{F_5}^B + {F_{5_i}}^F}^{Forcing} \tag{3.3}$$

where the term i represents the foil number, and:

${F_3}^B$ - heave excitation force due to waves
${F_5}^B$ - pitch excitation force due to waves
${F_3}^F$ - heave force due to submerged foils
${F_5}^F$ - pitch force due to submerged foils
M_B - total mass of the vessel including foils
I_B - moment of inertia for vessel including foils
A_{**} - added mass coefficient
B_{**} - damping coefficient
C_{**} - hydrostatic restoring coefficient for pure heave

The hydrodynamic coefficients and excitation forces are evaluated using the strip theory method which is applicable for; slender, rigid and wall-sided vessels; small amplitude motions; low Froude numbers; and deep water (Salvesen et al. 1970). The theory also assumes that the presence of the vessel has no effect on the incident wave pressure field, also known as the Froude Krylov hypothesis, and that the effects due to viscosity are disregarded. The solution of the flow around a heaving semi-circle is extended and transformed to describe the flow properties of the two-dimensional shape of the hull, known as conformal mapping, shown in Figure 3.3.

Transom effects are accounted for in the strip theory formulations with the addition of speed dependent functions for the aft-most sections (abbreviated with A). The global added mass, damping and restoring coefficients are evaluated by integrating over the length of the vessel and combining the coupled terms:

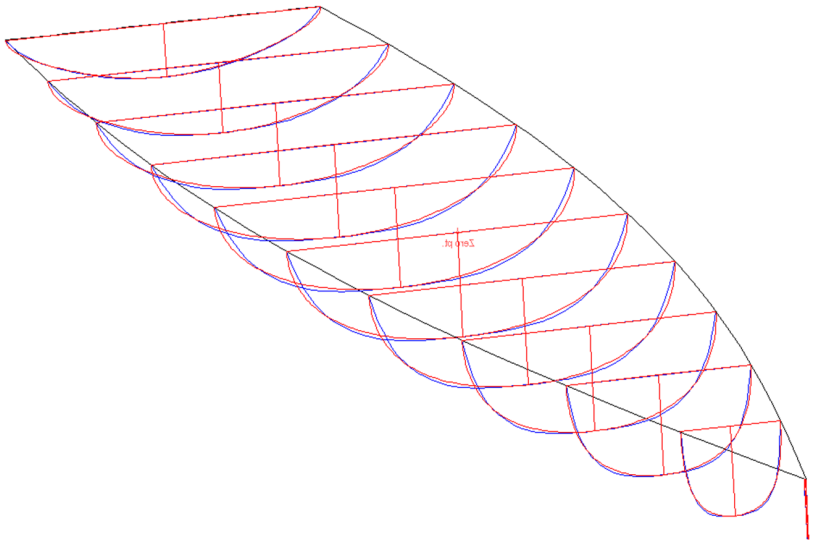

Figure 3.3: Conformal mapping of hull sections to evaluate sectional hydrodynamic coefficients

$$A_{33}{}^{0} = \int_{L} a_3 d\xi \tag{3.4}$$

$$A_{33} = A_{33}{}^{0} - \frac{U}{\omega_e{}^2} b_3{}^{A} \tag{3.5}$$

$$B_{33}{}^{0} = \int_{L} b_3 d\xi \tag{3.6}$$

$$A_{35} = -\int_{L} \xi a_3 d\xi - \frac{U}{\omega_e{}^2} B_{33}{}^{0} + \frac{U}{\omega_e{}^2} \xi^{A} b_3{}^{A} - \frac{U^2}{\omega_e{}^2} a_3{}^{A} \tag{3.7}$$

$$A_{53} = -\int_{L} \xi a_3 d\xi + \frac{U}{\omega_e{}^2} B_{33}{}^{0} + \frac{U}{\omega_e{}^2} \xi^{A} b_3{}^{A} \tag{3.8}$$

$$A_{55} = \int_L \xi^2 a_3 d\xi + \frac{U^2}{{\omega_e}^2} {A_{33}}^0 - \frac{U}{{\omega_e}^2} {\xi^A}^2 {b_3}^A + \frac{U^2}{{\omega_e}^2} \xi^A {a_3}^A \tag{3.9}$$

$$B_{33} = {B_{33}}^0 + U {a_3}^A \tag{3.10}$$

$$B_{35} = -\int_L \xi b_3 d\xi + U {A_{33}}^0 - U \xi^A {a_3}^A - \frac{U^2}{{\omega_e}^2} {b_3}^A \tag{3.11}$$

$$B_{53} = -\int_L \xi b_3 d\xi - U {A_{33}}^0 - U \xi^A {a_3}^A \tag{3.12}$$

$$B_{55} = \int_L \xi^2 b_3 d\xi + \frac{U^2}{{\omega_e}^2} {B_{33}}^0 + U {\xi^A}^2 {a_3}^A + \frac{U^2}{{\omega_e}^2} \xi^A {b_3}^A \tag{3.13}$$

where a_3 and b_3 are the frequency dependent sectional added mass and damping coefficients respectively. The following wave-independent hydrodynamic coefficients define the hydrostatic restoring forces and moments that are applied to the hull to maintain hydrostatic equilibrium:

$$C_{33} = \rho g \int_L b_\xi d\xi = \rho g A_{WP} \tag{3.14}$$

$$C_{35} = C_{53} = -\rho g \int_L \xi b_\xi d\xi = -\rho g M_{WP} \tag{3.15}$$

$$C_{55} = \rho g \int_L \xi^2 b_\xi d\xi = \rho g I_{WP} \tag{3.16}$$

where b_ξ is the sectional beam, A_{WP} is the waterplane area, and M_{WP} and I_{WP} are the first and second moment of areas respectively, acting about the transverse axis located at the centre of gravity.

The wave excitation forces and moments exerted on each strip are induced by the effects of both the sectional Froude-Krylov force (f_3) and the diffraction force (h_3). The Froude-Krylov force is

a result of the unsteady pressure field generated by an undisturbed incident wave. The diffraction force is due to changes made to the pressure field due to the presence of the strip. The global wave excitation forces are evaluated by integrating the Froude-Krylov and diffraction forces over the length of the vessel as follows (Salvesen et al. 1970):

$$F_3 = \rho\zeta_0 \int_L (f_3 + h_3) d\xi + \rho\zeta_0 \frac{U}{i\omega_e} {h_3}^A \tag{3.17}$$

$$F_5 = -\rho\zeta_0 \int_L \left[\xi(f_3 + h_3) + \frac{U}{i\omega_e} h_3\right] d\xi - \rho\zeta_0 \frac{U}{i\omega_e} \xi^A {h_3}^A \tag{3.18}$$

Salvesen et al (1970) derived the following expressions for the sectional Froude-Kriloff (f_3) and diffraction (h_3) force:

$$f_3 = g e^{ik\xi} e^{-kd_\xi s_\xi} b_\xi \tag{3.19}$$

$$h_3 = -\frac{1}{\rho} \frac{\omega_0}{\omega_e} e^{ik\xi} e^{-kd_\xi s_\xi} (\omega^2 a_3 - i\omega b_3) \tag{3.20}$$

where d_ξ is the sectional draft and s_ξ is the sectional area coefficient (Sectional Area / $[b_\xi \times d_\xi]$). Substituting the sectional forces into the equations for the global excitation forces yields the following approximations for head and following seas only (Salvesen et al. 1970):

$$\begin{aligned} F_3 = \zeta_0 \int_L e^{ik\xi} e^{-kd_\xi s_\xi} \Big[\rho g b - \omega(\omega_e a_3 - i b_3)\Big] d\xi \\ - \zeta_0 \frac{U}{i\omega_e} e^{ik\xi_A} e^{-kd_\xi s_\xi} \omega(\omega {a_3}^A - i {b_3}^A) \end{aligned} \tag{3.21}$$

$$\begin{aligned} F_5 = -\zeta_0 \int_L e^{ik\xi} e^{-kd_\xi s_\xi} \Bigg[\xi\Big(\rho g b - \omega(\omega_e a_3 - i b_3)\Big) \\ -\zeta_0 \frac{U}{i\omega_e} \omega(\omega a_3 - i b_3)\Big] d\xi \\ + \zeta_0 \frac{U}{i\omega_e} e^{ik\xi_A} e^{-kd_\xi s_\xi} \omega \xi_A (\omega {a_3}^A - i {b_3}^A) \end{aligned} \tag{3.22}$$

The heave and pitch forcing terms can be translated into the time domain by evaluating their complex identities:

$$F_{30} = |F_3| \; and \; \varphi_3 = tan^{-1}\Big(\frac{\Im(F_3)}{\Re(F_3)}\Big) \tag{3.23}$$

$$F_{50} = |F_5| \; and \; \varphi_5 = tan^{-1}\Big(\frac{\Im(F_5)}{\Re(F_5)}\Big) \tag{3.24}$$

where,

$${F_3}^B = F_{30} sin(\delta + \varphi_3) \tag{3.25}$$

$${F_5}^B = F_{50} sin(\delta + \varphi_5) \tag{3.26}$$

The inclusion of the time dependent variable, δ, ensures that the surge of the vessel, i.e the change in encountered frequency, is coupled with the heave and pitch equations of motion.

3.2.3 Foil heave

For wave propulsion, the foils are rigidly fixed to the vessel and the foil motions are, therefore, equivalent to a remote location onboard the vessel. In this way, the foil heave (h) is calculated from the wave-induced hull motions (η_3, η_5) with respect to the waterline at $z = 0$:

$$h = -\sqrt{({x_f}^2 + {d_f}^2)} \sin\big(\tan^{-1}\Big|\frac{d_f}{x_f}\Big| - \eta_5\big) + \eta_3 \tag{3.27}$$

where d_f is the initial foil depth.

3.2.4 Wavy flow

Due to the oscillatory nature of regular gravity waves and assuming deep water, the fluid particles adopt an oscillatory path. The amplitude of the wave-induced fluid particle velocity (u_0, v_0) at the

instantaneous depth of the submerged foils is as follows:

$$u_{0_i} = v_{0_i} = \frac{gk\zeta_0}{\omega} e^{kh} \tag{3.28}$$

The vertical and horizontal components of fluid velocities are evaluated with respect to the horizontal (x-direction) location of the submerged foils ($x_B + x_f$):

$$u_w = u_0 \sin\Big(k(x_B + x_f) \pm \omega t\Big) \tag{3.29}$$

$$v_w = v_0 \cos\Big(k(x_B + x_f) \pm \omega t\Big) \tag{3.30}$$

where x_B is the position of the vessel LCG in the x-direction and x_f is the foil location relative to the LCG.

3.2.5 Flapping foil theory

Numerous methods have been developed to compute the forces acting on an unsteady (flapping) foil. The classical, low order linear methods such as Theodorsen's theory were developed prior to the advent of computers and have since been proven to be surprisingly effective at predicting the forces generated by a flapping foil undergoing small amplitude oscillations in both heave and pitch (Jones and Platzer 1997). However, significant improvements can be gained with the implementation of higher order numerical methods such as unsteady potential flow panel methods, particularly for larger amplitude motions.

Such improvements include the inclusion of section profiles in the foil geometry, and the modelling of vorticity at numerous panels along the chord of the foil and in the nonlinear wake profile, which better captures the effect of shed vortices on the airfoil. Panel methods in 2D can also be extended to 3D surface panel computations whereby the effects of transverse vorticity can be considered and the losses due to finite wing span accounted for. However, panel methods must maintain the Kutta condition, which assumes that the pressure on the upper and lower sides of the foil are equal at the trailing edge. For high Strouhal numbers, flow separation is likely at the trailing edge and unsteady panel methods are unable to account for this effect on the resultant forces. In addition, panel methods are unable to account for viscous effects such as drag and boundary layer effects, and

in most cases an empirical correction is included in the computations to account for these effects.

In order to fully capture the viscous effects including flow separation and vortex shedding along the chord of the foil, Navier-Stokes solvers have been employed to accurately capture the fluid dynamic effects on a flapping foil. However, such solvers are computationally expensive and only practical for the invesitgation of flapping foils for a limited number of cases and oscillations, and are, therefore, not suitable for long duration free running simulations.

An increase in the complexity of the numerical computations directly increases the computation time. Whilst previous numerical analysis on flapping foil wave propulsion incorporated panel methods, linear theories have also been proved adequate for small amplitude motions. Furthermore, since the seakeeping approach assumes small amplitude motions and the aim is to investigate the coupled dynamic response, the numerical method implemented in this research employs the simplified linear theories and future work can be included to improve the numerical modelling of the flapping foils.

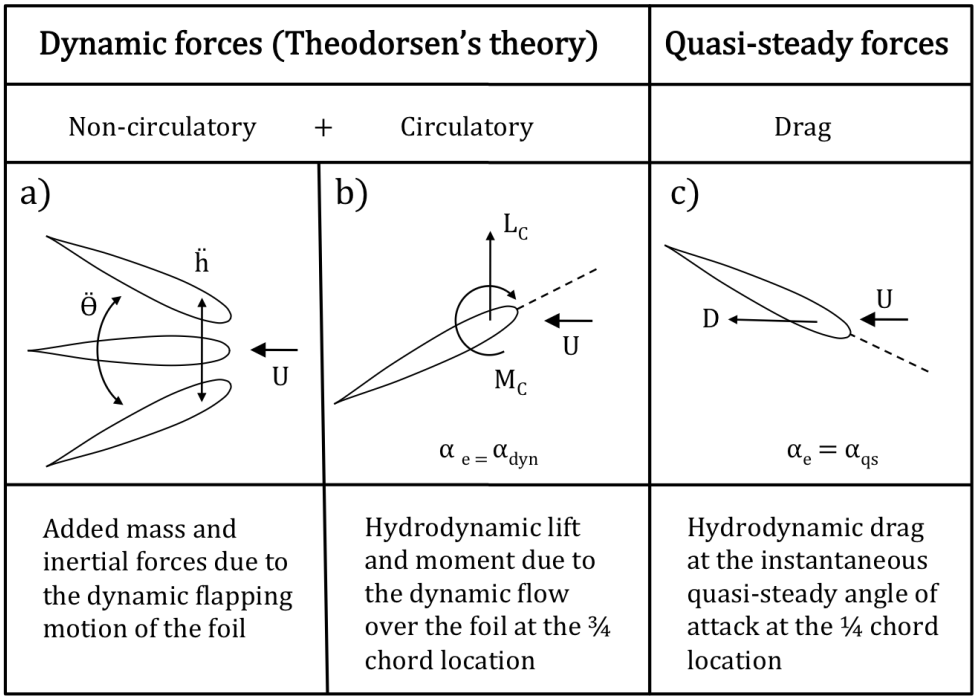

Figure 3.4: Forces acting on submerged flapping foil

The model uses Theodorsen's theory of aerodynamic flutter, which solves the forces acting on a flat plate undergoing harmonic flapping motions (Theodorsen 1935). Figure 3.4 shows how the theory is split into non-circulatory (added mass and inertial) forces (a) and circulatory (hydrodynamic lift)

forces (b). The theory assumes that the flow is always attached, the flow wake is inline with the forward direction, the foil is a flat plate and the pitch angles are small. The theory is unable to account for the hydrodynamic drag.

Relative flow

The relative flow speed in the x-direction at the foil location (u_f) is the sum of the vessel's forward speed (U) and the horizontal velocity component of the wave particle orbital motions (u_w):

$$u_f = U - u_w \tag{3.31}$$

The component of the relative flow speed in the z-direction at the foil location (v_f) is a combination of the foil heave velocity ($\dot{h}$), the vertical component of the wave particle orbital motions (v_w) and the foil pitch:

$$v_f = -\dot{h} + v_w - \frac{c}{4}(1-2a)\dot{\theta} \qquad \text{at the 3/4 chord location}$$

or

$$v_f = -\dot{h} + v_w + \frac{c}{4}(1+2a)\dot{\theta} \qquad \text{at the 1/4 chord location} \tag{3.32}$$

Drag force

The drag force can be estimated from experimental data, which has been compiled for a series of flow conditions and different foil geometries (Sheldahl & Kilmas 1981). For the calculation of the quasi steady drag force, the instantaneous flow speed (V) and the quasi steady angle of attack (α_{qs}) at the quarter chord location are defined as:

$$V = \sqrt{({u_f}^2 + {v_f}^2)} \tag{3.33}$$

$$\alpha_{qs} = tan^{-1}\left(\frac{v_f}{u_f}\right) - \theta \tag{3.34}$$

Therefore, the drag force is calculated with respect to the instantanoeus flow speed and angle of

attack:

$$D = \frac{1}{2}\rho C_D(\alpha_{qs})V^2 cs + D_i \tag{3.35}$$

where D_i is an induced drag due to three dimensional flow effects at the foil tips, and is therefore applicable for foils of finite span. This effect, approximated by Prandtl, is estimated as a proportion of the circulatory lift force (Katz & Plotkin 2001):

$$D_i = \frac{{L_C}^2}{\pi AR} \tag{3.36}$$

where the aspect ratio, AR, is the span to foil area ratio ($AR = \frac{s^2}{s \times c}$).

Non-circulatory forces

The non-circulatory forces include the force associated with accelerating the added mass of the surrounding fluid (abbreviated as NC) and the force associated with the mass of the foil (abbreviated as m). The former considers the relative heave acceleration of the surrounding fluid by substituting the inertial heave acceleration of the foil ($\ddot{h}$) in the original formulations with that of the relative heave acceleration ($\ddot{h}_r = \ddot{h} - \dot{v_f}$):

$$L_{NC} = m_a\left[\ddot{h}_r - \left(\frac{c}{2}\right)a\ddot{\theta} + U\dot{\theta}\right] \tag{3.37}$$

$$M_{NC} = m_a\left(\frac{c}{2}\right)\left[\left(\frac{c}{2}\right)\left(\frac{1}{8} + a^2\right)\ddot{\theta} - a\ddot{h}_r + \left(\frac{1}{2} - a\right)U\dot{\theta}\right] \tag{3.38}$$

where m_a is the added mass of a flat plate ($\pi\rho\left(\frac{c}{2}\right)^2 s$) (Katz & Plotkin 2001).

The inertial forces and moments are obtained by resolving the foil motions in the z-direction (L_m), the x-direction (D_m) and about the pivot point (M_m):

$$L_m = m_f\left[c\left(b_g - \frac{1}{2}(1+a)\right)\left(\ddot{\theta}\cos\theta - \theta^2\sin\theta\right) + \ddot{h}\right] \tag{3.39}$$

$$D_m = m_f\left[c\left(b_g - \frac{1}{2}(1+a)\right)\left(\ddot{\theta}\sin\theta + \theta^2\cos\theta\right)\right] \tag{3.40}$$

$$M_m = m_f c(b_g - b_{piv})\ddot{h}\cos\theta \tag{3.41}$$

where b_g is the centre of gravity of the foil.

Circulatory forces

The circulatory forces consider the hydrodynamic lift force due to the flow over the foil, which applies the small angle approximation ($\sin\alpha \approx \alpha$) and includes Prandtl's lifting line approximation for finite span foils (Katz & Plotkin 2001):

$$L_C = \frac{1}{2}\rho C_L U^2 cs \qquad \text{where} \quad C_L = 2\pi\frac{AR}{AR+2}\alpha_{dyn} \tag{3.42}$$

Assuming small angles, the flow angle relative to the foil chordline (the dynamic or effective angle of attack, α_{dyn}) is resolved at the three-quarter chord location and includes a lift deficiency factor known as Theordorsen's coefficient (C'):

$$\alpha_{dyn} = C'\left[\left(\frac{v_f}{u_f}\right) - \theta\right] \tag{3.43}$$

The lift deficiency factor is a function of the reduced frequency, k_{red}, which describes the nondimensional oscillatory frequency of the flapping foil with respect to the flow velocity, and is defined as:

$$k_{red} = \frac{\omega c}{2U} \tag{3.44}$$

where c is the foil chord.

For small amplitude oscillations, the Theodorsen's function is incorporated to account for the reduction in lift due to the effect of the wake. The function was originally solved for in terms of Bessel functions of the first and second kind. However, an approximation is more applicable, and for a reduced frequency of greater than or equal to 1 it can be shown that the magnitude of the coefficient C' approaches 0.52, shown in Figure 3.5a.

In addition, the unsteady effect of a flapping foil induces a phase difference between the foil motions and the circulatory lift force. The linear theory developed by Theodorsen includes this unsteady effect on the phase, as shown in Figure 3.5b. The current model assumes a quasi steady

response ($\angle C' \approx 0$) with regard to the phase between the flapping motions and the circulatory lift force. For wave propulsion, a reduced frequency of greater than 1 is expected and the phase effect of the circulatory lift force is assumed to be small in comparison the phase effect of the non-circulatory terms.

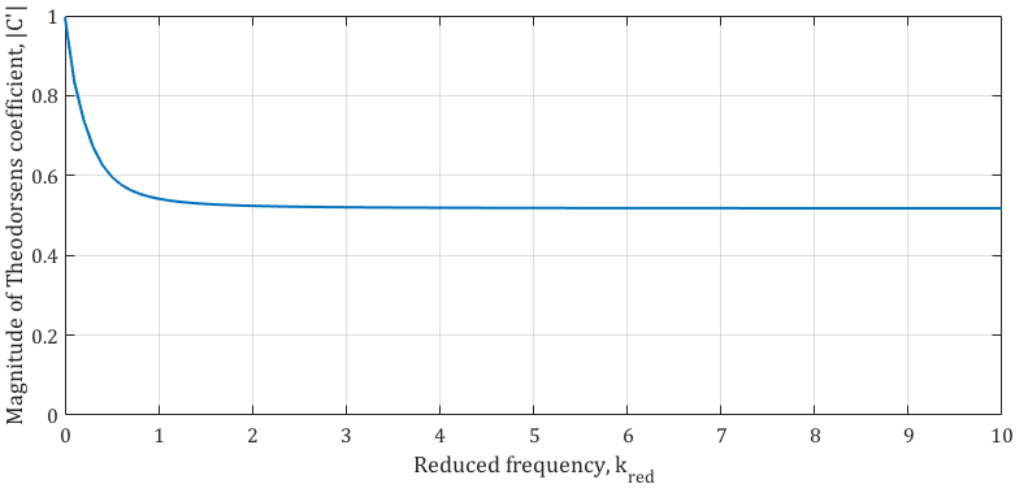

(a) Magnitude

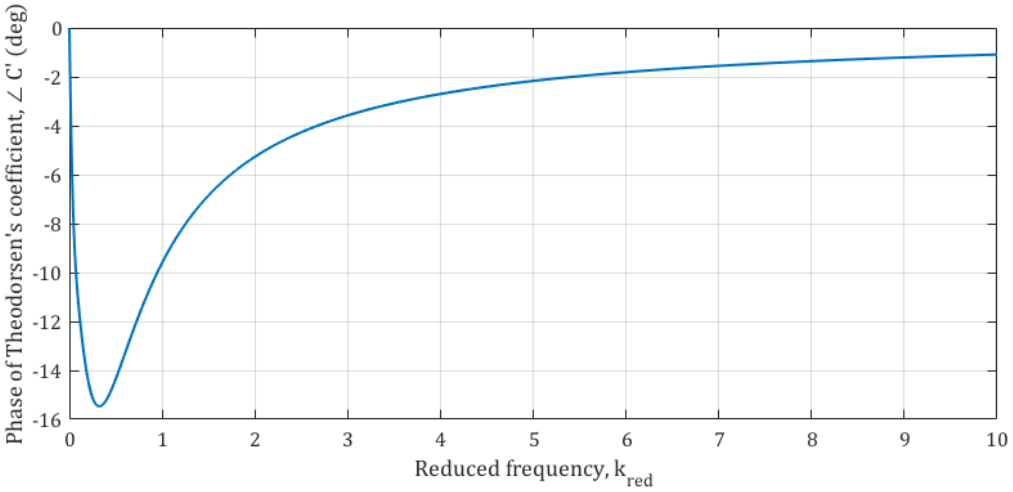

(b) Phase angle

Figure 3.5: Theodorsens coefficient as a function of the reduced frequency of a flapping foil

Substituting the dynamic angle of attack into Equ. 3.42 results in the following hydrodynamic lift force acting on the foil, which includes an approximation for finite span:

$$L_C = -\frac{AR}{AR+2}\pi\rho U c s C' \left[\dot{h}_r + \frac{c}{4}(1-2a)\dot{\theta} + U\theta\right] \tag{3.45}$$

and the moment about the pivot point due to the hydrodynamic lift force acting at the quarter chord location:

$$M_C = L_C \times \left(\frac{c}{4}\right)(2a+1) \tag{3.46}$$

The main limitations of this method are that it is only applicable for small amplitude oscillations of flat plates where there is no chordwise flow separation, and that it is incapable of resolving the drag forces on a flapping foil.

Resultant forces

The flapping foil pitch is passive and constrained by a rotational spring, and this needs to be factored in when considering foil pitch motions. The foil pitch is therefore solved using the following equation of motion:

$$\begin{aligned} M_\theta &= M_{NC} + M_C - D\sin(\alpha_{qs} - \beta)\left(\frac{c}{4}\right)(2a+1) \\ &= I_f\ddot{\theta} + k_\theta\theta + M_m \end{aligned} \tag{3.47}$$

where M_θ is the hydrodynamic moment, I_f is the rotational inertia of the foil, k_θ is the spring constant, and β is the sum of the vessel pitch and foil pitch ($\beta = \theta + \eta_5$). The resultant hydrodynamic and inertial lift forces (L_z) are resolved in the z-direction, and the corresponding thrust/drag forces (T_x) are resolved in the x-direction as follows:

$$L_z = (L_{NC} + L_C + L_m)\cos\beta + D_m\sin\beta + D\sin(\alpha_{qs} - \beta) \tag{3.48}$$

$$T_x = (L_{NC} + L_C + L_m)\sin\beta + D_m\cos\beta - D\cos(\alpha_{qs} + \beta) \tag{3.49}$$

The resultant vertical forces (${F_{3_i}}^F$) and moments acting on the vessel (${F_{5_i}}^F$) are the sum of the forces acting on each submerged flapping foil:

$${F_{3_i}}^F = \sum L_{z_i} \tag{3.50}$$

$$F_{5_i}{}^F = \sum x_{f_i} L_{z_i} \tag{3.51}$$

3.2.6 Wave propulsion

The surge force in the x-direction (F_1) is the combination of the flapping foil thrust (T_x) and the wave-induced surge force (F_ζ). The inertial and hydrodynamic damping forces are equal to the external surge force applied to the vessel and can, therefore, be solved to obtain the instantaneous forward speed ($\dot{\eta_1} = U$):

$$F_1 = \sum F_x = T_x + F_\zeta = (M_B + A_{11})\ddot{\eta}_1 + B_{11}\dot{\eta}_1 \tag{3.52}$$

where the added mass term, A_{11}, is regarded as neglible and the damping term, B_{11} is given as the derivative of the vessel's total resistance:

$B_{11} = \frac{dR_T}{d\dot{\eta}_1}$

A component of the wave-induced surge force, known as the Froude-Krylov surge force (F_ζ), is calculated by integrating the incident wave pressure field over the length of the vessel (Hashimoto et al. 2016):

$$F_\zeta = \mu_d \rho g k \zeta_0 \int_L A_\xi e^{-kd_\xi/2} \sin(kX_\xi) d\xi \tag{3.53}$$

where A_ξ is the hull sectional area, X_ξ is the longitudinal distance of the hull section from the incident wave trough and μ_d is an empirical correction to account for the absence of diffraction effects (discussed in more detail in the Appendix B).

The total resistance of the vessel moving with forward speed in waves is evaluated as the sum of the resistance of the vessel in still water (R_{SW}), the added resistance due to the waves (R_{AW}) and an additional resistance due to appendages (R_{APP}):

$$R_T = R_{SW} + R_{AW} + R_{APP} \tag{3.54}$$

The bare hull resistance in still water (R_{SW}) can be estimated using the ITTC'57 empirical formula and a form factor (ITTC 1957). As the Froude number of a wave-propelled boat is relatively

low, at approximately Fn = 0.1, it is possible to assume that the effect of wave making resistance is small in comparison to the skin friction resistance. For the purposes of this research, it is assumed that the contribution of wave making resistance is negligble.

A vessel moving with forward speed in a seaway imparts energy into the surrounding wave field due to the motions induced by the incident waves. Therefore, an added resistance (R_{AW}) due to the waves is exerted on the moving vessel. However, experimental analysis by Journee (1976) shows that the effect in following waves is minimal and, therefore, the following theory for added resistance in waves is only considered applicable for head waves.

The main methods that apply strip theory include the momentum and energy method, the integrated pressure method and the radiated energy method (Arribas 2007). The momentum and energy method is considered the most robust solution due to it's ability to accurately capture the peak resistance, and its stability in short waves (large $\omega_e\sqrt{L/\lambda}$) (Arribas 2007).

The following momentum and energy method developed by Joosen (1966) also includes additional terms to account for the presence of submerged foils:

$$R_{AW} = \frac{1}{2}\frac{{\omega_e}^3}{g}\big((B_{33} + \frac{F_L}{U})\eta_3{}^2 + (B_{55} + \frac{F_L {x_f}^2}{U})\eta_5{}^2 \\ -2(B_{35} + \frac{F_L x_f}{U})\eta_3\eta_5\big) \tag{3.55}$$

where $F_L = \pi\rho C' U^2 cs(\frac{AR}{AR+2})$ is the simplified Prandtl lifting line force for an unsteady flapping foil (Scalvonous & Borgen 2004).

The appendage resistance due to additional submerged struts, such as the mounts for the flapping foils, is evaluated as a viscous drag force:

$$R_{APP} = \frac{1}{2}\rho C_{D_A} U^2 A_{APP} \tag{3.56}$$

The drag coefficient of the struts (C_{D_A}) is estimated using the Hoener approximation (Hoener 1965):

$$C_{D_A} = 2C_F[1 + 2\frac{t_s}{c_s} + 60\frac{{t_s}^4}{c_s}] \tag{3.57}$$

where C_F is the ITTC '57 friction coefficient of the strut, t_s is the strut thickness and c_s is the strut chord.

3.2.7 Wave energy recovery

Figure 3.6 a) shows the free body diagram that represents a submerged foil coupled to a surface vessel via a spring and damper. For energy recovery, the submerged foil is free to heave relative to the vessel, and therefore the foil can perform work against the vessel and vice versa.

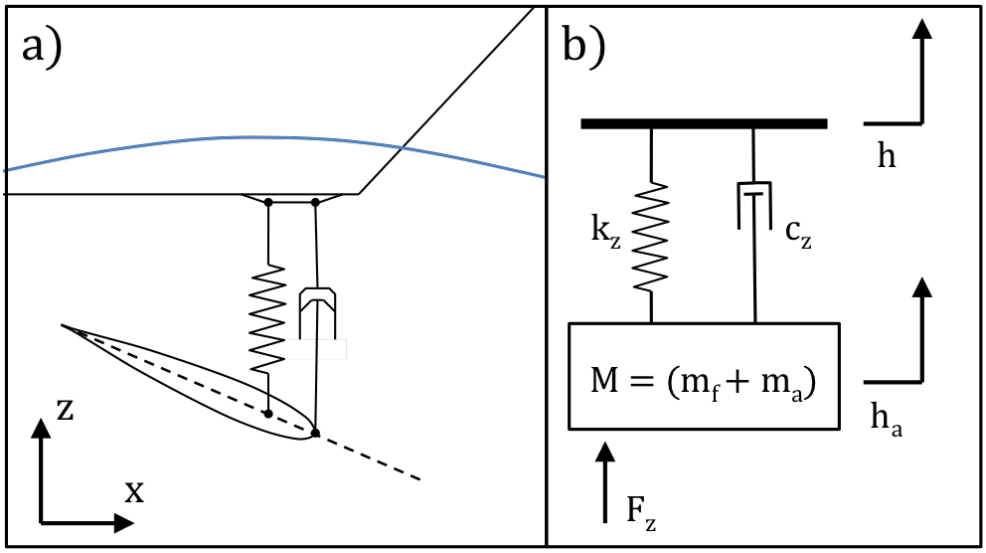

Figure 3.6: Flapping foil wave energy recovery free body diagram

The relative heave of the foil is solved by applying the same methods that are described in Section 3.2.2 to 3.2.7 with an additional equation of motion to address energy recovery. The equation of motion for energy recovery is defined as follows, with the excitation forces on the right hand side:

$$(m_f + m_a)\ddot{h}_a + c_z\dot{h}_a + k_z h_a = L_z + c_z\dot{h} + k_z h \tag{3.58}$$

where h_a is the absolute heave response of the foil, c_z is the damping constant that is representative of the damping applied by a PTO generator and by friction, k_z is the spring constant and L_z is the hydrodynamic excitation force acting on the foil. This arrangement is regarded as a 'base excited' mass spring damper (see Figure 3.6 b)), and with the substitution of the absolute heave, it is possible

to solve for the relative heave motion of the foil:

$$\big(m_f + m_a\big)\ddot{h}_e + c_z\dot{h}_e + k_z h_e = L_z - \big(m_f + m_a\big)\ddot{h} \tag{3.59}$$

where h_e is the foil effective heave, which is the difference between the wave-induced heave at the remote location of the flapping foil (h) and the absolute heave (h_a) of the foil with respect to the global frame of reference:

$$h_e = h_a - h \tag{3.60}$$

This relative motion is the source of the kinetic energy which can be absorbed by a PTO unit, and an idealized solution for the power absorption can be calculated as the work done against the damper:

$$P = L_z\dot{h}_e = c_z\dot{h}_e^2 \tag{3.61}$$

The wave energy recovery theory does not consider the losses associated with the conversion of kinetic energy into useful power, such as electrical. Experimental and numerical analysis has been included in subsequent chapters to investigate the complete wave energy conversion into electrical power, and the method for electromechanical energy conversion is described in the following section.

3.3 Hybrid numerical modelling

The numerical model aims to simulate the coupled dynamics of a vessel and submerged flapping foils, jointly referred to as the 'system'. Both the vessel and foil motions are defined by second order ordinary differential equations (ODEs) and, therefore, the system comprises of at least two ODEs in series, of which each ODE is referred to as a 'subsystem'. The method to solve this system of differential equations is complex due to the indirect interdependency of each subsystem. This means that the state variables of a subsystem are not directly coupled with the equations of another. Consequently, a hybrid method is derived, which can accommodate the solution of each subsystem

whilst ensuring that the subsystems remain coupled. A simplified flow chart of the numerical model is shown in Figure 3.7.

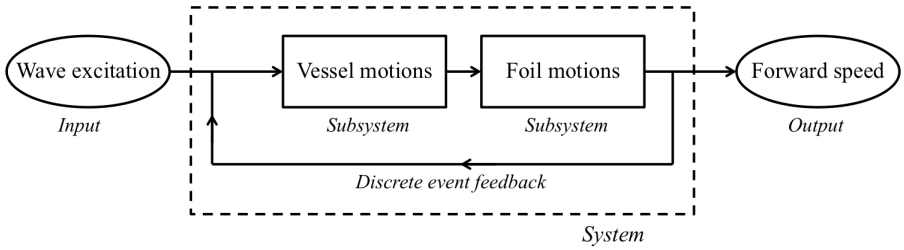

Figure 3.7: Example of the hybrid approach for free running wave propulsion

A hybrid discrete-continuous technique is applied to solve the response of the coupled dynamics in the time domain. The solution is achieved by the implementation of synchronous discrete events at a constant time step within a continuous-time framework. The discrete events are categorised as either changes in the state variables or as instantaneous forces, and the continuous-time framework refers to the continuous solution of the ODEs that define the dynamic response of the subsystems. Therefore, the coupled response of the entire system is simulated by considering the effect of one subsystem on another as a discrete event. For example, a change in the forward speed of the vessel or the pitch of the foil is regarded as a discrete event that effects the overall response of the system.

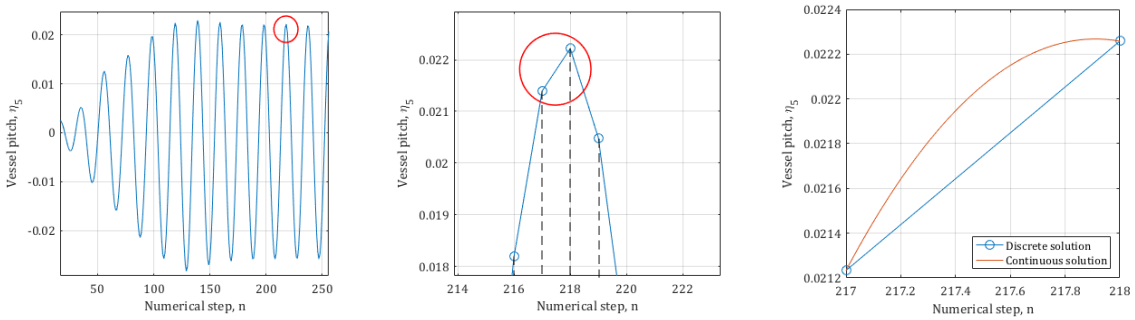

a) Harmonic reponse b) Discrete events c) Continuous solution

Figure 3.8: Detail of the hybrid discrete-continuous model with synchronous discrete events at time steps of t_n

Figure 3.8 shows an example of the numerical solution for the vessel pitch response. The solution of each subsystem forms a discrete event that effects the response of following subsystems. For example, at each instance of time (t_n) the hull motions are evaluated with respect to the resultant forces acting on the submerged foils at the previous time step, t_{n-1}. The ODEs for the vessel and

foil motions are solved by implementing a multi-step initial value Runge-Kutta algorithm, known as ODE45 (MatLaB 2017). In this case, the solver uses a variable time step, τ, with a time interval equal to the discrete time step, t_n. The initial values for each solution are equal to the state variables from the previous discrete time step, t_{n-1}. This hybrid method allows for the coupling of complex subsystems which otherwise cannot be solved simultaneously.

The hybrid method can effectively couple the various subsystems to predict the instantaneous response and model the transient effect of an accelerating free running model. However, the numerical model does not fully capture the transient effects. In particular, transient effects such as fluid memory effects in the radiation and damping forces are not accounted for in the hydrid time domain model. Most seakeeping simulation tools implement the Cummins equation to model the fluid memory effect in the time domain, which is an integro-differential solution that involves convolution terms. However, this solution involves an onerous process which can be simplified using alternative methods, such as frequency domain regression (similar to the current method but including fluid memory effects), impulse response curve fitting and realization theory (Taghipour et al. 2008).

The hybrid seakeeping method described in this chapter is, therefore, limited to modelling only a dynamic system with no fluid dynamic effects. However, within the numerical framework described in the following section, these effects could be accounted for in future analysis using the methods detailed by Taghipour et al. (2008).

3.3.1 Numerical algorithm

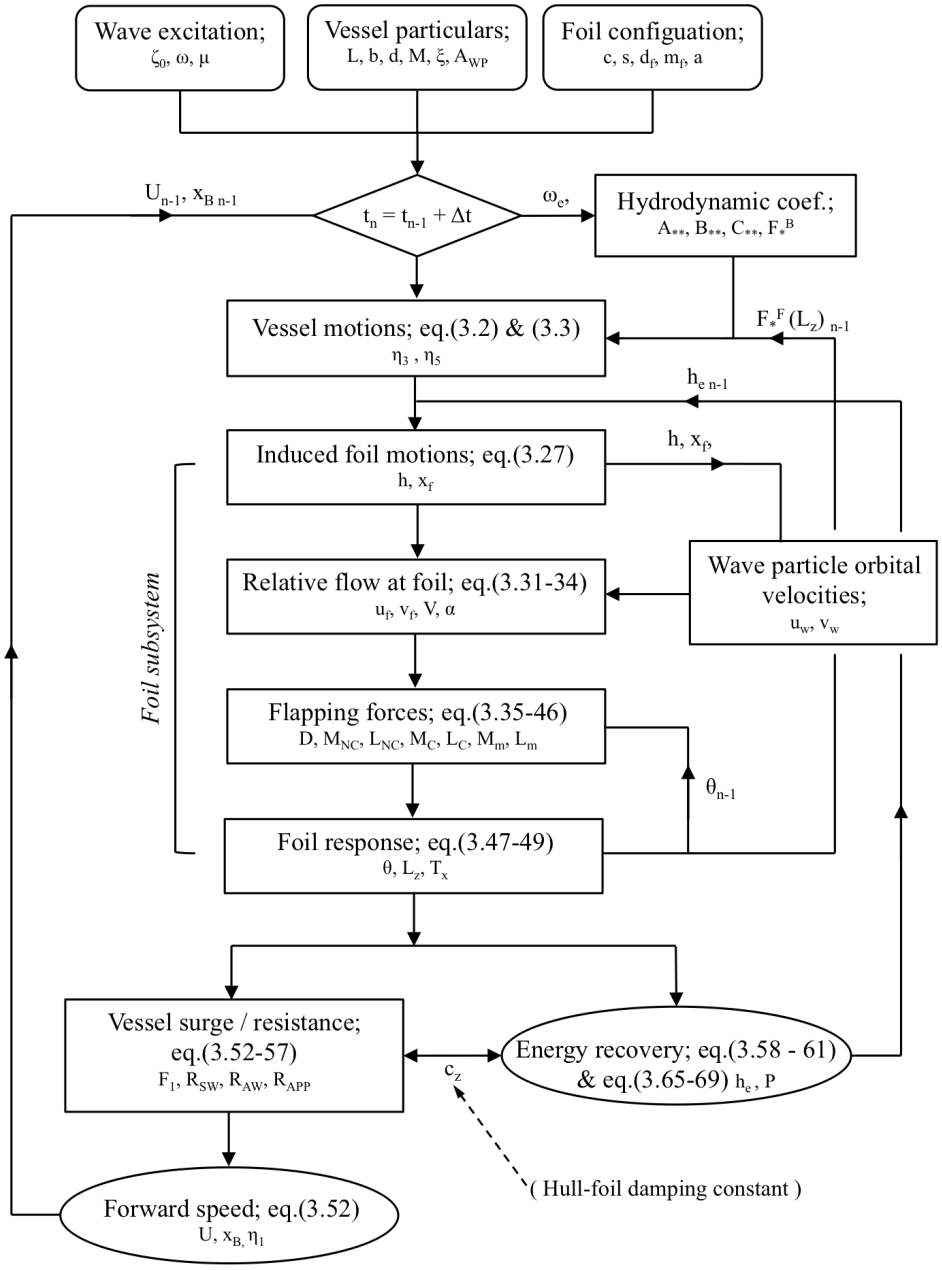

Figure 3.9: Flowchart of the numerical model for wave propulsion and energy recovery

Figure 3.9 shows the flowchart for the numerical model, which includes both wave propulsion and energy recovery. The input parameters for the wave characteristics, the vessel particulars and the

foil particulars are predefined using a graphical user interface (GUI), shown in Figure 3.10. It is possible to import the hydrodynamic sectional coefficients for any hull shape. The algorithm has been setup to simulate the response of the system for a range of wave frequencies simultaneously.

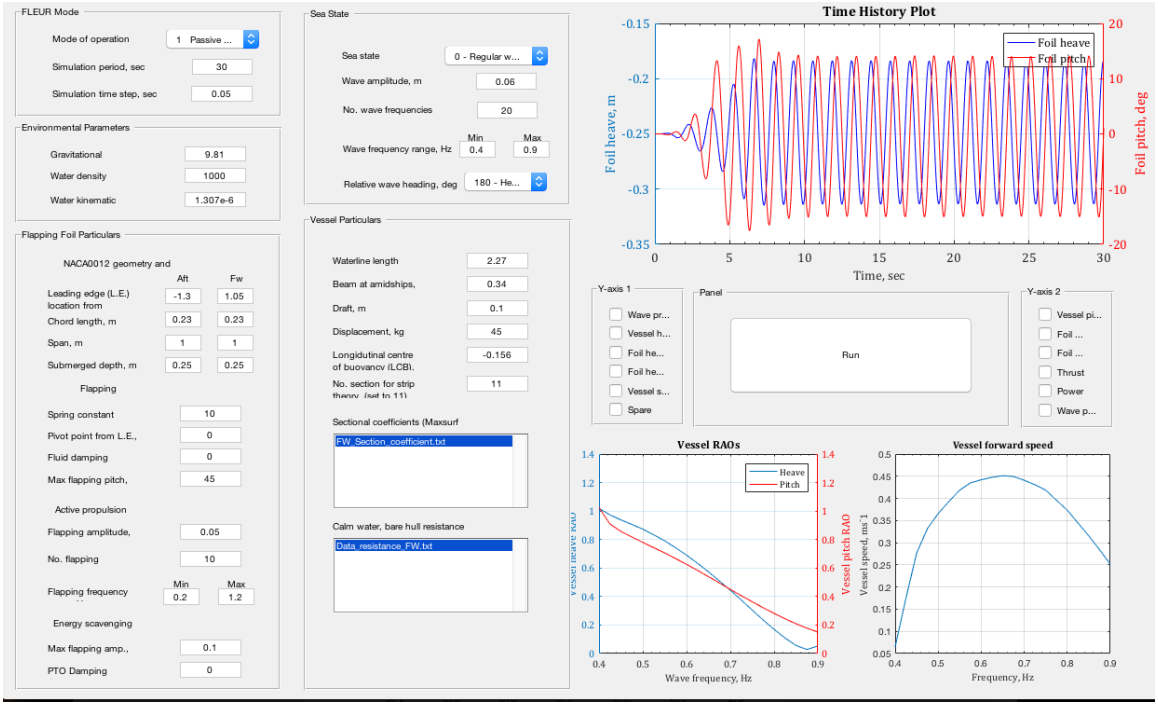

Figure 3.10: Numerical model MATLAB graphical user interface (GUI) for all simulations

The simulation is initiated with a ramp increase in the wave elevation from zero to the predefined wave amplitude. Within each time step, the algorithm loops through each of the subroutines detailed in Figure 3.9. With this process, it is possible to predict the vessel forward speed and estimate the power generated using the PMTLG method. The key elements of the model are: the effect of the forward speed on the wave encountered frequency (Doppler effect), which is considered at the beginning of each time step; the vessel response, i.e heave, pitch and surge; the pitch response of the submerged flapping foils; and the power take off. These are detailed in the following sections.

Doppler effect

As the numerical model is setup to simulate a free running scenario, the spatial term of the wave profile in Equation 3.1 is required to model the vessel at the correct location in the wave with respect

to time. Due to the forward speed of the vessel, there is an encountered wave frequency (ω_e), which defines the instantaneous wave profile, and is a function of the vessel's forward speed (U or $\dot{\eta}_1$):

$$\omega_e = |\omega - kU\cos\mu| \tag{3.62}$$

where μ is the vessel heading and defined as 0 for following waves and π for head waves. Regardless of the vessel heading, positive forward speed results in the vessel moving away from the origin in the positive x-direction. To simulate head waves, the wave propagates in the negative x-direction and, for following waves, the wave propagates in the positive x-direction. As the encountered wave frequency is a function of the vessel speed (Doppler effect) it is necessary to evaluate the encountered wave profile at each time step. This is achieved by solving the angular position of the vessel on the wave (ϑ) in space and time at the previous time-step:

$$\vartheta_{n-1} = kx_{n-1} \pm \omega t_{n-1} \tag{3.63}$$

where n is the numerical step and $\vartheta = 0$ for $n = 1$. The encountered wave profile for the next time-step (ζ_{e_n}) is then computed to include the Doppler effect by calculating the change in the observed wave profile (encountered wave) relative to the moving vessel within the time interval of one time step (Δt):

$$\zeta_{e_n} = \zeta_0 \sin(\delta) \tag{3.64}$$

where $\delta = \vartheta_{n-1} \pm \omega_e \Delta t$

Vessel motions

The strip theory makes use of the conformal mapping method, discussed in Section 3.2.3, to evaluate the sectional added mass and damping coefficients. This technique is implemented in a ship motion software tool called Maxsurf Motions Advanced (Bentley Software 2014). The three dimensional hull form is split into 11 equal sections (see Figure 3.3), which are located at a distance, ξ, from the LCG.

Since the hydrodynamic coefficients are frequency dependent, a look up table of sectional added mass and damping coefficients is exported from Maxsurf. Each coefficient relates to a particular

frequency, and the quantity and range of frequencies is specified by the user (in this case, 50 look up points have been exported ranging from a frequency of 0.6 $rads^{-1}$ to 13.6 $rads^{-1}$). The same look up table method is used to determine the sectional Froude-Krilov and diffraction forces. The numerical model interpolates the sectional coefficients and forces from the conformal mapping results with respect to the instantaneous encountered wave frequency. In this way, the vessel pitch and heave are evaluated with the Doppler effect taken into account. Lastly, the equations of motion for the vessel heave and pitch are solved using the Runge-Kutta method (Dormand & Prince 1980).

Foil motions

As previously mentioned in Chapter 3, the unsteady foil theory of Theodorsen does not account for the drag force acting on the foil. Therefore, the drag force is obtained using a lookup table of drag coefficients for a NACA0012 foil, which is compiled from the data published by Sheldahl and Kilmas (1981). The drag coefficient is interpolated at the quasi steady angle of attack, α_{qs}, and a Reynolds number of 3.6×10^5, which is at the higher spectrum of the flow characteristic noted at this scale.

The hydrodynamic and inertial forces acting on the foil result in a moment that acts about the foil pivot point. As the foil is spring loaded, the resultant foil pitch motion is defined by an ordinary differential equation (Equation 3.30), which is solved using the Runge-Kutta method. Therefore, foil pitch is solved at each time step, and the resultant forces are accounted for with respect to the vessel motion, forward speed and energy recovery.

The change in foil heave relative to the hull (h_e) is accounted for in the calculation of the wave-induced foil motions by the simple addition of the foil heave kinematics at each time step, and is shown as a feedback loop in Figure 3.9.

Electromechanical energy conversion

The electromechanical energy conversion is achieved by using a permanent magnet tubular linear generator (PMTLG), which works on the same principles as a DC rotary generator but is driven by translational components. The principle of energy conversion is based on Faraday's law of electromagnetic induction whereby an electromagnetic force (emf) is induced in nearby conductors due to the dynamic interaction with a magnetic field. For a PMTLG, the magnetic field is generated by a permanent magnet rod that moves within a stator, which houses a series of wire coils, as shown in

Figure 3.11.

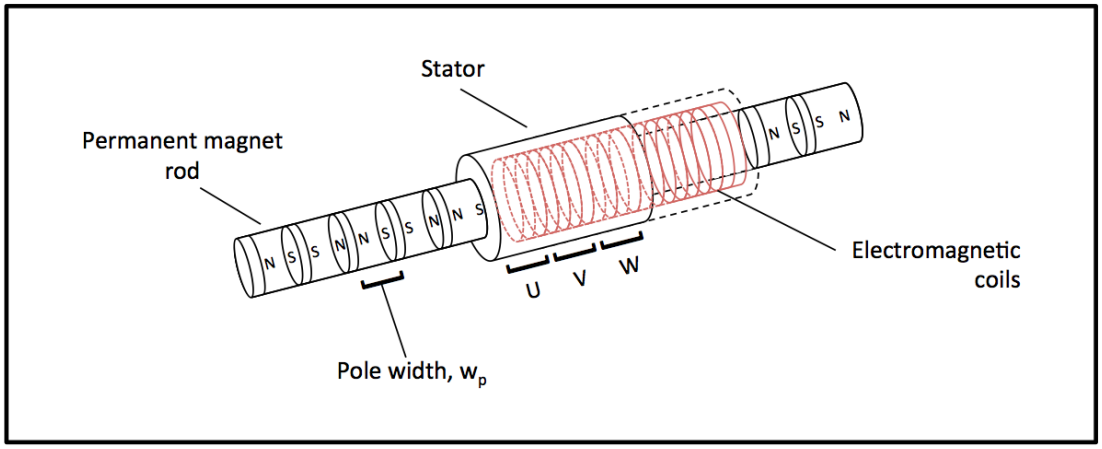

Figure 3.11: Schematic of a PMTLG, with three electrical phases; U, V and W

The induced emf (e) is derived from the Faraday-Maxwell electromagnetic laws. Compared to a permanent magnet synchronous generator, the modelling of a PMTLG is more complex as the motion of the permanent magnet rod is not constant and, therefore, a different approach is required. It is possible to model the PMTLG using finite element methods as demonstrated by Zheng et al. (2015), but an analytical method developed by Thorburn and Leijon (2007) has been shown to achieve reasonable results. Faraday's law states that the induced emf is equivalent to the rate of change of magnetic flux. By assuming the input motion is sinusoidal, Thorburn and Leijon (2007) have derived a model for the magnetic flux and therefore the induced emf for a linear permanent magnet generator. As the induced emf is linearly proportional to the electromagnetic parameters of the linear generator and the motion of the permanet magnet rod, an emf constant (e_c) can be introduced to simplify the problem. The emf constant is defined as the amplitude of the induced emf with respect to the amplitude of the permanent magnet rod velocity. The induced emf per phase (e_{ph}) is proportional to the relative velocity of the permanent magnet rod or, in this case, the relative heave velocity of the submerged foil:

$$e_{ph}(t) = e_c \dot{h}_e \cos\left((\frac{2\pi}{w_p})h_e - \delta_e\right) \tag{3.65}$$

where w_p is the pole width of the permanent magnet rod, which consists of several permanent magnets mounted inline with the poles opposing each other, as shown in Figure 3.11. Assuming a multiple phase linear generator, δ_e is the equivalent phase angle between each electrical circuit or

phase.

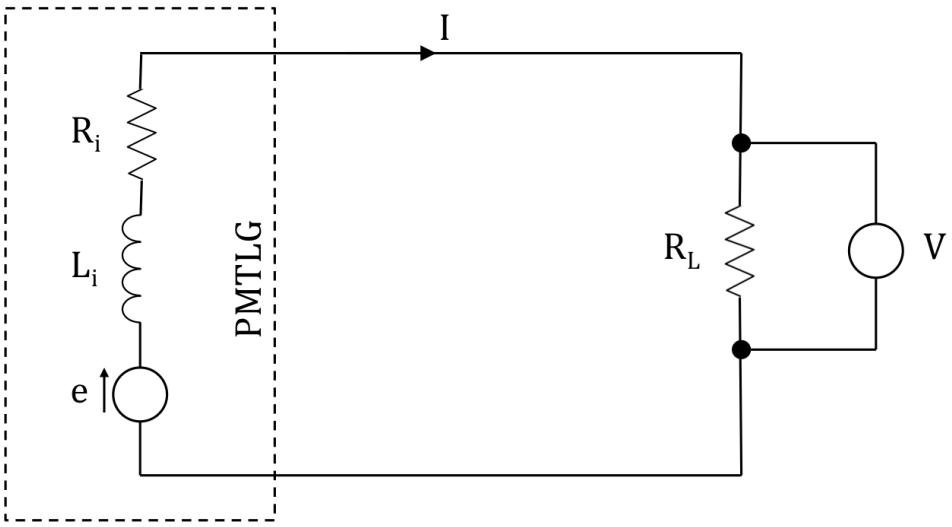

Figure 3.12: Circuit diagram of electrical power take-off using a PMTLG

Figure 3.12 shows the electrical circuit diagram of the PTO setup. The circuit consists of the induced emf (e), a load resistance (R_L), the internal resistance (R_i) and the inductance (L_i) of the linear generator. The phase voltage delivered to the terminal across the load resistor is given as:

$$V_{ph}(t) = e_{ph}(t) - R_i I - L_i \frac{dI}{dt} \tag{3.66}$$

where I is the current, and the equivalent electrical power for a multiple phase generator is:

$$P = \sum IV_{ph} = \sum \frac{{V_{ph}}^2}{R_L} \tag{3.67}$$

The induced emf generates an opposing force that acts to dampen the motion of the permanent magnetic rod, which is equivalent to the power generated:

$$F_M = \frac{P}{\dot{h}_e \eta_g} \tag{3.68}$$

where η_g is the efficiency of the generator. This force can be considered as the damping force applied by the PTO unit and any further damping can be attributed to friction in the system. Therefore,

the complete equation of motion for the relative foil heave which includes the effect of a PTO unit can be written as:

$$\big(m_f + m_a\big)\ddot{h}_e + \big(c_f + \frac{\big(e_c \cos(\frac{2\pi}{w_p} h_e - \delta_e\big)^2}{\eta_g R_L}\big)\dot{h}_e + k_z h_e = L_z - \big(m_f + m_a\big)\ddot{h} \tag{3.69}$$

where c_f is the frictional damping constant.

3.3.2 Assumptions and limitations

The assumptions and limitations of linear wave theory, strip theory and Theodorsens theory apply. Therefore, it is necessary to adhere to the following criteria:

1. Harmonic motions:

   The equations of motions for both the vessel and foil motions are representative the harmonic response of a force mass spring damper system, which oscillates at the encountered wave frequency.

2. Small foil pitch angles ($\theta < \frac{\pi}{4}$)

   The numerical model does not account for dynamic stall or hysteresis in the lift response of the flapping foils. Therefore, caution is required for large pitch where the effect of dynamic stall and lift hysteresis becomes a dominant effect.

3. Small vessel motions

   The prediction of vessel motions is limited by the strip theory method implemented in the numerical model, which assumes small vessel motions. For validation purposes, experiments should aim to maximise the response whilst remaining within the limit of the strip theory.

4. Low Froude numbers ($Fn < 0.4$)

   This assumptions is easily satisfied for free running wave propelled vessels, which operate at low forward speeds.

5. Negligble fluid interaction effects between the foils and/or hull

   This is a limitation in the numerical modelling whereby the combined linear theories can only capture the kinematics of the coupled response and cannot model the hydrodynamic interactions between the foils and/or hull. The impact of this is discussed in Chapter 6.

6. Deep water (Water depth $\gg \lambda$)

Reynolds number effect

Viscous effects from a change in Reynolds number will affect the calm water resistance of the hull and the hydrodynamic forces acting on the foils. The latter affect on the foil lift and drag is not considered in this analysis, which assumes a constant Reynolds number. Therefore, caution is required when considering for viscous effects on the foil response at different scales, for example laminar to turbulent boundary layers, stall angles and flow separation.

Free surface effect

The effect of the free surface is neglected in the current method on the basis that previous research has shown that the effect is minimal for depth Froude numbers less than 1 (Hough and Moran 1969).

3.3.3 Sensitivity study

A reduced order sensitivity study of the numerical model has been conducted where only the key numerical parameters are assessed. Numerical parameters which have not been assessed include the number of hull sections, the frequency increment for the hydrodynamic coefficient look up table and the angle of attack increment for the foil drag coefficient look up table. The number of hull sections are selected to adequately capture the hull shape over the length of the vessel, and ample increments are implemented for the hydrodynamic and drag coefficient look up tables. The key numerical parameters which require investigation include the numerical time-step, numerical ramp and simulation period, and the following analysis of these parameters proves that the numerical method is suitably robust for this application.

Time-step

The numerical time step or time increment, Δt, is a critical parameter that requires a compromise between accuracy and simulation run time. A comparatively small time step of 1000th of a second ($\Delta t = 0.001$) was set as a reference for which it was assumed that the model achieves acceptable convergence.

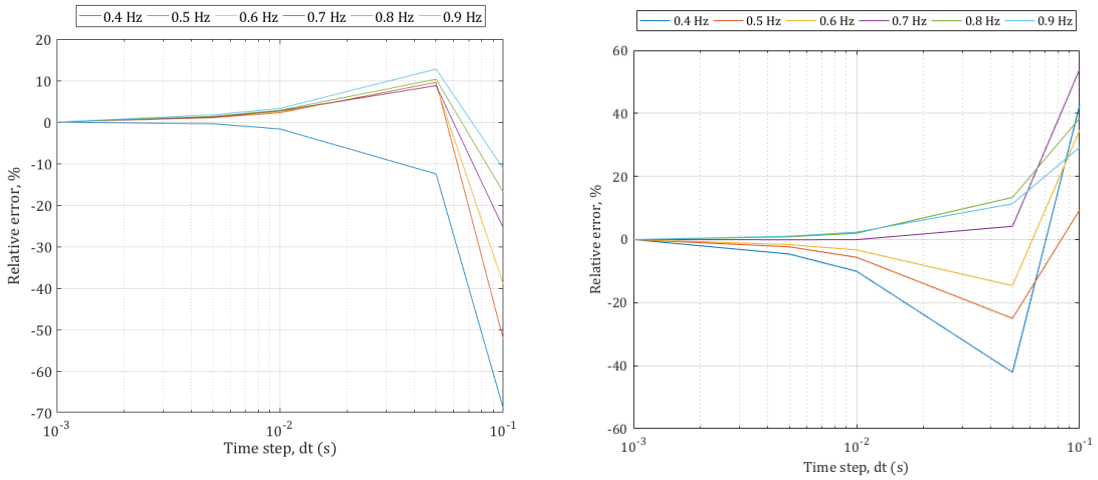

a) Wave propulsion

b) Energy recovery

Figure 3.13: Time-step verification

Figure 3.13 shows the convergence of the numerical model for each mode with decreasing time step. Significant errors are incurred at time increments greater that than 0.05 seconds, and therefore a time step of 0.01 seconds is selected, which achieves a manageable computation time and an acceptable relative error of less than 5% for the entire wave frequency range. This analysis proves that the method of solving a system of ordinary equations with a discrete difference method is numerically stable.

Numerical ramp and simulation period

As with the time step, a suitable simulation period is required to ensure convergence towards a steady state whilst maintaining a reasonably low run time. Figure 3.14 shows that, for all cases, the numerical ramp has a significant effect on the convergence time, but does not affect the overall result. For this scale, the results show that a simulation period of greater than 20 seconds and a

ramp factor of 5 ensures that simulation converges to a steady state. The transient acceleration period is also frequency dependent, and therefore simulations must be run at a simulation period suitable for the lowest frequency.

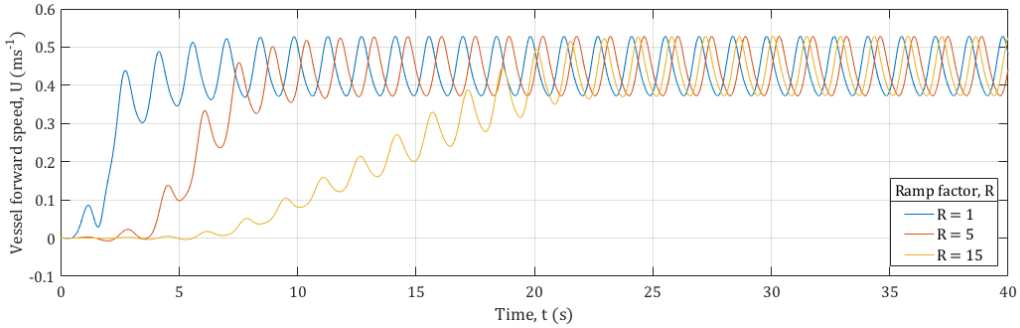

(a) Wave propulsion

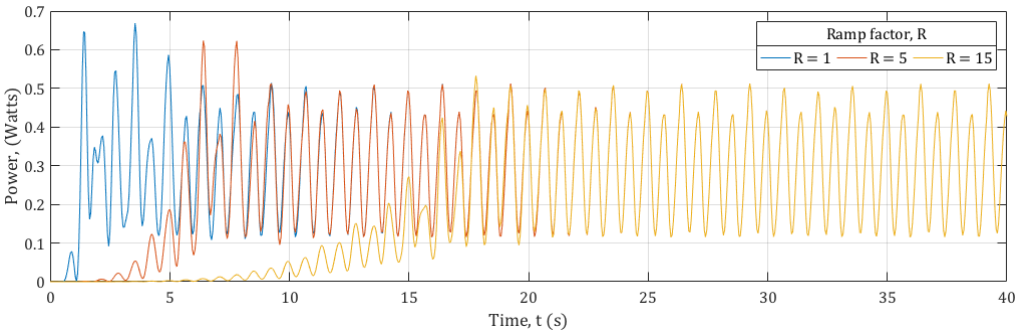

(b) Energy recovery

Figure 3.14: Simulation period verification for all numerical case studies

3.4 Summary

The sensitivity study shows that the numerical model achieves suitable convergence with respect to important numerical parameters and is, therefore, suitable for free running simulations.

With a defined geometry for the vessel and foils, a given sea state and a predefined forward speed, it is possible to solve for wave propulsion and/or energy recovery. The problem is made more complex when the forward speed is unknown, and, to predict the forward speed, an iterative or free running time domain process is required. Therefore, a hybrid numerical approach has been implemented which can account for the Doppler effect, the effect of the foils on the vessel and vice versa. The numerical method also accommodates the prediction of wave energy recovery, which is

based on a base excited mass spring damper model, and incorporates PTO with the modelling of a permanent magnet tubular linear generator (PMTLG).

The numerical model requires that the wave-induced motions are harmonic and relatively small; a result of the applied linear theories. Additional limitations are associated with the absence of certain nonlinear effects. In particular, the numerical model does not completely capture the unsteady lift force acting on the foil at high pitch angles. The linear theory does not account for dynamic stall at high pitch angles, which occurs when a large vortex is shed at the leading edge and rolls up the back face of the foil. A flapping foil is also subject to dynamic effects, such as hysteresis, which is not accounted for in the linear theory. Furthermore, the method neglects the added resistance due to following waves. Whilst these effects are important, it is shown in the following chapter that they do not, for the most part, have a significant impact on the overall coupled dynamic response.

Chapter 4

Free running and restrained towing tank experiments

The aim of the experimental analysis is to validate the numerical model, to provide a proof of concept for wave energy recovery, and also to further investigate the physical response of the coupled dynamics.

The numerical model consists of two main dynamic subsystems; the vessel motions and the foil motions. Both aspects require separate validation to be confident that the simulation accurately captures the individual physical responses. Furthermore, as the subsystems are coupled, it is necessary to change a dependent variable such as the foil location to validate the physical response of the coupled system. To ensure that the numerical model can capture the physical response in a range of differing environments and scenarios, comparisons need to be made with respect to a changing independent variable such as the wave profile and vessel heading.

The experiments were conducted using two towing tank methods; restrained, i.e. fixed to the carriage, and free running. The experimental analysis covers the following areas; the overall response (i.e. wave propulsion or energy recovery), the vessel motions and the foil motions. The experiments have been conducted for a range of wave parameters with foils mounted at both the bow and stern. Three different experiments have been carried out to support this research:

1. Preliminary experiments (fixed to the carriage) - to investigate the suitability of the experimental platform, validate the fixed speed strip theory method, and assess the mechanisms for wave propulsion and energy recovery;

2. Wave propulsion (free running) - to validate the free running numerical model for wave propulsion including the vessel and foil motions, and to investigate the coupled dynamic response with a change in the foil location for head and following waves;

3. Wave energy recovery (restrained) - to investigate the feasibility of a wave energy recovery device utilizing submerged flapping foils, to validate the wave energy recovery part of the numerical modelling and to assess the coupled effect of the foils on the vessel motions.

4.1 Experimental setup

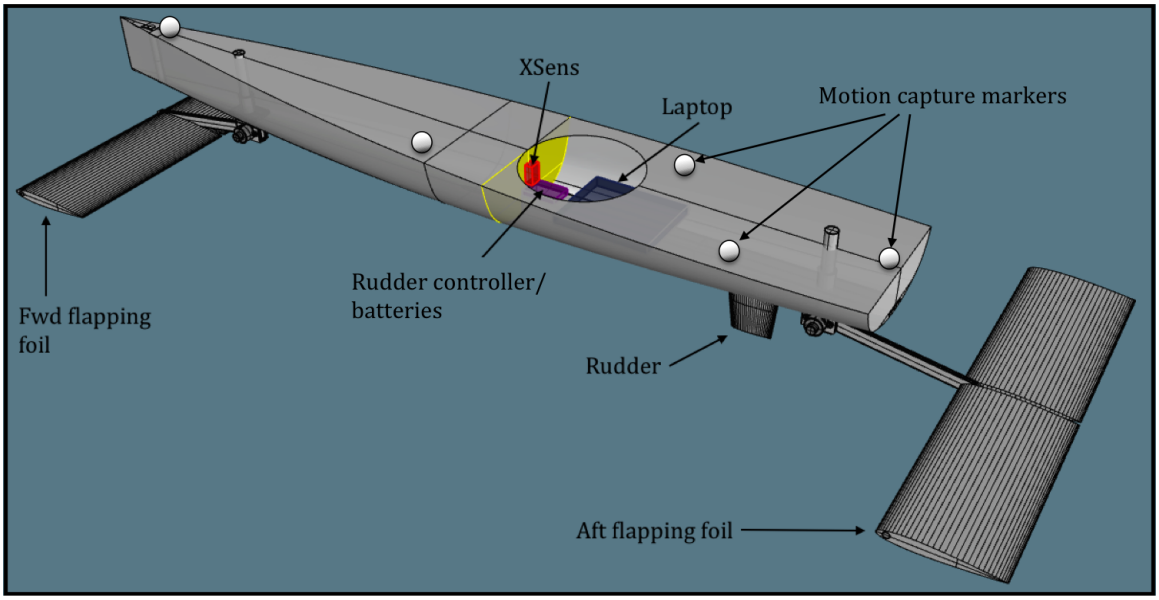

Figure 4.1: General arrangement of the final experimental platfrom

4.1.1 Experimental platform

An existing towing tank hull was modified for the purpose of the experiments and a series of updates were implemented as the experimental programme progressed. The updated hull form is called FLEUR and is referred to later in the simulation analysis. The hull is strengthened for testing in

Table 4.1: Experimental particulars for FLEUR tank model

Parameter	**Value**	**Units**
Hull particulars		
Waterline length, L_{WL}	2.27	m
Beam, B	0.34	m
Draft, T	0.107	m
Displacement excl. foils, M	44.8	kg
LCG, LCG	-0.156	m (from amidships)
Block coef., C_B	0.521	-
Prismatic coef., C_P	0.704	-
Waterplane area coef., C_{WP}	0.745	-
Max section area coef,. C_M	0.804	-
Water density, ρ	1000	kg/m^3
Foil particulars		
Foil mass, m_f	5.2	kg
Foil chord, c	0.23	m
Foil span, s	1	m
Foil depth, d_f	0.25	m
Foil type	NACA0012	-
Pivot point, a	-1	see Section 3.2.1
Spring constant, k_θ	10	Nm/rad
Pitch radius of gyrations		
Condition (Foil location)	k_5	
With foils ($\pm 0.6m$)	0.563	m
With foils ($\pm 1.2m$)	0.664	m
With foils ($\pm 1.8m$)	0.807	m
Hull only	0.476	m

waves with the addition of a longitudinal stiffener, which also provides the housing for the flapping foil mounts.

The model has been designed to accommodate the testing of various parameters in both free running and restrained testing scenarios. The foils are mounted at the end of aluminium 'pivot arms' that are fixed to vertical stainless steel tubes via a shaft mount, as shown in Figure 4.2 and Figure 4.3 for the aft foil. The model and foil particulars are detailed in Table 4.1. Pitch radius of gyration tests were performed on a rig for varying conditions such as foil locations, and the results are also presented in Table 4.1. Figure 4.1 shows a general arrangement of the final design used in the main body of experiments.

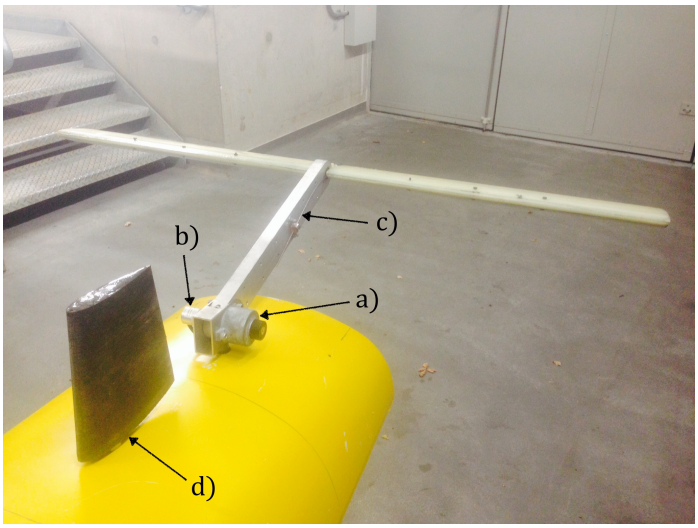

Figure 4.2: Submerged foil mounts and rudder location forward of the aft foil; a) Rotational damper/spring b) Rotational encoder c) Pivot arm with foil pitch spring mechanism d) Rudder

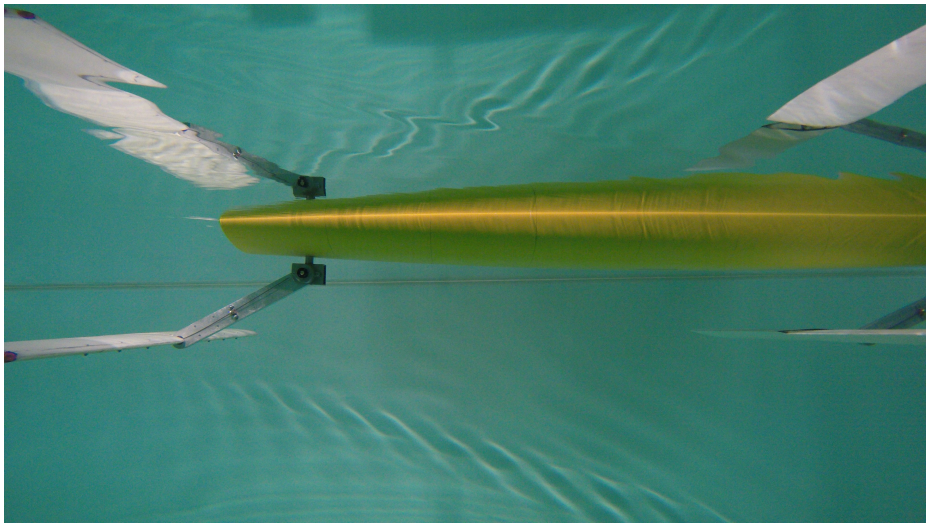

Figure 4.3: Preliminary setup fixed to the carriage

The stainless steel tubes are secured through the keel of the hull at the forward and aft locations. This setup provides the capability to alter the foil orientation and depth. The foils are mounted in two halves either side of the pivot arm and fixed via a shaft that rotates through three bearings that are pressed into the pivot arm, as can be seen in Figure 4.4.

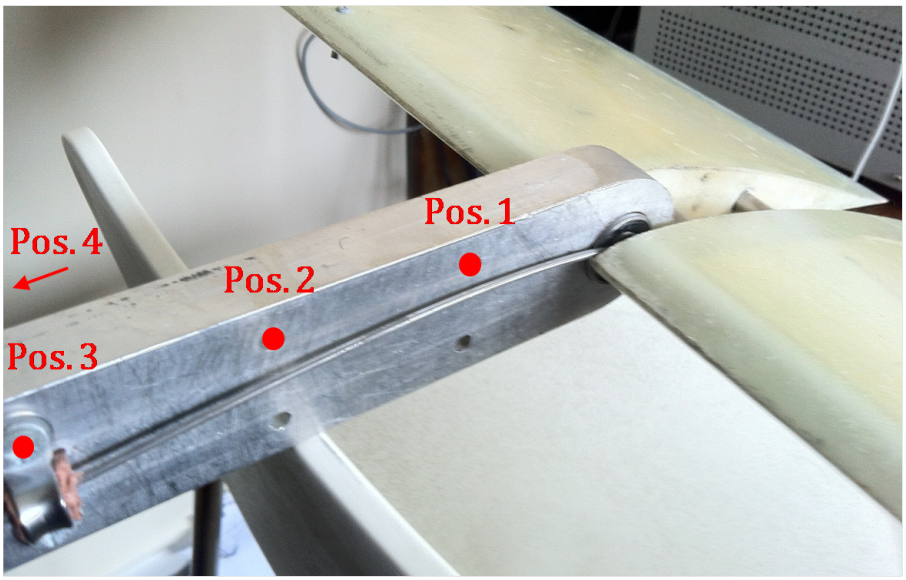

Figure 4.4: Pivot arm and rotational spring setup

A length of spring steel is fixed to the foil rotational shaft either side of the bearing mounting, shown in Figure 4.4. The working length of the spring steel can be adjusted by fixing the rod at different locations on the pivot arm, thus changing the spring constant. The spring constant can be altered using the same technique used by Bockmann et al. (2014) in their experiments to test the performance of a flapping foil under passive and active pitch conditions (Bockmann & Steen 2014). The centre of foil pitch can be set at the leading edge, one-quarter chord and half chord.

The centre of foil pitch was located at the leading edge and the spring constant was calibrated for a range of settings. By adjusting the height of the vertical mounting and angle of the aluminium pivot arm relative to the hull, the aft and forward foil depth was set to 0.25m below the waterline, shown in Figure 4.5 a) and Figure 4.6 a). The foils are neutrally buoyant to prevent buoyancy forces or weight from applying a torque to the pivot arm. The depth of the foils was, therefore, maintained at 0.25m in the neutral condition and the neutral foil pitch angle was set to be parallel to the free surface.

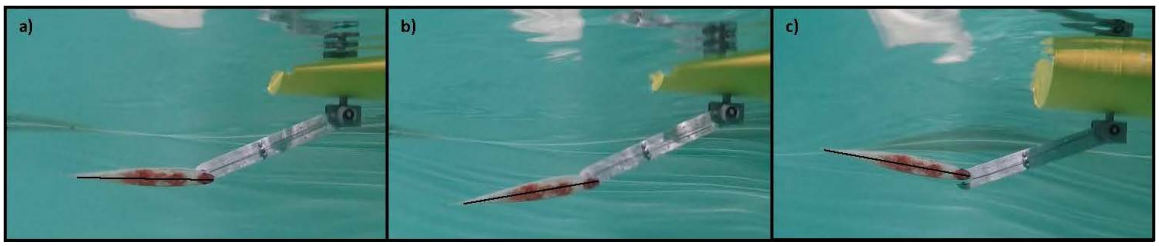

Figure 4.5: Aft foil spring loaded motion: a) Neutral angle b) Negative pitch c) Positive pitch

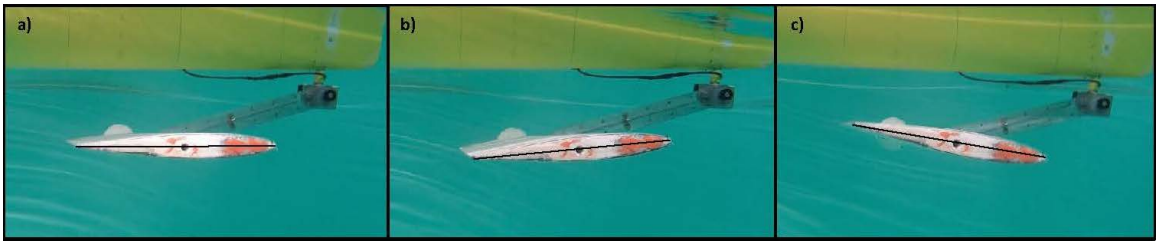

Figure 4.6: Forward foil spring loaded motion: a) Neutral angle b) Negative pitch c) Positive pitch

Further additions to the experimental platform were made throughout the experiments and, where relevant, these are introduced in the following sections.

4.1.2 Testing facilities (towing tanks)

Southampton Solent University 60m tank

The Southampton Solent University towing tank is 60m long, 3m wide and 1.8m deep. The wave machine is capable of generating waves of up to 0.1m amplitude and a frequency of 1.2 Hz. An experimental platform can be secured to the tow carriage via a tow post which is restrained by transverse and longitudinal dynamometers.

University of Southampton 138m tank

The University of Southampton Boldrewood towing tank is 138m long, 6m wide and 3m deep. The wave maker consists of nine paddles which can produce waves of up to 0.5m amplitude and frequency of 1 Hz (depending on wave amplitude). The towing tank has the capability to run motion capture

cameras, and it is therefore possible to conduct free running remote data acquisition using the motion capture setup over a data capture volume approximately 20m long, 4m wide and 2m deep.

4.1.3 Calibrations

General

In-situ calibrations were performed prior to experiments in the towing tank. This included using calibration weights for the dynamometer, distance measurements for linear potentiometers and wave probes, and angular measurements for rotational potentiometers and encoders.

Foil pitch spring constant

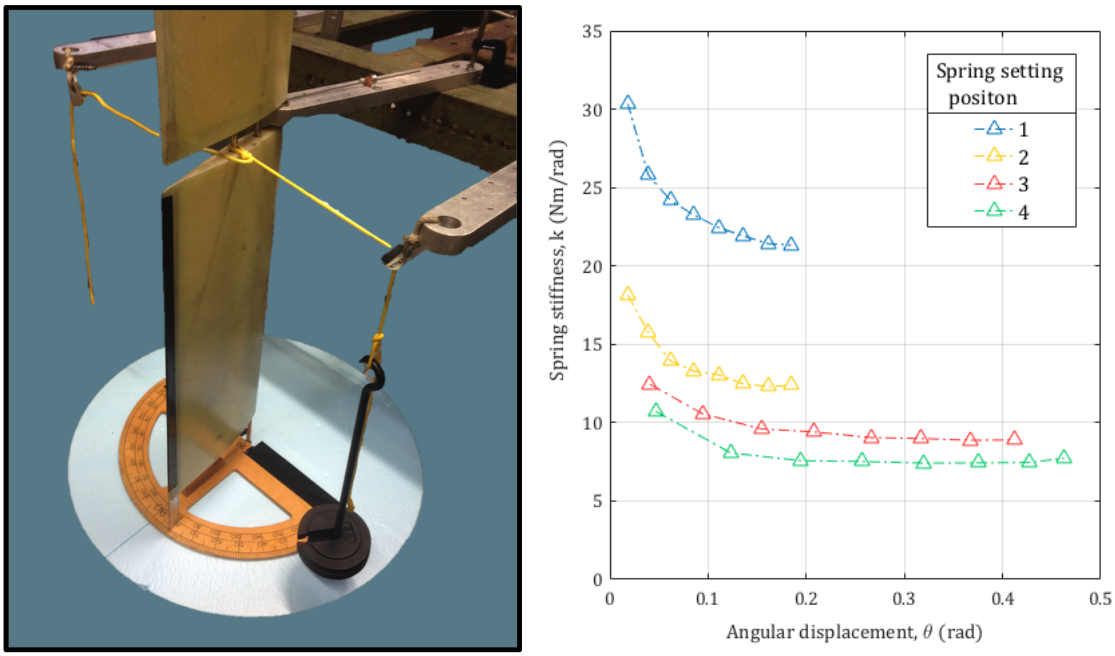

(a) Spring calibration setup

(b) Spring calibration results

Figure 4.7: Foil pitch rotational spring calibration

The spring setup for the experimental platform enables the setting of four different spring constants. This is achieved by adjusting the distance along the pivot arm at which the linear spring rod is

clamped. The distances for each spring setup are presented in Table 4.2.

Table 4.2: Spring positions

Spring position	**Distance from the foil pivot point / m**
1	0.05
2	0.10
3	0.15
4	0.20

Figure 4.7a shows the setup for the calibration. Weights, at increments of 5N and up to 40N, were used to apply a known moment about the pivot point of the foil via a pulley system. The spring constant for each setting was acquired by relating the angular displacement of the foil to the moment about the pivot point.

Results from the spring calibration are shown in Figure 4.7b. The calibration results show a strong non-linear trend at low angular displacements, but it was possible to describe this trend using a polynomial empirical equation.

Rotary damping constant

The damper was adjusted using a screw, which altered the size of an orifice between two fluid reservoirs. Calibration experiments were conducted to calculate the damping constant values for the various screw settings. The number of turns from the highest damping setting (fully screwed in) relates to the damping constant, as shown in Table 4.3.

Table 4.3: Damping constant calibration

No. of Turns	**Damping constant, ζ / Nm/rads^{-1}**
0	6.76
0.5	4.90
1	4.34
2	4.36

4.2 Data acquisition sensors and methods

Due to the range of experiments conducted, a variety of sensors have been used to acquire the data. Table 4.4 summarises which sensors or methods have been implemented for each experiment.

Table 4.4: Sensors used for data acquistion

Experiment	Vessel speed	Vessel motions	Foil motions	Wave profile
Preliminary	Stopwatch Dynamometer	Potentiometer (linear and rotary)	Rotary encoder	Wave probe
Wave propulson	Stopwatch Video (Qualisys) Doppler method	Inertial (XSens) Video (Qualisys)	Video (GoPro)	Wave probe
Energy recovery	Stopwatch	Potentiometer (linear and rotary)	PMTLG data	Wave probe

4.2.1 Vessel speed

Stopwatch

Using five markers, placed along the tank wall at set intervals of 3m, an assistant recorded the split time at which the bow of the vessel passed each marker. The first marker was located at a distance of 5m from the starting location of the vessel in order to allow for the acceleration of the vessel to a steady state forward speed. A comparison with this method and that of the Doppler method is shown in Figure 4.12.

Doppler method

The inertial sensor onboard the platform records the vessel motions, and the encounter frequency can be estimated by applying frequency domain analysis by calculating the power spectral density shown in Figure 4.8. It can be seen that there is a significant shift in the encountered frequency towards a high frequency in head waves and towards a low frequency in following waves. The difference between the encounter frequency of the vessel and the incident frequency of the waves is then used to estimate the forward speed of the vessel.

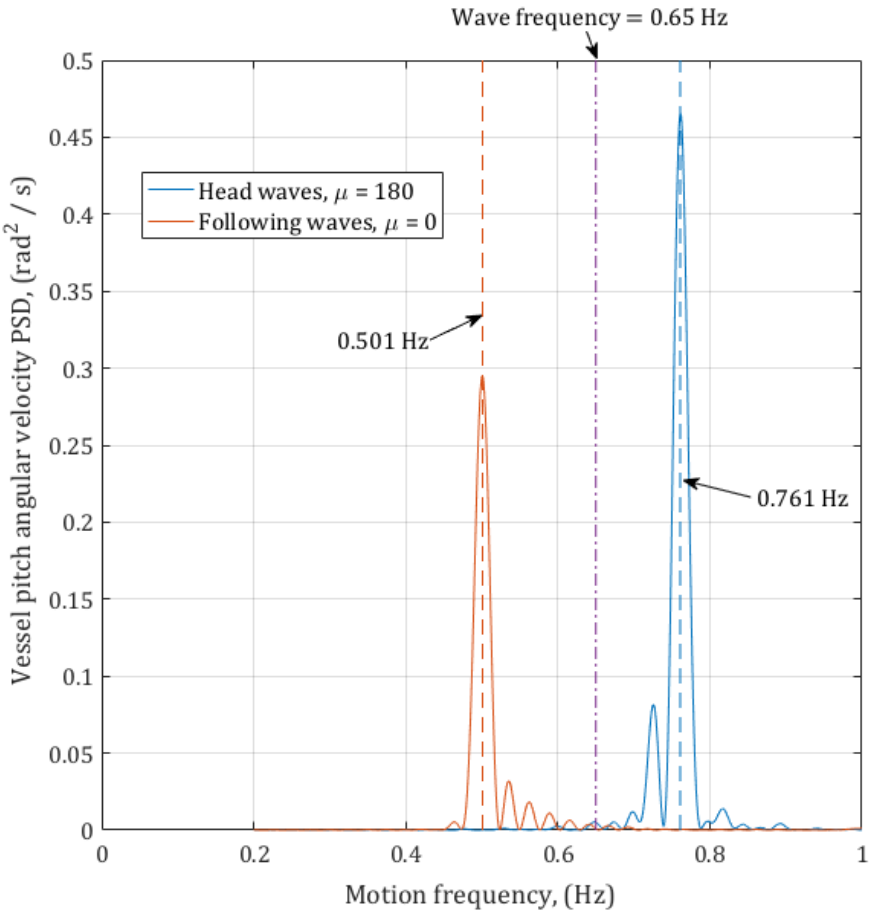

Figure 4.8: Doppler effect (change in encountered wave frequency) due to the forward speed in head and following waves estimated using the power spectral density function

Video (Qualisys)

The motion capture system utilizes a series of cameras that combine to track the motion of a marker in a three-dimensional volume. The Qualisys setup enables the system to identify a 'body' which can be tracked within the 3D volume with respect to an inertial frame of reference in 6 degrees of freedom. The setup can track the exact position of a marker within 0.5mm and at a sample rate of 60Hz. The setup could track the free running motion of the vessel over a calibrated volume 20 metres in length, as shown in Figure 4.9. This method of data acquisition is considered the most accurate method for acquiring the vessel motions and forward speed.

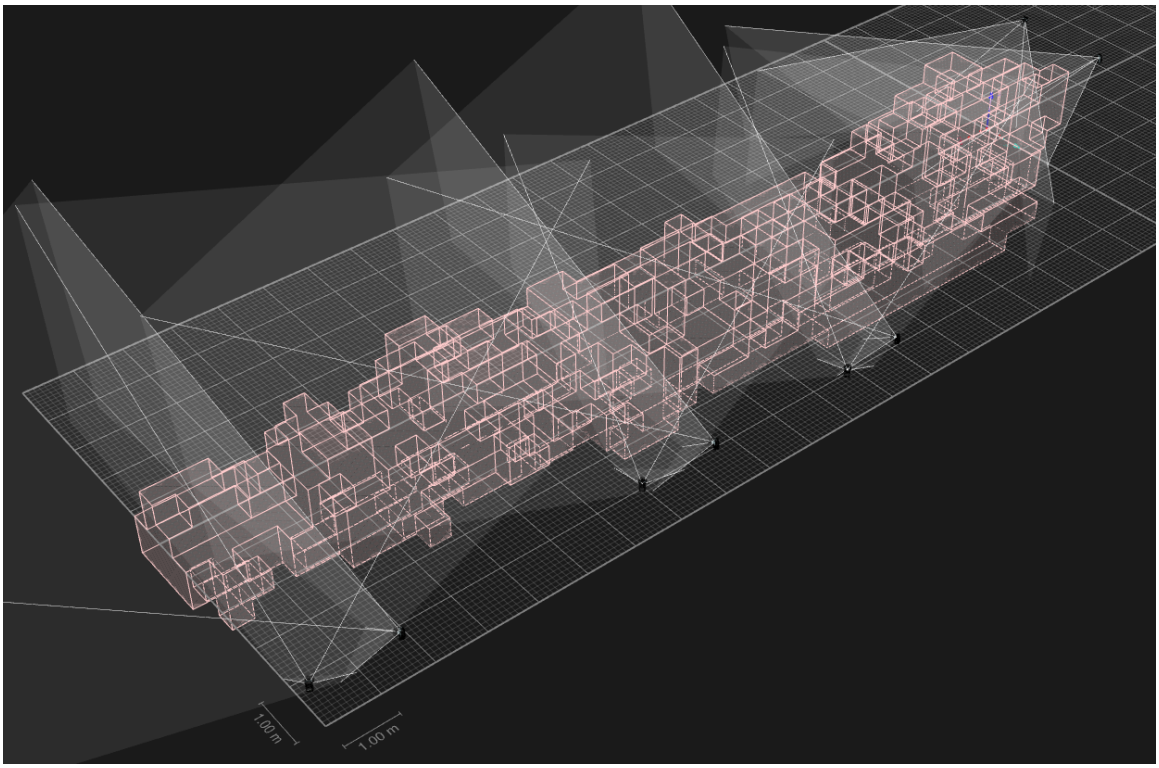

Figure 4.9: Camera motion capture (Qualisys) calibrated volume

4.2.2 Vessel motions

Inertial sensor (XSens)

The inertial sensor used was an XSens MTi 100 sensor, which measures the translational accelerations and rotational velocities. The data was acquired on a laptop located in the central compartment of the experimental platform, as shown in Figure 4.1. The inertial sensor was placed approximately at the LCG and VCG (vertical centre of gravity) in order to reduce any pitch induced accelerations that may occur in the heave data. The raw data requires significant post processing to acquire the translational and angular displacement. The sample frequency of 100Hz was set for all the experiments.

Carriage sensors; potentiometers and dynamometers

For the experiments that involved securing the model to the towing tank carriage, it is possible to acquire the relative motions and forces with relation to the tow post mount. The tow post is mounted on to a dynamometer which measures the transverse or 'side' forces and the longitudinal or 'drag' forces. The tow post is free to move in the heave orientation and a linear potentiometer records this motion. The tow post is secured to the model via a fixing that bolts on to the model 100mm aft of the LCG. Potentiometers on the tow post fixing on the model measure the roll and pitch motions of the vessel. All sensors are calibrated before a series of experiments and record at a sample frequency of 100 Hz.

4.2.3 Wave amplitude

Wave probes (Ultrasonic and resistance wires)

A wave probe is located on the carriage at a position equidistant from the model and the wall of the tank to avoid reflections from either objects. Two types of sensors have been implemented; resistance wires and an ultrasonic sensor. The former measures the change in voltage over two semi-submerged wires, which is due to a linear change in resistance with the relative submergence of the wires. The latter is located above the free surface and uses ultrasound to measure the distance between the water and the sensor. The wave probes were used to check the wave amplitude during experiments, and also to calculate the transfer function or response amplitude operator (RAO) of the vessel motions. Both sensors measured at a sample frequency of 100Hz.

4.2.4 Foil motions and power take off

Video (GoPro)

A GoPro camera was located underwater to capture the flapping motion of the foils during the free running experiments. In order to acquire data from the video footage, a tracking software was utilized to track the location of the trailing and leading edge of both foils, see Figure 4.10. This technique involved setting a scale which was based on the chord length of the foil. The relative distances of the data points were normalised with respect to the foil chord, which accounted for the

varying distance of the model from the camera for each experiment. The relative motion between the trailing edge and the leading edge was used to calculate the foil pitch and the flapping phase was calculated as the phase difference between the calculated pitch and the leading edge data point. The GoPro camera recorded video at a sample rate of 30Hz.

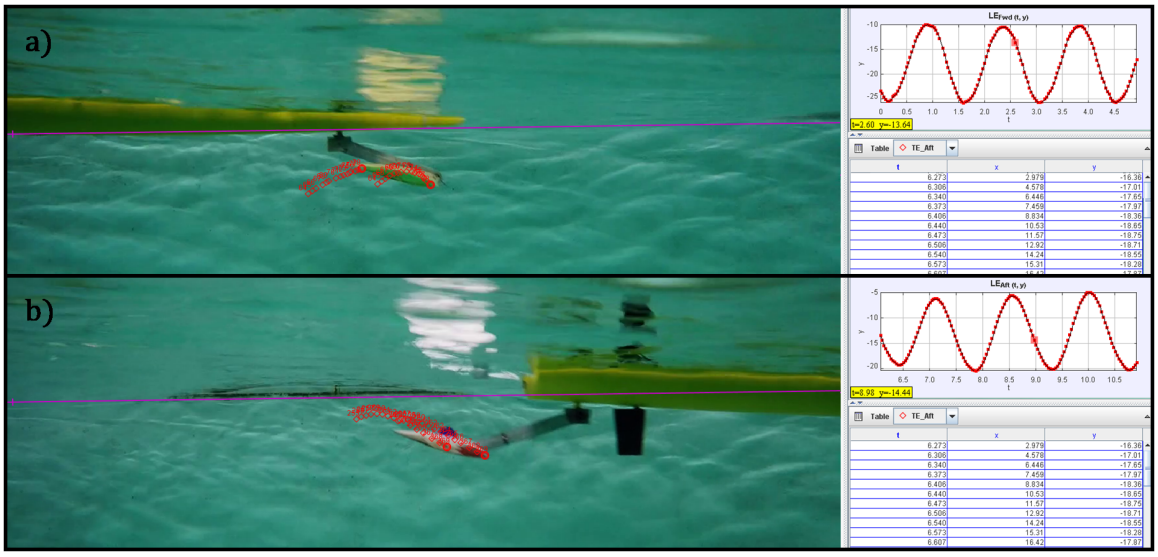

Figure 4.10: Underwater flapping foil motion tracking; a) Forward foil and b) Aft foil

Rotary encoder

For the preliminary experiments it was necessary to measure the relative motion of the submerged foils about the rotary dampers. This was achieved using waterproof rotary encoders that were secured to the shaft of the rotary damper, on which the pivot arm of the foil was mounted, see Figure 4.11. The signal outputs of the encoders were in the form of two quadrature sinusoidal analogue signals which can be interpolated and filtered to acquire the angular position and direction of rotation. The rotary encoder has an accuracy of $\pm 0.3^o$ and a sample frequency of 10 Hz.

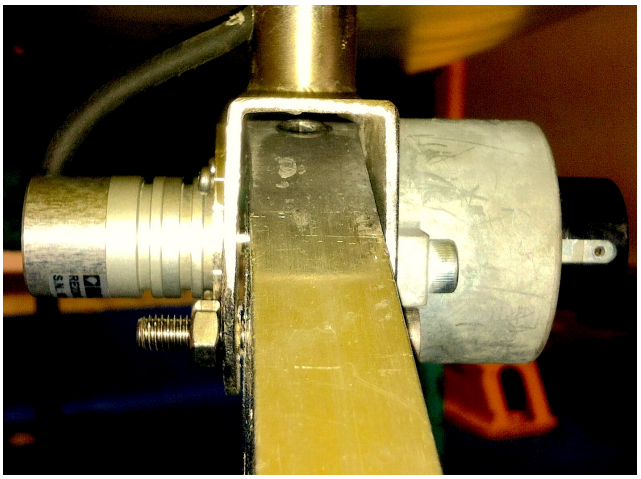

Figure 4.11: Rotary encoder located on the shaft that connects the pivot arm to vessel - left handside of the photograph

PMTLG

The permanent magnet tubular linear generators have the same output as a 3-phase permanent magnet rotary generator or motor. The voltage was measured over each phase in relation to the stator coils. Applying a resistor or load circuit made it possible to calculate the power generated by each PMTLG unit. The data was acquired using the CompactRio data acquisition hardware and post-processed using the LabView software. The data was recorded at a sample frequency of 100Hz. The PMTLG units are also fitted with Hall sensors which made it possible to measure the exact position of the permanent magnet thruster rod and, therefore, the relative heave of the submerged foils.

4.3 Uncertainty analysis and sensor comparison

For the experimental results, the overall uncertainty is either stated or depicted on graphs with use of error bars. Overall, the results show good repeatability, and that the majority of the uncertainty within the results is low. In the few cases where there is large uncertainty ($> 10\%$), errors could be attributed to the difficulty of maintaining a fixed heading for a free running experiment, for example. As the vessel was remotely operated, errors could have been caused by extreme motions of the rudder, resulting in additional drag or oversteer.

4.3.1 Uncertainty analysis methodology

The ITTC Committee recommends two types of uncertainty analysis for seakeeping experiments according to the International Organization for Standardization (ISO) (ITTC 2008):

- Type A (Precision error); a measure of the experimental repeatability using repeated experiments, otherwise known as precision error.
- Type B (Bias error): uncertainty associated with the entire experiment including model geometry, instrumentations measurements, calibration, data acquisiton and post processing.

The overall uncertainty/error is estimated as a combination of both types of uncertainty/error:

$$Overall\ error = \sqrt{(Precision\ error^2\ +\ Bias\ error^2)} \tag{4.1}$$

Type A uncertainty

For the two main experiments detailed in the following sections (4.5 and 4.6), at least three runs were carried out for each condition in order to assess the repeatability of the experiment and assess the uncertainty of the results. This is quantified from the standard deviation (σ) of the repeated results using the following formulae:

$$Precision\ error = \sigma = \sqrt{\frac{\sum_{i=1}^{N}(x_i - \bar{x})^2}{N-1}} \tag{4.2}$$

where N is the number of repeats, x_i is the recorded value and $\bar{x}$ is the mean of the N repeats.

Type B uncertainty

Type B uncertainty requires detailed data of the instrumentation used for each experiment. In this case, the Type B uncertainty is closely associated with the accuracy of the experimental setup and the measurement devices. Table 4.5 presents the error (ϵ_{xx}) associated with the calibration and measurement processes. The error associated with the data analysis is particular to each run and type of experiment. An overall average for each experiment is presented in Table 4.5 for the harmonic measurements. The overall bias error for each experiment can then be calculated as the square root sum of squares (RSS):

$$Bias\ error = RSS = \sqrt{\epsilon_{calibration}^2 + \epsilon_{measurement}^2 + \epsilon_{analysis}^2} \tag{4.3}$$

The calibration error is evaluated for the wave resistance probe from the standard error of estimate (SEE) (ITTC 2008):

$$\epsilon_{calibration} = SEE = \sqrt{\frac{1}{M-1}\sum_{n=1}^{M}(y_n - y_{LS,n})^2} \tag{4.4}$$

where M is the number of data points used for the calibration, y_n is the measured data and $y_{LS,n}$ is the estimated data using the linear fitting function (constant rate in this case). The measurement error is calculated as plus/minus half the resolution of the instrumentation:

$$\epsilon_{measured} = \pm\frac{Resolution}{2} \tag{4.5}$$

This assumes that the sensors are operating in a constant environment and within the specified range. This method of estimating the measurement error does not consider the accuracy of the instrumentation. Therefore, in order to assess the degree of accuracy, a comparison between particular sensors is given in Section 4.3.2.

As the experiments are conducted in regular waves, the bias error associed with the data analysis

is calulated as the absolute difference between the fitted harmonic amplitude and the average peak to peak amplitude. For example, the analysis error for the wave amplitude is calculated as follows:

$$\epsilon_{analysis} = \sqrt{2} \times \zeta_{RMS} \quad - \quad \frac{\overline{(\zeta_{p_n} - \zeta_{t_n})}}{2} \tag{4.6}$$

where ζ_{p_n} and ζ_{t_n} is the consecutive wave peak and trough in a time history of n waves. For non dimensional results, where the uncertainty is a function of both the wave amplitude and the measured response, the uncertainty of both measurements is applied using the RSS method.

Table 4.5: Bias error for calibration, measurement and analysis

Calibration, $\epsilon_{calibrated}$		
Element	**Source**	**Error**
Wave amplitude	Resistance probe Ultrasonic probe	1.2mm[a] Live calibration
Free running	Accelerometers Qualisys	0.06 deg/s (N/A for mm/s^2) 0.5mm

Measured, $\epsilon_{measured}$			
Element	**Source**	**Resolution**	**Error**
Speed	Qualisys Stopwatch Doppler effect	1mm/s 20mm/s 5mm/s[c]	± 0.5mm/s ± 10mm/s ± 2.5mm/s
Wave amplitude	Resistance probe Ultrasonic probe	1.5mm[b] 1mm	± 0.75mm ± 0.5mm
Heave amplitude	Qualisys Accelerometer Potentiometer	0.5mm 3mm 0.3mm[b]	± 0.25mm 1.5mm 0.15mm[b]
Pitch amplitdue	Qualisys Accelerometer Potentiometer	0.05 deg 0.1 deg 0.3 deg[b]	± 0.025 deg ± 0.05 deg ± 0.15 deg
Relative foil heave amplitude	PMTLG	0.006mm	± 0.003mm

Analysis, $\epsilon_{analysis}$		
Element	**Free running error**	**Restrained error** $\zeta_a = 0.06m$ | $\zeta_a = 0.09m$
Wave amplitude	1.54mm	$1.52mm$ | $2.04mm$
Heave amplitude	0.9mm	$0.46mm$ | $0.77mm$
Pitch amplitude	0.0005 deg	$0.05deg$ | $0.04deg$
Relative foil heave amplitude	N/A	$1.45mm$ | $2.22mm$

[a] SEE
[b] estimated from ITTC recommendations
[c] assuming an encountered frequency measurement sensitivity of 0.001 Hz

Wave measurement

Other uncertainties include the measurment of the wave profile at various locations along the length of a free running experiment. The wave probes were situated close to the wave makers and any deterioration in the wave along the length of the tank was not recorded. Also it was not possible to exactly gauge when the wave reflections from the beach would effect the model. A run length of 20 metres was set at a particular location in the tank where it was considered that the reflections would not interfere significantly with the experiments. Tank side wall reflections were of concern due to the low forward speed of the free running model but the low speed also meant that the waves generated by the vessel were minimal and the effect was assumed to be negligible.

4.3.2 Sensor comparison

Figure 4.12 shows the standard deviation of vessel forward speed for both the stopwatch and the Doppler methods. In this case, the Doppler method was used as the base method for comparison. The standard deviations are approximately 10% or less from the mean. Whilst this is quite significant, it is acceptable considering the variable response of a free running experiment.

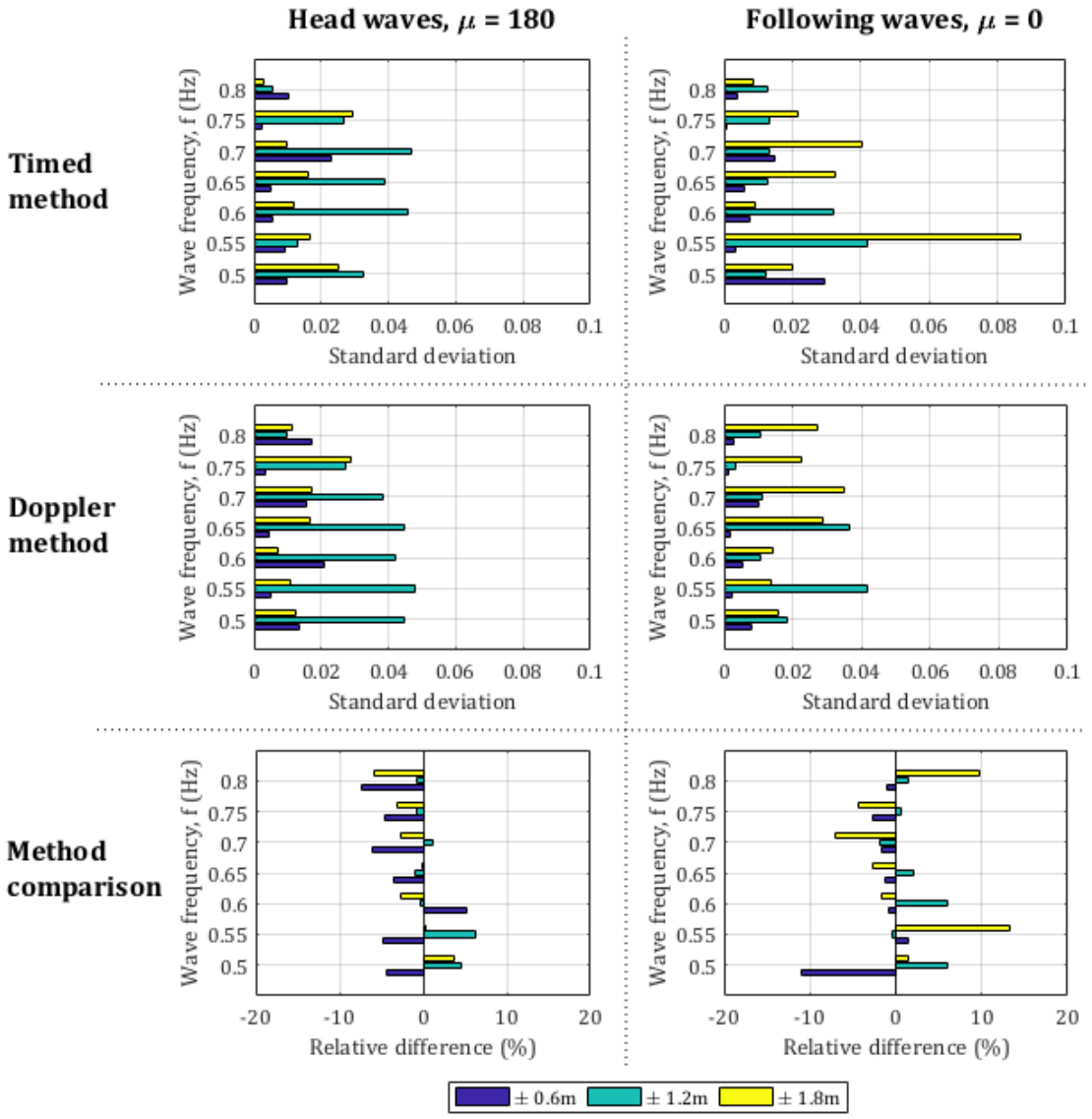

Figure 4.12: Standard deviation in forward speed for the stopwatch and Doppler methods

Although the stopwatch technique was susceptible to human error, the vessel forward speed was low, and frequent time splits were taken to ensure a reliable average. It can be seen that the stopwatch method is in good agreement with the Doppler method and the relative error between the two methods amounts to less that 5% for most cases. In following waves, there are several cases where the relative error is greater than 10%, which may be attributed to human error in the stopwatch method.

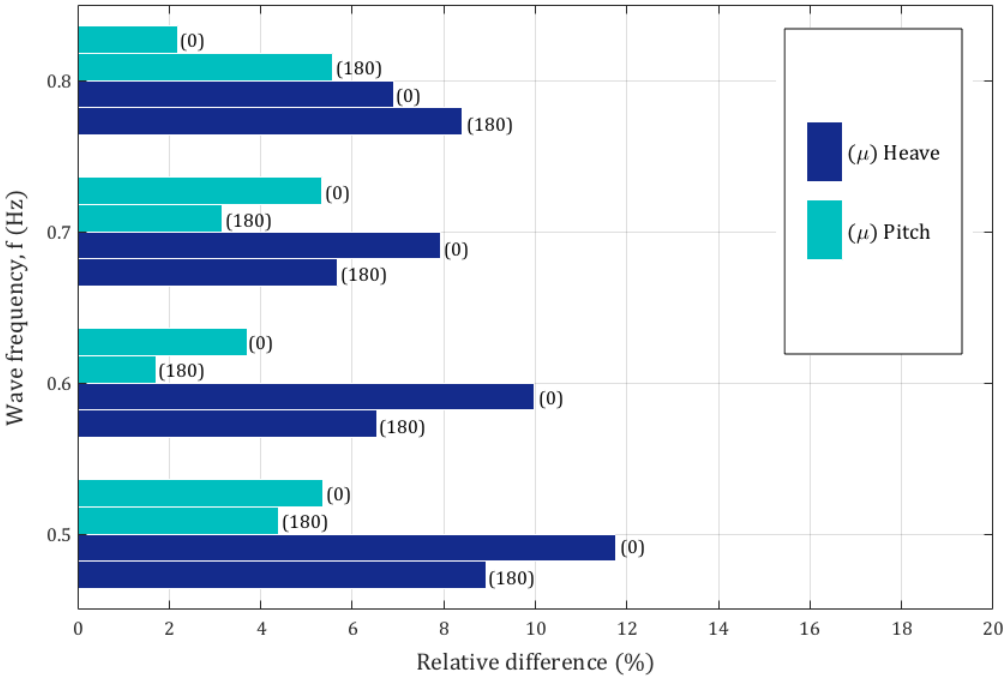

Figure 4.13: Comparison between motion capture cameras and inertial sensors

Figure 4.13 shows a comparison between the inertial sensors and the motion capture cameras for the vessel motions. In this case, the Qualysis motion capture method is used as the base method due to its marker acquisition accuracy of less than 0.5mm. The inertial sensors show reasonably good agreement with the motion capture cameras for vessel pitch, and are almost all within 5% for head and following waves. However, the results from the inertial sensors for vessel heave are in less agreement with those of Qualysis. This is mainly due to the requirement to post process and integrate the raw acceleration data from the inertial sensor to acquire the heave displacement. Only one step is required for the pitch motion as the raw data is recorded as an angular velocity, and therefore less error is incurred.

For future free running experiments, the Qualysis data should be used to capture both the motions and forward speed of the vessel, which would eliminate the requirement to post process data from an inertial sensor.

4.4 Restrained, wave-induced (Preliminary)

The preliminary experiments were designed to assess the suitability of the experimental platform for the main body of experiments by considering the following:

1. Coupled dynamics in relation to the vessel motions.
2. Thrust generation by the submerged flapping foils for various carriage speeds and wave frequencies.
3. Energy recovery by the foils when free to move relative to the vessel at varying damping constants and forward speeds for a range of wave frequencies.

4.4.1 Methodology

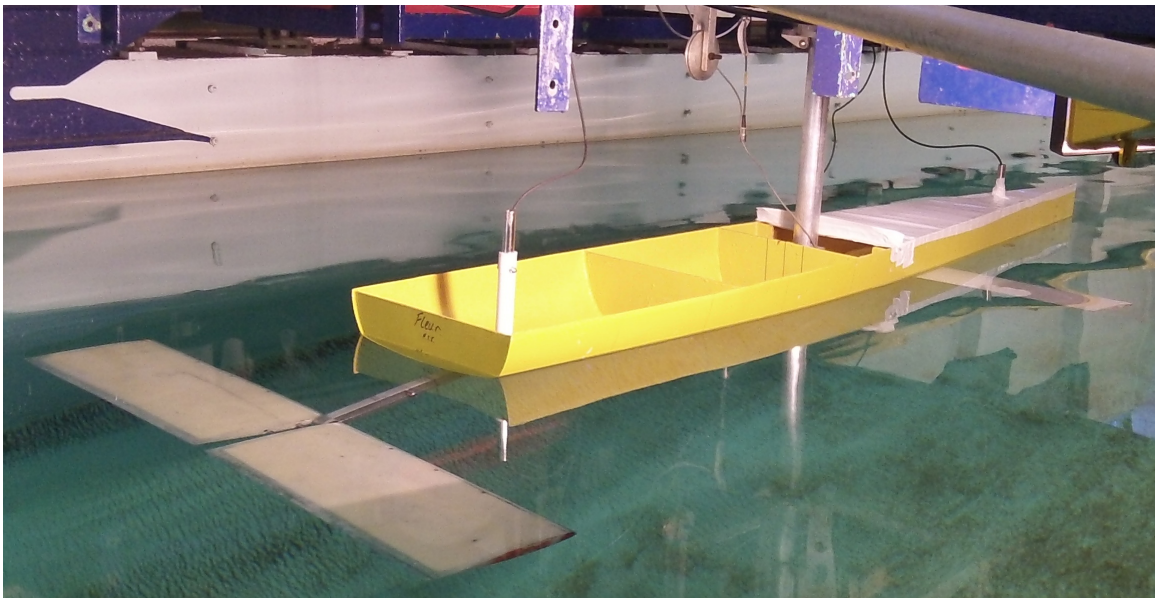

Figure 4.14: Preliminary setup - restrained at the tow post of the carriage

The setup implemented in the preliminary experiments used submerged foils located at approximately 1.3m abaft of the LCG of the vessel and 0.95m forward of the LCG. The model was fixed to the carriage (see Figure 4.14), which was either moved at 0.5knots towards the wave maker or kept stationary. The experiments were carried out under two different conditions; bollard pull (zero

carriage forward speed) and towed condition. For each condition, the extent to which the pivot arm was able to rotate about its pivot point was altered by applying an adjustable damping force. The damping force is applied by a rotational damper, shown in Figure 4.2, which simulates the power take-off of a generator.

The angular positions of the pivot arms were recorded using incremental magnetic rotary encoders. The signal outputs of the encoders were in the form of two quadrature sinusoidal analogue signals, which were interpolated to acquire the angular position and direction of rotation. The rotary damper and encoder are both mounted on a box section that forms the shaft connection for the pivot arm. The stainless steel box sections are welded to the vertical stainless steel tubes through which the cables for the rotary encoders pass to connect to the data acquisition setup.

In order to investigate the response of the foils and the vessel motions in head waves, the system was tested over a series of increasing wave frequencies, from 0.4 to 1 Hz, and at a wave amplitude of 0.04m. The set of wave frequencies encompass the wavelength to length ratios of 0.7 to 4, which is close to the recommendations suggested by the ITTC Seakeeping Committee (ITTC 2005).

Data was acquired for the wave amplitude, vessel heave and pitch, drag and the angular position of the pivot arm (estimation of power take-off). A test matrix of the preliminary experiments is given in Table 4.6. The preliminary experiments do not include repeat tests as the aim was to assess the suitability of the experimental setup and procedure for future experiments.

Table 4.6: Test matrix for preliminary experiments with wave parameters

Damping setting	Zero speed	0.5 knots
Fixed	✓ f = 0.4,0.6,0.8 and 1.0 Hz (λ/L = 4.3, 1.9, 1.1, 0.7)	✓ f = 0.4,0.6,0.8 and 1.0 Hz (λ/L = 4.3, 1.9, 1.1, 0.7)
0	✓ f = 0.8 Hz (λ/L = 1.1)	✓ f = 0.8 Hz (λ/L = 1.1)
0.5	✓ f = 0.8 Hz (λ/L = 1.1)	✓ f = 0.8 Hz (λ/L = 1.1)
1	✓ f = 0.8 Hz (λ/L = 1.1)	✓ f = 0.8 Hz (λ/L = 1.1)
2	✓ f = 0.8 Hz (λ/L = 1.1)	✓ f = 0.8 Hz (λ/L = 1.1)
No foils	✓ f = 0.8 Hz (λ/L = 1.1)	✓ f = 0.8 Hz (λ/L = 1.1)

4.4.2 Results

Vessel motions

Figure 4.15 shows the RMS pitch response of the model whilst restrained at the carriage in a wave of 0.8 Hz frequency and 0.04m amplitude. As expected, the RMS pitch motion of the vessel is notably less with foils at the bow and stern in comparison to the barehull model. Where the foils are free to heave, the vessel pitch motion decreases with an increase of pivot arm damping.

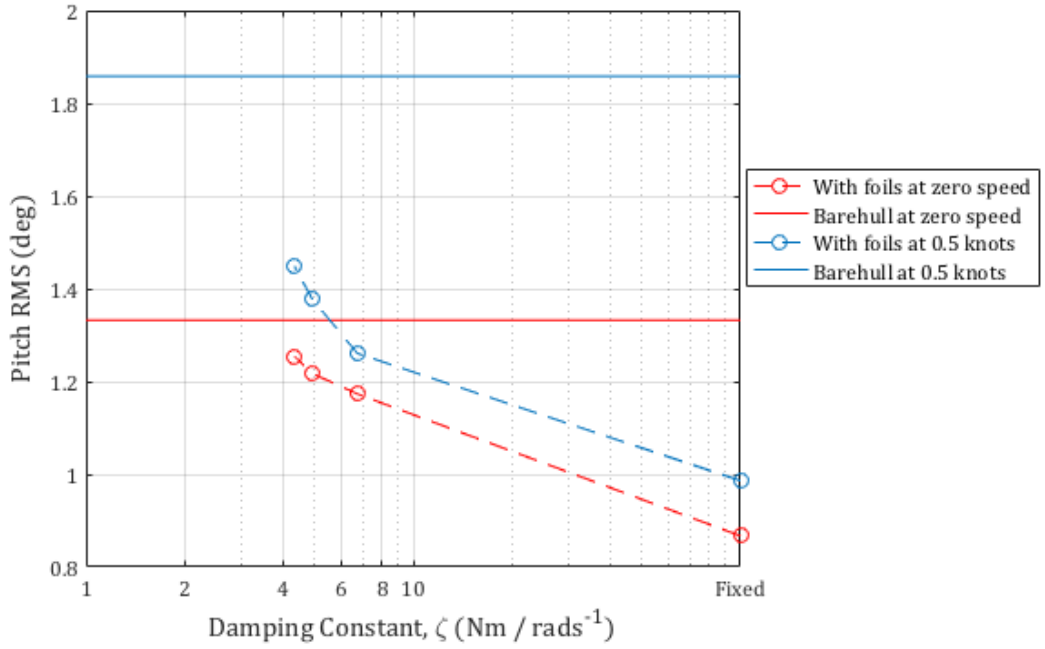

Figure 4.15: Change in vessel pitch motion with increasing effect of submerged foils from bare hull, to free foils with damping, through to fixed foils in regular waves ($\zeta_0 = 0.04m, f = 0.8Hz$)

Thrust generation

Figure 4.16 shows the time-averaged force measured in the x-direction for different speeds, with and without waves, where positive force is net thrust and negative is drag. For zero forward speed, a net thrust force was generated by the foils at the median wave frequencies of 0.6 and 0.8 Hz. For a forward speed of 0.5 knots and for the median wave frequencies, the foils also generated a net thrust force similar to that in the zero speed case. This is estimated by taking into account the experimental result for the calm water drag at 0.5 knots (solid red line in Figure 4.16).

Both sets of results identify that there is an optimum frequency of approximately 0.8 Hz; at which the foils generate thrust due to the combined vessel motions at this frequency. However, the increments in wave frequencies are relatively large and the peak response of either case could be between 0.7 and 0.9 Hz. Future experiments should include more wave frequencies at smaller increments.

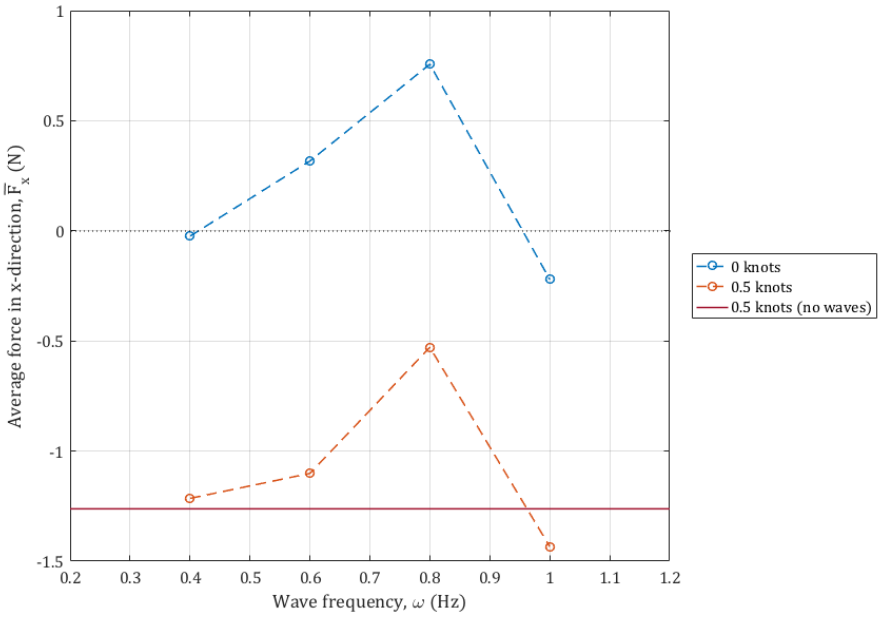

Figure 4.16: Average force in the x-direction for different speed, with and without waves ($\zeta_0 = 0.04m$)

Energy recovery

Assuming that all of the kinetic energy absorbed via the damper can be converted into electrical energy, the power generated by a foil is the work done by the flapping foils at the rotary damper:

$$P_\omega = M_z\omega_z = L_z a_z \omega_z = c_z {\omega_z}^2 \tag{4.7}$$

where M_z is the moment about the rotary damper, L_z is the vertical force acting on the foil, a_z is the length of the pivot arm, c_z is the damping constant and ω_z is the angular velocity of the pivot arm about the pivot point at the rotary damper.

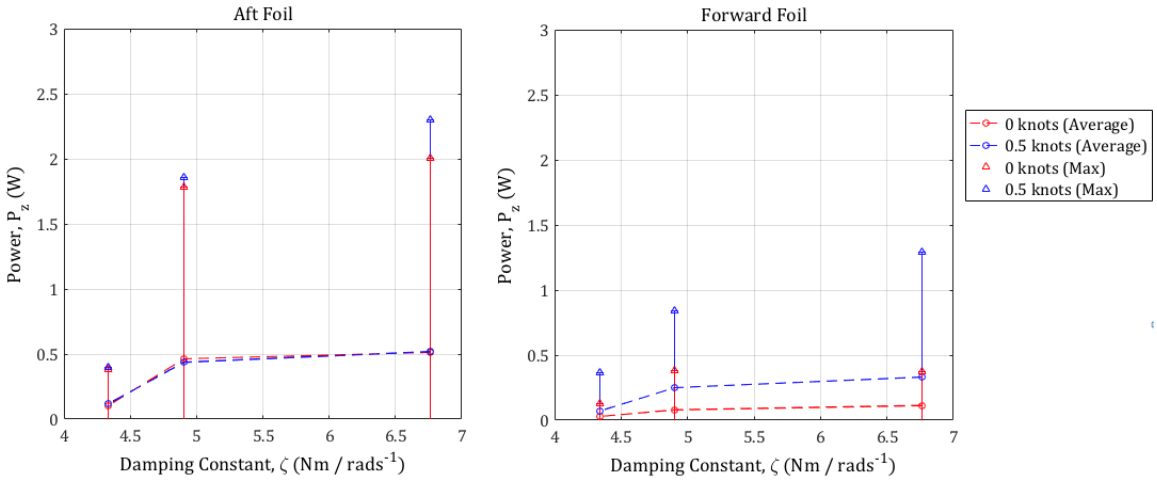

Figure 4.17: Mean and max power absorbed at the aft and forward foil location for varying damping constants at zero and 0.5 knots forward speed ($\zeta_0 = 0.04m$, $f = 0.8Hz$)

By adjusting the damping settings, as detailed in Table 4.3, it was possible to assess the effect of foil heave on the power generated. Figure 4.17 shows the maximum and average power generated by the forward and aft foil respectively. Both figures show a trend of increasing power generation with an increase in damping. As the damping constant tends to infinity, the power generated should approach zero, and there should exist an optimum damping constant, which is greater than the values tested. However, this is not representative of a true PTO device and further work is required in this area.

As expected, the forward foil generates less power than the aft foil. This is because, in the preliminary experiments, the foils are not located equidistant from the longitudinal centre of rotation (the tow post fitting in this case). Consequently, the pitch induced heave is significantly less for the forward foil and, therefore, the rate at which the forward foil heaves relative to the vessel is less than that of the aft foil.

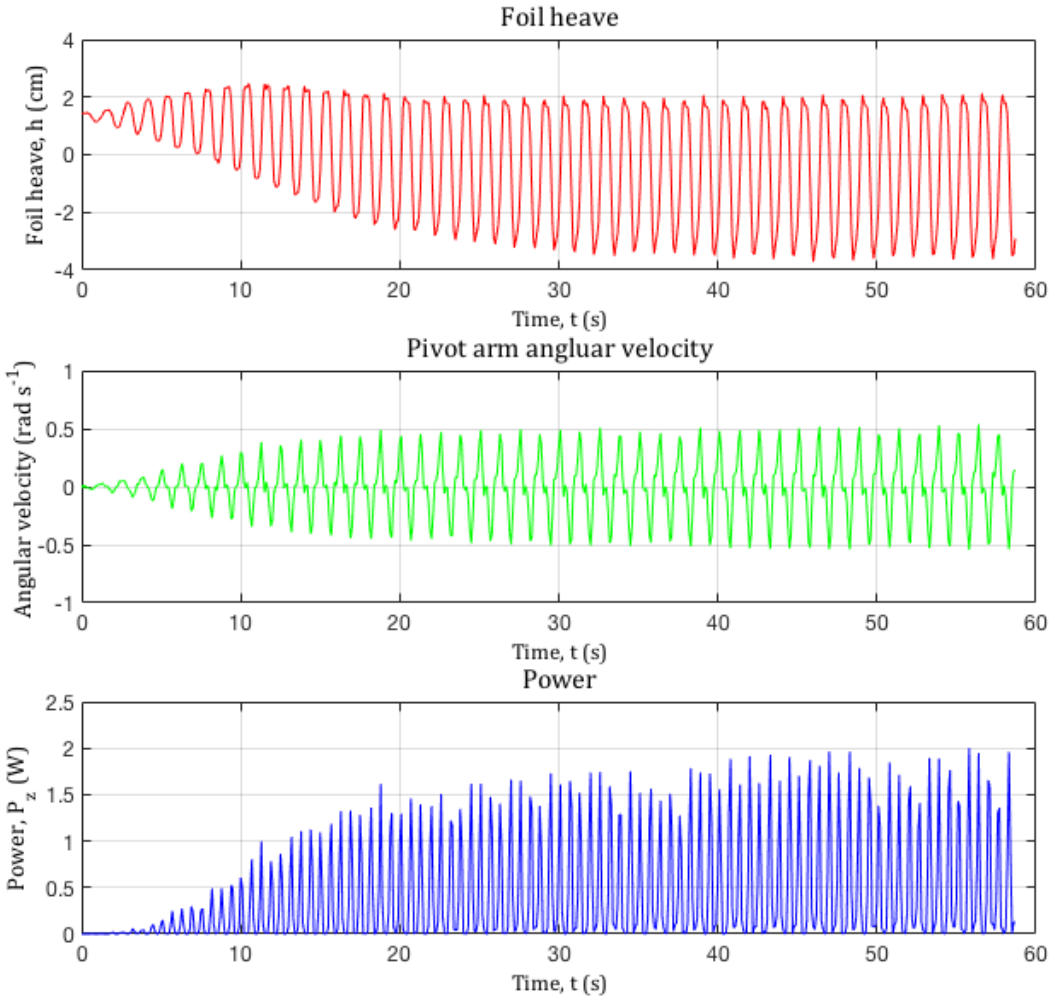

Figure 4.18: Time history of power generated by the aft foil in the preliminary experiments

Figure 4.18 shows the time history of foil heave, pivot arm angular velocity and the equivalent power generated by the aft foil at zero speed in an incoming wave of amplitude, 0.04m, and frequency, 0.8 Hz with the damping setting at zero turns (6.76 $Nm/rads^{-1}$). The foil heave was evaluated from the rotational data acquired by the rotary encoder using trigonometry. The foil is seen to start at an initial depth slightly shallower than its neutral position before settling into a steady oscillation about a steady state position. The cyclic response of the foil is reflected in the power generated at the rotary damper. The results indicate a promising generation of power, up to a maximum of 2 watts per foil, and prove that it is possible to recover wave energy using submerged flapping foils.

4.4.3 Validation

The comparisons between the numerical and experimental vessel motions with submerged foils at zero speed and 0.5 knots can be seen in Figure 4.19. The numerical results capture the overall trend and peak response of the experimental vessel motions.

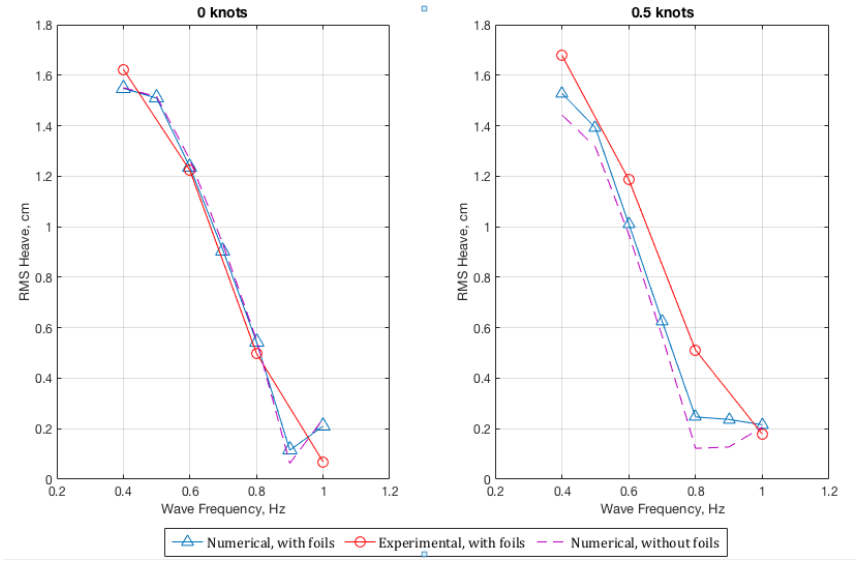

(a) RMS heave motion

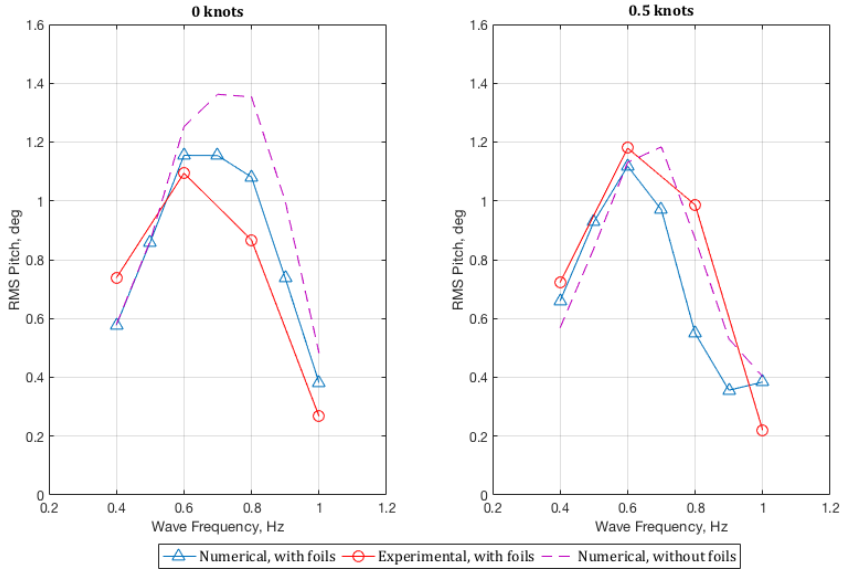

(b) RMS pitch motion

Figure 4.19: Validation of vessel motion response with submerged flapping foils in head waves of 0.04m amplitude, at a constant speed and restrained in surge

In conclusion, the current method is regarded as suitable for an initial validation of the coupled strip theory but further work is required to confidently validate the vessel motions over a wider range of external parameters, and should include repeat experimental runs.

4.4.4 Summary

The preliminary results provide a useful insight into the mechanisms of wave propulsion and wave energy recovery, and were successful at informing the structure of the main body of experiments. Additionally, the numerical results show reasonable agreement with the experimental results, and demonstrates that the coupled strip theory is acceptable for the purposes of this particular constant speed case with foils located near to the bow and stern. Key points to be considered for the main body of experiments were:

- self-propulsion could not be achieved, and therefore free running experiments are necessary:

  The carriage speed of 0.5 knots proved too high for self propulsion (only drag was recorded). Whilst lowering the speed would achieve self propulsion, this speed would be dependent on the wave frequency and would generate large vibrations on the carriage.

- the effect of foil location on the coupled dynamics:

  It has been shown that the effect of the submerged foils significantly effects the pitch response of the vessel at zero speed, and to further invesitgate this coupled response the foil location should be altered.

- the frequency dependency of thrust generation:

  Figure 4.16 clearly shows a resonant response at around 0.8Hz for both zero speed and forward speed. However, further analysis is required to investigate the frequency response for smaller increments of wave frequency.

- future wave energy recovery experiments can be conducted with the vessel restrained at the carriage:

  For free running, the vessel kept station whilst the foils were free to heave relative to the vessel (i.e. in the energy recovery mode). This observation demonstrates that changing the coupling between the submerged flapping foils and the surface vehicle alters the mode of operation from generating thrust or power.

- the foils should be locate equidistant from the LCG;

  The preliminary experiments identified that the aft foil generated more power than the forward foil. This is mostly due to a larger distance of the aft foil from the LCG. To directly compare the repsonse of the aft and forward foils, future experiments require that the foils are equidistant from the LCG.

- future experiments should include a more complete setup with a PTO device:

  The method to estimate the power absorption for energy recovery is too approximate, and a setup that can convert the incident wave power into electrical power would provide an improved estimate on the viability of a such a system

- further validation of the coupled strip theory method:

  The numerical results, which include the effect of submerged foils, show good agreement with the preliminary experimental results. However, further validation is required for a free running scenario (i.e. free to surge) and also for following waves.

4.5 Free running, wave propelled

In free running experiments the model is self propelled over a predefined distance in the towing tank. In this case, the vessel is propelled by the waves, and is propelled either towards the wave maker (head waves) or away from the wave maker (following waves), as shown in Figure 4.20. The principle measurement was the vessel's forward speed, but data was also acquired for the vessel and foil motions. The following objectives were set for these experiments:

1. Assess the free running wave propulsion response for varying wave frequencies in head and following waves.
2. Investigate the effect of foil location on the coupled dynamics.
3. Measure the flapping response of the forward and aft foil.

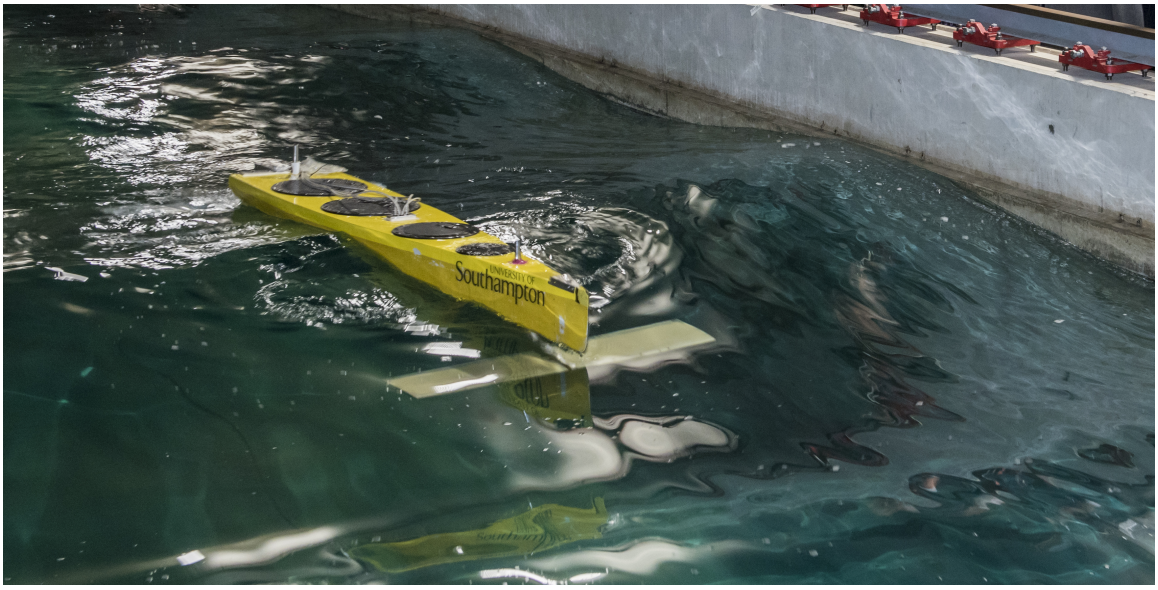

Figure 4.20: Photo of the improved design of experimental platform for free running experiments with watertight deck and bulkheads, taken in the 138m tank ($\zeta_a = 0.08$m, $\omega = 0.6$ Hz)

4.5.1 Methodology

A significant difference between restrained carriage and free running experiments is the requirement to acquire data remotely for the latter case. A watertight deck was therefore added to enable

electronic equipment to be accommodated in the model, see Figure 4.20. A remotely controlled rudder was also fitted, as shown in Figure 4.2. The experiments were conducted in head and following waves with a specific focus on the effect of foil location on the vessel motions and propulsive response.

The foils were located at varying locations from the vessel LCG; ±0.6m, ±1.2m and ±1.8m, as shown in Figure 4.21. This corresponds approximately to 50%, 100% and 150% of the half waterline length about the vessel LCG as shown in Figure 4.22. To capture the peak response, the analysis was conducted over a range of wave frequencies from 0.5 Hz ($\lambda = 2.75L$) to 0.8Hz ($\lambda = 1.1L$) at intervals of 0.05Hz. The wave amplitude was increased to 0.06m (as opposed to the 0.04m in the preliminary exerpiments) to ensure sufficient forward speed for rudder control. The experiments were conducted in the 60m tank and the wave amplitude was kept at a constant of 0.06m. A test matrix for the free running wave propelled experimental analysis is presented in Table 4.7.

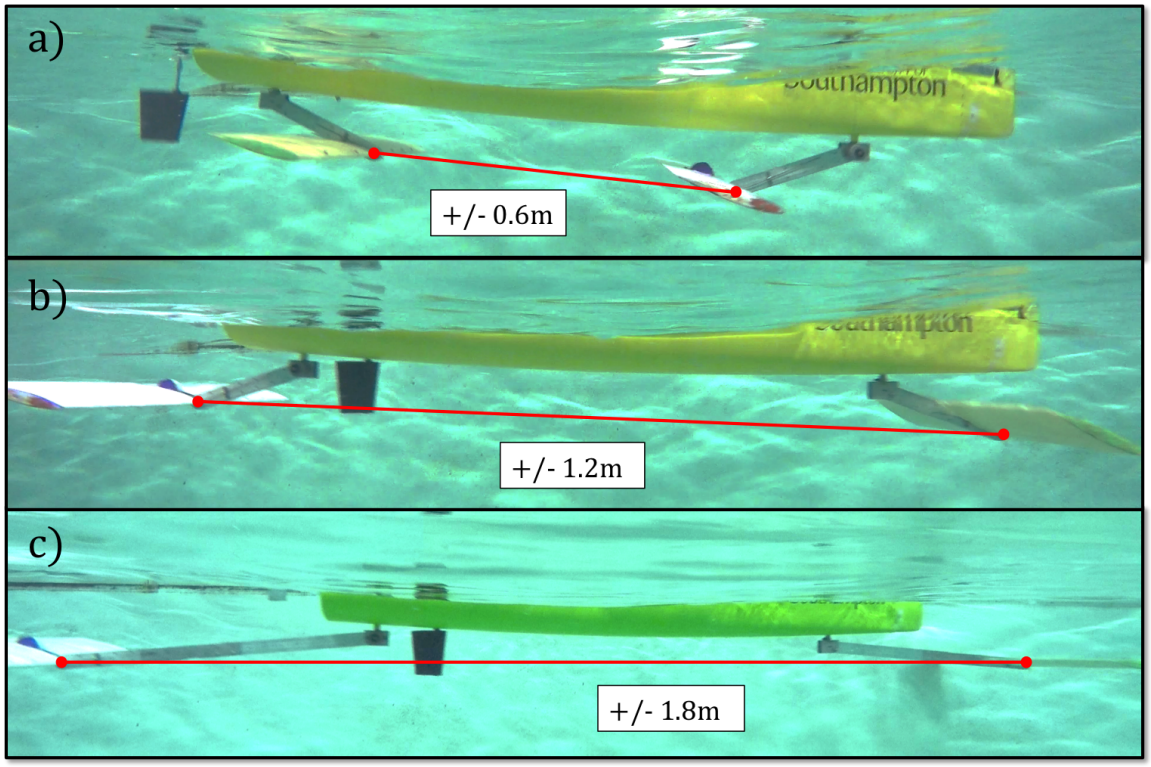

Figure 4.21: Foil distance from LCG; a) ±0.6m b) ±1.2m c) ±1.8m

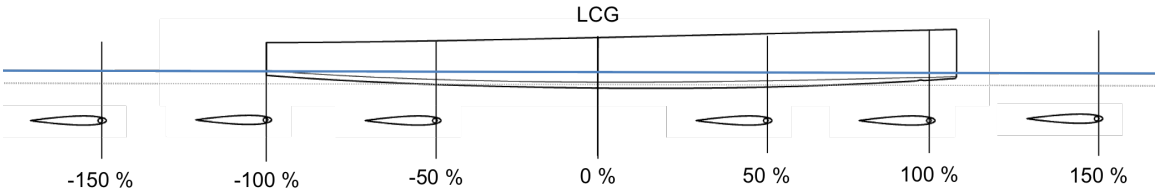

Figure 4.22: Location of foils as a percentage of the half vessel length from the LCG

Three methods were used to acquire the forward speed of the vessel: a stopwatch with split times at measured distances; an accelerometer method which makes use of the Doppler effect; and motion capture cameras. Cameras were located underwater to capture the motion of the foils as the vessel passed by, and onboard accelerometers were used to measure the vessel motions. The capture zone or area of the tank where the data was acquired was marked out as a 20m length with an initial length to allow for the model to accelerate and reach a steady state speed. The capture zone was located at the longitudinal centre of the tank to provide adequate space for the model to accelerate without the interference of reflected waves from the beach end of the tank.

It was expected that there would be a considerable oscillation in the forward speed of the wave propelled model. In order to record the oscillating forward speed response rather than the average speed, a series of additional free running experiments were conducted in the 138m tank using the Qualisys motion capture cameras.

Table 4.7: Test matrix for free running wave propelled experiments in both head and following waves. (The unbracketed values represent the total number of runs, the bracketed values represent the number of runs recorded using the underwater cameras and an asterix represents runs using the Qualisys motion capture cameras)

		Foil location		
Wave frequency Hz	λ/L	± 0.6**m**	± 1.2**m**	± 1.8**m**
0.50	2.75	3 (1)	3 (2)*	3 (1)
0.55	2.27	3 (1)	3 (2)	3 (1)
0.60	1.91	3 (1)	3 (2)*	3 (1)
0.65	1.63	3 (1)	3 (2)	3 (1)
0.70	1.40	3 (1)	3 (2)*	3 (1)
0.75	1.22	3 (1)	3 (2)	3 (1)
0.80	1.07	3 (1)	3 (2)*	3 (1)

4.5.2 Results

Coupled response; forward speed

Figure 4.23 shows the free running forward speed response of the vessel in varying wave frequencies and headings. As expected, an oscillation in forward speed was observed, and at low wave frequencies, the oscillations in the forward speed amount to almost 100% of the steady state mean speed. As the encountered wave frequency increases, the amplitude of speed fluctuation decreases, which suggests either an increase in the added wave resistance and/or a decrease in the wave-induced surge force.

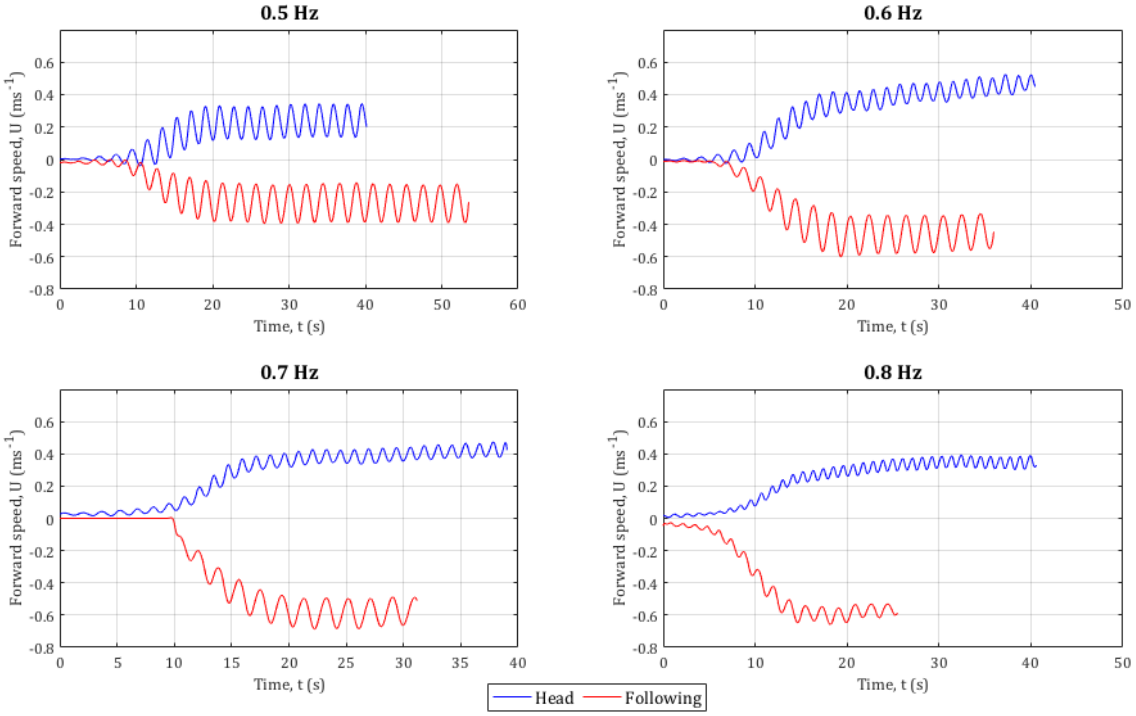

Figure 4.23: Vessel forward speed time history for head and following waves, with forward speed logged as negative for following waves ($\zeta_a = 0.06m$)

The time averaged, free running forward speed in head and following waves with the foils at varying locations, is shown in Figure 4.24. Error bars are also presented in Figure 4.24 and show, in general, good repeatability of the experiment. The average standard deviation for all free running experiments in head and following waves is $0.024ms^{-1}$.

As expected, the forward speed of the vessel is greatest with the foils at either the forward and

aft perpendiculars or beyond ($x_f = \pm 1.2m$ or $\pm 1.8m$). Although foils closer to the LCG have less of a reduction effect on the vessel pitch, the pitch induced heave of the foils in comparison to other foil locations is significantly reduced. Also, for the foil location nearest to the LCG, the foils are in very close proximity to the hull and each other, which will have a significant effect on the local flow field.

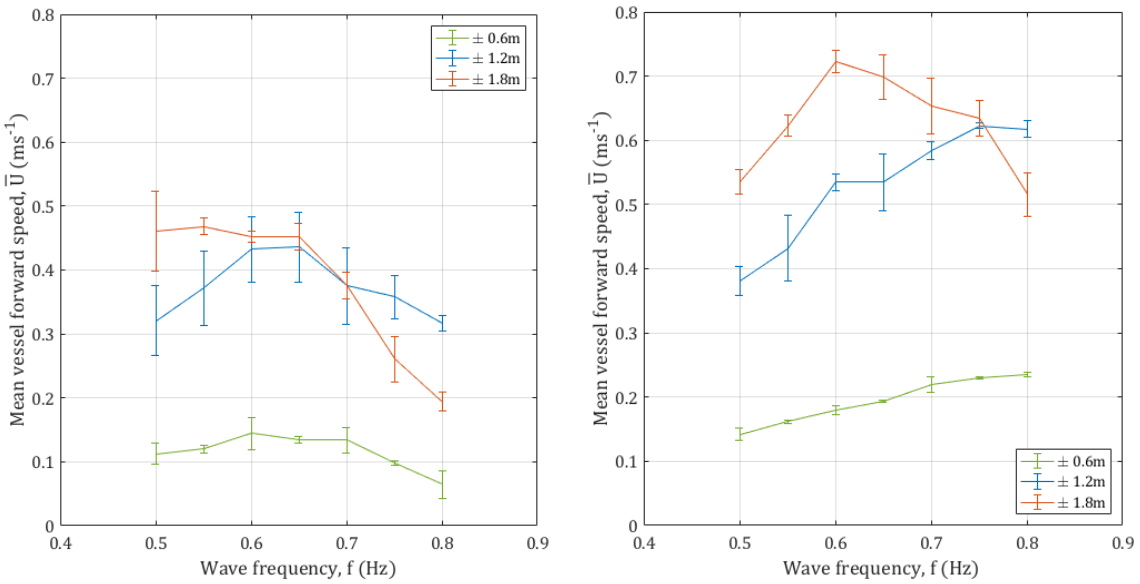

(a) Head waves

(b) Following waves

Figure 4.24: Mean free running vessel forward speed for varying foil locations in head and following waves ($\zeta_a = 0.06m$), calculated using the Doppler effect method. (Error bars represent the Type A uncertainty)

Vessel motions

Figure 4.25 shows the pitch motion Response Amplitude Operator (RAO) of the vessel for the varying foil location in head and following seas (equivalent non-dimensional results are presented in Appendix C). As expected, the location of the foils has a significant effect on the vessel pitch for both head and following waves. The plots are presented against the vessel encountered frequency to compare the vessel motions in the same steady state encountered wave profile and in all cases there is a trend of significantly less vessel pitch with an increase in the distance of the foils from the LCG.

Due to the significant effect of the encountered frequency on the vessel motions, it is difficult to quantatively compare the effect of foil location. However, the relative difference in the encountered

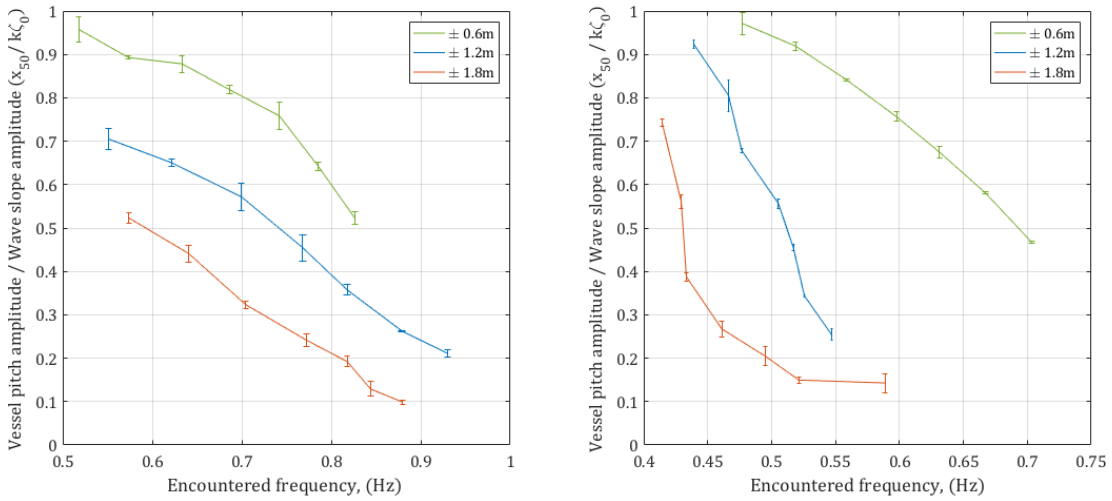

(a) Head waves

(b) Following waves

Figure 4.25: Free running vessel pitch response for varying foil locations in head and following waves ($\zeta_a = 0.06m$) (error bars represent the Type A uncertainty)

frequency for the experiments with the foils located at and beyond the AP and FP is less than 10%. Therefore, comparing the vessel pitch between these two cases, the percentage reduction in vessel pitch is approximately proportional to the percentage difference between the location of the foils, i.e 50% reduction in pitch for 50% change in distance from the LCG. This reduction in pitch is shown in Figure 4.26 for both head and following waves. Although, at lower wave frequencies the percentage reduction is only approximately 25%, there is a consistent reduction of approximately 50% for the remaining frequencies.

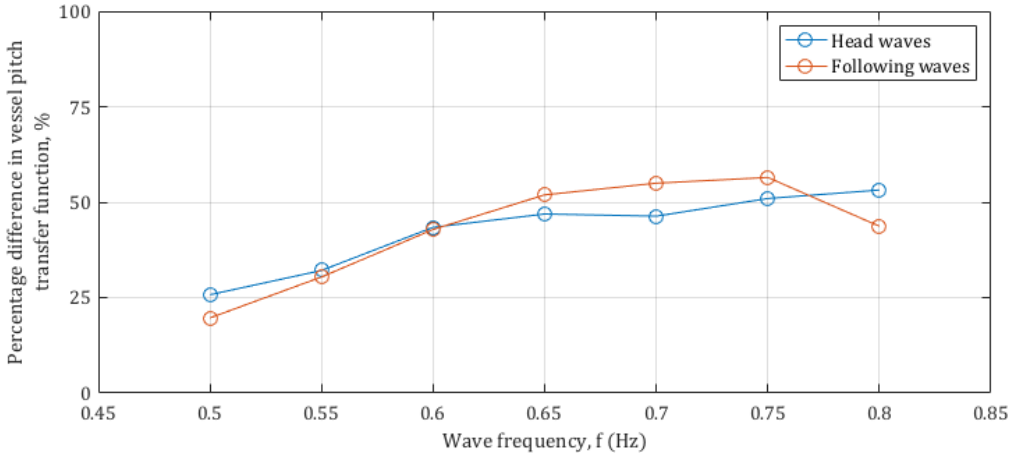

Figure 4.26: Percentage difference between the vessel pitch for a 50% increase in foil distance from the LCG; between $\pm 1.2m$ and $\pm 1.8m$ foil location

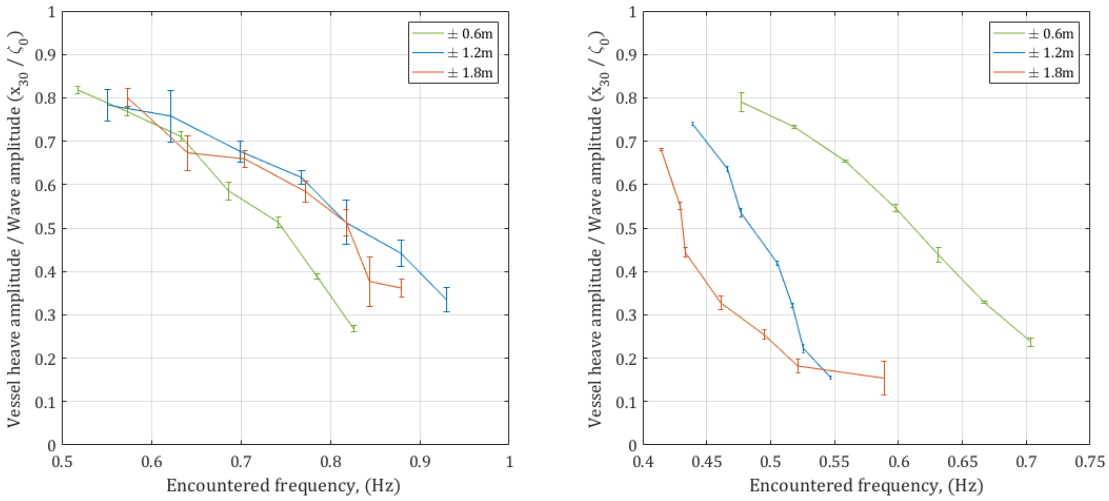

(a) Head waves

(b) Following waves

Figure 4.27: Free running vessel heave response for varying foil locations in head and following waves ($\zeta_a = 0.06m$) (error bars represent the Type A uncertainty)

Figure 4.27 shows the heave motion RAO of the vessel in head and following waves (equivalent non-dimensional results are presented in Appendix C). In head waves, it is clear that the effect of the foil location has a minimal effect on the vessel heave response. In following waves, however, there is a noticeable decrease in the heave of the vessel with increasing foil distance from the LCG, which is difficult to explain. However, it can be seen that the vessel heave in following waves shows a

strong correlation with the vessel pitch response in terms of the trends with respect to encountered wave frequency. Therefore, it is considered that the hull motions accelerometer is not just recording the vessel heave but a proportion of pitch-induced heave, which makes it difficult ascertain the true heave response of the vessel.

Foil motions

An indication of the forces acting on the submerged foils can be gained from the foil pitch response. Since, the lift force acting on the foil also acts as a moment about the foil pivot point it can be assumed that the foil pitch is, therefore, proportional to the forces acting on the foil. However, it was not possible to ascertain the exact direction of the lift forces to determine the forward thrust of the foils. This can only be estimated if self propulsion is achieved with a constant speed towing tank experiment. Therefore, the pitch motion of the foils is only considered an indication of the hydrodynamic forces acting on the forward and aft foils.

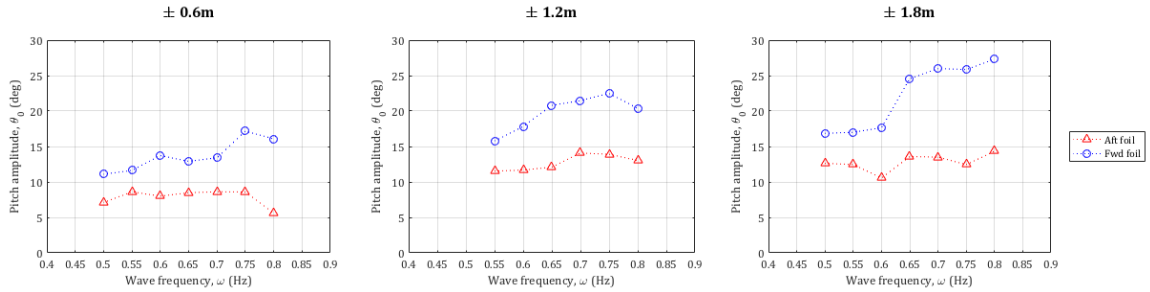

(a) Head waves

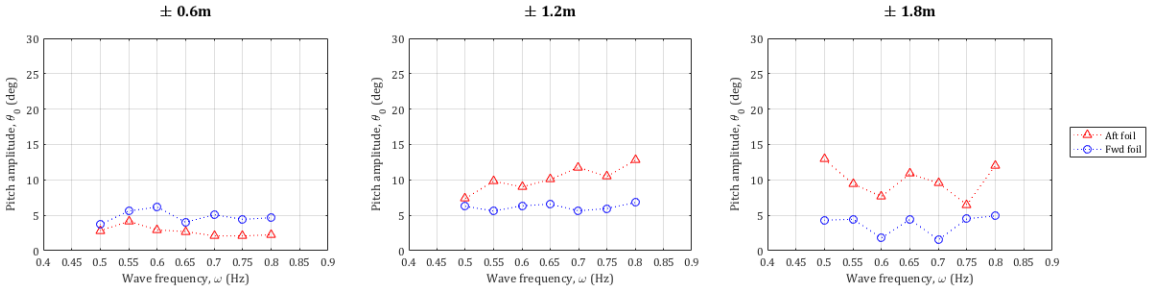

(b) Following waves

Figure 4.28: Flapping foil pitch amplitudes for the aft and forward foil

Figure 4.28 shows the foil pitch amplitude for head and following waves with the foils located at different distances from the LCG. The most interesting aspect of these results is that for head waves

the forward foil pitch amplitude is significantly greater than that of the aft foil for all three cases. The opposite is observed in following waves with the exception of the case with the foils located closest to the LCG, which is considered to be the result of second order effects due to the close proximity of the foils to the hull. The noticeable differences in the foil pitch amplitude suggests differences between the forces acting on the forward and aft foil. This would imply that a greater resultant force is generated by the forward foil in head waves, and a greater force at the aft foil in following waves. This is an important outcome, and will be discussed in more detail in Chapter 6.

As expected, the foil pitch increases with foil distance from the LCG, and more so in head waves. This is an indication that the forces acting on the foils are greater when the foils are located further from the LCG. However, it is difficult to attribute this increase in the force to one specific cause as it will be a combination of the vessel-induced motions and the incident wave effect at the foils, which will vary considerably depending on the foil location.

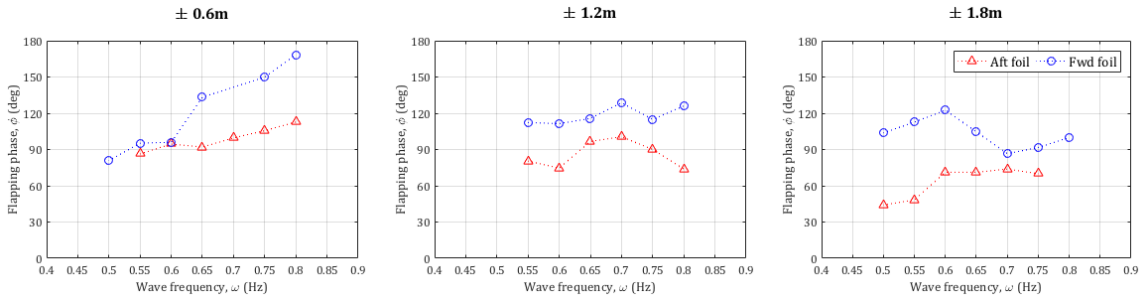

Figure 4.29: Flapping foil phase in head waves for the aft and forward foil at varying locations

Figure 4.29 shows the flapping foil phase of the aft and forward foil in head waves. The flapping foil phase is defined as the phase difference between the foil heave and pitch. Again, the results show a significant difference in the response of the forward and aft foils: the average flapping phase of the aft foil is approximately 91^o, whilst the average forward foil flapping phase is approximately 114^o.

4.5.3 Validation

Coupled response; forward speed

Figure 4.30 presents a comparison of free running numerical and experimental results in head and following waves with the foils located at the forward and aft perpendiculars. For validation purposes, a ramp factor of 10 is applied to mimic the generation of waves in the towing tank, and the start point of the experimental data has been cropped to match that of the numerical simulations. Reasonable agreement is shown between the numerical and experimental results, which proves that the numerical model is capable of capturing the transient response of the wave propelled vessel.

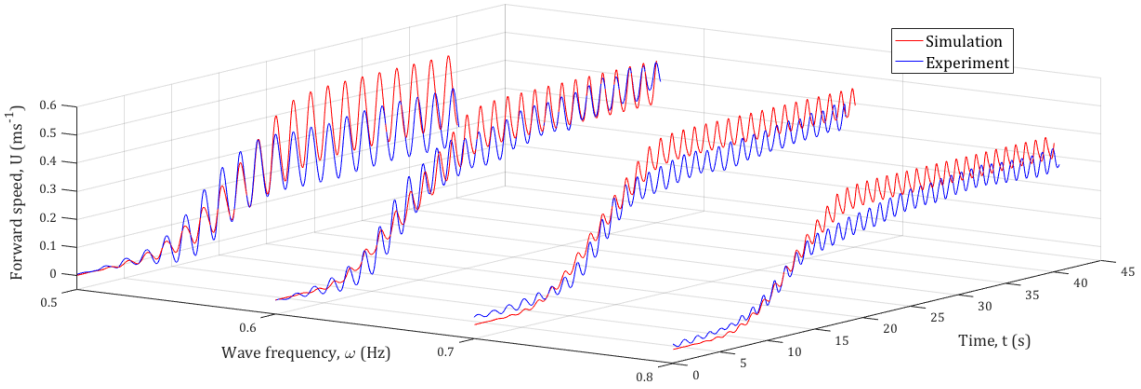

(a) Head waves

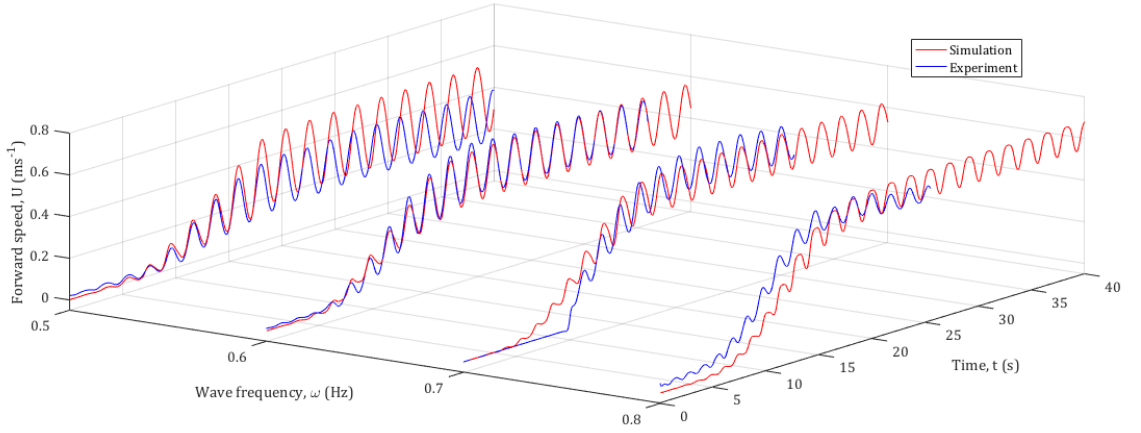

(b) Following waves

Figure 4.30: Time history of the vessel forward speed from experimental results and numerical simulations ($\zeta_0 = 0.06m$)

The speed oscillation is mostly attributable to the wave-induced surge force acting on the vessel and an empirical correction is required to numerically model this at high frequencies. The surge force is shown to have a minimum effect on the time average speed and is, therefore, considered to have a negligible effect on the overall response of the vessel. Further investigation into the wave-induced surge force and the empirical correction factor is discussed in Appendix B.

Figure 4.31 shows a comparison between the numerical and experimental results for the mean free running forward speed in head and following waves. The numerical results show reasonable agreement with experimental results with the foils at differing locations for head waves. For following waves, there is also reasonable agreement for the foil location at or beyond the forward and aft perpendiculars, but the numerical model overestimates the forward speed in following waves when the foils are located closest to the centre of the vessel. The cause of this overestimation in following waves is considered to be due to the assumed absence of added resistance due to following waves in the numerical model. Although the added resistance in following waves is assumed to be negligible, it will actually become significant at lower speeds, and this is not factored into the numerical model.

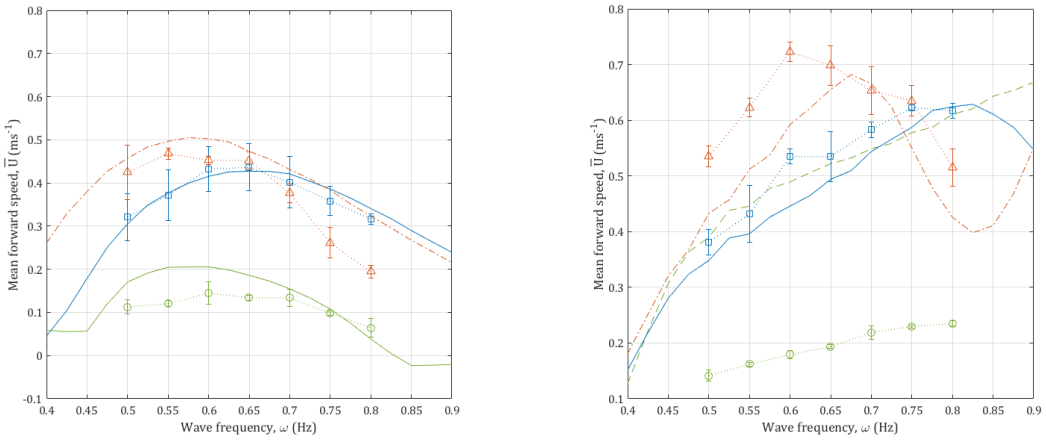

(a) Head waves (b) Following waves

Figure 4.31: Numerical and experimental comparison of mean vessel forward speed for different foil locations and wave frequencies ($\zeta_0 = 0.06m$) (error bars are reperesentative of the overall uncertainty)

In head waves, the model also overestimates the forward speed response at higher frequencies when the foils are located beyond the aft and forward perpendiculars, which could be due to the diffraction effect caused by the forward foil.

Vessel motions

Figures 4.32a and 4.32b show the numerical and experimental results for the vessel pitch motion in head and following waves respectively. In head waves, the numerical prediction of the pitch response does not exactly match the experimental results, but more importantly the numerical model is able to capture the effect of the foil location on the coupled response. In following waves, although the numerical model captures the trend of decreasing pitch with increasing foil distance from the LCG, the numerical predictions are shown to deviate significantly from the experimental results.

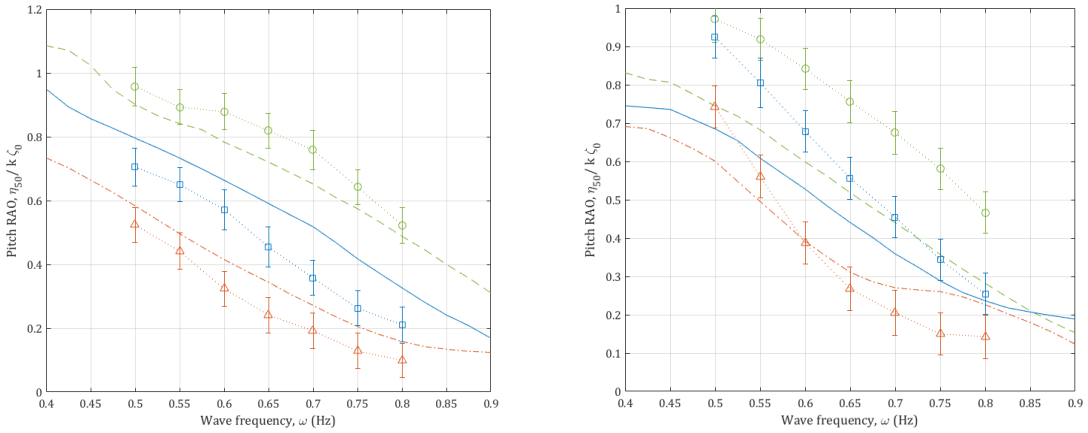

(a) Head waves

(b) Following waves

Figure 4.32: Numerical and experimental comparison of vessel pitch (error bars are reperesentative of the overall uncertainty)

In head waves, the relative effect of the foils on the vessel heave is minimal, as shown in Figure 4.33a, which is also confirmed in the numerical simulations. In following waves, the numerical results show considerably less agreement with the experiment results for the vessel motions, see Figure 4.33b. In this case, the numerical results show a significant difference in the vessel heave response with respect to the foil location. However, this discrepancy in the heave response is considered to be associated with the data acquisition rather than errors in the numerical model. Further investigation shows that the vessel heave response in following waves shows a close correlation to the corresponding vessel pitch, which suggests that the heave response includes a fraction of pitch-induced heave.

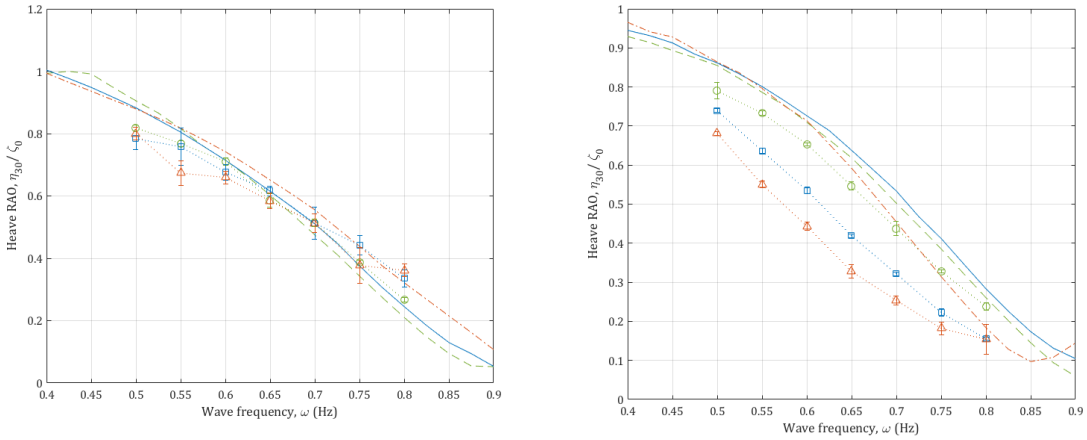

(a) Head waves

(b) Following waves

Figure 4.33: Numerical and experimental comparison of vessel heave (error bars are reperesentative of the overall uncertainty)

Foil motions

Figure 4.34a and Figure 4.34b compare the numerical pitch response of the aft and forward foils with the equivalent experimental results. In head waves, the experimental results show that the pitch response of the forward foil is significantly greater than that of the aft foil, which is also reflected in the numerical results (Figure 4.34a).

The numerical results show a steady increase in the pitch amplitude with increasing wave frequency, which is also evident in the experimental data for wave frequencies less than 0.7 Hz. The discrepancies with the experimental data at frequencies greater than 0.7Hz may be attributed to the overestimation of the vessel's response at higher frequencies. Overall, there is a reasonable agreement between the numerical and experimental results in head waves.

In following waves, the numerical results are less in agreement with the experimental data. However, the numerical model does capture the difference between the forward and aft foils; supporting the experimental result that the aft foil pitch is greater than that of the forward foil in following waves. The numerical results show that the pitch response of the aft foil is significantly greater than that of the forward foil, which is in agreement with experimental results and is a reversal of the effect in head waves.

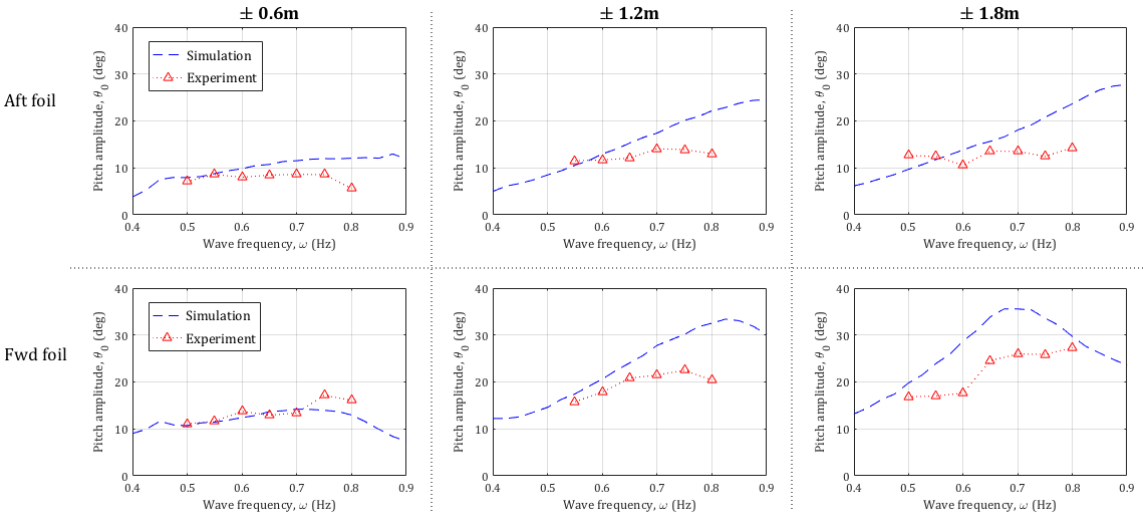

(a) Head waves

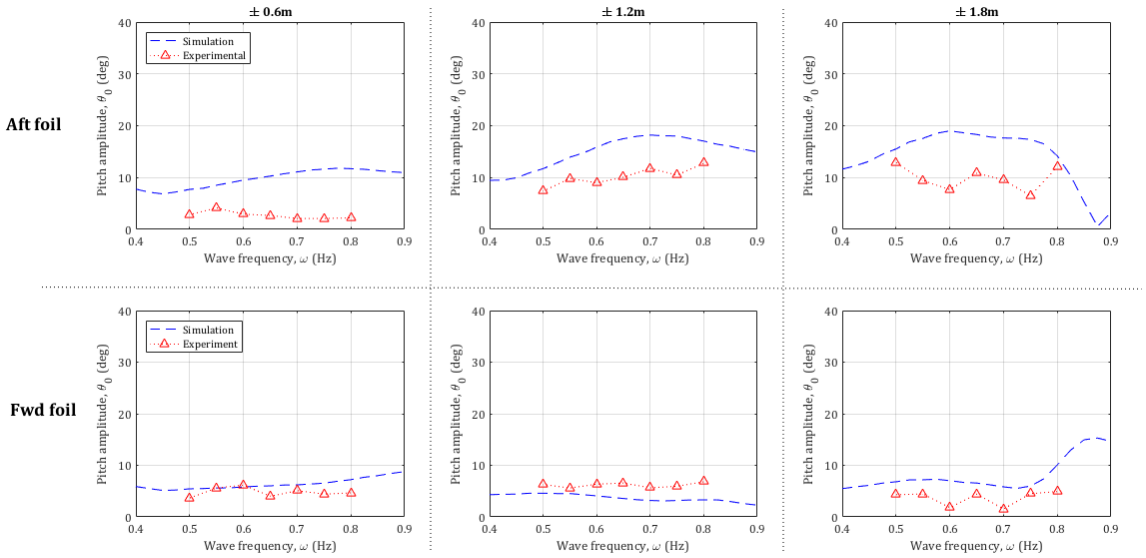

(b) Following waves

Figure 4.34: Numerical and experimental comparison of foil pitch

The flapping phase, ϕ, is defined as the phase difference between the foil heave and pitch, shown in Figure 4.35. Figure 4.36 presents the numerical and experimental results for the forward and aft flapping phase. The numerical results for the flapping characteristics show good agreement with the experimental results, especially with regard to the differences between the forward and aft foil. Unfortunately, it was not possible to capture the flapping phase of the foils in following waves due to a limited motion capture time, which was due to an increase in forward speed in following waves

and a decrease in the flapping frequency.

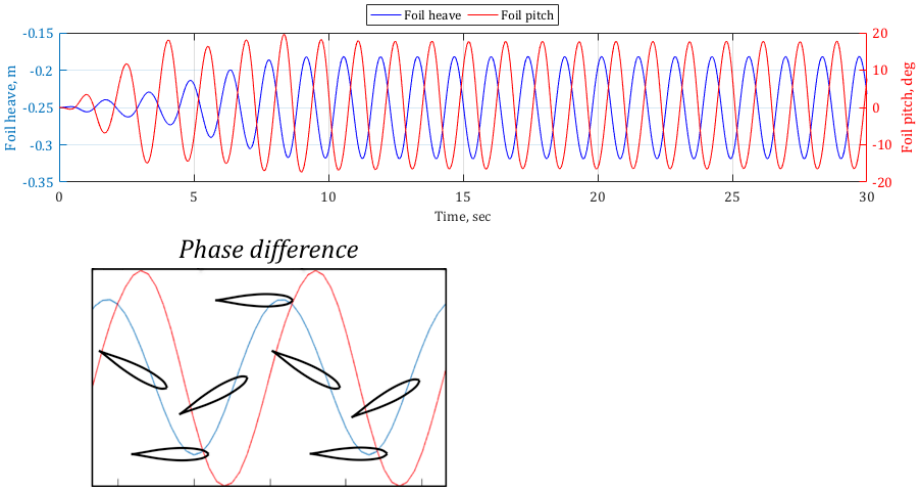

Figure 4.35: Definiton of flapping phase from time domain numerical simulation

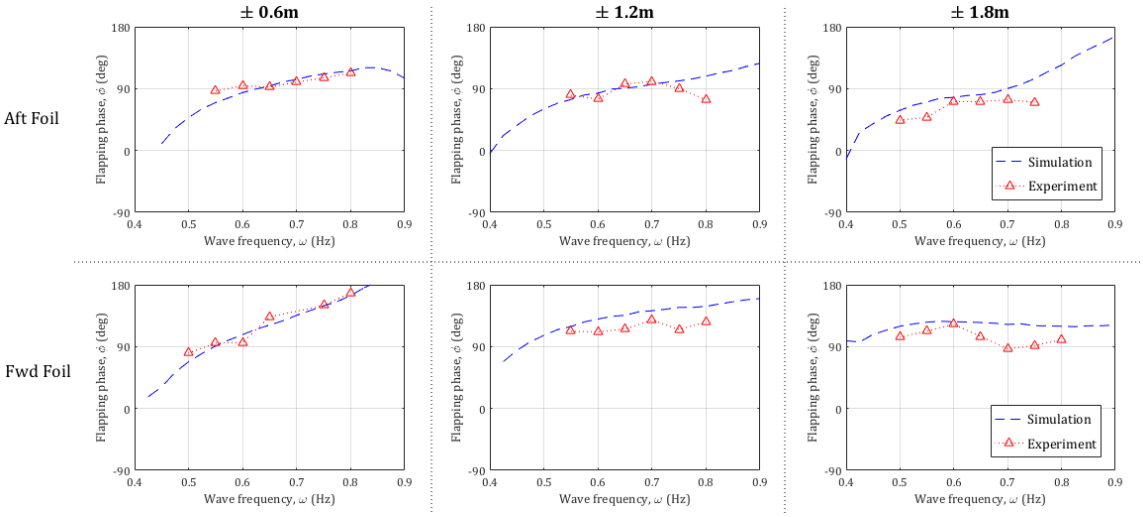

Figure 4.36: Comparison of the forward and aft foil flapping phase in head waves

4.5.4 Summary

The comparisons with experimental data shows that the numerical model, in general, adequately captures the free running forward speed of a wave propelled vessel. An obvious exception is the case where the foils are located closest to the vessel's LCG in following waves. Therefore, for following

waves, the validity of the numerical model is restricted to cases where the foils are located either at or beyond the aft and forward perpendiculars.

With regard to vessel motions, the numerical model captures the effect of the foil location on the vessel pitch and heave, but in following waves the numerical results are considerably different to that of the experiments. The most likely explanation for this discrepancy is the use of the strip theory method in following waves. However, it is difficult to use this explanation for vessel heave in following waves because the experimental results are thought to include an erroneous element of pitch induced heave. Furthermore, the numerical model does not include the diffraction or scattering of incident waves by the forward foil and, as the foil represents a relatively large wetted surface area in comparison to the hull, the unsteady incident wave pressure acting on the hull will be significantly decreased by the presence of the forward foil. This could explain the overestimation by numerical model of the vessel response at higher wave frequencies.

With regard to the foil motions, both the numerical and experimental results are in good agreement, and show a significant difference between the response of the forward and aft foil, for both flapping amplitude and phase. The results confirm that mounting a foil at the forward perpendicular is preferable in head waves, whilst mounting a foil at the aft perpendicular is preferable in following waves. This difference for head and following waves can be partly accounted for by the kinematic motions of the vessel, which are explained in Chapter 6.

4.6 Restrained, wave energy recovery

The preliminary experiments identified that it was possible to recover energy utilizing the relative motion of submerged flapping foils. However, the estimation of power generation was approximate, and based upon the energy absorbed by a damper rather than an actual power take off device. Therefore, the following objectives were set for this series of experiments:

1. Analysis of power generation, to include PTO, over a range of wave frequencies and wave amplitudes.
2. Assess the effect on vessel motions due to the presence of submerged foils, which are free to heave.

4.6.1 Methodology

Energy recovery experiments were performed in the 60m tank with the model secured to the carriage. The model was constrained in head waves, and the flapping foils were free to move relative to the permanent magnet tubular linear generators (PMTLGs), mounted above the forward and aft foils (see Figures 4.37 and 4.38). The PMTLG devices are capable of converting linear drive into electrical power through electromagnetic induction by the movement of a permanent magnet rod within a series of coils.

The foil was constrained by the damping of the generator and a restoring spring force. The damping force is an opposing electromotive force (emf) exerted on the permanent magnet rod due to the current induced in the stator coils. A load of 0.47 ohms was applied to the PTO circuit and the voltage recorded. The PMTLG devices used are Servotube STA1108 actuators, which have inbuilt Hall sensors to measure the position of the rod. The actuators are designed as linear drive systems rather than generators, and, therefore, the efficiency of this device for energy recovery is low. The devices can also be used for actively driven flapping foil propulsion and the FLEUR model has been used to demonstrate this, but is outwith the scope of this thesis.

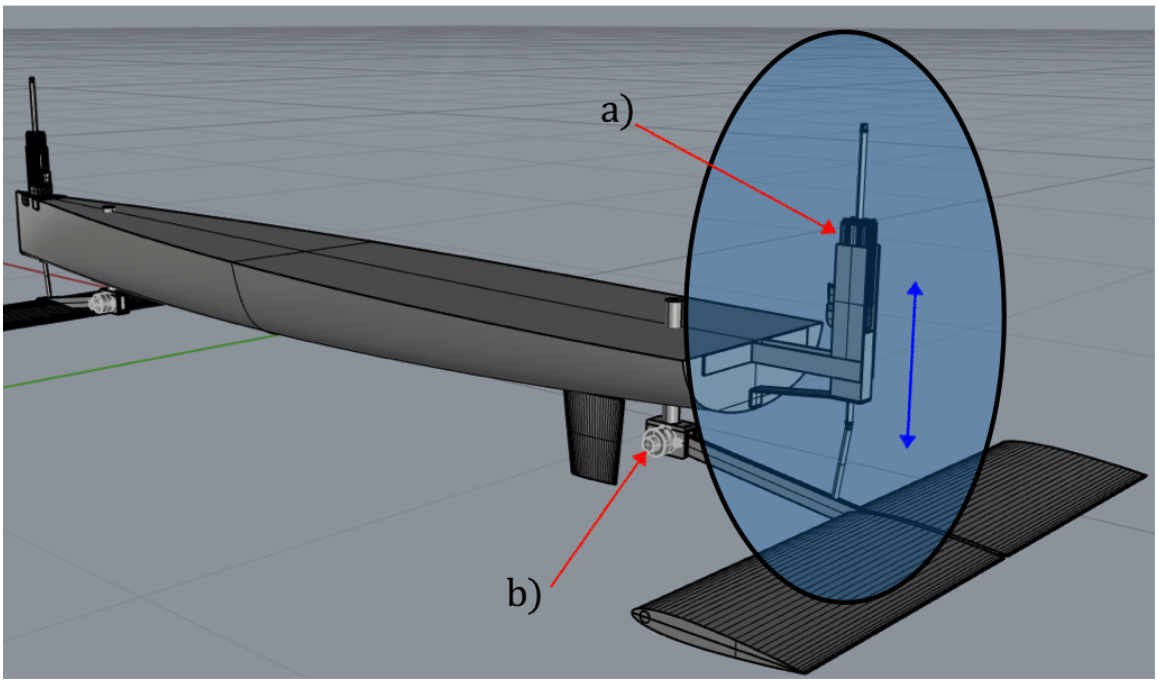

Figure 4.37: General arrangement of the power take-off unit; a) PMTLG device secured above the foils with the thruster rod connected to the foil; b) Rotational spring for pivot arm

The power cables and hall sensor wires were fed back to the carriage where the position of the submerged foils and the generated power was recorded. During each test, the wave height, vessel motions, relative foil position and induced voltage was recorded. The tests were repeated three times, and carried out in a range of regular waves at two different waves heights (0.12m and 0.18m) and a range of wave frequencies (0.4 - 1.0 Hz) at increments of 0.1 Hz. In order to analyse the difference in the vessel motions for fixed and free foils, the same experiments were repeated but with the foils fixed.

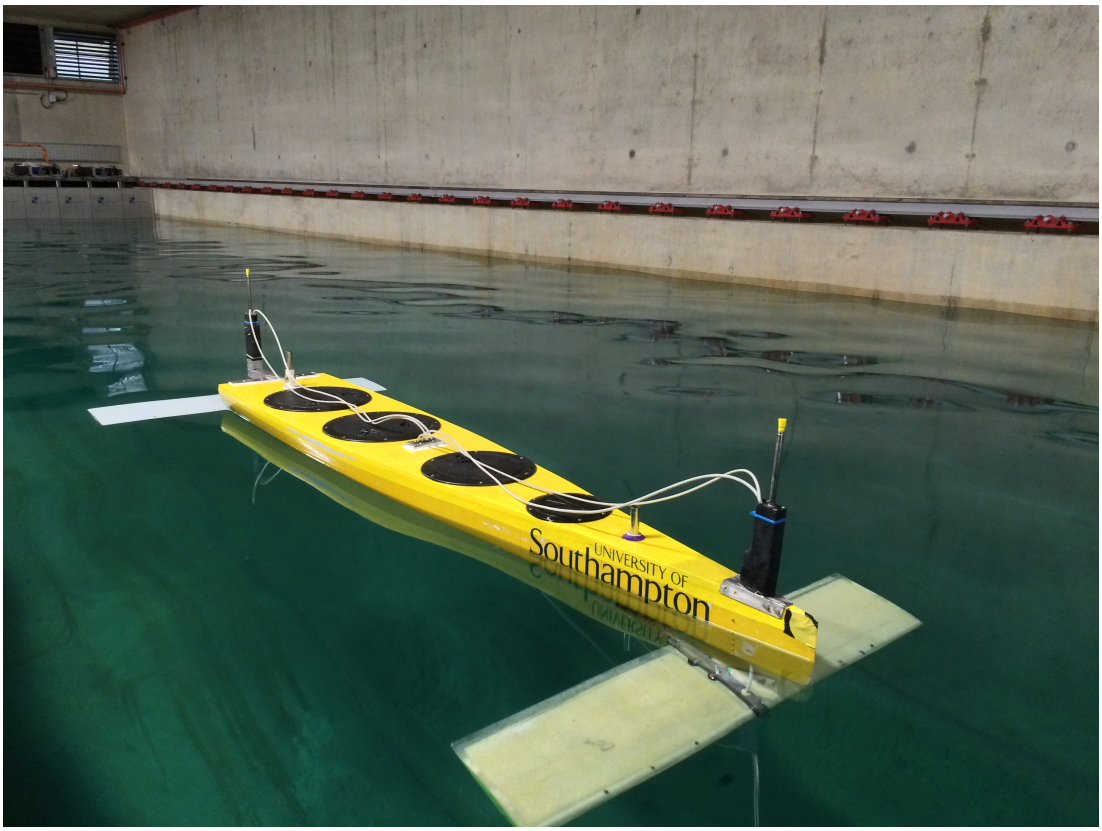

Figure 4.38: Photo of the experimental platform with PMTLG devices fitted at the bow and stern of the model

4.6.2 Results

Foil motions

The circled parts of Figure 4.39 show the change in relative position of the thruster rod which directly relates to the position of the forward foil (an underwater view is shown in Figure 4.40). The submerged foil is effectively acting as a sea anchor which resists the induced motions from the hull through a drag force acting on the foil.

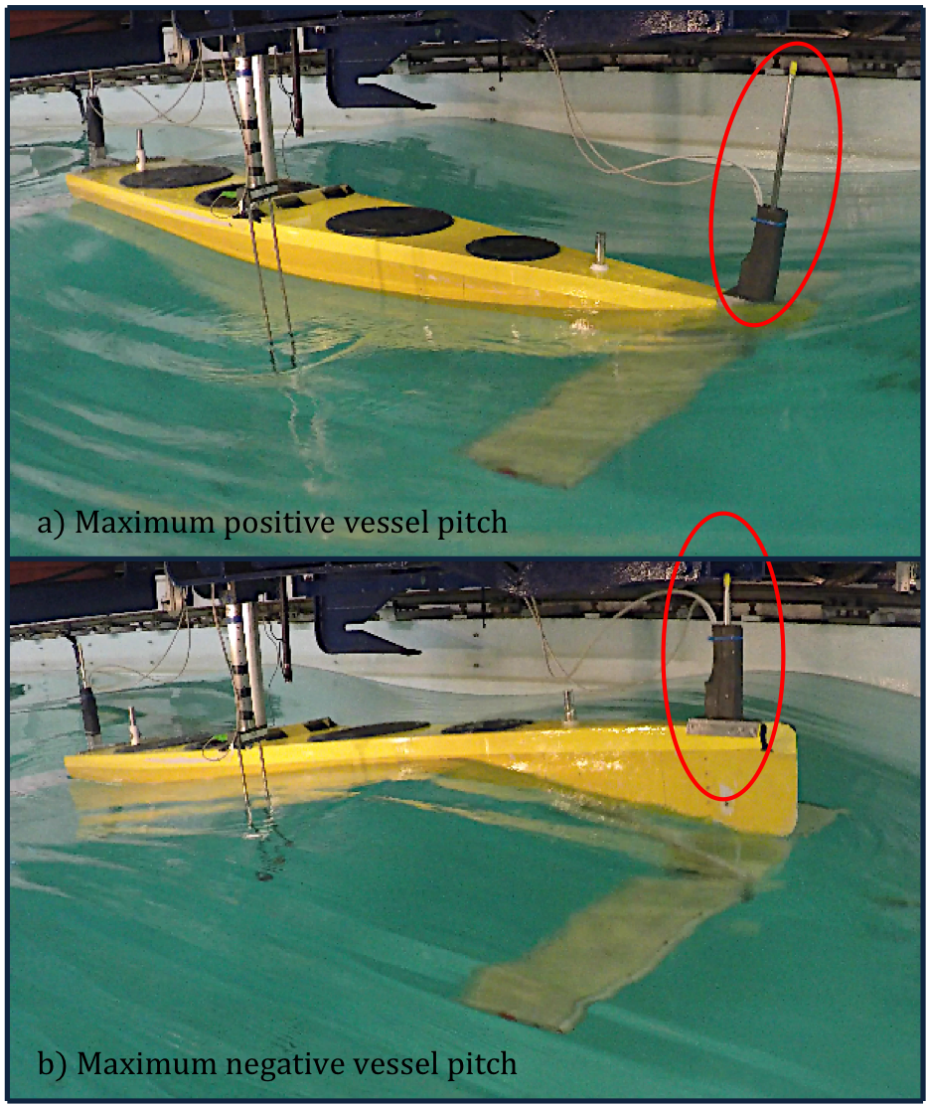

Figure 4.39: Minimum and maximum thruster rod positions for PMTLG energy recovery ($\zeta_a = 0.09$m, $\omega = 0.7$ Hz)

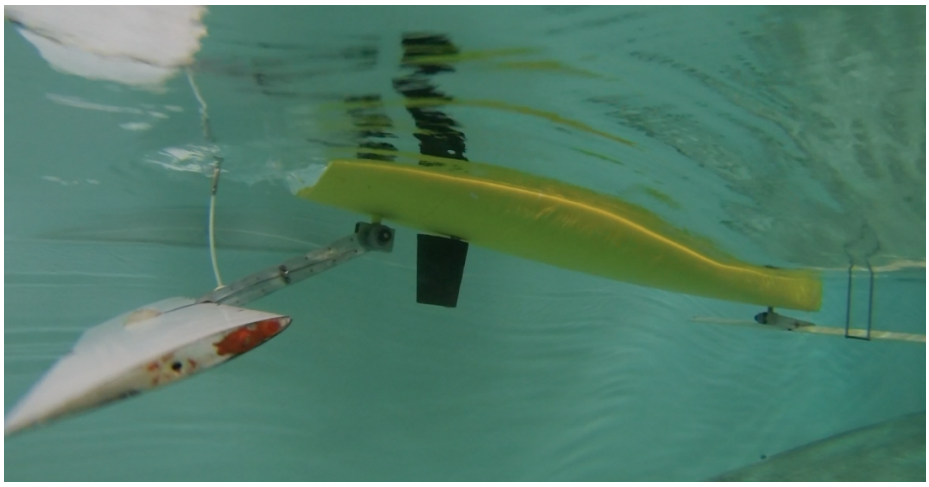

Figure 4.40: Underwater view of PTO setup - maximum positive vessel pitch ($\zeta_a = 0.09$m, $\omega = 0.7$ Hz)

A time history of the wave energy recovery experiment is shown in Figure 4.41. Although the tow post fixing is positioned close to the vessel's LCG, the effective motion of the aft foil is considerably less than that of the forward foil. This is true for all the energy recovery tests and a summary of the effective foil motions is presented in Figure 4.42a.

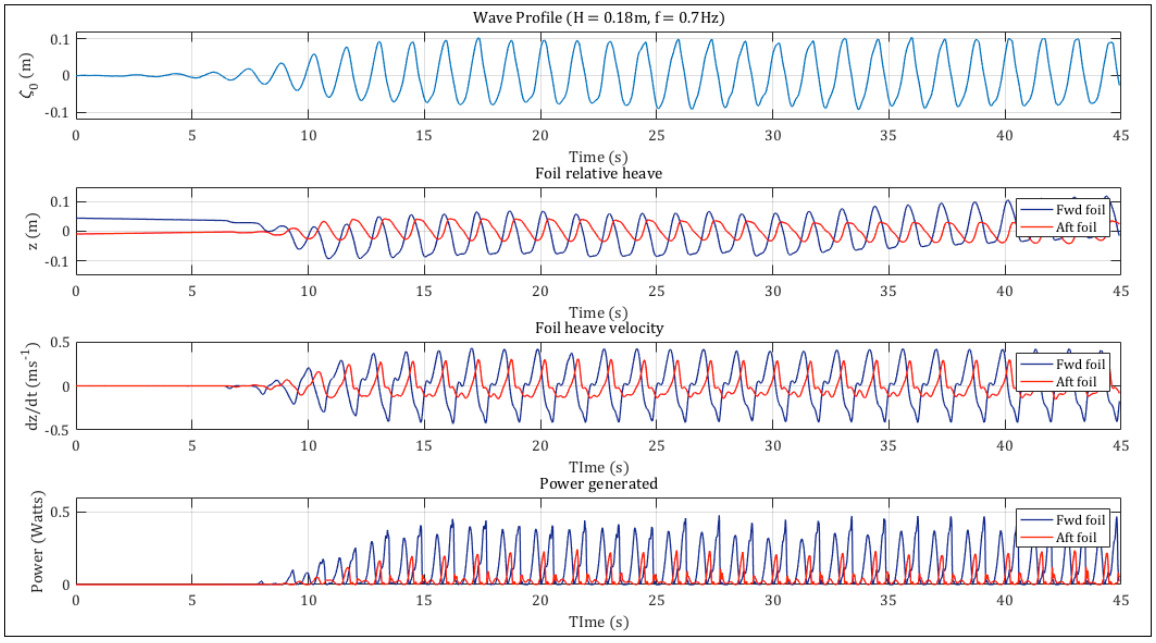

Figure 4.41: Example time history of wave profile, relative foil motions and corresponding power generation for a regular wave ($\zeta_a = 0.09$m, $\omega = 0.7$Hz)

The error bars shown in Figure 4.42a represent the standard deviation of the the results. Overall it is shown that the experiments are very repeatable with the majority of standard deviations at each wave frequency and amplitude less than 5% of the mean value. Directly comparing the response of the forward and aft foils across the entirety of all the runs yields the result that the motion of the aft foil is approximately 45% less than that of the forward foil. The peak effective heave of the foward foil is approximately equal to the wave amplitude and the equivalent transfer function for the aft foil is approximately 0.6.

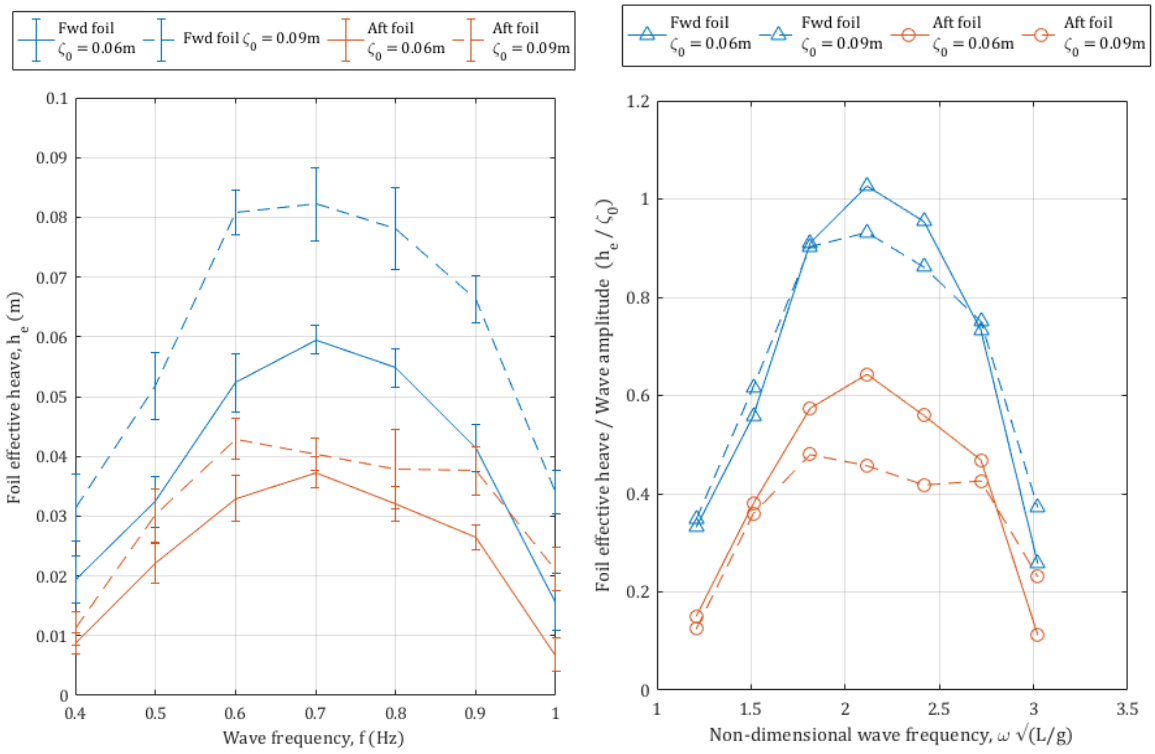

(a) Foil effective heave

(b) Foil transfer function

Figure 4.42: a) Foil effective heave amplitude (error bars represent the overall uncertainty) and b) transfer function of PMTLGs for the forward and aft foils in varying wave heights and frequencies (error bars are reperesentative of the overall uncertainty)

Coupled response: power generation

The power generated by each foil was calculated by measuring the induced voltage over a resistance load of 0.47 Ω on each phase and taking the mean generated power ($\bar{P}_z$) for each test case. From applying linear wave theory, the input wave power for each test can be estimated using the following

definition for wave power, P_w (Watts):

$$P_w = \frac{\rho g H c_g B}{8} \tag{4.8}$$

where H is the wave height, c_g is the wave group celerity or velocity and B is the maximum beam of the surface vehicle, and it is assumed that the surface vehicle is the primary wave converter. This equation for wave power represents the power of the entire water column and is, therefore, only used as a basis energy for each wave frequency for ease of comparison. The energy recovery efficiency can, therefore, be defined as:

$$\eta_{recovery} = \frac{\bar{P}_z}{P_w} \tag{4.9}$$

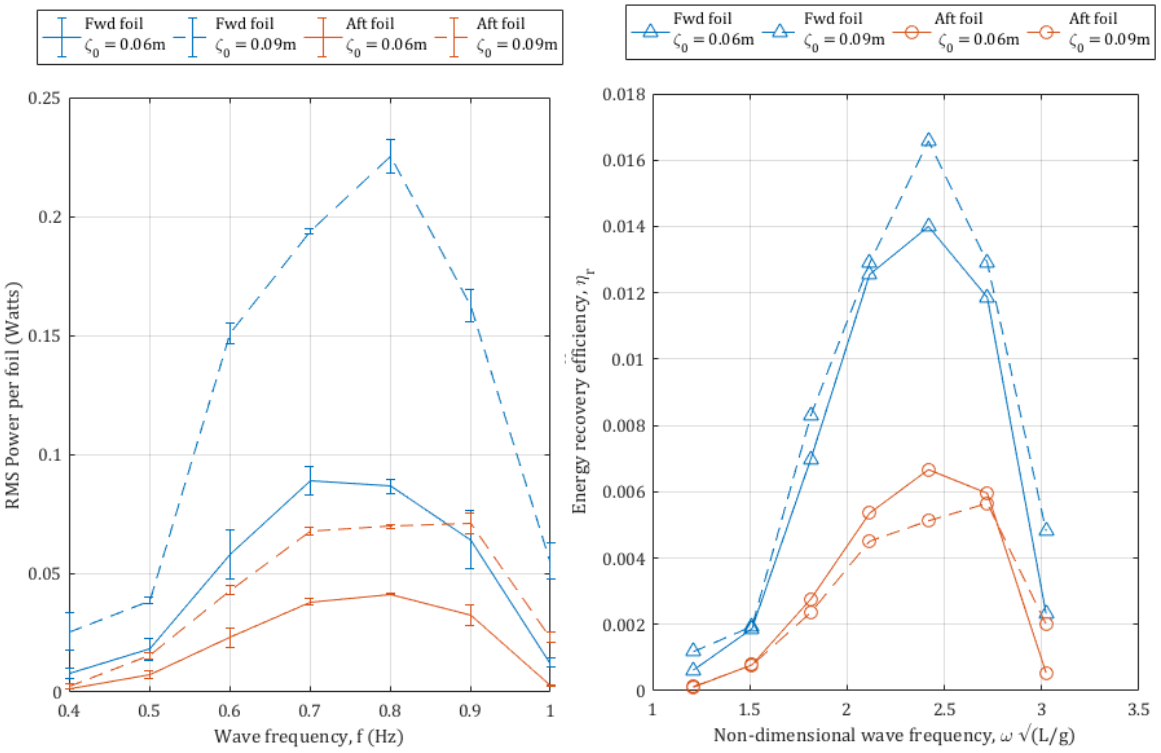

(a) RMS generated power

(b) Energy recovery efficiency

Figure 4.43: a) RMS power generated (error bars represent the overall uncertainty) and b) PTO efficiency of PMTLGs for the forward and aft foils in varying wave heights and frequencies

Figure 4.43 shows the resulting RMS generated power and energy recovery efficiency with respect to wave frequency. Reasonable repeatability is found with the experiment, and the same trend with respect to wave frequency is found for both the forward and aft foil. The recovery of wave energy in this case is shown to be fairly inefficient, but this is mostly due to a suboptimal PTO setup. However, the experiments have highlighted several key issues for the application of using submerged flapping foils as wave energy recovery devices. Most notable is the frequency dependent response of the system. Like most wave energy devices there is a significant peak in the generation of power about the resonant motion of the wave energy converter, i.e the hull. For the median wave frequencies (0.5-0.9 Hz), the mean generated power is almost directly proportional to the square of the wave height (12 and 18 cm):

Fwd foil: $\frac{\bar{P}_{18}}{\bar{P}_{12}} \simeq 1.1 \times \frac{H_{18}}{H_{12}}^2$

Aft foil: $\frac{\bar{P}_{18}}{\bar{P}_{12}} \simeq 0.9 \times \frac{H_{18}}{H_{12}}^2$

Vessel motions

Figure 4.44 b) shows the transfer functions for pitch in regular waves of varying height and frequency. There is a reduction of up to 50% in the vessel pitch amplitude due to the presence of the foils when in the fixed foil condition, which is similar to the results of (Bockmann 2015). Figure 4.44 a) shows that the heave motion of the surface vehicle remains relatively unchanged with or without the foils free to move, which agrees with the preliminary and free running results.

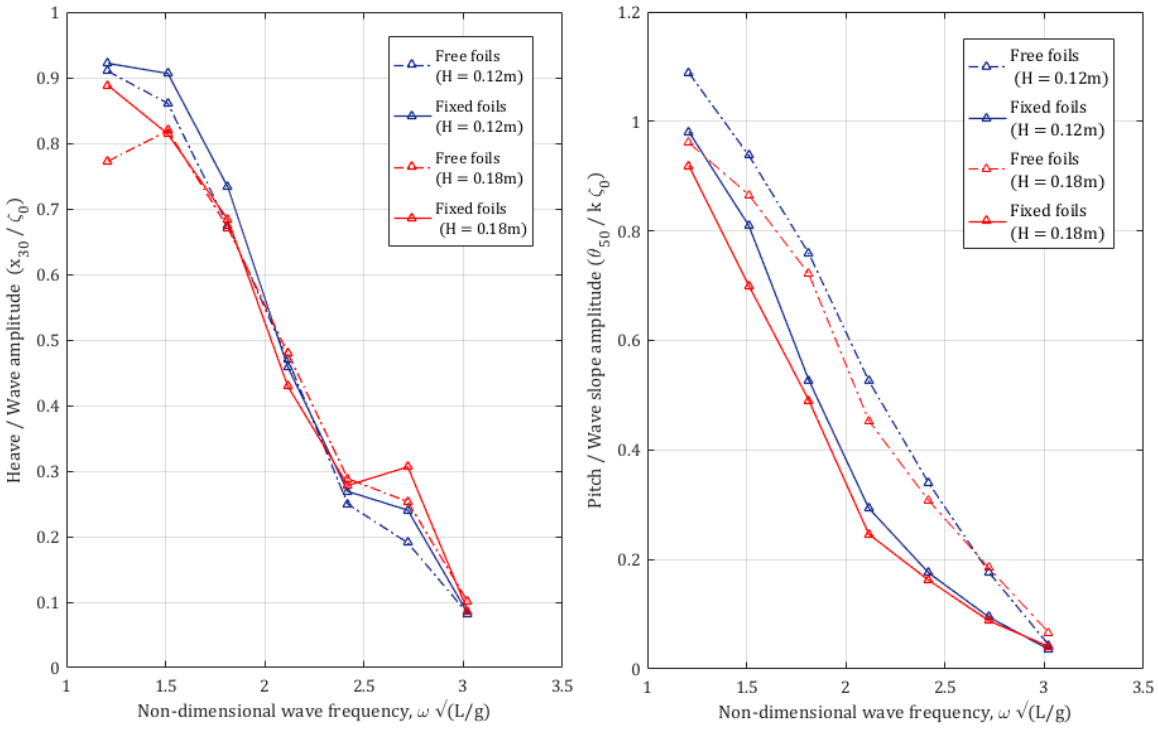

(a) Heave (b) Pitch

Figure 4.44: Effect of submerged foils on the vessel motions in different wave amplitudes

4.6.3 Validation

For the purposes of validating the numerical model in relation to the actual power generated rather than the theoretical equivalent, the electromechanical energy conversion has been modelled to simulate the PMTLG used in the experiments. Details of the PMTLG numerical modelling are presented in Section 3.4.1.

Foil motions

Validating the numerical model against the experimental foil relative heave and the hull motions during energy recovery involved securing the vessel to the stationary carriage and testing in head waves only. Therefore, for the purposes of validation, the forward speed of the vessel is set to zero for the numerical simulations. Figure 4.45 shows the nondimensional effective heave of the forward and aft foil, which is equivalent to the position of the permanent magnet rod relative to the PMTLG

device.

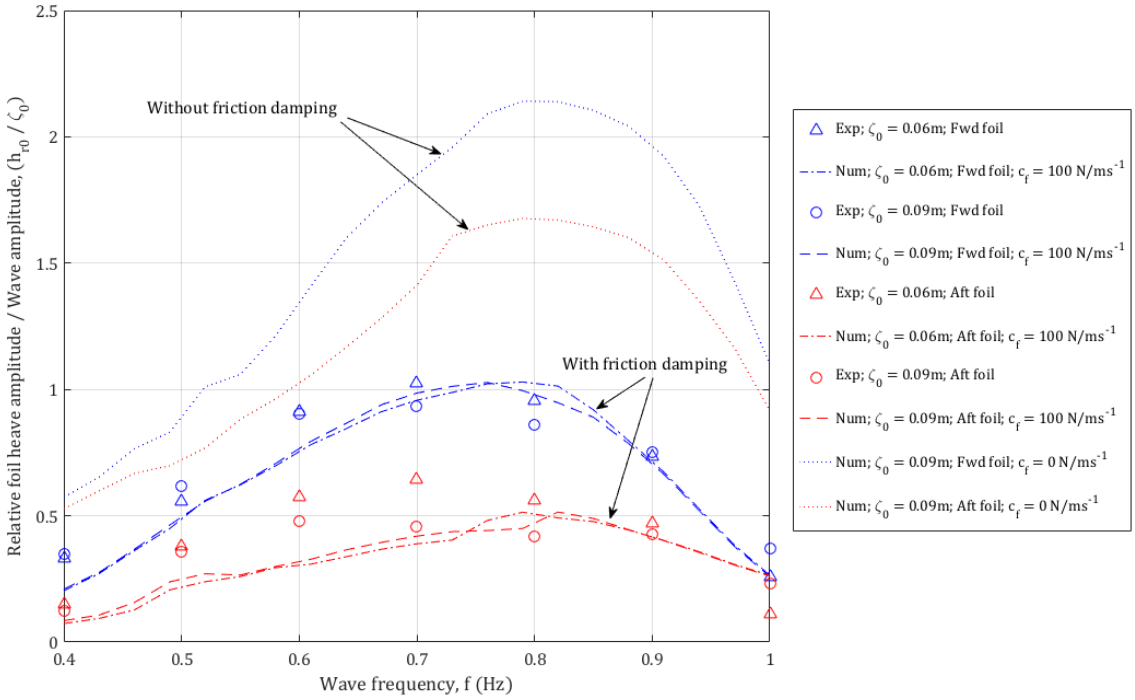

Figure 4.45: Numerical and experimental results of the relative foil heave for the forward and aft foils, nondimensionalised with respect to the wave amplitude (ζ_a = 0.06m and 0.09m

Without the consideration of frictional losses or other additional damping effects the numerical model significantly overestimates the response of the foils in comparison to the experimental data. However, the inclusion of a frictional or an additional damping force in the numerics yields results that show good agreement with the experimental data. Most notably, the numerical results also agree with the experimental data in relation to the response of the aft foil, which is almost half that of the forward foil. Both the numerical and experimental results show a linear response with respect to wave amplitude.

Power generation

Figure 4.46 shows the energy recovery efficiency comparison between the numerical and experimental results. The numerical model captures the large differences between the response of the forward and aft foils, and the peak power generated with respect to wave frequency shows reasonable agreement with the experimental data. Figure 4.46 also identifies the difference between an ideal power take

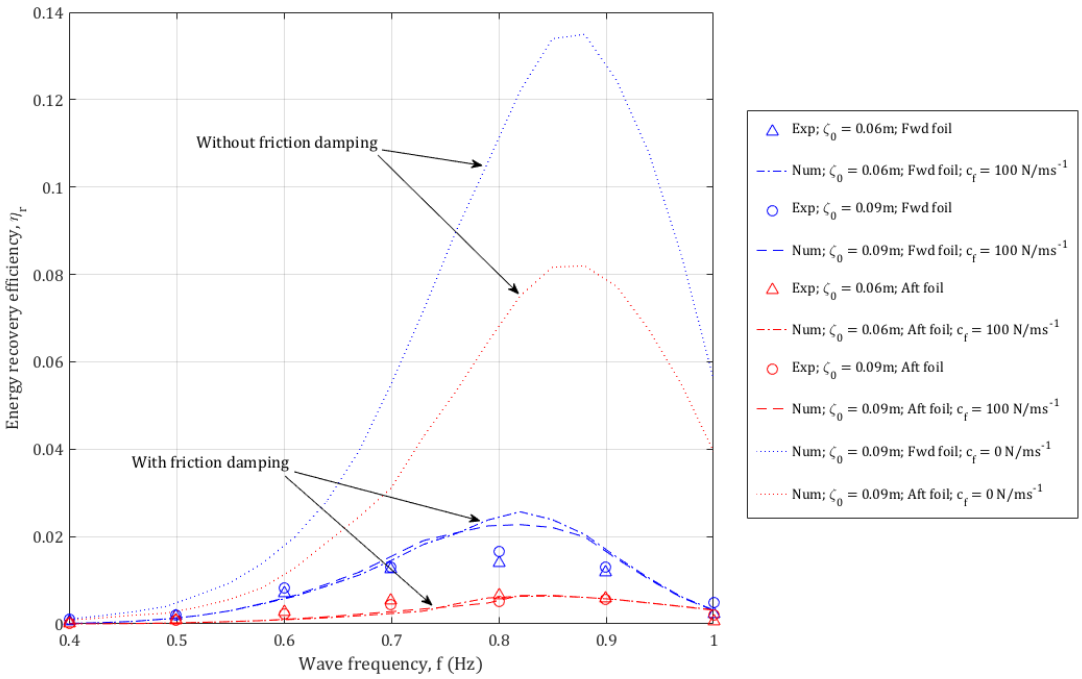

Figure 4.46: Numerical and experimental comparison for the energy recovery efficiency of the aft and forward foils at two different wave amplitudes; 0.06m and 0.09m

off setup with zero friction and an unoptimized setup like the experimental platform.

Vessel motions

Figure 4.47 shows the numerical and experimental results of the vessel motions with the foils free to heave relative to the vessel, i.e. in the wave energy recovery mode. The numerical results for the vessel motions are in strong agreement with the corresponding experimental data. Figure 4.47 also includes the numerical result for the ideal case without an additional frictional or damping force. The numerical results are consistent with the experimental results, both showing that a reduction in the damping force effectively reduces the opposing force acting on the vessel and, therefore, reduces the stabilizing effect of the submerged foils with respect to the vessel pitch.

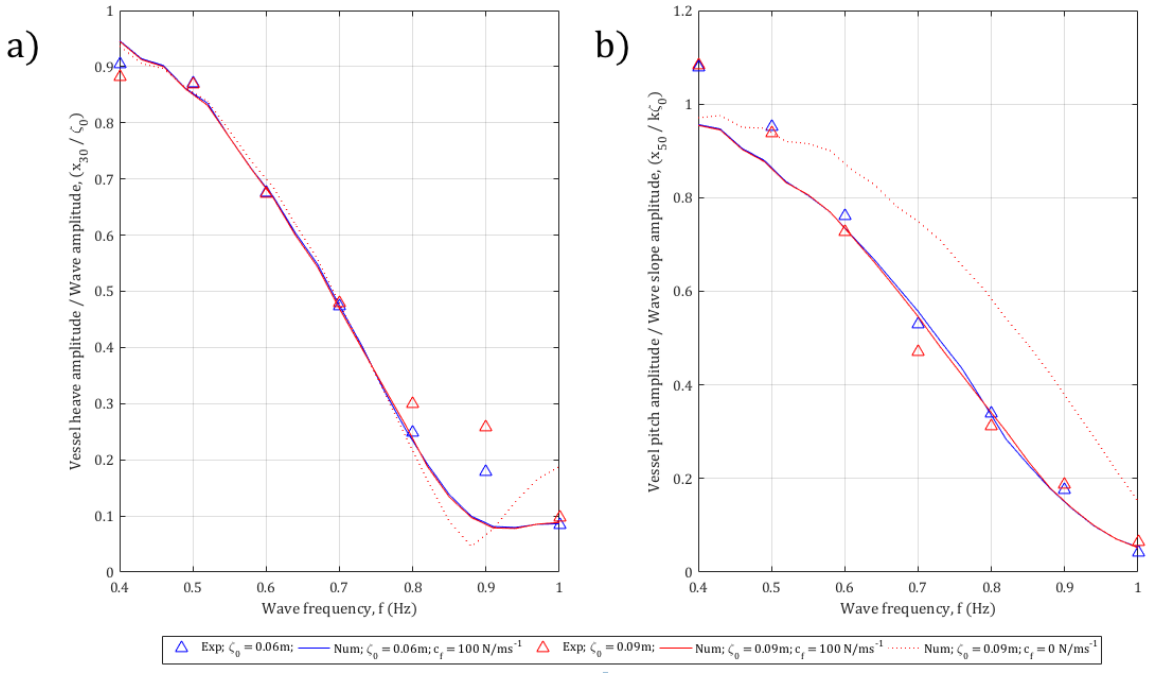

Figure 4.47: Comparison between numerical and experimental results for the vessel a) heave and b) pitch reponse with the foils free to heave relative to the vessel and for two different wave amplitudes; 0.06m and 0.09m

4.6.4 Summary

With a consideration for frictional losses, a reasonable agreement is found between the experimental and numerical results, and this validates the numerical method described in Section 3.4.1. The numerical model can, therefore, be applied as an optimization tool for improving wave energy recovery for a wave powered vessel.

Both the numerical and experimental results show a significant difference between the response of the forward and aft foils, which agrees with the free running wave propulsion results. This is principally due to the kinematics of the vessel motions, but also associated with the relative flow of the local wave particles, which is explained in more detail in Chapter 6.

Without the incorporation of an additional damping factor, the numerical results are shown to significantly overestimate the relative heave of the foil, which also results in an overestimaton of the power generated. However, increasing the damping force acting on the foil reduces the relative motion of the foil considerably, and results in an accurate prediction of the power generated. This suggests that either the numerical model is not capturing additional forces such as friction or the model is underestimating the opposing electromagnetic force acting on the permanent magnet rod. Future work, beyond the scope of this research, is required further investigate this aspect of wave energy recovery.

In conclusion, the experimental results prove that it is possible to recover energy from incoming waves using the submerged foil setup.

Chapter 5

Numerical simulations of the coupled response

The validated numerical model provides the capability to: comprehensively investigate the coupled dynamics of a wave powered vessel; predict the forward speed of the vessel; and estimate the potential for power generation. The aim of this chapter is to investigate, through numerical simulations, the effect of the following key areas on the coupled response of a wave powered vessel; wave parameters, foil particulars and hull shape.

The simulation method applies the numerical algorithm described in Chapter 3. The parameters for investigation are shown in Table 5.1. For the foil and vessel particulars, the input variables are discretised over a suitable range and simulations are performed with respect to wave frequency. For energy recovery analysis, the number of parameters for investigation has been significantly reduced as the problem is less complex in terms of hydrodynamics.

The wave amplitude and frequency is analysed initially to assess the linearity of the response and the frequency dependency. Using the same FLEUR hull form from the experimental analysis, simulations are carried out for wave propulsion in head and followings waves, and for wave energy recovery with a zero forward speed. Changes to foil particulars, including location, size, spring constant and PTO damping, are applied for a foil located aft of amidships and another located forward of amidships. The investigation of the effect of the hull form on the response is carried

Table 5.1: Simulation parameters for investigation

	Parameters		
Mode	**Wave**	**Foil (Fwd & Aft)**	**Hull** (Wigley form)
Wave propulsion	Amplitude Frequency	Size Location Spring	Waterplane area coef. Length/beam ratio Length/draught ratio
Energy recovery	Amplitude Frequency	PTO damping	-

out for varying shapes of the Wigley hull form, which is defined by a constant length (L = 3m) and proportions altered by a change in length to beam or draught ratios. This hull form has been extensively used for seakeeping research, and is a convenient reference hull form that can be described in a single formula (Wigley 1934):

$$y(x,z) = \frac{B}{2}\Big[1 - \big(\frac{2x}{L}\big)^2\Big]\Big[1 - \big(\frac{z}{T}\big)^2\Big] \tag{5.1}$$

Further simulations investigate the effect of scale on nondimensional parameters, and assess the similiarity of the coupled response. For this analysis, the Wigley hull form was scaled using the length parameter and by maintaining geometric similiarity.

5.1 Wave parameters

Wave propulsion

Figure 5.1 presents the numerical results of the free running forward speed for varying wave amplitudes and frequencies in head waves. It can be seen that the results vary considerably with wave frequency and the peak forward speed is achieved at a frequency of 0.65-0.7 Hz. An incremental increase in the wave amplitude is shown to increase the forward speed of the vessel but the response is not directly proportional.

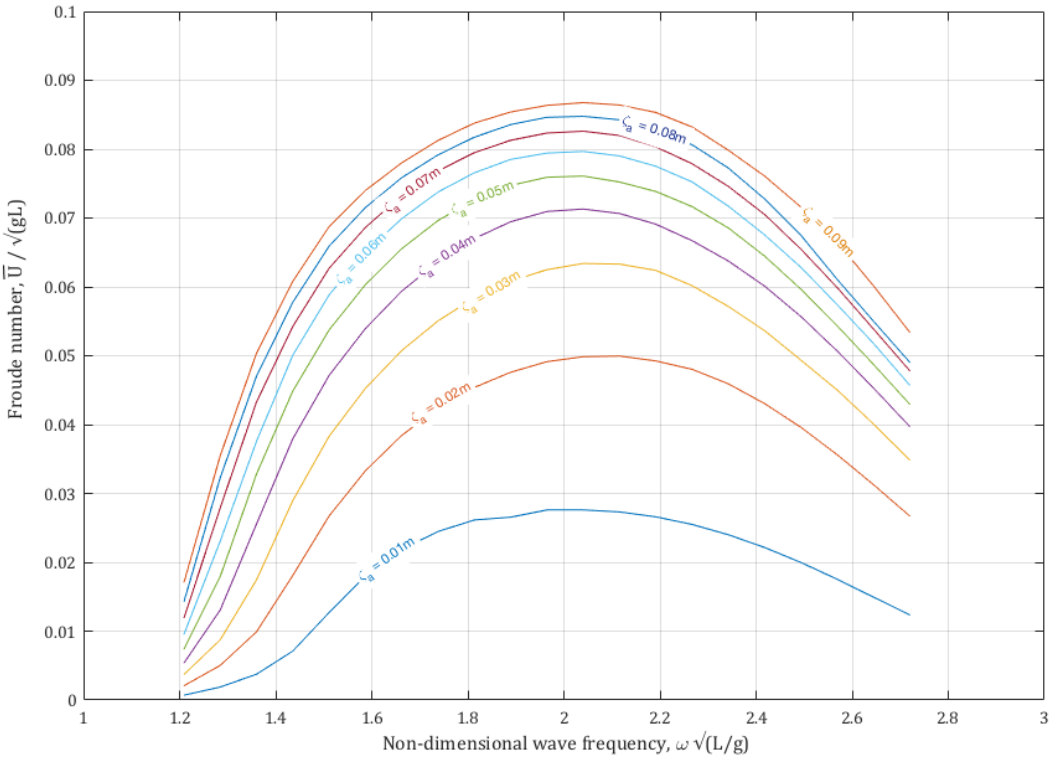

Figure 5.1: Mean non-dimensional vessel forward speed response for a range of wave parameters in head seas; amplitude (ζ_a) in metres and wave frequency

The steady state forward speed is achieved at the point at which the wave-induced thrust is matched by the total resistance of the vessel, i.e. the acceleration is equal to zero. The components of total resistance can be separated into speed dependent drag, such as viscous (form drag) and skin friction, and wave dependent drag (added resistance due to waves), which is a function of the vessel motion. The viscous and skin friction drag is proportional to the square of flow speed whilst the wave dependent drag is proportional to the square of the wave amplitude.

Assuming that the wave-induced thrust force is also proportional to the square of the wave amplitude, this force is directly proportional to the added resistance due to waves, and a directly proportional forward speed response would be expected. However, the speed dependent drag becomes the limiting factor in the vessel's response at higher forward speeds and, hence, higher wave amplitudes.

Figure 5.2 uses the same data as Figure 5.1, but plotted with the wave amplitude on the x-axis. This figure clearly shows the effect of the speed dependent drag for wave frequencies other

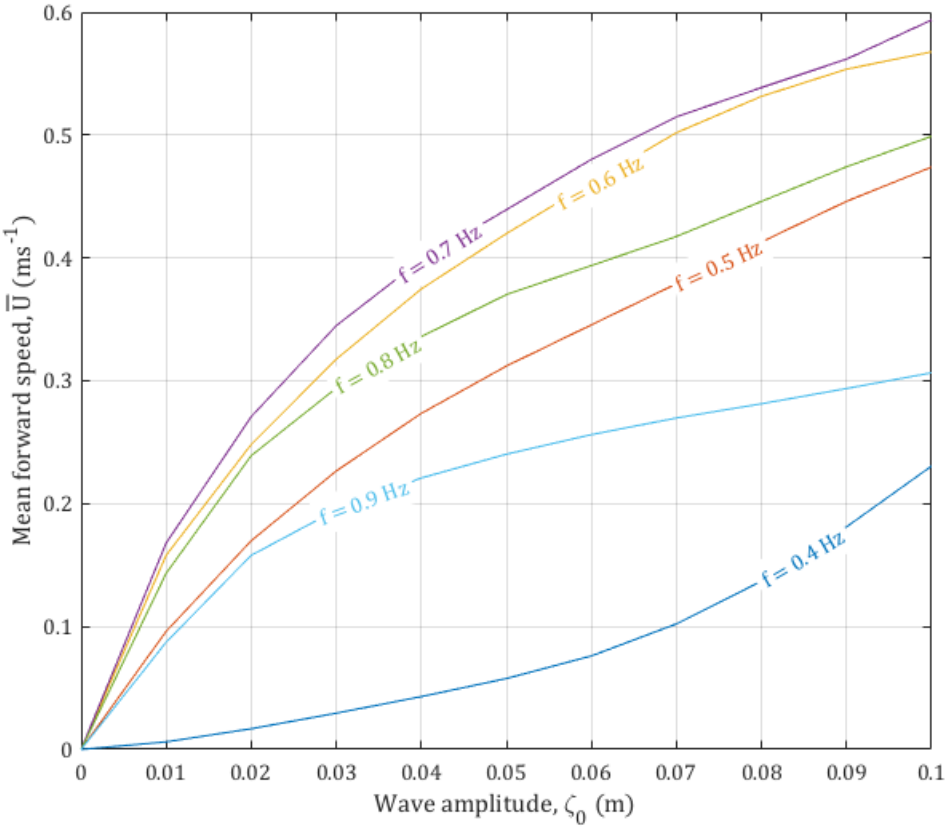

Figure 5.2: Mean vessel forward speed response for increasing wave amplitude in head seas at varying wave frequencies

than 0.4 Hz. The most noticeable difference in proportionality is between the highest and lowest frequency, which agrees with the free running experimental analysis conducted by Isshiki in varying wave heights (Isshiki 1994). This difference can be attributed to the Doppler effect. In head waves, and for wave frequencies lower than the peak frequency of 0.65-0.7 Hz, the vessel forward speed results in a shift towards the peak frequency. In contrast, for higher wave frequencies, a forward speed results in a shift away from the peak response. As the response of the vessel is very frequency dependent, this effect is magnified at lowest and highest wave frequencies.

For following waves, the opposite effect occurs, which is clearly reflected in the peak forward speed response with respect to wave frequency as shown in Figure 5.3. The peak response is achieved at a wave frequency of approximately 0.8 Hz. This is also a result of the Doppler effect which shifts the encountered wave frequency towards the resonant frequency of 0.65 Hz for high wave frequencies and amplitudes. This highlights the importance of the effect of forward speed on the vessel motions,

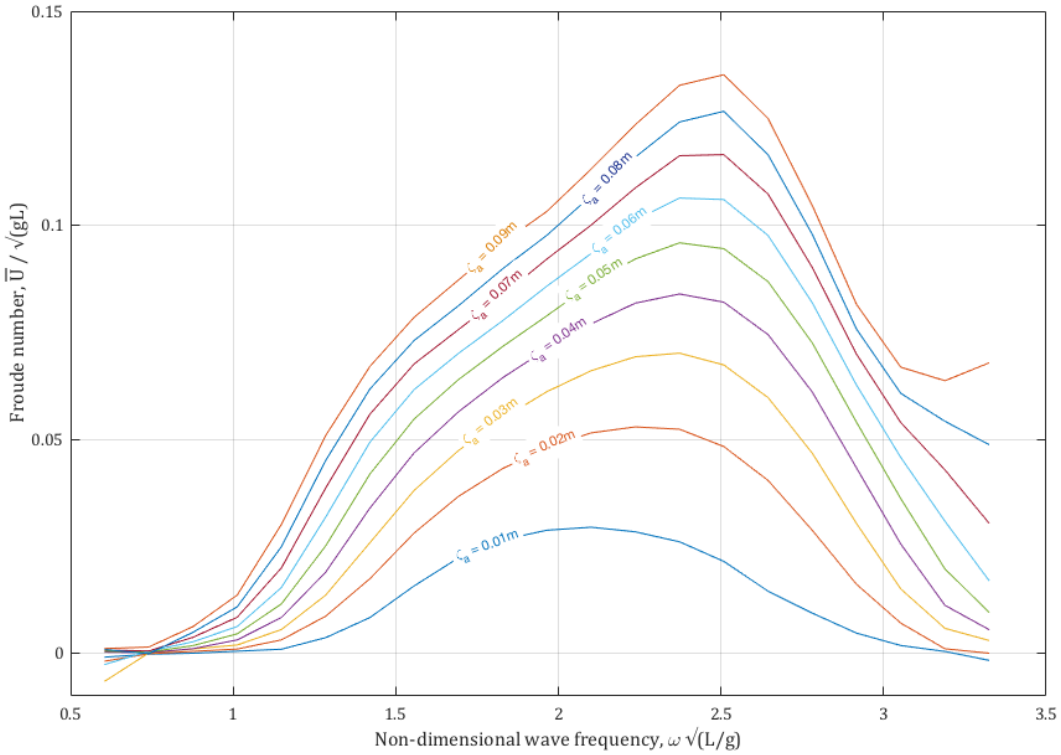

Figure 5.3: Mean non-dimensional vessel forward speed response for a range of wave parameters in following seas; amplitude and wave frequency

showing that the two responses are interdependent. As with head waves, the speed dependent drag term becomes more dominant with increasing forward speed, and hence limits the response of the vessel with respect to wave amplitude.

Energy recovery

Figure 5.4 shows the total average power generation from both the aft and forward foil in fixed (zero speed) condition with increasing wave amplitude. For consistency, the simulation used the FLEUR hull form and the validated PMTLG method for calculating the power take-off. The simulations include a consideration for energy losses with the application of a frictional damping constant of 100 N/ms^{-1}, as discussed in Chapter 4.

The numerical results show that, as expected, the generated power is proportional to the square of the wave amplitude and has a significant frequency dependence with the peak response at exactly

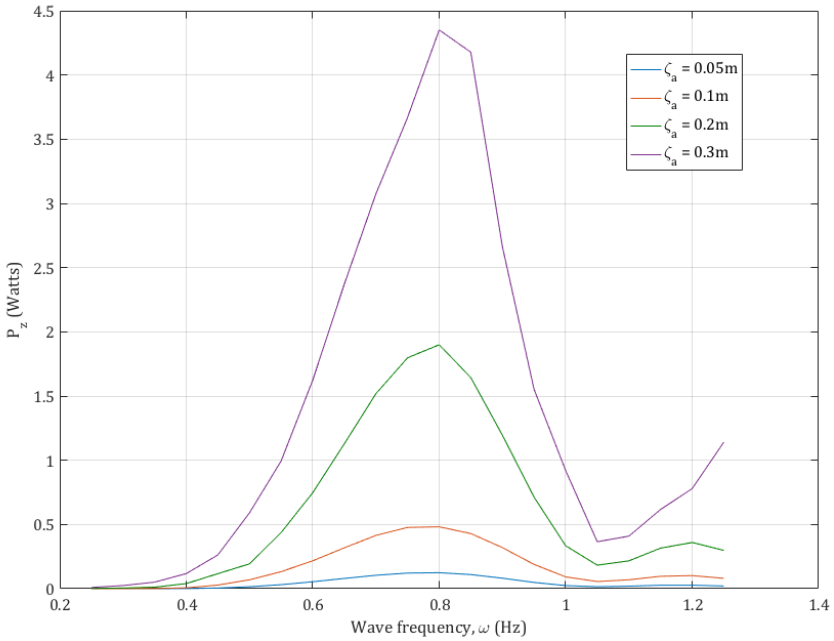

Figure 5.4: Average power recovered for varying wave amplitudes and frequencies

0.8 Hz, which is the same resonant response observed for thrust generation from the constant speed experiments in Section 4.2.2.

The average power generation of 4 Watts in regular waves of 0.3m amplitude and 0.8 Hz is a moderate extraction of power for a wave energy recovery device. It is comparatively small compared to the 125 Watt rated photovoltaic cells installed on a similar sized USV, AutoNaut. However, as explained in the previous Chapter, this includes a consideration for losses such as friction. An improved PTO design, with reduced losses, would significantly increase the power generation performance of submerged flapping foils and could yield an average power of upto 20 Watts in wave amplitudes of 0.3m and at the peak frequency of 0.8Hz. This compares favourably to solar energy recovery considering that the 125 Watt solar rating does not take into account day/night hours or adverse weather conditions such as clouds.

Although it is difficult to directly compare wave and solar energy, recent research has shown that a hybrid system that utlizies wind, wave and solar energy is more effective for a given route, particularly for small vehicles such as USVs (Cao et al. 2017). Therefore, the submerged flapping foil wave energy recovery system could serve as a useful contribution to a hybrid system.

As with the rated power of photovoltaic cells, the prediction of wave energy recovery is based upon ideal conditions (i.e. regular waves), and future analysis is required for short crested irregular waves. In addition, the analysis at higher wave amplitudes is beyond the linearity assumptions of small amplitude motions, and, although the generated power is shown to be directly proportional to the wave amplitude, this law may not be maintained for comparatively large waves. A weakly or fully non-linear simulation and/or further experiments would need to be completed to validate this response at higher wave amplitudes, as depicted in Figure 3.2. Additionally, the power generation is only significant when the waves are large relative to the size of the vessel, which is the case for a small USV in high frequency wind waves: a reasonable peak average power generation could therefore be achieved with USVs. Furthermore, an improved design and a reduction in the mechanical energy losses could result in significant gains in the wave energy conversion efficiency. The effect of wave energy recovery on the propulsive performance of the submerged flapping foils is investigated in Section 5.2.4.

5.2 Foil particulars

5.2.1 Foil location

Following on from the experimental analysis, the effect of foil location has been investigated in more detail to determine whether there is a significant change in the frequency dependent coupled response due to the foil location for different wave frequencies. This analysis has been carried out in head waves because the validity of the numerical model in following waves is only applicable for cases with the foils positioned at or beyond the AP and FP, as highlighted in Chapter 4.

Figure 5.5 shows the forward speed response for varied forward (x_{f1}) and aft (x_{f2}) foil location. The foils are referenced to the LCG as a percentage of the half waterline length. The simulations are repeated over the modal frequency range, and show that the optimum forward speed is, in general, achieved with the foils situated beyond the forward and aft perpendiculars. This result is in agreement with the constant speed numerical analysis for thrust generation carried out by Bockmann and Isshiki (Isshiki & Murakami 1984, Bockmann 2015). There is little evidence to suggest that the wave frequency has a significant effect on this conclusion.

Figure 5.6 shows the change in vessel pitch with forward and aft foil location for different wave

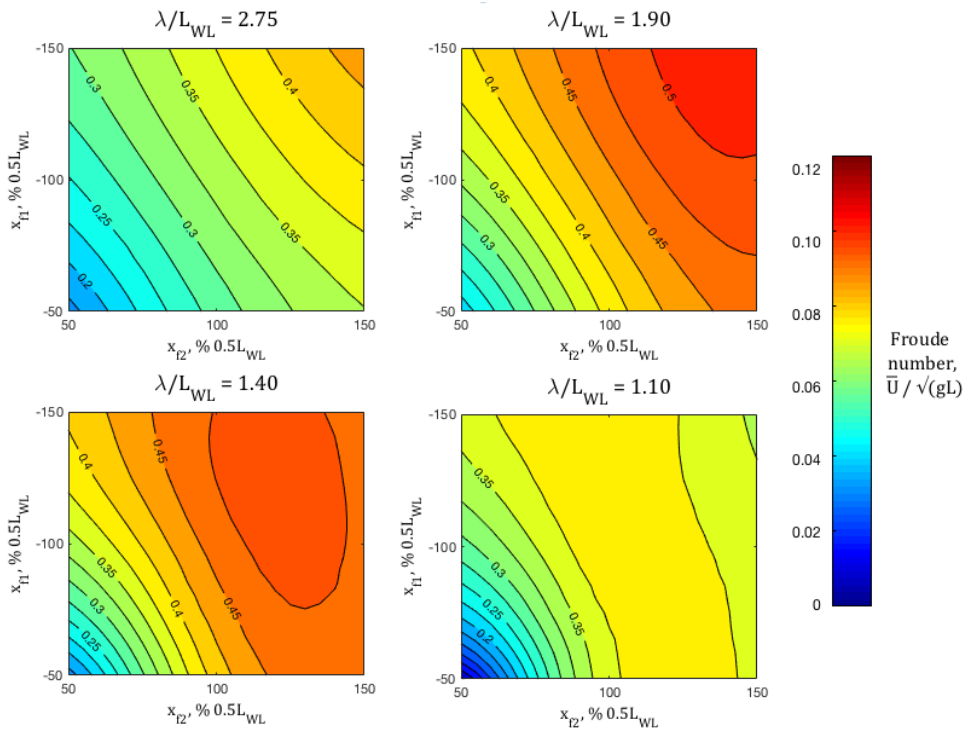

Figure 5.5: Simulation of vessel forward speed with foil location, relative to the vessel LCG ($\zeta_a = 0.06m$)

frequencies. The vessel pitch is significantly reduced as the foil location moves away from the LCG, which is evident from the experimental results and expected due to the increased stabilizing effect of foils situated further away from the LCG.

The vessel pitch is also affected by the encountered frequency of the wave and, therefore, related to the forward speed of the vessel. As the foils are extended beyond the aft and forward perpendiculars there is a significant reduction in the vessel pitch due to both an increased effect from the foils and the effect of the forward speed (encountered wave frequency).

5.2.2 Foil size

The foil size was varied by changing the foil span as a ratio of the vessel beam and maintaining the foil chord at a constant, which is proportional to vessel length ($c/L_{WL} = 0.1$). Figure 5.7 shows the effect of changing foil size on the forward speed response for different wave frequencies in head waves. The forward speed response is represented by the non-dimensional Froude number ($\frac{U}{\sqrt{gL}}$),

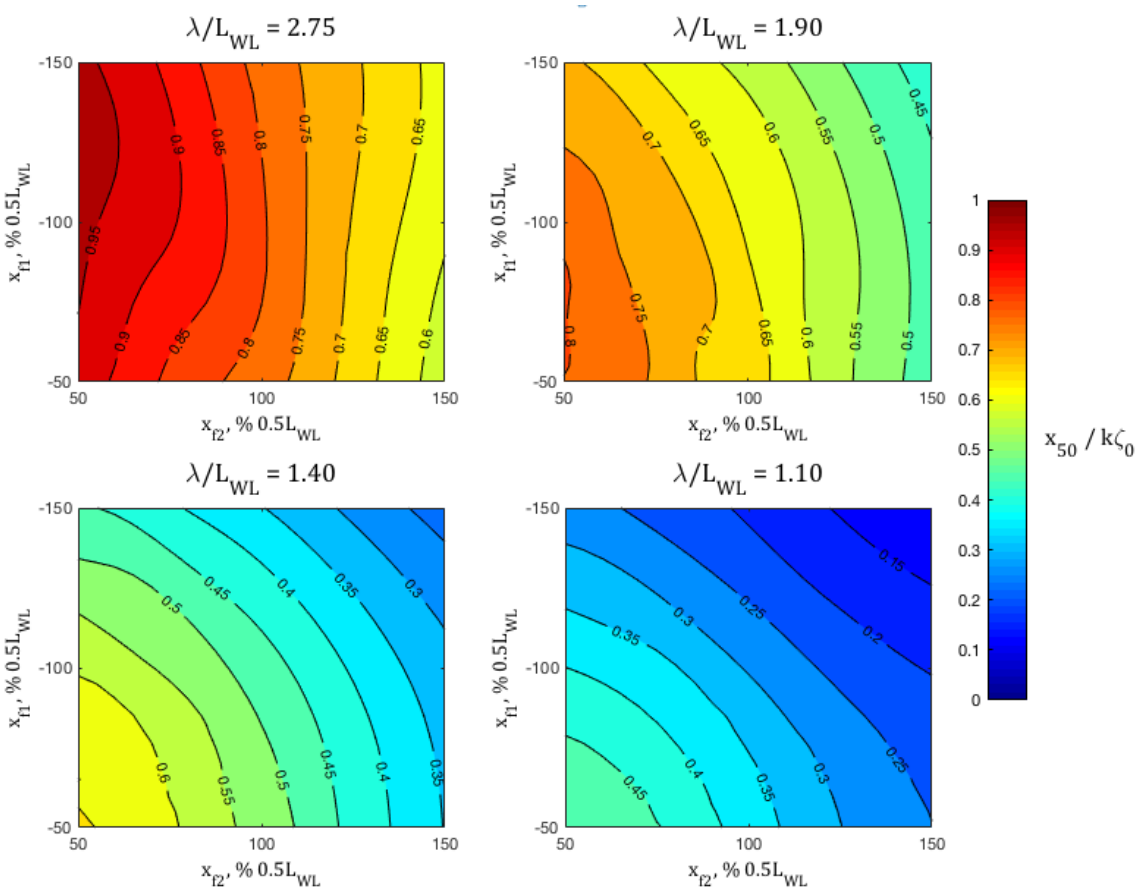

Figure 5.6: Simulation of pitch motion with foil location relative to the vessel LCG ($\zeta_a = 0.06$m)

the foil size is represented by the non-dimensional foil span to maximum beam ratio (s/B_{max}) and the wave frequency is non-dimensionalised as the wavelength to length ratio (λ/L_{WL}).

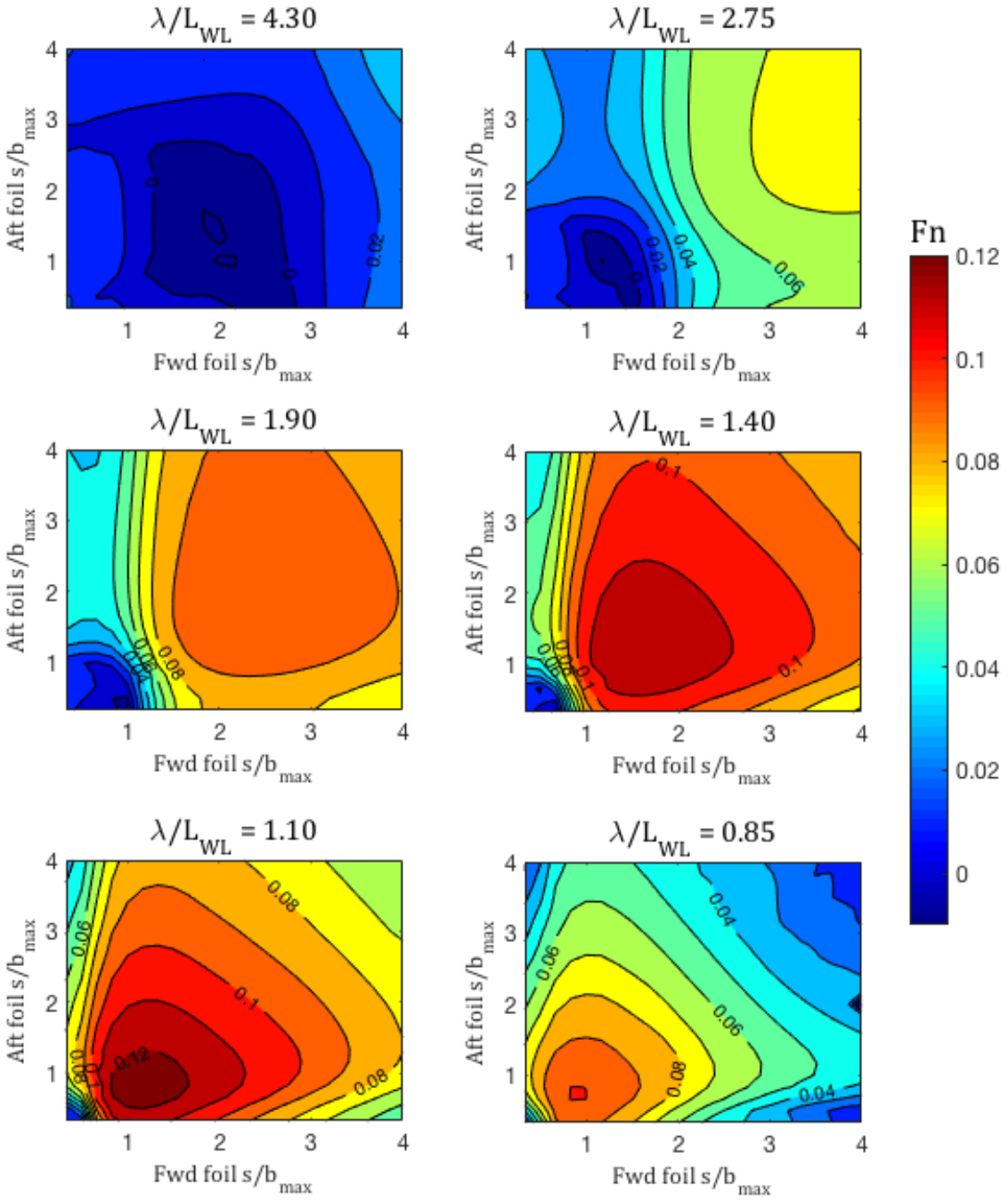

Figure 5.7: Froude number for varying span to beam ratios in head waves

In contrast to the effect of changing foil location, the optimum foil size varies considerably over the range of wave frequencies in head waves. For optimum foil size, the results show a general trend

from larger foils at lower wave frequencies towards smaller foils at higher frequencies. This is clearly shown in Figure 5.8. However, this effect is consistent for head waves only.

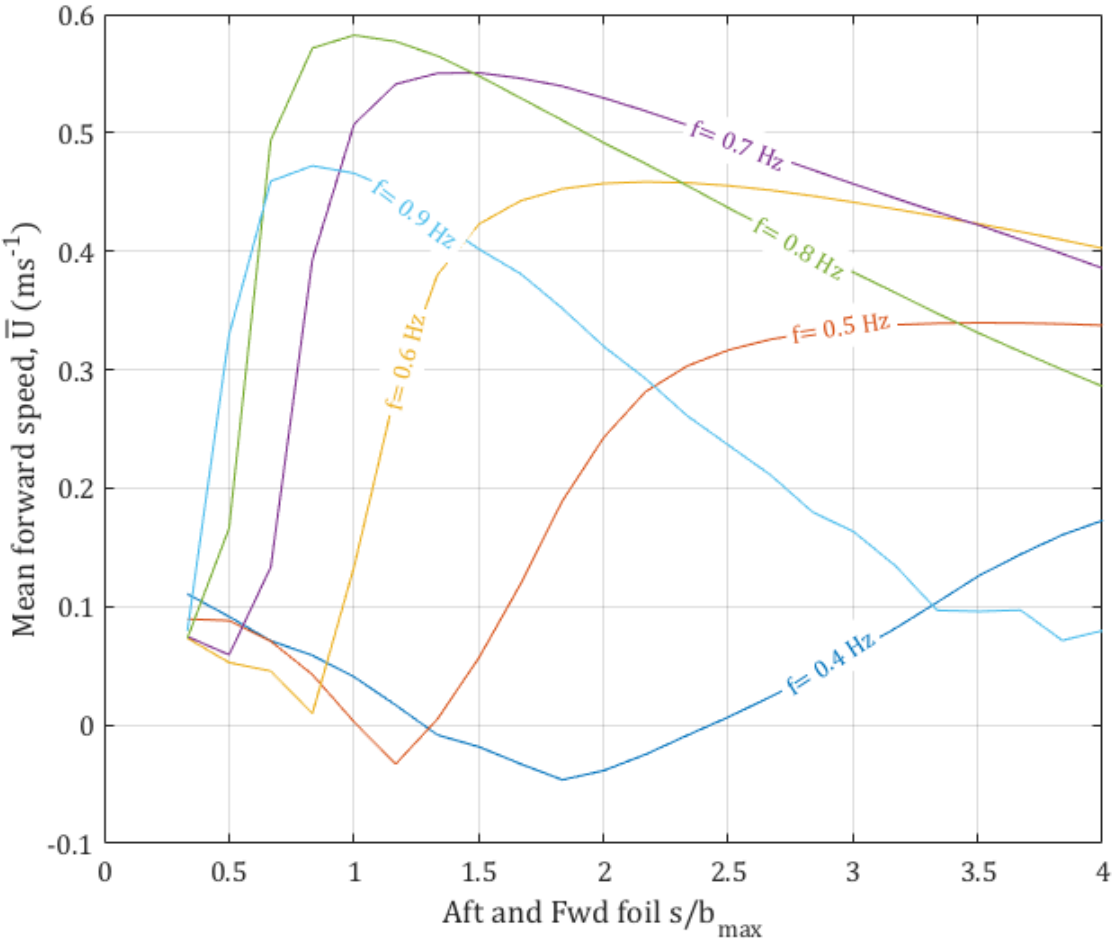

Figure 5.8: Mean forward speed response with the aft and forward foils at the same span to maximum beam ratio in head waves (dimensional diagonal slice of Figure 5.7)

For following waves, the optimal response is less frequency dependent and achieved with a larger aft foil (see Figure 5.9). There is a minimal effect from changes to the forward foil size. These results show that the aft foil provides the majority of the thrust in following waves.

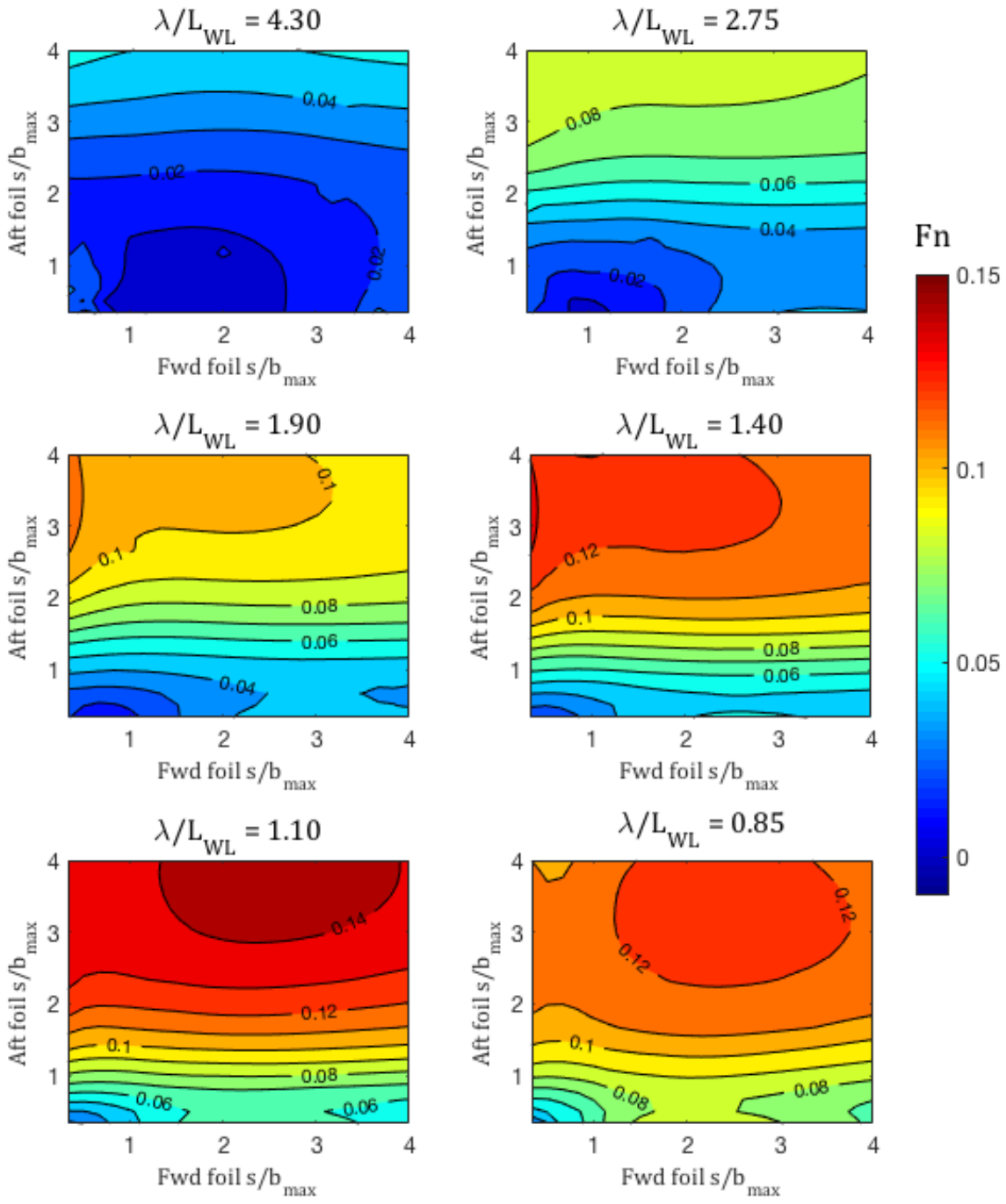

Figure 5.9: Froude number for varying span to beam ratios in following waves

Figures 5.10a and 5.10b show the thrust coefficients for the forward and aft foils with respect to foil size in head and following waves. It can be seen that the forward foil thrust and the aft foil

thrust are asynchronous. This indicates a coupling between the foil thrust and the hull motions. For example, as the foils are rigidly connected to the vessel, the instantaneous lift force acting on one of the foils will influence the vessel motions and, therefore, the driving force for the other foil. Therefore, one foil becomes dominant over the other which is clearly shown in the case of following waves when the aft foil span to beam ratio is greater than 1. This is also associated with the location of the foil within the wave profile, known as wave-phasing, which will be explained in Chapter 6.

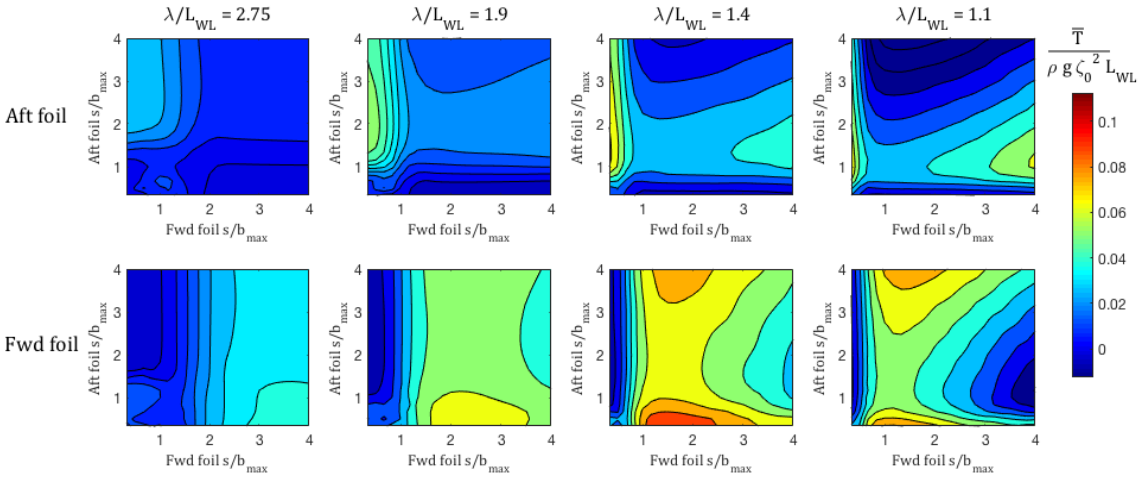

(a) Head waves

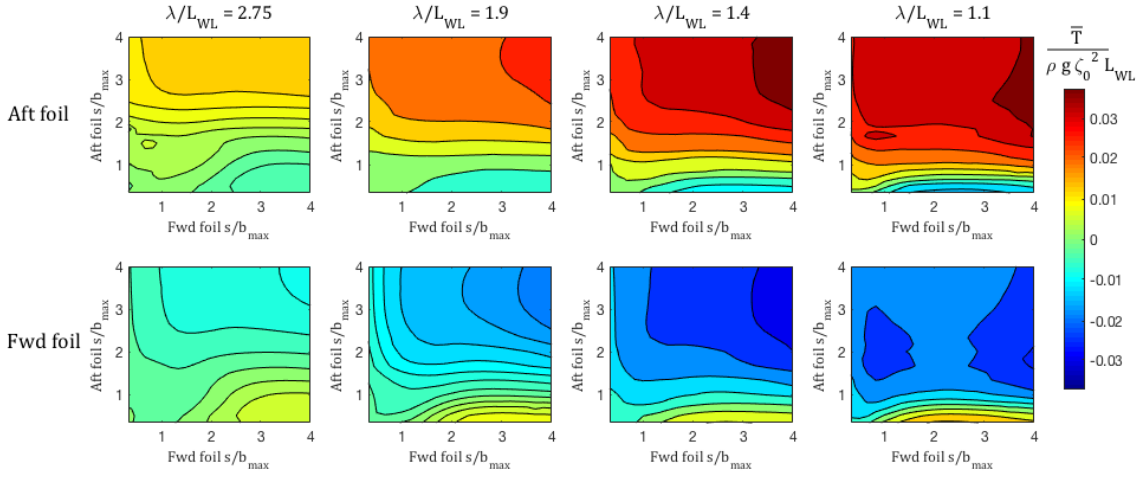

(b) Following waves

Figure 5.10: Comparison of thrust generation for the forward and aft foils in head and following waves

5.2.3 Foil spring constant

The foil pitch is modelled as a rotational mass spring damper, and is therefore defined by the hydrodynamic forces, the inertial force and the restoring force from the rotational spring. The restoring force is assumed to be directly proportional to the angular displacement (pitch) of the foil, and therefore will always act to restore the pitch angle to zero. The spring constant can be tuned to achieve an optimum foil pitch with respect to the hydrodynamic and inertial forces, i.e. the foil pitch which generates maximum net thrust.

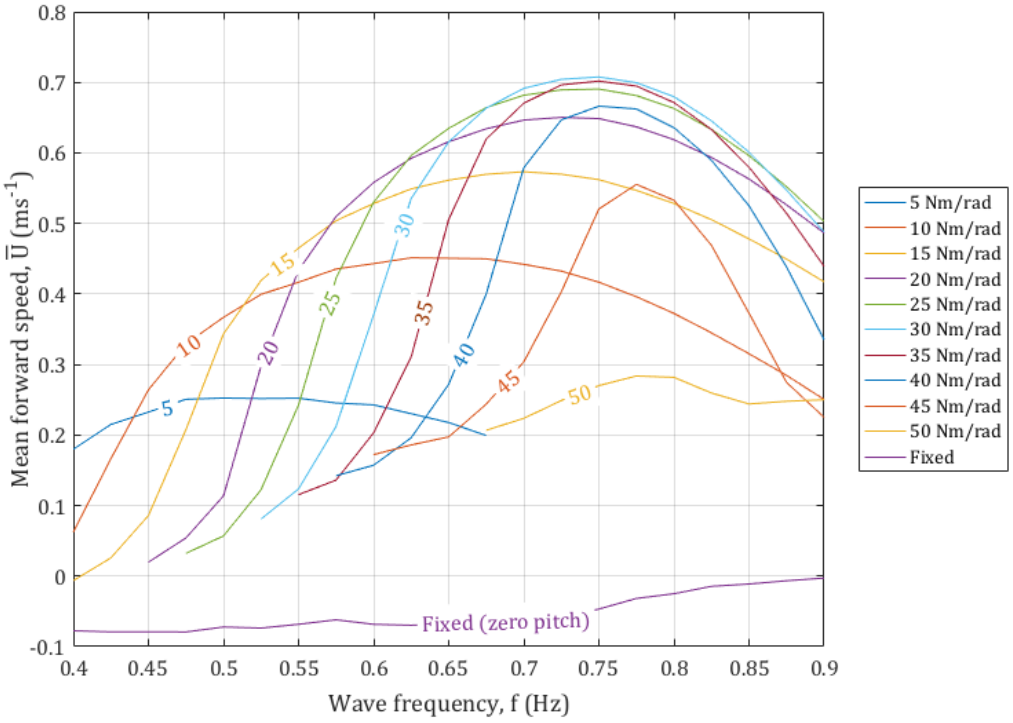

Figure 5.11: Mean forward speed response for varied spring constant and fixed pitch (zero pitch) in head waves

Figure 5.11 shows that the effect of the spring constant is significant and also frequency dependent in head waves. The hydrodynamic forces vary significantly with wave frequency and, consequently, the optimum spring constant ranges from 15Nm/rad at 0.55 Hz to 35 Nm/rad at 0.75 Hz. Additionally, the optimum spring constant is not the same for head and following waves.

Figure 5.12 shows the effect of varying the foil spring constant in following waves. The results

show that the optimum spring constant (10 Nm/rad) is generally independent of wave frequency, except for at high frequencies where there is a second resonance. The second resonance is a result of the vessel motions at high wave frequencies.

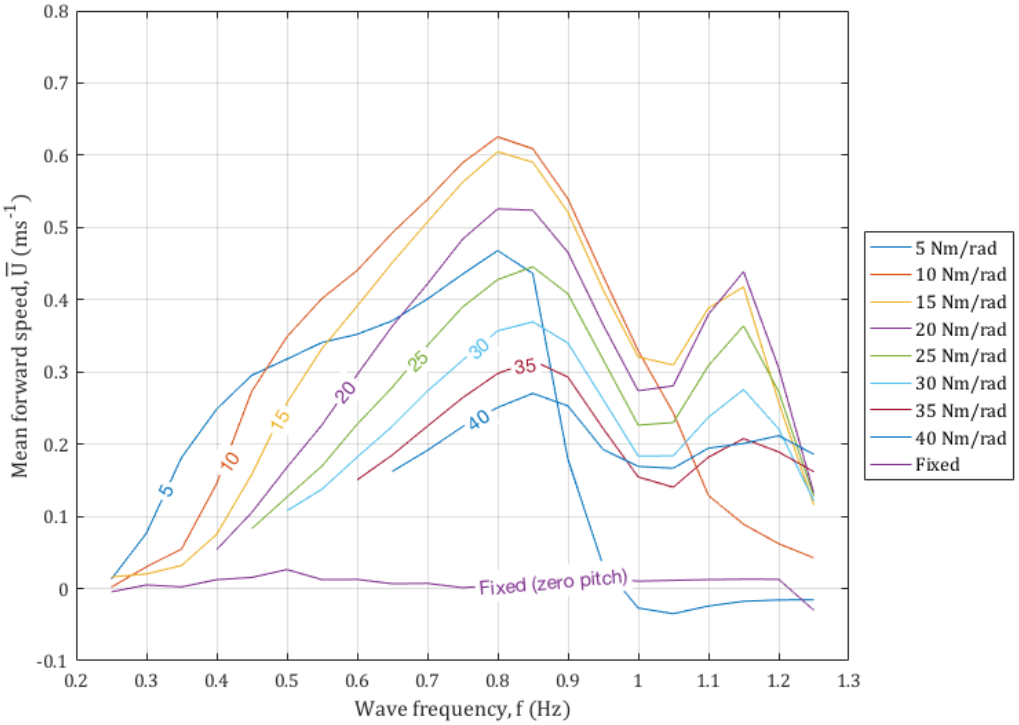

Figure 5.12: Mean forward speed response for varied spring constant and fixed pitch (zero pitch) in following waves

The restoring spring force does not only affect the magnitude of the foil pitch but also the phase difference between foil heave and pitch, referred to as flapping phase. The effect of the flapping phase will be discussed in Chapter 6.

A significantly large spring constant, which causes the resultant foil pitch to approach zero, results in a very poor propulsive response: for fixed foil pitch the resultant forward speed is in the negative x-direction in head waves and almost zero in following waves (see Figure 5.12). Although previous research has shown that a fixed foil at zero pitch is capable of generating thrust in a wavy flow, this free running simulation shows that the foils are unable to generate sufficient thrust to overcome the hull resistance and added resistance due to waves.

5.2.4 PTO damping

The research problem, depicted in Figure 1.5, highlights that wave propulsion and energy recovery are interchangeable through heave control of the submerged foil. In theory, the energy for forward propulsion can be maximised at the expense of the energy recovered for onboard power and vice versa. The determining variable is the damping factor that dictates the magnitude of the relative foil heave.

Figures 5.13a and 5.13b show both the propulsion and power generation results from the same free running simulation for varying damping constants. By adjusting the damping constant, a combination of both propulsion and power generation is delivered simultaneously. The results show that a decrease in the PTO damping reduces the propulsive performance and increases the energy recovered. This effect is reversed for an increase in PTO damping. Therefore, changing the PTO damping can control the mode of the wave powered vessel.

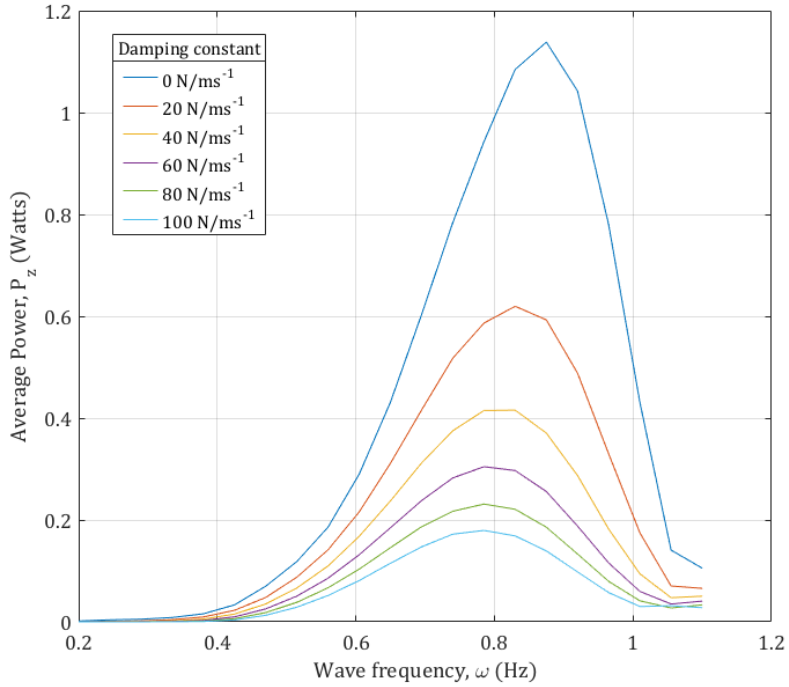

(a) Average power recovered for a range of foil damping

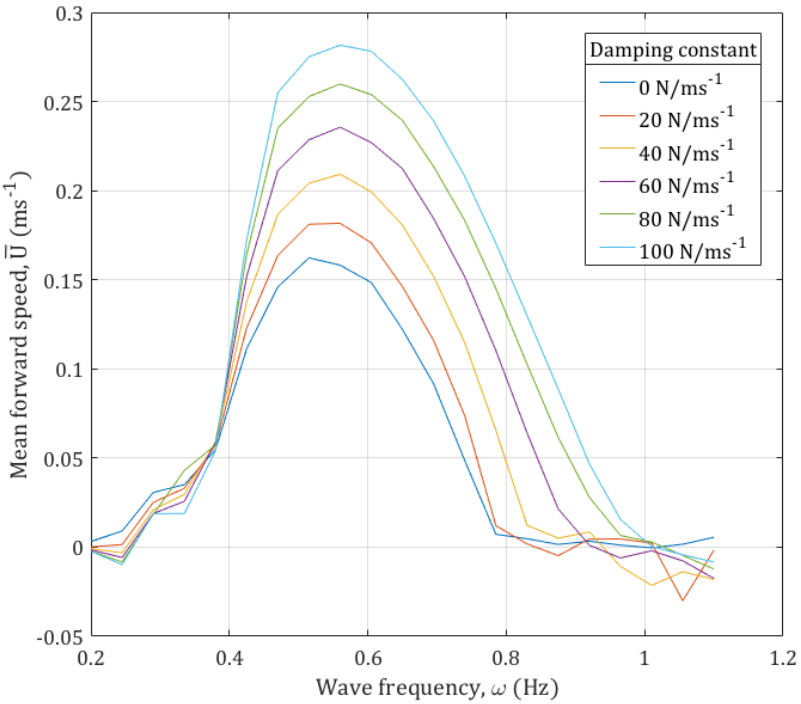

(b) Resultant mean vessel forward speed

Figure 5.13: Effect of varying damping constant on the response of a wave powered vessel in head waves

5.3 Hull particulars

The hydrodynamic effects of changing the local sectional forms are accounted for in the strip theory method for both vessel motions and added resistance due to waves. The numerical model can only assess the first order hydrodynamic effects due to a change in hull form and second order effects due to extreme changes, such as excessive slamming or deck wetness, are not considered.

The following analysis focuses on three main changes in hull form; waterplane area coefficient, length/beam ratio and volumetric ratio. These coefficients are considered to have an important effect on the seakeeping response of most monohull ship types (Lloyd 1998).

5.3.1 Waterplane area coefficient

The waterplane coefficient is the ratio of waterplane area to the product of vessel length and beam, i.e. how much the waterplane area resembles a rectangle. The results show that the waterplane coefficient has a significant impact on the forward speed, shown in Figure 5.14.

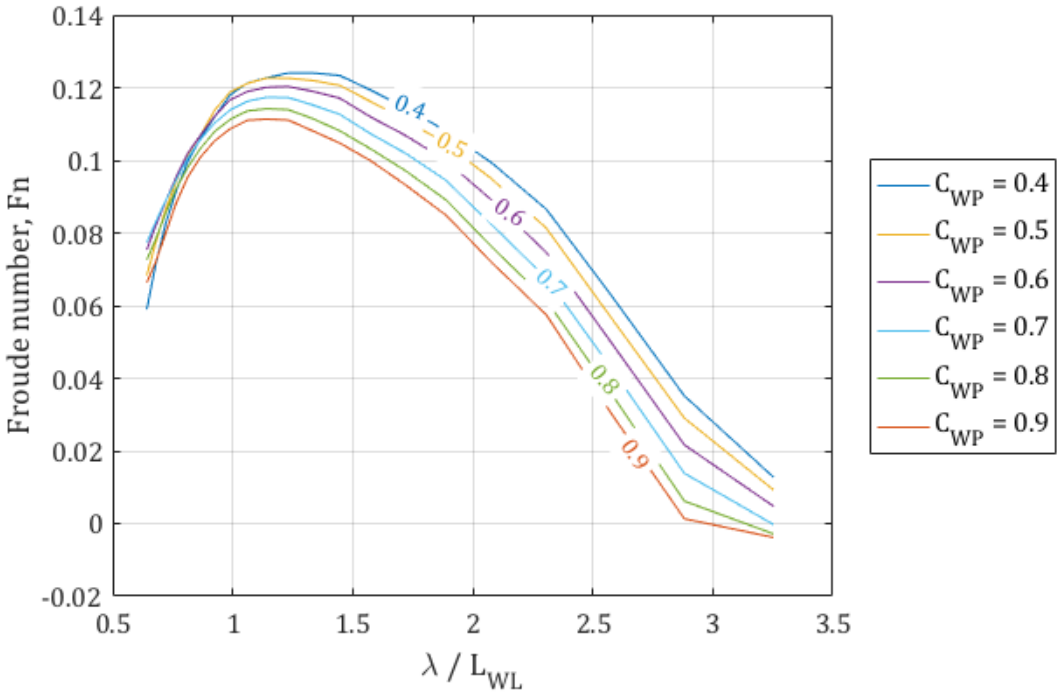

Figure 5.14: Effect of varying waterplane area coefficient in head waves

The waterplane coefficient has a minimal effect on the vessel pitch (see Figure 5.15), which is expected as the Wigley hull shape is symmetrical about amidships. The effect on vessel heave is significant (see Figure 5.15) and results in a directly proportional change in the induced heave of the foil. This is reflected in the propulsive response, which shows that a reduced waterplane coefficient is preferable for optimum wave propulsion due to an increase in the heave response of the vessel and, therefore, the submerged foils.

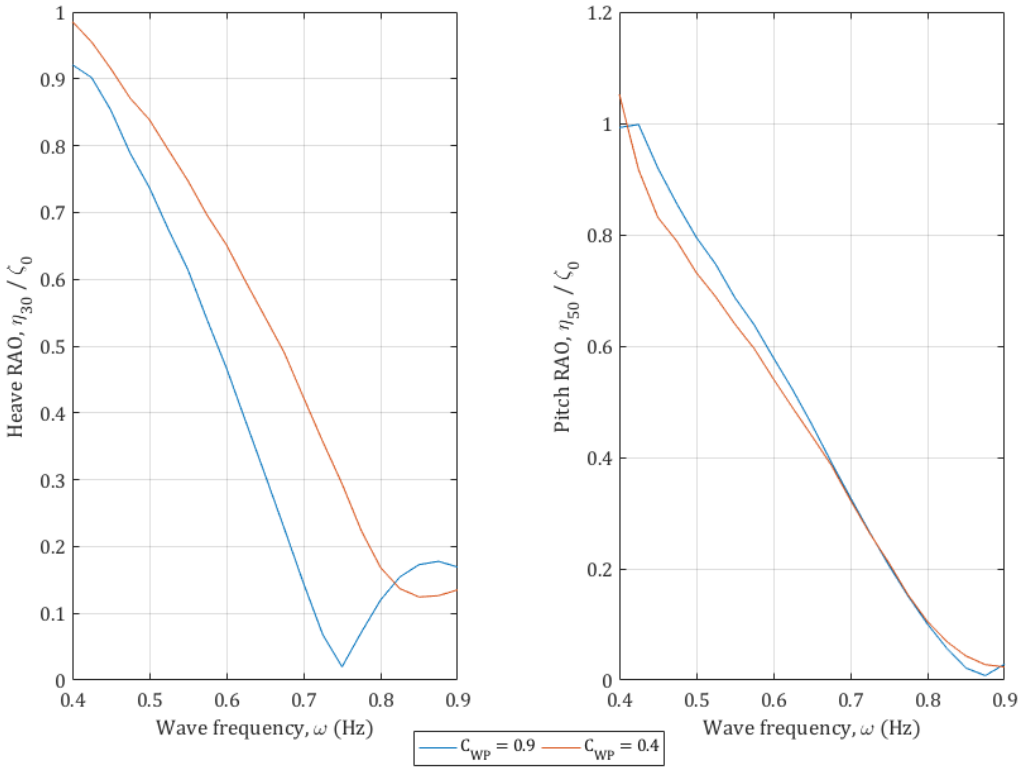

Figure 5.15: Vessel heave and pitch motions for extreme waterplane coefficients in head waves

5.3.2 Length/beam ratio

The length/beam ratio is changed by maintaining a constant vessel length and varying the beam. The block coefficient is kept constant, which results in a change in displacement and wetted surface area.

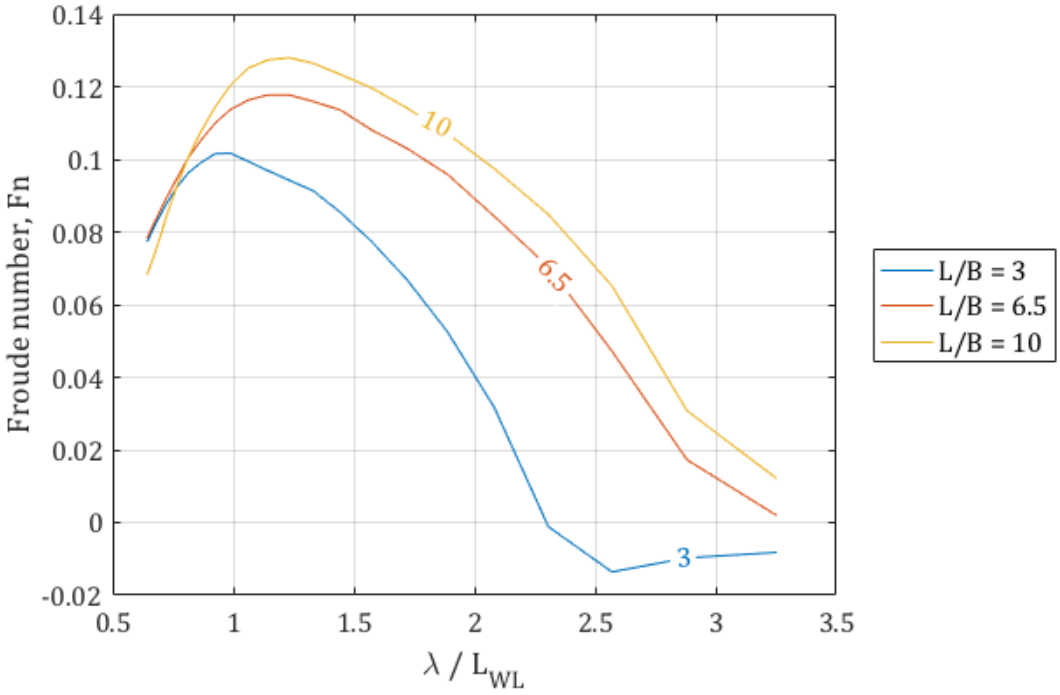

(a) Head waves

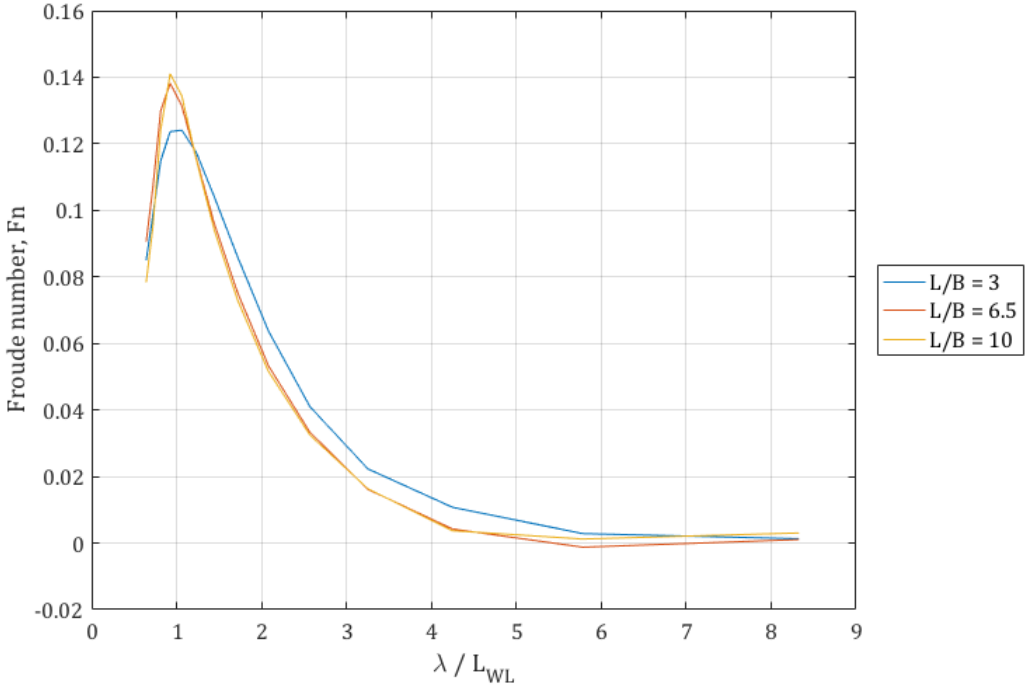

(b) Following waves

Figure 5.16: Effect of length-beam ratio on the vessel response for varying wave frequencies in head and following waves

Figure 5.16 shows the results for three significantly different length/beam ratios in head and following seas. As with the waterplane area coefficient, the effect of changing the hull form has a minimal effect on the propulsive response of the vessel in following waves. In head waves, the effect is significant showing that a larger length/beam ratio is more effective for wave propulsion. This is counter-intuitive as an increase in the length/beam ratio reduces the vessel motions and, therefore, reduces the motion induced heave of the submerged foils. However, this can be explained by the fact that the length/beam ratio also significantly affects the pitch response of the vessel. An overall reduction of vessel heave and pitch causes a decrease in the added resistance due to waves, as shown in Figure 5.17. Therefore, the optimum length/beam ratio is mainly driven by the reduction in added resistance.

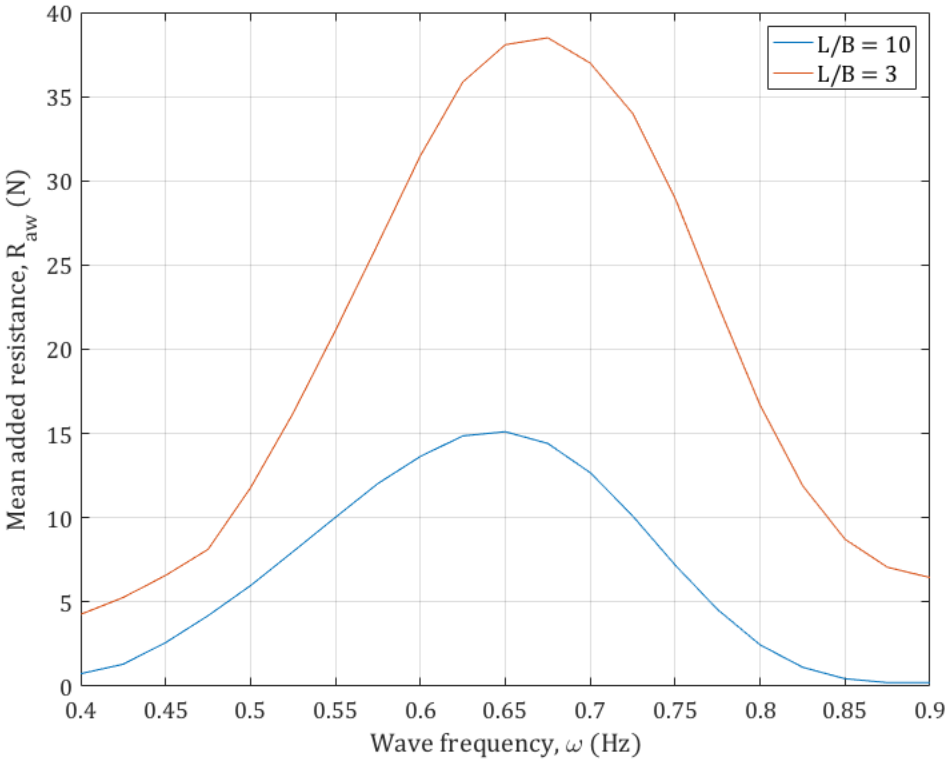

Figure 5.17: Effect of length/beam ratio on added resistance in head seas

5.3.3 Volumetric ratio

The volumetric ratio is defined as the vessel length divided by the cubic root of displaced volume ($L/\nabla^{\frac{1}{3}}$). For discretisation of the parameter, the vessel draft is increased at constant increments whilst the remaining geometric parameters are kept constant. A low volumetric ratio represents an increase in displacement and, therefore, the ratio captures the effect of increasing the payload of the vessel.

Figure 5.18 shows the response of the Wigley hull form for increasing volumetic ratios in head waves. It can be seen that the forward speed response for low volumetric ratios is noticeably less than for high volumetric ratio. In following waves, a lower volumetric ratio results in an increase in the propulsive performance at the resonant frequency but the effect is minimal, shown in Figure 5.19.

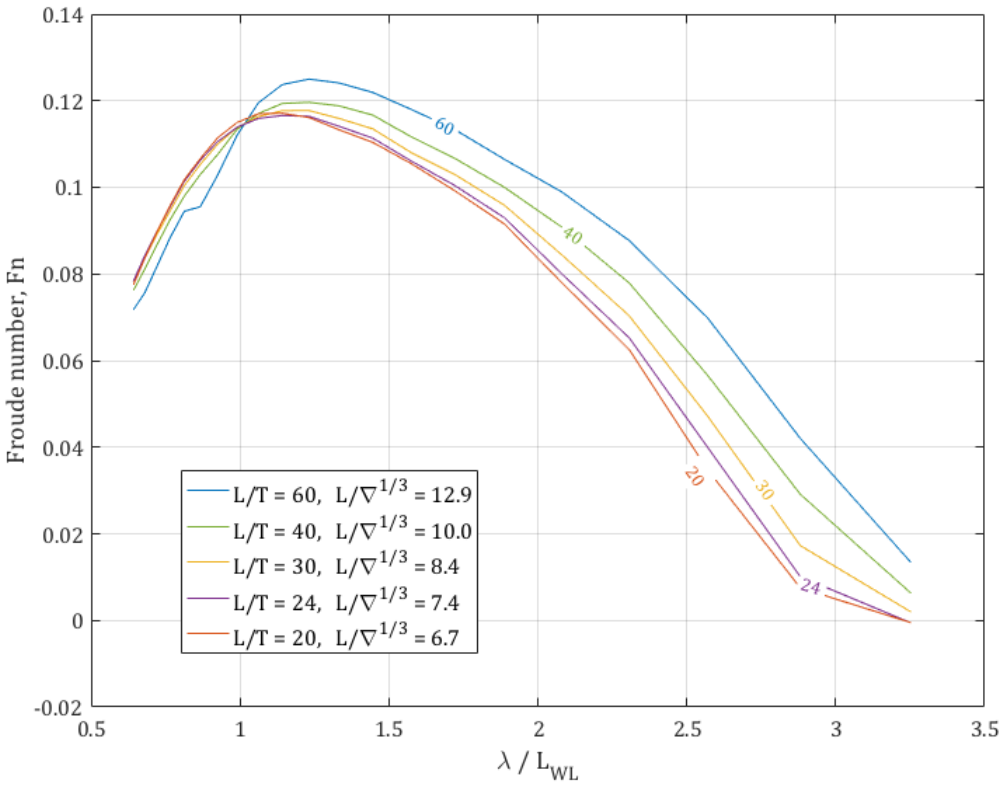

Figure 5.18: Effect of length-draught ratio on the vessel response for varying wave frequencies in head waves

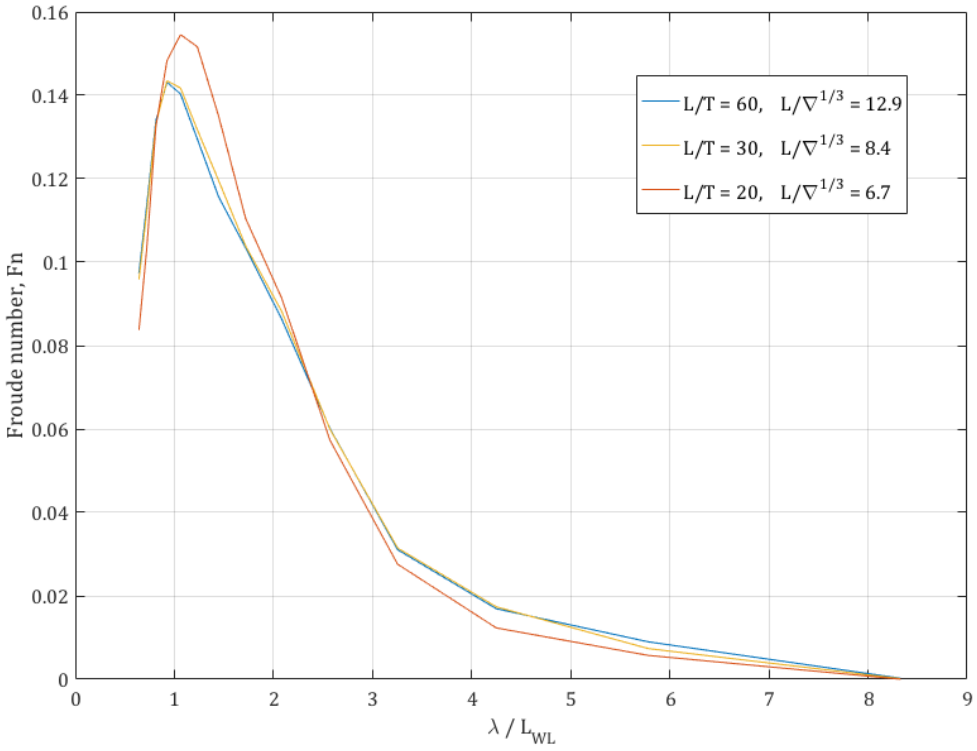

Figure 5.19: Effect of length-draught ratio on the vessel response for varying wave frequencies in following waves

The motions of the vessel in head waves increase with an increase in displacement (see Figure 5.20), which is consistent with the results of Lloyd (1998). The increase in displacement results in the added resistance due to waves almost doubling (see Figure 5.20 c), which in turn results in a significant difference in the forward speed shown in Figure 5.18. In following waves, it is assumed that there is a negligible added resistance due to waves, and therefore the effect of vessel motions is less significant. As an approximation, a volumetric ratio of 10 is shown to yield reasonable propulsive performance.

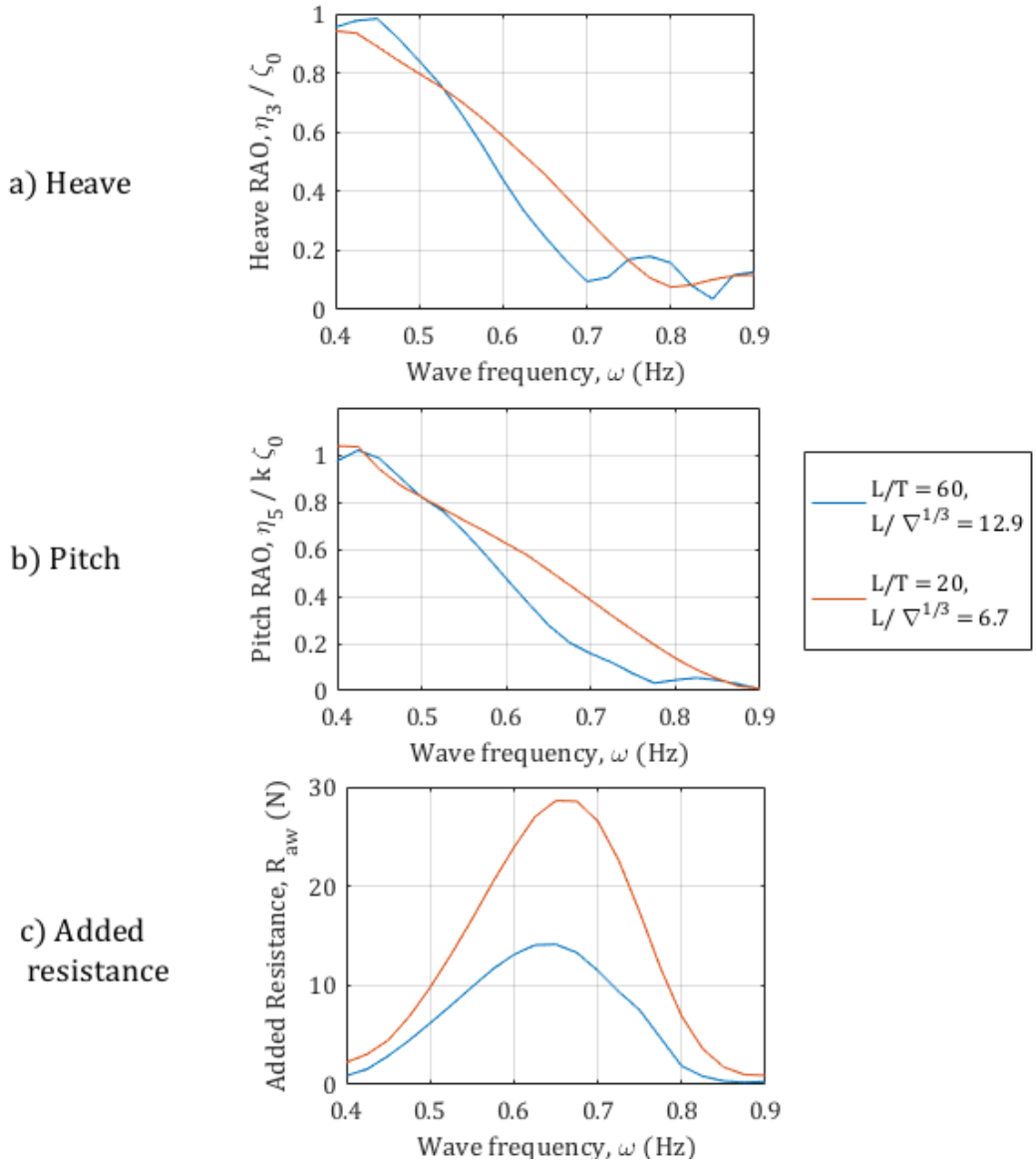

Figure 5.20: Effect of volumetic ratio on vessel motions and added resistance in head waves

5.4 Geometric scaling

Assuming dynamic similarity, the response of a wave propelled vessel is equivalent to a function that consists of a series of non-dimensional coefficients. Dimensional analysis has been performed to obtain a series of non-dimensional coefficients from a set of variables and parameters. For seakeeping,

it is convenient to set the vessel surge motion equivalent to the following function:

$$\eta_{10} = f[\zeta_0, \lambda, U, L, B, I, \rho, \mu_w, g, T_x, R_{AW}] \tag{5.2}$$

This function states that the vessel surge can be defined by a formulae that consists of the bracketed variables. Deriving a singular function for the vessel surge is an onerous task, and it is more efficient to define the response of a system using non-dimensional values. Assuming linearity and hull form consistency, the non-dimensional surge response is equivalent to a set of non-dimensional variables:

$$\frac{\eta_{10}}{\zeta_0} = f\Big[\frac{\zeta_0}{L}, \frac{\lambda}{L}, \frac{U}{\sqrt{gL}}, \frac{B}{L}, \frac{I}{\rho L^5}, \frac{\rho U L}{\mu_w}, \frac{T_x}{\rho g {\zeta_0}^2 \frac{B^2}{L}}, \frac{R_{AW}}{\rho g {\zeta_0}^2 \frac{B^2}{L}}\Big] \tag{5.3}$$

This method enables the analysis of the response as a function of non-dimensional coefficients, as demonstrated in Chapter 6. The fundamental dimensional coefficients that are commonly associated with seakeeping are; the Froude number, wavelength to length ratio; and the added resistance due to waves coefficient. The Froude number is a ratio of the inertial and gravitational forces, which is used extensively for the scaling of hydrodynamic experiments to full scale. This is particularly useful in the analysis of seakeeping, which is governed by gravitational waves and, therefore, scalable to the Froude number.

The Reynolds number is a ratio of the inertial and viscous forces, and is directly proportional to the length of the vessel. It is, therefore, impossible to satisfy both the Froude number and Reynolds number at a given scale. However, given that the vessel is wave powered, it can be assumed that the dominant non-dimensional coefficient is the Froude number. For investigating the response of the system at various scales, the hull form and foils have been geometrically scaled according to the length of the vessel, and Table 5.2 presents a list of the associated vessel particulars, foil particulars and wave parameters.

Table 5.2: Table of parameters for geometry scaling

	Vessel parameters				Foil parameters				Wave parameters	
Scale Ratio	L (m)	B (m)	T (m)	Δ (kg)	s (m)	c (m)	d (m)	k (m^{-1})	ζ_0 (m)	ω (Hz)
1	1	0.134	0.04	2	0.308	0.1	0.1	0.5	0.05	0.59-2.00
2	2	0.268	0.08	16	0.8	0.2	0.2	8	0.1	0.42-1.42
4	4	0.536	0.16	126	1.6	0.4	0.4	128	0.2	0.30-1.00
6	6	0.804	0.24	426	2.4	0.6	0.6	648	0.3	0.24-0.80
8	8	1.072	0.32	1010	3.2	0.8	0.8	2048	0.4	0.21-0.69
10	10	1.34	0.40	1972	4	1	1	5000	0.5	0.19-0.63
100	100	13.4	4.00	1.972×10^6	40	10	10	50×10^6	0.5	0.06-0.16

Figures 5.21 and 5.22 shows the coupled response with respect to the Froude number and the wavelength to length ratio for increasing scale for head and following waves, respectively. For each scale, the non-dimensional coupled response is very similar, which proves that the system exhibits kinematic similiarity. The analysis shows that the optimum wavelength to length ratio is approximately 1.25 for head waves and 1 for following waves. The difference between the two ratios is due to the Doppler effect, which shifts the encountered wave frequency to higher frequencies in head waves and lower frequencies in following waves. Konstantinov and Yakimov (1995) predicted that the optimum ratio is 1.05 in head waves and 0.9 in following waves, but this was for a fixed speed case that does not include a shift in the wave frequency due to the Doppler effect.

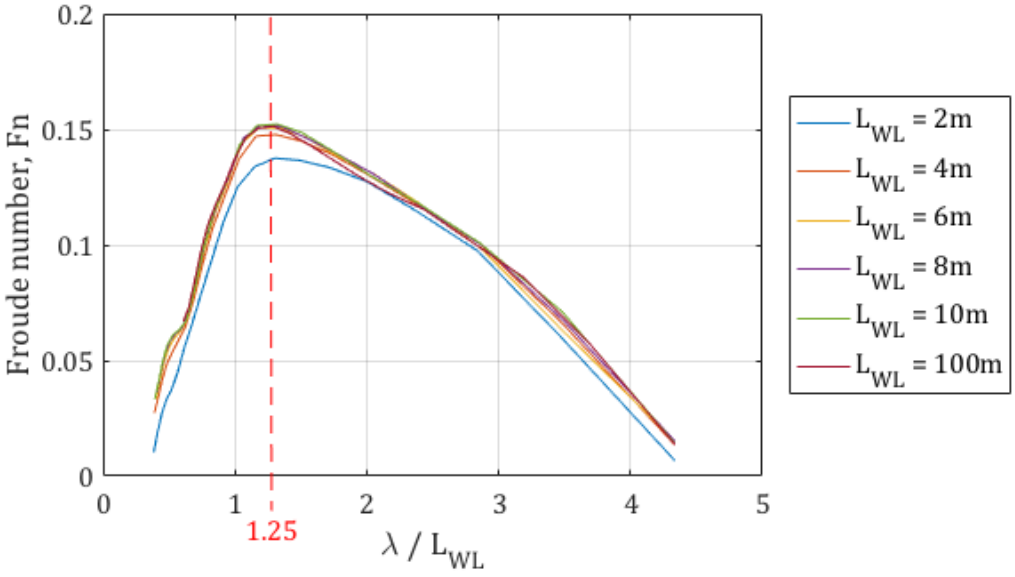

Figure 5.21: Free running resultant Froude number scale comparison for varying wave frequencies in head waves

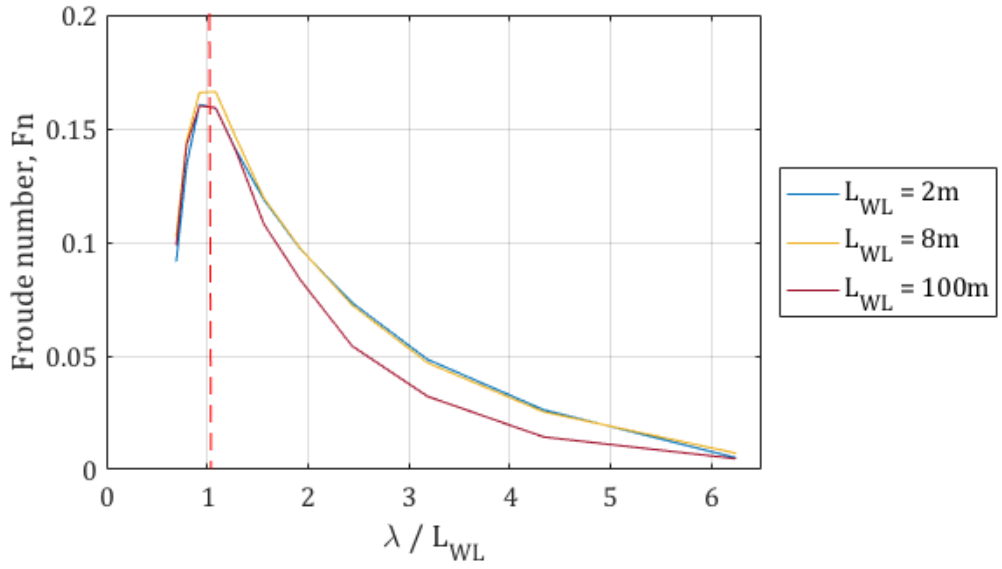

Figure 5.22: Free running resultant Froude number scale comparison for varying wave frequencies in following waves

Figures 5.23a and 5.23b show the resultant non-dimensional thrust and non-dimensional added resistance for a 10m and 100m vessel. The results are shown to be very similar between the two

scales and could be used to perform spectral analysis for the estimation of forward speed in irregular waves, which is discussed in Chapter 6 and highlighted as a recommendation for future work.

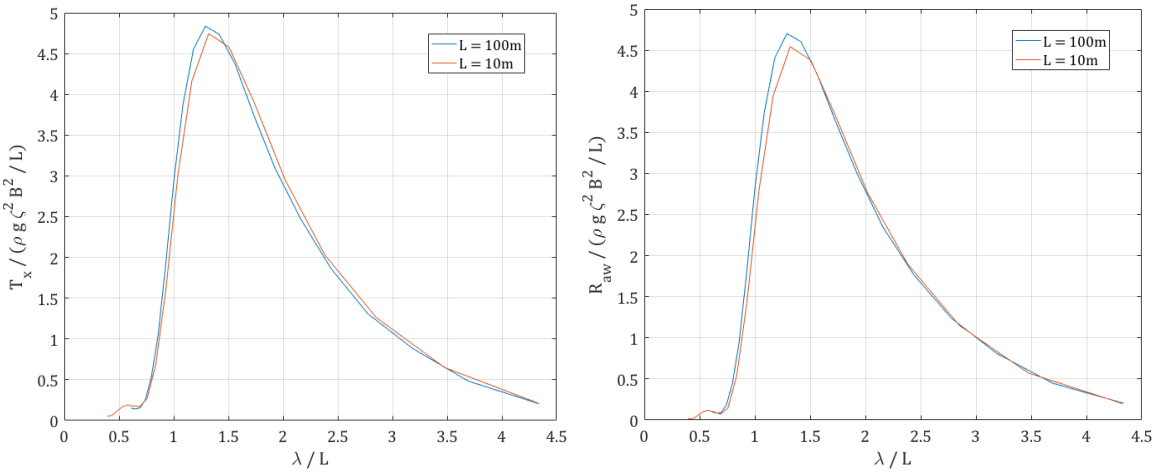

(a) Non-dimensional thrust

(b) Non-dimensional added resistance

Figure 5.23: Non-dimensional thrust and added resistance for a 10m and 100m vessel

5.5 Wave-induced mechanism

Figures 5.24 and 5.25 show the speed response and the non-dimensional equivalent, respectively, of the two main propulsive mechanisms; heave or pitch driven submerged flapping foils. To investigate the heave driven case, the numerical model was adapted to remove the pitch induced foil response, and both foils were submerged to a significant depth of 5m (2.2 L_{WL}) and located beneath the LCG (illustrated in Figure 1.2). The pitch driven case was simulated using the FLEUR setup, with foils located at the forward and aft perpendiculars.

The results show a similar average forward speed but a significantly different resonance response. The pitch driven case is optimum for a higher wave frequency ($\lambda/L_{WL} = 1$) which is due to an increase in the pitch rate of the vessel. In contrast, the heave driven case is more suited to lower frequency waves ($\lambda/L_{WL} = 5$) as the amplitude of the heave response is the determining factor in the magnitude of the forward speed response.

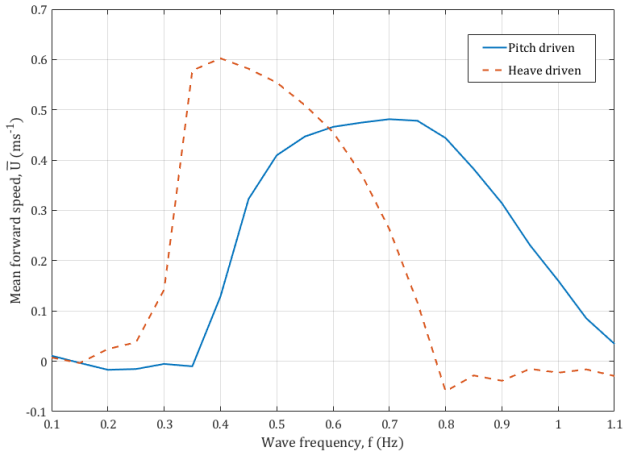

Figure 5.24: Mean forward speed comparison of pitch driven and heave driven mechanisms in head waves ($\zeta_a = 0.1$m)

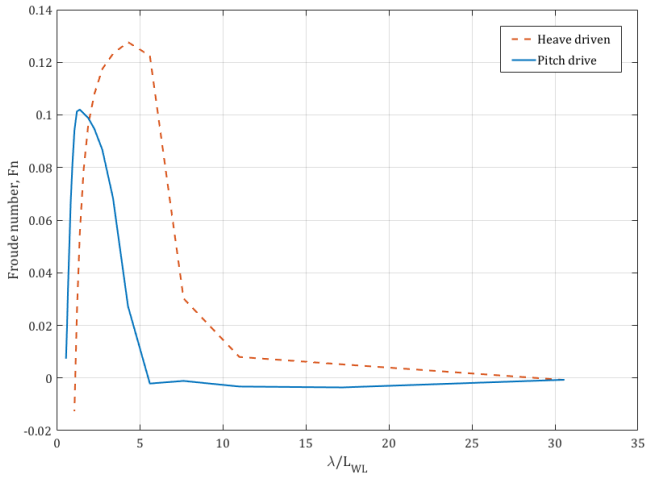

Figure 5.25: Non dimensional comparison of pitch driven and heave driven mechanisms in head waves ($\zeta_a = 0.1$m)

5.6 Implications for the design of wave powered vessels

This section translates the findings from the numerical analysis into design guidance for wave powered vessels. Based upon the numerical analysis of a pitch driven system, Table 5.3 provides guidelines for

the various design parameters for head and following waves, and for high and low wave frequencies in the case of foil size. The following subsections discuss the design considerations for each parameter, and provide discussion on the mechanisms for wave propulsion and the type of vessel. There are numerous additional parameters that could be considered such as foil flexibility, sweep angle and taper, depth of submergence, heading angles and wave conditions. However, these parameters form an area of future work that would complement the design basis guidelines detailed in Table 5.3.

Table 5.3: Guidelines for optimal propulsive performance

		Head seas		**Following seas**	
Parameter		$\lambda/L_{WL} > 1.5$	$\lambda/L_{WL} < 1.5$	$\lambda/L_{WL} > 1.5$	$\lambda/L_{WL} < 1.5$
Foil	*Size*[1] *(%* $\frac{sc}{L_{WL}B_{max}}$*)*	$> 20\%$	$< 20\%$	$> 30\%$	$> 20\%$
	Location (%$0.5L_{WL}$ about amidships)	± 100			
	Spring constant[1] *(non-dimensional,* $\frac{k}{\rho g \zeta_0 sc^2}$*)*	1.5 to 2.5 $\times 10^{-4}$		0.75 to 1.5 $\times 10^{-4}$	
Hull	*Waterplane coef.*	0.5 to 0.6			
	Length/beam ratio	> 6.5		-	
	Volumetric ratio	10			
Scale	*Geometric* λ/L_{WL}	1.25		1	

[1] assuming foil chord is 10% L_{WL}

5.6.1 Foil design

Foil size

For foil design, a considerable compromise is required between the optimum foil size in following waves, in head waves, and for low and high wave frequencies. However, a passive or active mechanism to control the foil size, such as telescopic foils, could optimize the propulsive performance for a given incoming wave frequency or wave direction. This would yield a significant widening of the wave frequency range in which wave powered vessels can operate effectively, but would be difficult to implement. Without the capability to change the size of the foils in-situ, it is recommended that the foils are approximately 20% of the L $\times$ B area of the vessel in order to operate effectively in a range of wave conditions.

Foil location

To achieve good propulsive performance in both head and following waves, it is clear that both a forward and aft foil should be incorporated in the design. The optimum foil location is at or beyond the aft and forward perpendiculars. This is observed for both head and following waves regardless of the wave frequency in both experimental and numerical analysis. Positioning the foils within the perpendiculars results in poor propulsive performance, and positioning the foils much further beyond the perpendiculars yields a small gain, which is offset by the design complications of extended foils. The most effective method of increasing the distance of the foil location from the LCG is to increase the length of the vessel. However, the optimum length of the vessel is frequency dependent, and this factor also needs to be considered.

Spring constant

The numerical and experimental results show that the flapping phase and pitch amplitude of a spring loaded foil varies considerably with respect to wave frequency and foil location. The optimal flapping phase and amplitude for thrust generation is achieved at a particular spring constant (discussed in more detail in Section 6.4.1). This is particularly difficult to satisfy for a range of different wave frequencies and headings, and the guidelines for spring constant in Table 5.3 are provided as upper and lower bounds to achieve a reasonable propulsive performance.

Experiments performed by Bockmann & Steen (2015) showed that an actively pitching foil for wave propulsion was marginally less effective than a spring loaded foil. Therefore, the most effective method of control is to alter the passive wave-induced response of a spring loaded foil by changing the spring constant. Naito & Isshiki (2005) also suggested a method for pitch control through the varying of a spring constant and this research supports this conclusion. Alternatively, a method could be designed to pitch the foil relative to the incoming wave. Experiments conducted by Hao et al. (2017) have shown this method to be effective.

5.6.2 Hull design

Waterplane area coefficient

Decreasing the waterplane area coefficient was shown to produce an improved propulsive performance in head waves. However, the numerical simulations show that this effect is only significant with extreme changes in the waterplane coefficient. It is concluded that a wave powered vessel should have a low waterplane area coefficent.

Length/beam ratio

With respect to hull design, the length/beam ratio has been shown to have a significant effect on wave propulsion. Designing a hull that converts more of the wave energy into kinetic energy, in the form of vessel motions would appear to be a desirable characteristic: a larger vessel motion increases the induced response of the foils, and therefore an increases the thrust generation. However, the numerical analysis shows that the added resistance in waves becomes the dominant factor at low length/beam ratios and efforts to improve the efficiency of wave propulsion with an increase in vessel motions are thwarted by an opposing increase in the added resistance. This analysis leads to the conclusion that, in the case of the length/beam ratio, the hull should be designed for a reduction in added resistance to improve the propulsive efficiency. In following waves, it is not possible to ascertain whether the same conclusion is applicable as the numerical model assumes a negligible added resistance due to waves.

Volumetric ratio

As with the waterplane coefficient, changes to the volumetric ratio show a marginal effect on the propulsive performance unless the changes to the ratio are extreme. This is encouraging for the design of wave powered vessels as less consideration of payload is necessary. Although, the numerical simulation shows that the optimum volumetric ratio is approximately 10 for both head and following waves, small deviations from this due to a change in payload (displacement) will not have large adverse effect on the propulsive performance. However, a volumetric ratio of 10 represents a relatively light displacement design, and heavily loaded wave powered vessels should, therefore, be avoided.

5.6.3 Scale

The length of the vessel has been used as the determining scale factor for geometric scaling. The results from the numerical analysis show that there is significant change in the speed response with respect to scale for varying wave frequencies, as shown in Figure 5.26. This presents a significant constraint for the design of a wave powered vessel as the scale must be designed for a specific wave spectrum.

Figure 5.26 shows the same results as those presented in Figure 5.21 but with dimensional parameters. The figure shows a shift in the frequency response due to the scale, and a linear change in the magnitude of the speed, both of which are to be expected due to the proportional effect of vessel length. It can be seen that a larger vessel is more suitable for low frequency waves, but only over a narrow range. For smaller vessels this effect is reversed.

In Figure 5.22, the optimum length to wavelength ratio was shown to be different for head and following waves due to the Doppler effect, but the same for varied geometric scales. For a pitch driven system, the length to wavelength ratio should be approximately equal to 1 in head waves and 1.25 in following waves, and therefore to operate in both wave headings the length to wavelength ratio of the vessel should be between 1 and 1.25.

5.6.4 Pitch vs. heave induced propulsion

The similarity in the magnitude of the forward speed response for the two mechanisms shows that both are equally suitable for the purpose of converting wave energy into propulsive thrust. However,

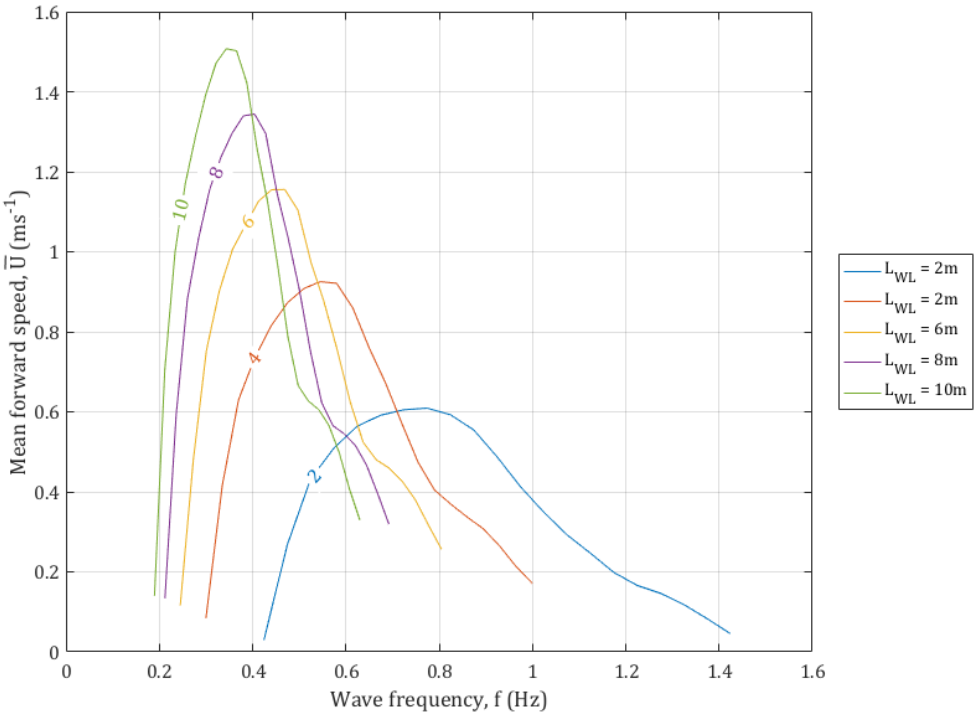

Figure 5.26: Mean forward speed response and different scales in head waves

the significant difference in the frequency response makes it difficult to design a single setup that can operate effectively over a large range of wave frequencies. For converting energy from ocean swell for wave propulsion, a heave driven setup is clearly the optimum method. However, in wind driven short fetch sea states such as enclosed seas or sheltered coastal regions, a pitch driven method is more advantageous.

Both types of propulsion methods exist as commercially operated unmanned surface vehicles, i.e. the Autonaut (pitch driven) and the Wave Glider (heave driven), and a useful in-situ trial could be performed to compare the two methods.

5.6.5 Catamaran vs monohull

Section 5.6.2 proposed guidance for the hull design of a wave powered vessel, which showed that a light, slender vessel with a low waterplane coefficient is optimal for wave propulsion. This is in

agreement with the WDPS ASV developed by Terao (2012), which is a wave propelled catamaran with slender hullforms.

A brief study has been conducted to compare the propulsive performance of a flapping foil wave powered catamaran versus a flapping foil wave powered monohull. The study was carried out by comparing a monohull, which is identical to the FLEUR model, and a catamaran with the same hull form but the beam of each demi hull set to half that of the FLEUR design. The analysis was conducted in head waves at a wave amplitude of 0.05m and the results are presented in Figure 5.27.

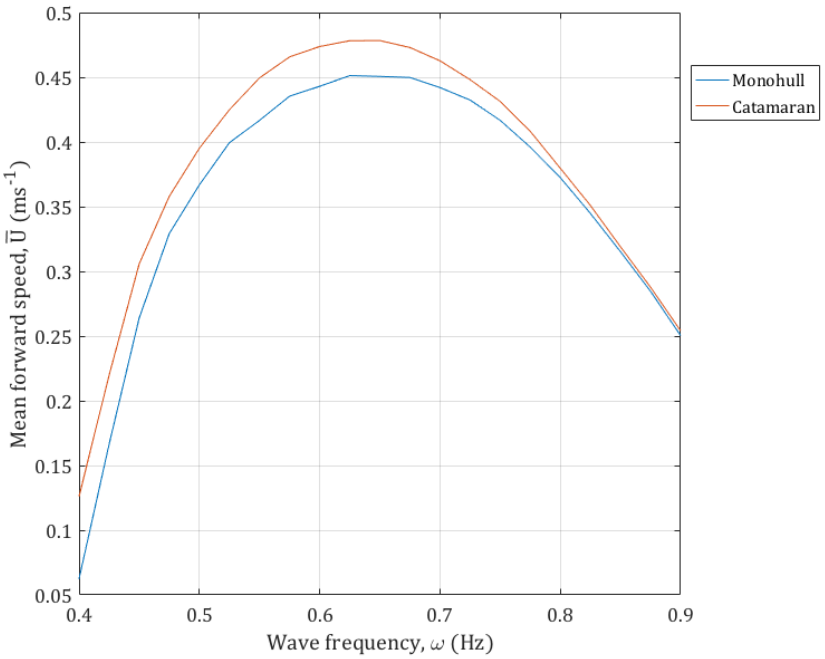

Figure 5.27: Comparison between a catamaran and monohull design in head waves

Despite a larger wetted surface area, the catamaran design shows an improved propulsive performance in head waves due to the increase length beam ratio of each hull. However, the difference is marginal and, in a real sea state with short crested waves, a catamaran will be more dynamically stable than a monohull and any beneficial effects from additional motions such as roll would be lost.

5.6.6 Speed control, energy recovery and station keeping

Part of the research problem, highlighted in Figure 1.5, is the transition between propulsion and energy recovery, achieved by changing the coupled relationship between the hull and foils. An experimental observation showed that, by allowing the foils to heave relative to the vessel, zero forward speed was generated and the vessel held its position in the waves. The numerical analysis has shown that the vessel can simultaneously be propelled and recover energy by changing the damping applied to PTO.

This outcome is particularly relevant for wave powered ASV station keeping. The AutoNaut ASV adopts a circular pattern to remain close to a given waypoint. The radius of this circle is dependent on the ambient wave energy, and therefore speed of the vessel. The shape of the circle is also dependent on the ocean current or tide at the particular location, which can significantly distort the station keeping track.

The wave energy recovery method of controlling the forward speed of a wave powered vessel would eliminate the requirement to station keep by circling about a waypoint. The method effectively works by converting the energy that would be used to circle a waypoint into useful power onboard the wave powered vessel through energy recovery at the foils. Future work could be conducted to investigate the implementation of this system for an in-situ flapping foil wave powered ASV.

Chapter 6

Discussion

The experimental and numerical results highlight a number of areas of interest relating the coupled response of a wave powered vessel. The following areas merit a more detailed discussion:

- wave frequency dependence - the effect of wave frequency on the coupled response;
- aft and forward foil response - the difference in the response of aft and forward foil;
- wave-phasing parameter - a parameter to describe the interaction between the foil and an incident wave;
- flapping foil characteristics - the wave-induced response of a spring loaded flapping foil;

Some of these factors are in agreement with previous research whilst others present new insights.

6.1 Wave frequency dependence

6.1.1 Regular waves

Both the experimental and numerical analysis show that wave frequency has a significant impact on the coupled response. This is a characteristic of most wave energy converters (McCormick 2007), and previous research has highlighted that optimal wave propulsion is restricted to a narrow range

of wave frequencies (Naito & Isshiki 2005). This presents great difficulty for the engineering design of wave powered vessels due to the broad spectrum of wave frequencies observed at sea.

For small amplitude motions, the response in regular waves is assumed to be harmonic and the vessel heave and pitch equations of motion can be described with respect to the wave frequency, as shown in Equations 6.1 and 6.2, respectively. These equations of motion are representative of a forced mass-spring-damper, and a resonant response is expected at the natural frequency. The spring loaded response of the submerged foils, combined with a non constant forward speed, makes it difficult to solve for the natural frequency and motions in the frequency domain, but the fundamental resonance is retained in the coupled response of a wave powered vessel.

$$\begin{aligned}\omega^2(M_B + A_{33}(\omega))\eta_3 - i\omega B_{33}(\omega)\eta_3 + C_{33}\eta_3 + \omega^2 A_{35}(\omega)\eta_5 - i\omega B_{35}(\omega)\eta_5 + C_{35}\eta_5 \\ = {F_3}^B e^{-i\omega t} + {F_{3_i}}^F(\omega)\end{aligned} \tag{6.1}$$

$$\begin{aligned}\omega^2(I_B + A_{55}(\omega))\eta_5 - i\omega B_{55}(\omega)\eta_5 + C_{55}\eta_5 + \omega^2 A_{53}(\omega)\eta_3 - i\omega B_{53}(\omega)\eta_3 + C_{53}\eta_3 \\ = {F_5}^B e^{-i\omega t} + {F_{5_i}}^F(\omega)\end{aligned} \tag{6.2}$$

A shift in the resonant frequency could achieve an improved response with respect to the incoming wave energy. However, this would still result in a narrow range of wave frequency for effective propulsion or energy recovery. For wave powered vessels, there are only two options to manage the frequency dependency. Firstly, the peak response of the vessel should be designed to match the modal wave frequency in a particular sea state. Secondly, the foil parameters could be designed to adapt to a change in wave frequency.

6.1.2 Irregular waves

A more realistic sea state is comprised of a series of regular waves at varying frequencies, which are known as linear irregular waves. An irregular wave is defined by a wave spectrum, which represents the energy density of a given sea state over a range of wave frequencies, i.e. the total combination of the regular waves results in an irregular sea state with a known density of energy.

In Chapter 5, it was shown that the relationship of the vessel forward speed with the wave amplitude is linear and is therefore theoretically possible to predict for irregular waves. The remainder of this section describes how this can be achieved for both wave propulsion and energy recovery.

Wave propulsion

The regular wave analysis at Section 5.1 showed that the linearity of the forward speed response with respect to wave amplitude is complicated by the combination of speed and wave dependent resistance components. Furthermore, as shown in Section 5.4 and in Figure 6.1, the average thrust generation and added resistance due to waves was found to be proportional to the square of the wave amplitude. This proportionality is an important requirement for the analysis in irregular waves.

The classic resistance and propulsion problem is solved by equating the propulsive force to the force required to overcome the vessel's total resistance at constant speed. For a free running propelled vessel in waves, this is not an accurate representation as the wave-induced motions result in an oscillatory forward speed. Therefore, for the purpose of this analysis, the average forces and speeds are considered in the frequency domain rather than the oscillatory equivalents in the time domain.

In regular waves, the resistance and propulsion method maintains that the vessel's forward speed can be calculated if the wave-induced thrust and added resistance are known:

$$\begin{aligned} &\dot{V} = 0, \quad then \;\; T_x = R_T = R_{SW} + R_{AW} + R_{APP} \\ &\therefore \\ &V = 0 \;\; or \;\; \bar{V} = \sqrt{\Big[\frac{\bar{T}_x - \bar{R}_{AW}}{\frac{1}{2}\rho(C_{F_{SW}} A_{SW} + C_{F_{APP}} A_{APP})}\Big]} \end{aligned} \tag{6.3}$$

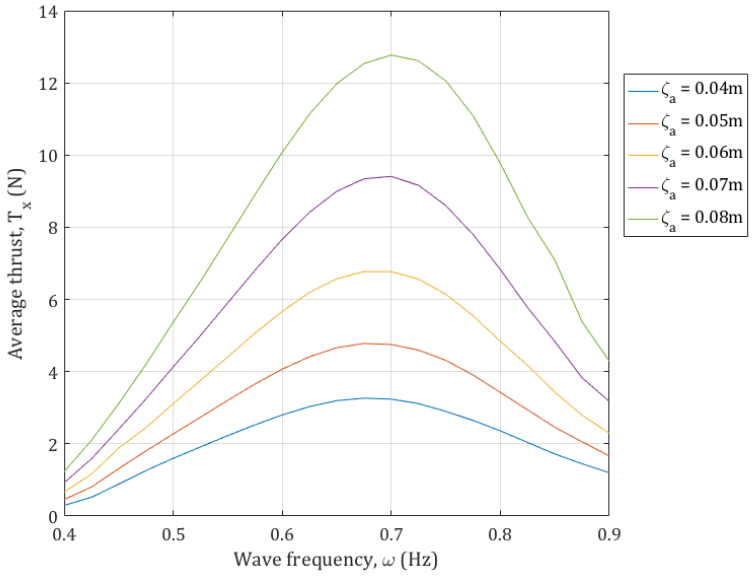

(a) Average thrust

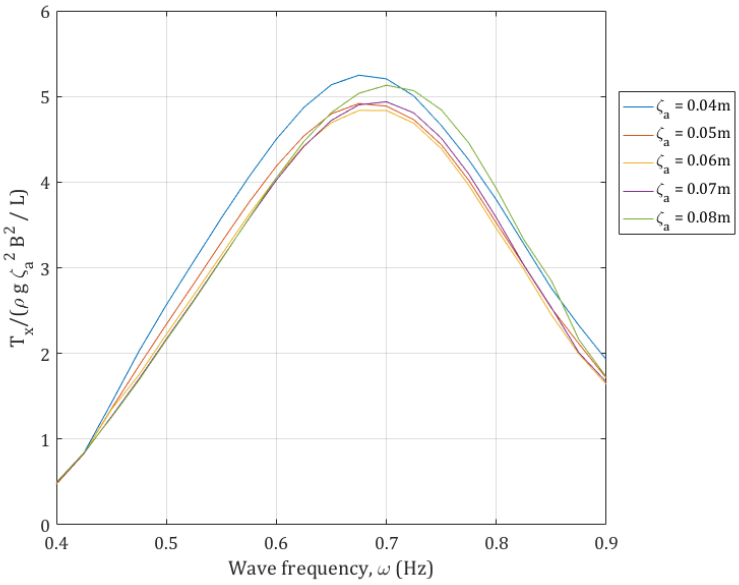

(b) Thrust coefficient, τ

Figure 6.1: Non dimensional thrust in head waves

Using spectral analysis and applying transfer functions, it is possible to estimate the mean wave-induced thrust and added resistance in an irregular sea state. This analysis is directly linked to

the regular waves analysis as it is necessary to gain a transfer function of the vessel response with respect to wave frequency; non-dimensionalised with respect to wave amplitude. The following formulas are used to estimate the wave-induced thrust and added resistance transfer functions, σ_{AW} and τ, respectively:

$$\sigma_{AW}(\omega, V) = \frac{R_{AW}(\omega, V)}{\rho g {\zeta_a}^2 \frac{B^2}{L}} \tag{6.4}$$

$$\tau(\omega, V) = \frac{T_x(\omega, V)}{\rho g {\zeta_a}^2 \frac{B^2}{L}} \tag{6.5}$$

By combining the wave-induced thrust transfer functions, shown in Figure 6.1b, with the spectral energy density function of a particular seastate (S_ω), the equivalent spectral density function for the wave-induced thrust can be obtained. The area under the spectral density function curve with respect to wave frequency is equal to the mean wave-induced thrust. The same spectral analysis can be conducted for the wave-induced added resistance, and the associated formulas are as follows (Kim et al. 2017):

$$\bar{R}_{AW} = 2 \int_0^\infty R_{AW}(\omega, V) S_\omega(\omega) d\omega \tag{6.6}$$

$$\bar{T}_{AW} = 2 \int_0^\infty T_x(\omega, V) S_\omega(\omega) d\omega \tag{6.7}$$

where S_ω is the wave spectrum of an irregular wave sea state.

By obtaining the mean wave-induced thrust and added resistance, it is possible to estimate the forward speed in irregular waves using Equation 6.3. This is highlighted as an area for future theoretical and experimental research, which could lead to the prediction of the forward speed response of a wave propelled vessel depending on its planned route across the oceans, seasonal weather patterns and knowledge of the local sea state.

Energy recovery

As with wave propulsion, a calculation of the energy recovery in irregular waves can be achieved by spectral analysis. In this case, the transfer function is the conversion efficiency from wave power to generated electrical power, and the frequency dependent response of the foils in regular waves can be used to construct a transfer function.

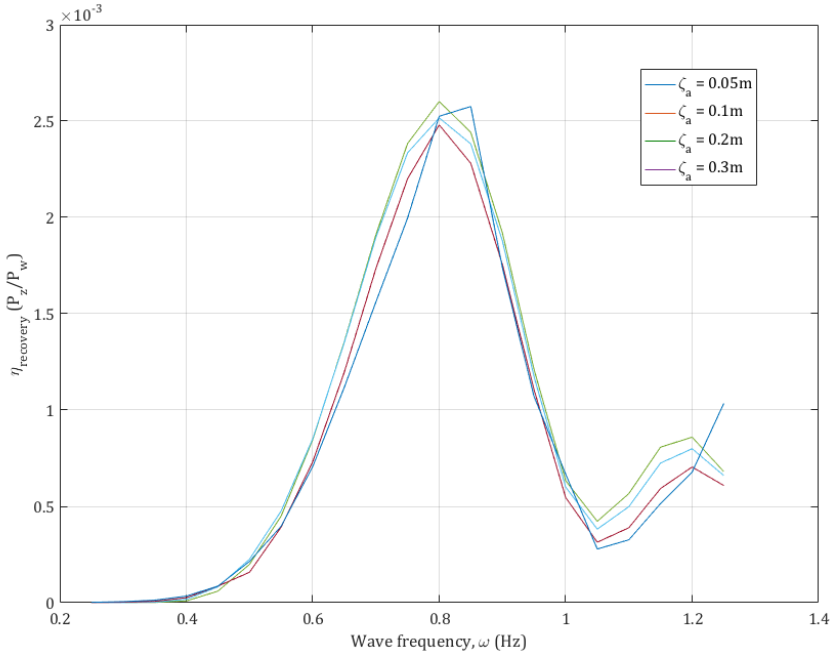

Figure 6.2: Energy recovery efficiency, $\eta_{recovery}$

Figure 6.2 shows the energy recovery from incoming regular waves of differing wave frequency. It is shown that the power recovered is proportional to the square of the wave amplitude and, therefore, the mean power recovered in a particular sea state is calculated as follows:

$$\bar{P}_Z = \int \eta_{recovery}(\omega) S_\omega(\omega) d\omega \tag{6.8}$$

This method has not yet been tested and it is suggested that future experiments are conducted in irregular waves to investigate whether the linearity of the response is retained. If so, this simplified method could be applied for certain known wave spectra in the areas of operation, and the PTO can be designed accordingly.

6.1.3 Following waves

For the condition with the foils located at or beyond the aft and forward perpendiculars, the experimental results show a significant increase in forward speed in following waves when compared to the equivalent frequencies in head waves. At high wave frequencies, this can be attributed to a decrease in the encountered wave frequency due to the vessel's forward speed. However, the increase in forward speed is universal across all the tested wave frequencies, which indicates that the difference is not exclusively governed by the frequency of the waves. Comparing the numerical and experimental results, it is evident that the difference is associated with the added resistance due to waves, which was assumed to be negligible for following waves. In larger waves, other instabilities such as the surf-riding would also positively contribute to the vessel's forward speed. Future experimental and numerical analysis should involve increasing the relative wave amplitude to assess these nonlinear effects.

6.1.4 Additional wave headings and short crested waves

The analysis in this thesis is focused on head and following regular waves with only a consideration for the vessel heave, pitch and surge. Whilst it is possible to adapt the current numerical method to predict the forward speed in irregular head and following waves, the inclusion of the effect of roll is necessary to simulate the response of a wave powered vessel in various headings. In addition, it is expected that the postive effect of pitch on the coupled response would diminish as the vessel headings tends to beam seas. Further analysis is required to understand the effect of roll, which may have positive effects by inducing flow over the tips of the foils. This would suggest that the starboard side of the foil should be separetly sprung from the port side, thus enabling alternate flapping in beam seas.

A more accurate representation of a sea state is the short crested irregular wave. This sea state is compiled of a series of irregular waves which are propagating in a dominant direction, yet a proportion of the waves propagate at at an offset angle from the main direction. This would reguire the prediction of roll to include the effect of different headings, and the response would be weighted using a similar method for seakeeping responses in short crested waves.

6.2 Aft and forward foil response

Both the numerical and experimental analysis highlight a significant difference between the forward and aft foils for wave propulsion and energy recovery. It was observed during the experiments that the response of the foil closest to the incoming wave profile, referred to as the leading foil, was greater than that of the foil furthest away, referred to as the trailing foil. This difference could be partly due to the dissipation of wave energy by the presence of the leading foil. However, the main reasons for the difference between the forward and aft foil response are the kinematics of the vessel motions and the location of the foils within the wave profile.

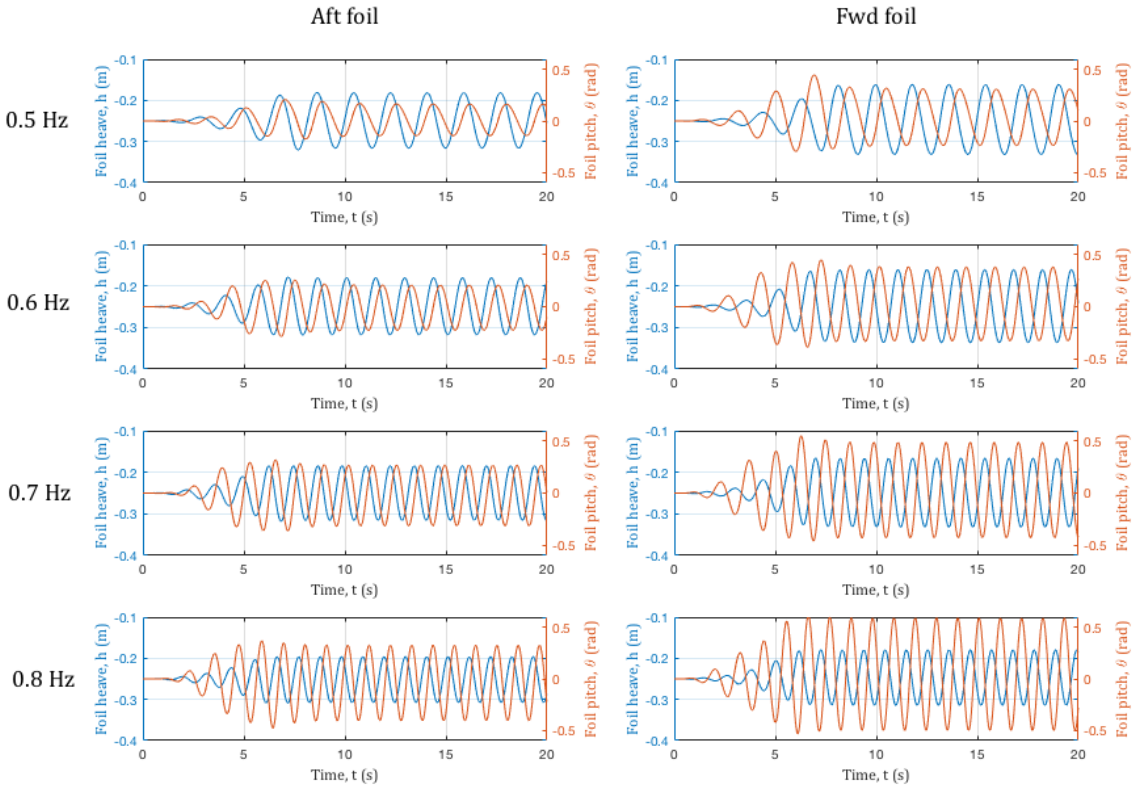

Figure 6.3: Induced heave and pitch of aft and forward foils in head waves for different wave frequencies ($\zeta_a = 0.06$m)

Figure 6.3 shows a significant difference in the induced response (heave and pitch) of the forward and aft foil in head waves for a range of wave frequencies. In agreement with experimental results in Section 4.3.2, the response of the forward foil is noticeably greater than that of the aft foil in head waves, and the effect is reversed for following waves. This can be explained by the change in phase

of the vessel motions between head and following waves.

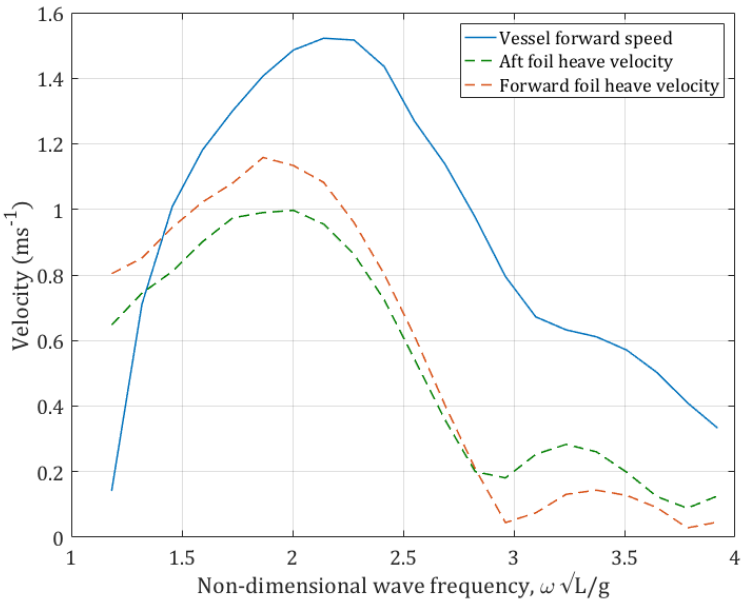

Figure 6.4: Simulaton of the mean vessel forward speed, and forward and aft foils heave velocity for a scaled Wigley hull form of 10m in length (from Table 5.2) in head waves ($\zeta_a = 0.06$m)

In head waves, maximum positive vessel pitch results in maximum negative pitch-induced heave at the remote location of the forward foil. In this case, the vessel LCG is also moving in the negative z direction of the global frame of reference. Therefore, the result is a positive superposition of the motions at the forward foil location. The same response is valid for the case of maximum negative vessel pitch. For the aft foil the exact opposite is the case where the pitch-induced heave is out of phase with the absolute heave of the vessel, and a negative superposition occurs, which consequently reduces the relative motion at the location of the aft foil. This kinematic difference between the forward and aft foil occurs for all head waves that have a wavelength of equal to or greater than the waterline length of the vessel. A reversal of this effect is observed for following waves and at high waves frequencies in head waves. The latter is a result of a change in the phase of the vessel motion which is independent of heading and due to the response of the vessel in waves of a wavelength less than the length of the vessel. The result is that the pitch motion of the vessel changes phase with respect to the vessel heave. This effect is shown in Figure 6.4 where the response of the aft foil is greater than the forward foil for higher wave frequencies.

The difference between the forward and aft foil could also be attributed to the effect of the leading foil on the trailing foil with regard to vortices shed from the leading foil. The shed vortices

interact with the trailing foil, which results in either an increase or decrease the propulsive efficiency. This interaction is governed by the state of the vortical flow at the instantaneous location of the trailing foil. Kinsey and Dumas (2012) proposed the following phase parameter for tandem foil configurations that defines the relative position of the trailing foil to the vortex street:

$$\frac{\Psi_f}{2\pi} = \frac{\xi_f}{VT_f} + \frac{\epsilon_f}{2\pi} \tag{6.9}$$

where ξ_f is the interfoil spacing, T_f is the flapping period of both foils, V is the relative flow speed and ϵ is the phase difference between the flapping heave of the two foils. For a wave propelled vessel with foils located at the forward and aft perpendiculars the flapping frequency is equal to the encountered wave period and the phase difference is positively out of phase for head waves and negatively for following waves, and Equation 6.9 reduces to:

$$\frac{\Psi_f}{2\pi} = \frac{L_{WL}}{UT_e} \pm \frac{1}{2} \tag{6.10}$$

Boschitsch et al. (2014) performed experiments on tandem flapping foils in a water channel at a reduced frequency of 1 and Strouhal number of 0.25: values which are similar to those observed for wave propulsion. These experimental results show that, depending on the phase difference and the interfoil spacing, the efficiency of the trailing foil fluctuates between 1.5 and 0.5 times the efficiency of a single foil. This effect is prominent at low interfoil spacing to foil chord ratios ($\xi_f/c < 2.5$), and decreases with an increase in interfoil spacing (Boschitsch et al. 2014). Epps et al. (2016) presented these results with respect to the flow stream velocity and flapping period, which showed that the analysis is equivalent for the non-dimensional interfoil spacing parameter in Equation 6.9 ($\frac{\xi_f}{VT_f}$). For a non-dimensional interfoil spacing parameter of greater than 4, the experimental results show that the effect on the trailing foil propulsive efficiency is minimal. For the free running experiments in head waves presented in Chapter 4, the non-dimensional interfoil spacing parameter ranges from 3.5 to 15, which results in a limited effect of the leading foil on the trailing foil, and it is, therefore, acceptable to neglect this effect in the numerical model. However, for constant speed wave augmented propulsion it is important to consider this effect and adjust the flapping phase or forward speed to ensure a positive effect on the efficiency of the trailing foil. This effect also has consequences for semi-active wave propulsion, whereby the submerged foils are actively actuated to enhance the propulsive efficiency in waves.

6.3 Wave-phasing parameter

The experimental results show that the pitch amplitude (θ_0) and flapping phase (ϕ) of the forward foil are both noticeably greater that that of the aft foil in head waves, see Figures 4.28a and 4.29. This can be partly attributed to the increase in foil heave amplitude, but the foil-wave interaction is also a key factor. The foil-wave interaction is defined by a 'wave-phasing' parameter (Ψ_{rel}). The wave-phasing is the phase difference between the vertical wave orbital velocity and the flapping foil heave displacement. The wave-phasing parameter is equal to $\pi/2$ if the foil heave velocity and the vertical wave orbital velocity are exactly out of phase. De Silva & Yamaguchi (2012) showed that, for a foil oscillating beneath waves, a wave-phasing parameter of $\pm\pi/2$ results in optimum thrust generation.

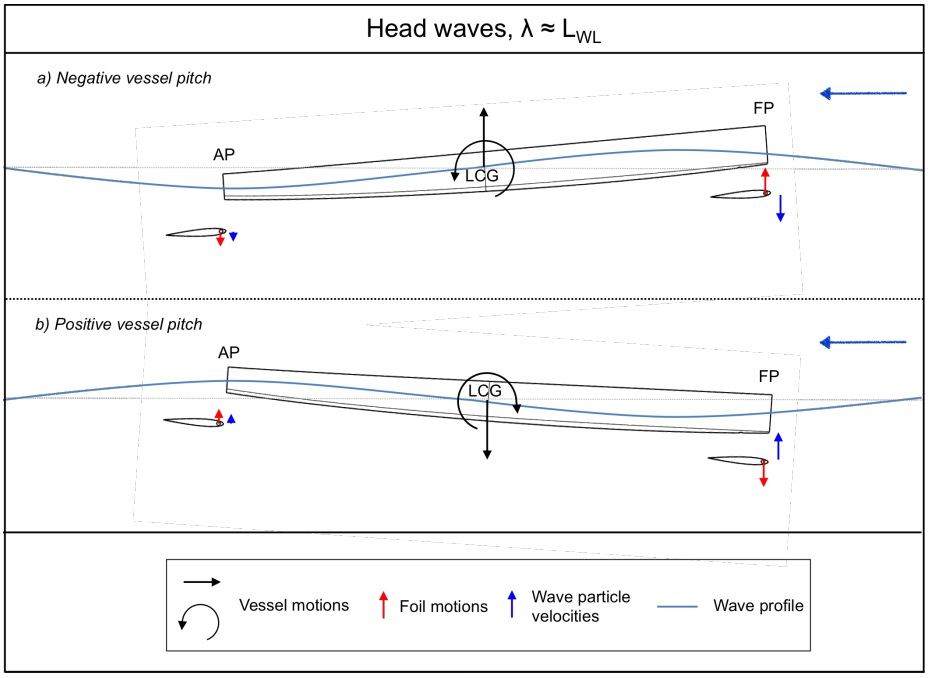

Figure 6.5: Head waves; 'wave-phasing'

This can be explained by the phasing of the wave-induced vessel motions. In head waves, the combination of negative vessel pitch (bow up) and positive vessel heave, drives the forward foil in the positive z-direction, which opposes the local motions of the wave particles, illustrated in Figure 6.5. Similarly, for negative vessel pitch, the forward foil is forced in the negative z-direction and is also out of phase with the wave particle motions. In contrast, the aft foil is out of phase with the vessel

heave motion and in phase with the wave particle motions, which has an adverse effect on the thrust generated at the aft foil.

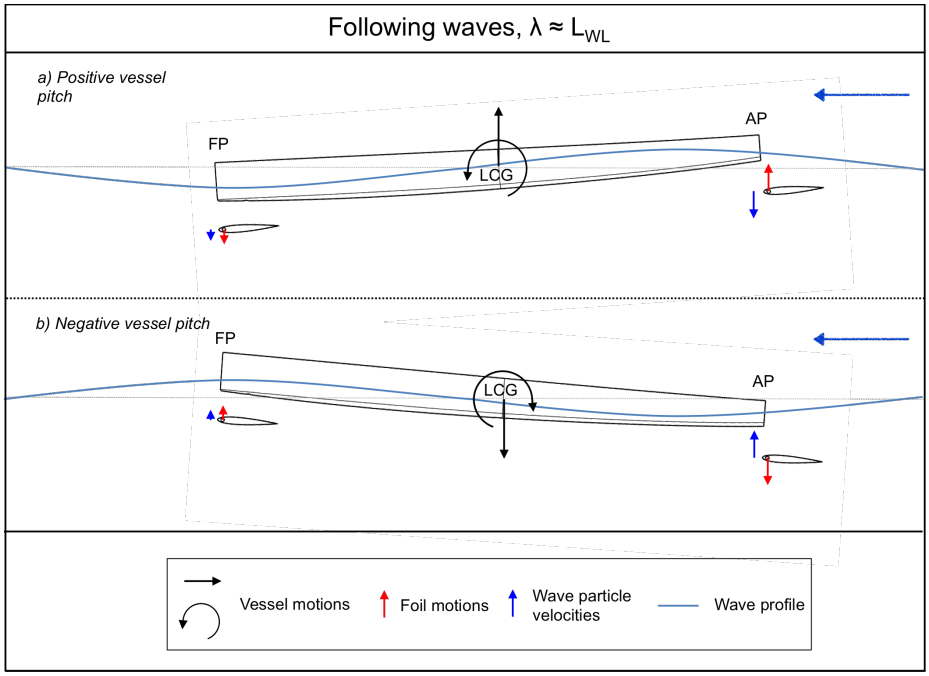

Figure 6.6: Following waves; 'wave-phasing'

This mechanism is reversed in following waves (illustrated in Figure 6.6), which supports the case for aft and forward mounted foils onboard wave propelled boats, contrary to the conclusion drawn by Bockmann (2015) but in agreement with the preliminary results of Feng et al. (2014).

In comparison to the aft foil, the forward foil is more out of phase with the incoming wave orbital motions, which causes an increase in the force acting on the foil and an increase in the flapping phase, as shown in Figure 6.7. This can be explained by considering the location of the foil at the point of maximum vessel pitch, which is assumed to be at the inflection point of the incoming wave profile. The location of the foil in relation to the wave at this instance determines the apparent heave of the foil (h_r), which is the sum of the foil heave and local relative vertical wave particle motion.

To maximise the energy extracted from the incoming wave in terms of thrust, the foil must be at a location where the maximum induced foil heave is out of phase with the vertical component of the wave particle trajectory, which is equivalent to a wave-phasing equal to $\pm\pi/2$. Figures 6.8a and 6.8b show the effect of the forward foil location on the wave-phasing and the resultant thrust,

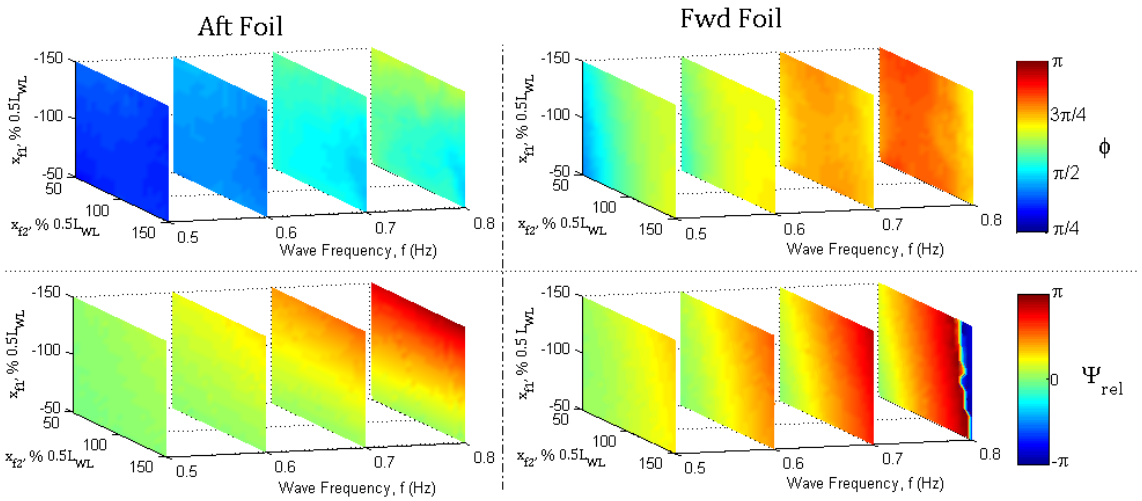

Figure 6.7: Simulation of flapping foil phase and 'wave-phasing' for different foil locations in head waves

respectively. The results are in agreement with the conclusions of De Silva and Yamaguchi (2012).

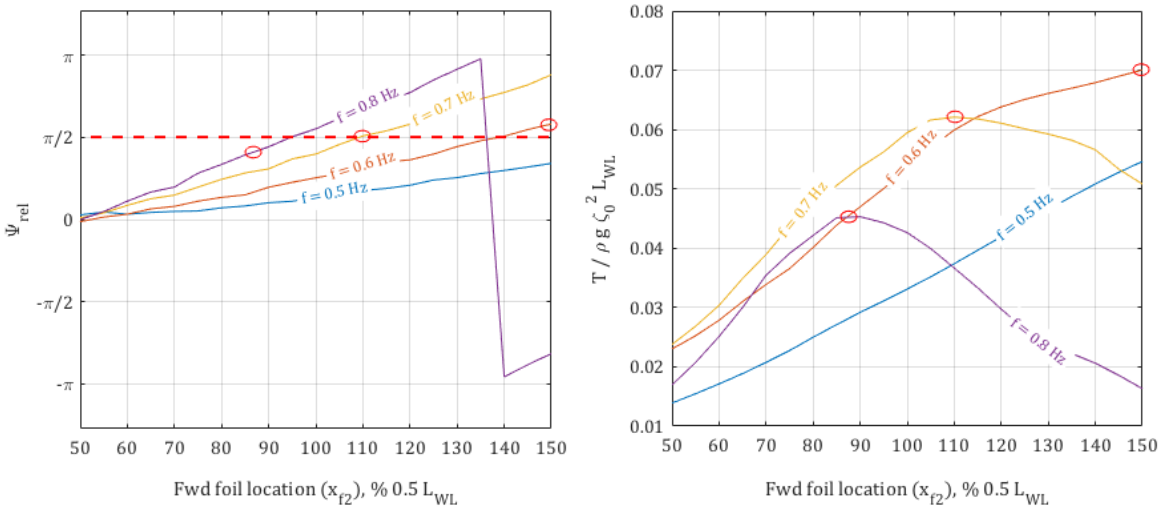

(a) Wave-phasing parameter

(b) Non-dimensional thrust coefficient

Figure 6.8: Simulation results for varying forward foil location with the aft foil size equal to that of the forward foil in head waves (the circular markers highlight the peak response)

With respect to the foil location, Figure 6.8b is in agreement with previous research, which also showed that the optimal forward foil location moves forward with a decrease in wave frequency (Naito et al. 1986). By comparing the Figure 6.8a and 6.8b, it can be seen that the peak thrust is

generated at a foil location where the wave-phasing is approximately equal to $\pi/2$, which shows the importance of the wave-phasing parameter on the wave-induced thrust generation.

The numerical analysis shows that the foil location has a significant effect on the wave-phasing parameter, particularly for the forward foil with head waves. In this case, the increased thrust from the forward foil is due to an increase in the flapping amplitude, which is discussed in the next section.

6.4 Flapping foil characteristics

6.4.1 Spring constant

The analysis in Section 5.3.3 shows that the optimal spring constant is highly frequency dependent and is, therefore, an important parameter for wave propulsion. The spring restoring force defines the amplitude of the foil pitch and the phase difference between the foil heave and pitch. Figure 6.9 shows the time history of the heave and pitch response of the forward and aft foil for head waves. As expected, an increase in the spring constant reduces the pitch amplitude of the foil, but there is an additional effect due to the forward speed and change in vessel motions.

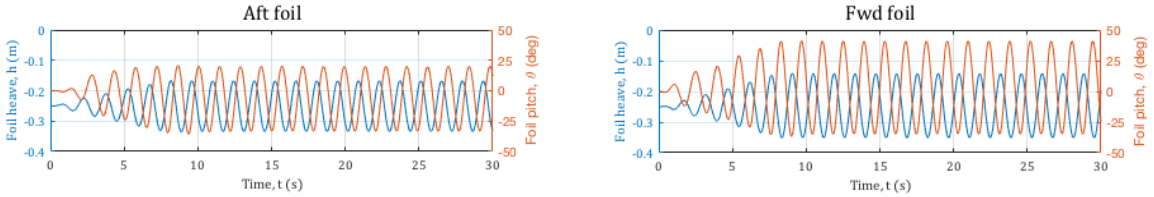

(a) 5 Nm/rad, $\bar{U} = 0.22ms^{-1}$

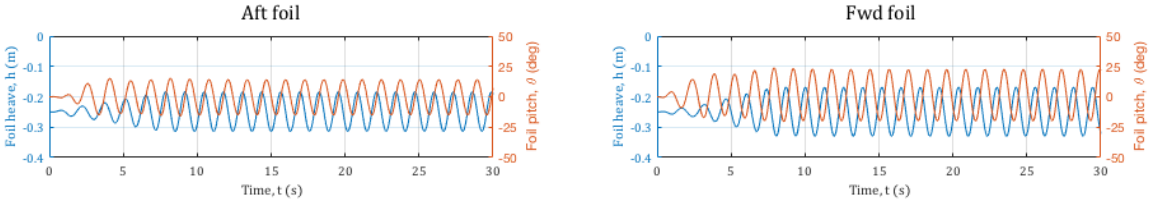

(b) 10 Nm/rad, $\bar{U} = 0.45ms^{-1}$

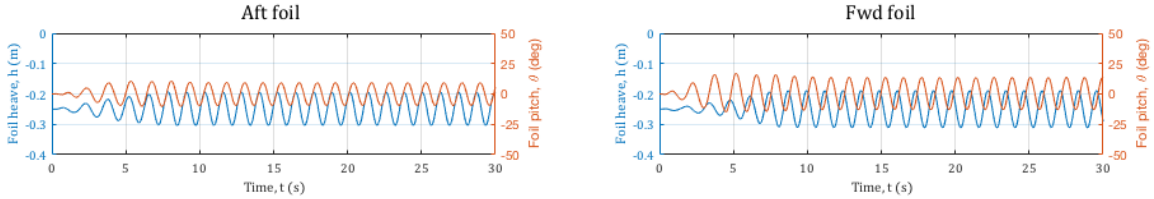

(c) 20 Nm/rad, $\bar{U} = 0.62ms^{-1}$

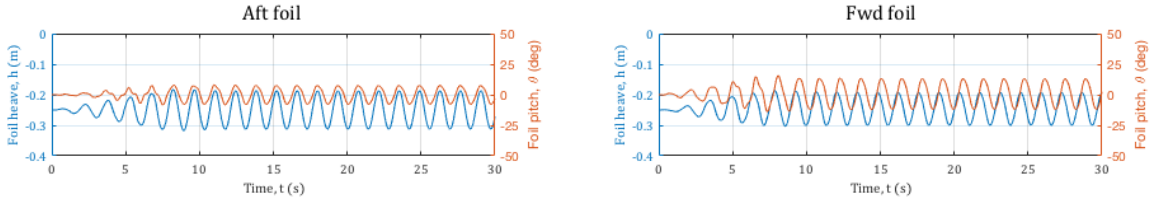

(d) 40 Nm/rad, $\bar{U} = 0.27ms^{-1}$

Figure 6.9: Time histories of the hydrodynamic force resolved in the x-direction (T_x) of the forward and aft foil for different spring constants in head waves ($\zeta_0 = 0.06m, \omega = 0.65Hz$)

The magnitude of the vessel motions varies with wave frequency and the forward speed of the vessel. However, in the case of the two extreme spring constants the forward speeds are the same but the induced foil heave is significantly different. For the higher spring constant (40 Nm/rad) the foil pitch is reduced, which results in larger proportion of the lift force acting in the vertical plane and opposing the vessel pitch moment. This effect has the consequence of reducing the induced foil heave.

Although the resultant foil heave amplitudes in Figures 6.9c and 6.9d are similar, the higher spring constant of 40 Nm/rad is more than 50% less efficient than the 20 Nm/rad case. Whilst the amplitudes are similar, the flapping frequencies are significantly less for lower speed case, for which the flapping phases are also far from the optimum phase of between 90^o and 110^o, shown in Table 6.1. The foil pitch amplitude for the cases of the two highest spring constants are also similar, but this is misleading due the effect of the forward speed on the foil pitch response: an increase in forward speed reduces the amplitude of the foil pitch. This can be seen in Figure 6.9c by comparing the foil pitch at 5 seconds (16.8^o) and the pitch amplitude beyond 15 seconds (13.5^o), after which a steady state forward speed is achieved.

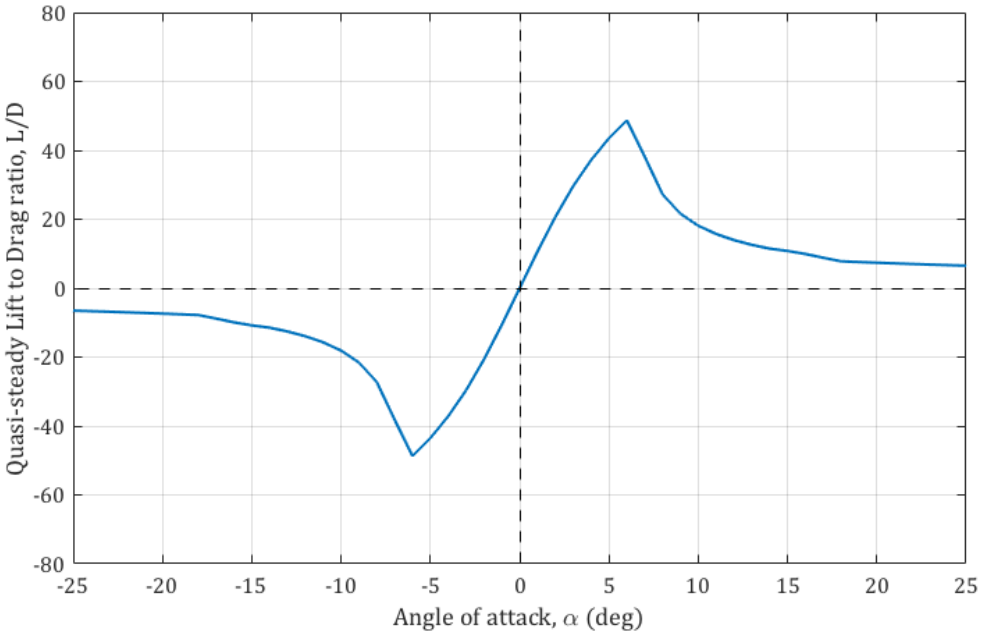

Figure 6.10: Quasi-steady lift to drag ratio for a NACA0012 foil at Reynolds number of 3.6×10^5

Furthermore, by investigating the quasi-steady lift to drag ratio, it is shown in Figure 6.10 that

there is an optimal angle of attack of approximately 6^o for the maximum lift to drag ratio. Although this does not account for the dynamic effect of the flapping foil, it provides a useful indication of the hydrodynamic effect of the angle of attack on the propulsive performance. Table 6.1 shows the average flapping phase and RMS angle of attack for the different spring constants. In this case, a spring constant of 20 Nm/rad is shown to produce the optimum flapping characteristics, which is evident in the propulsive performance of the overall coupled response. Therefore, the combination of vessel motions and foil setup is a key consideration for the optimal design of wave propelled vessels.

Table 6.1: Flapping phase of the aft and forward foil for different spring constants in head waves ($\zeta_0 = 0.06m, \omega = 0.65Hz$)

	Flapping phase ϕ (deg)		**RMS Angle of attack,** α (deg)		**Forward speed** $\bar{U}$ (ms^{-1})
Spring const.	**Aft**	**Fwd**	**Aft**	**Fwd**	-
5 Nm/rad	119.5^o	153.2^o	44.4^o	42.4^o	0.22
10 Nm/rad	83.4^o	138.9^o	12.8^o	13.8^o	0.45
20 Nm/rad	68.6^o	117.5^o	6.3^o	7.9^o	0.62
40 Nm/rad	351.7^o	44.5^o	34.6^o	41.2^o	0.27

Figure 6.11 shows a time history of the forces resolved in the x-direction for the forward and aft foil. At the extreme spring constants (5 Nm/rad and 40 Nm/rad) the forces are shown to oscillate approximately about zero with a double peak in positive thrust. In contrast, for the median spring constants (10 Nm/rad and 20 Nm/rad), the thrust generation for the both the forward and aft foil oscillates about a positive value, which results in a considerable increase in the overall vessel forward speed. This further highlights the importance of flapping foil characteristics on the propulsive performance of wave propelled vessels, and a method to tune the spring constant in-situ would be a significant development.

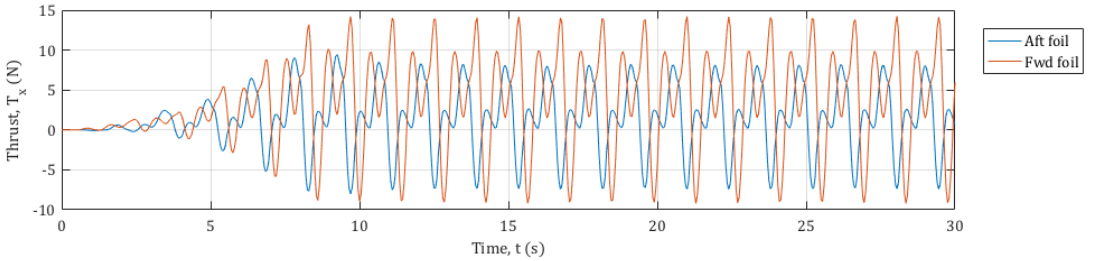

(a) 5 Nm/rad, $\bar{U} = 0.22ms^{-1}$

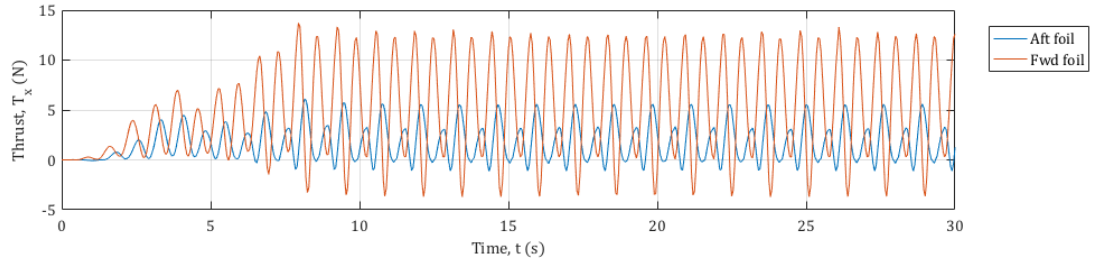

(b) 10 Nm/rad, $\bar{U} = 0.45ms^{-1}$

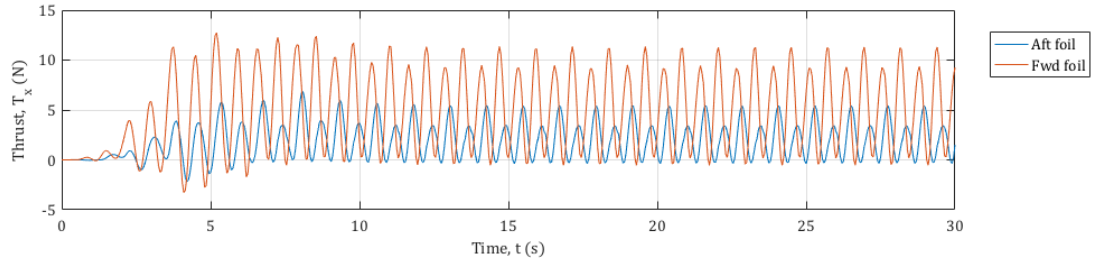

(c) 20 Nm/rad, $\bar{U} = 0.62ms^{-1}$

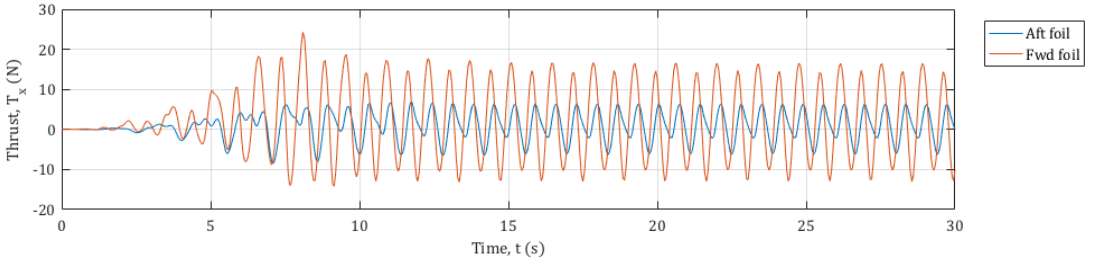

(d) 40 Nm/rad, $\bar{U} = 0.27ms^{-1}$

Figure 6.11: Time histories of the hydrodynamic force resolved in the x-direction (T_x) of the forward and aft foil for different spring constants ($\zeta_0 = 0.06m, \omega = 0.65Hz$)

6.4.2 Stouhal number

Figure 6.12 shows the numerical results of the dynamic induced heave of the forward and aft foil in head waves. As explained in Section 6.2, the difference between the aft and forward foil is due to the kinematics of the coupled response.

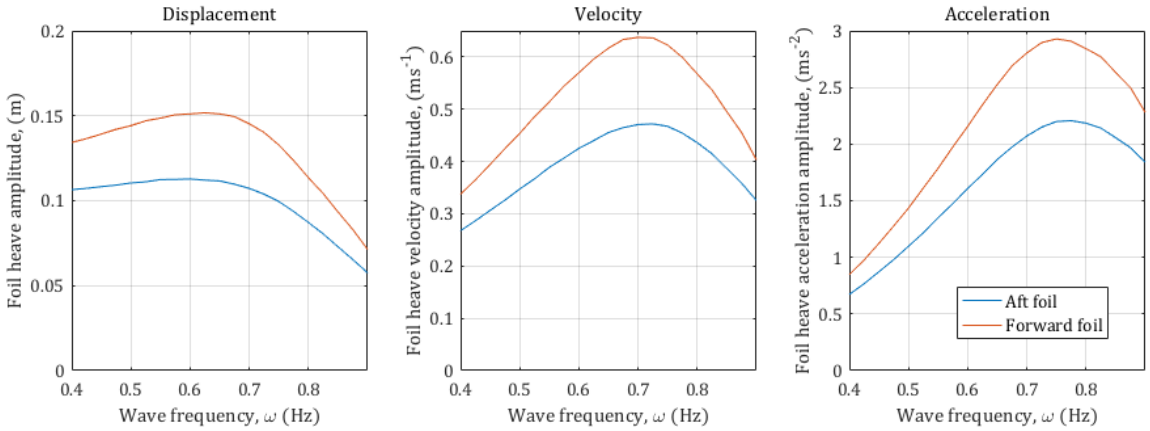

Figure 6.12: Simulation results of the induced foil heave, velocity and acceleration for head waves with the foils located at the AP and FP ($\zeta_a = 0.06$m)

The flapping foil generates a lift force, which is proportional to the square of the flow velocity, and an additional force due to the added mass, which is proportional to its acceleration. The combined effect of an increase in the foil heave velocity and acceleration results in a significant gain in propulsive thrust, as shown in Figure 6.13. A decrease in the induced foil heave at higher wave frequencies results in a significant drop in the generation of thrust for both the forward and aft foil. The significant difference between the thrust generation of the forward and aft foil is not solely due to the wave-phasing parameter, but also the difference in Strouhal number.

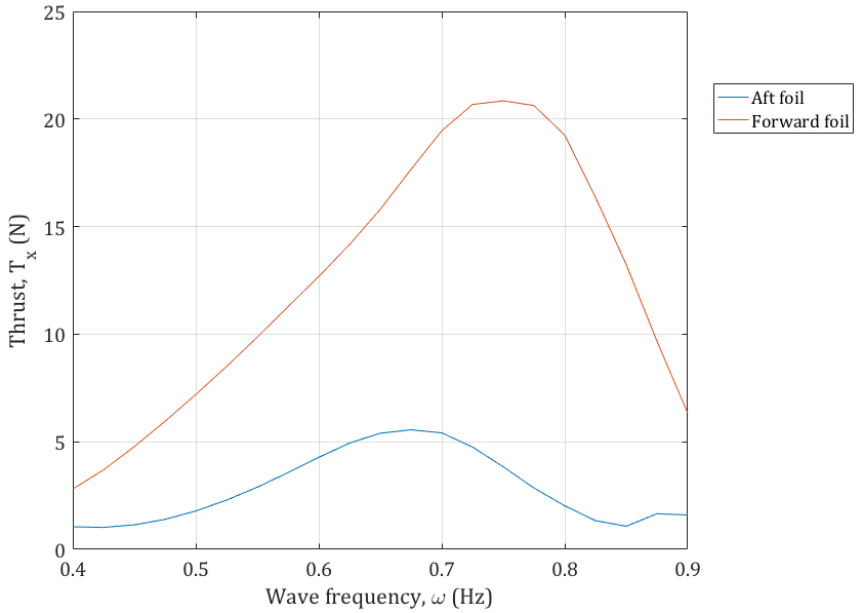

Figure 6.13: Simulation results for average thrust generated by the aft and forward foils in head waves with the foils located at the AP and FP ($\zeta_a = 0.06$m)

The Strouhal number is a dimensionless parameter that describes the frequency of vortex shedding from behind a body. For an oscillating body within a uniform flow the Strouhal number is defined by the oscillation frequency (f), the amplitude (h_0) and the flow speed(U):

$$St = \frac{2h_0 f}{U} \tag{6.11}$$

For wave propulsion, the flapping amplitude is set as the vessel-induced heave, the frequency is equal to the encountered wave frequency and the flow speed is equal to the vessel's forward speed. The Strouhal number provides a useful indication of the propulsive performance of flappings foils.

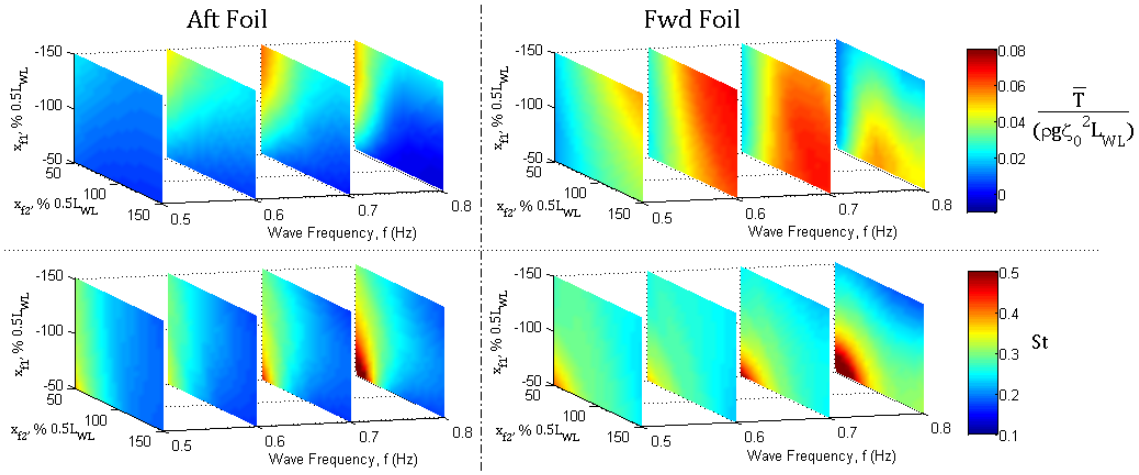

Figure 6.14: Simulation results of the flapping foil thrust coefficient and Strouhal number for varying foil locations in head waves ($\zeta_a = 0.06$m)

Figure 6.14 presents the thrust coefficient and Strouhal number for the aft and forward foils at varying foil locations and for a range of wave frequencies in head waves. The forward foil generates significantly more thrust in comparison to the aft foil and operates at a Strouhal number of approximately 0.3. Interestingly, research has shown that Strouhal numbers from 0.2 to 0.4 are associated with the peak propulsive efficiency obtained by flying animals (Taylor et al. 2003) and 0.25 to 0.35 for aquatic swimming animals (Triantafyllou et al. 1991). For cases where the forward foil is located beyond the forward perpendicular, the aft foil operates at a Strouhal number of approximately 0.2. In this case, the extended forward foil significantly reduces the wave-induced motions so that the flapping heave amplitude of the aft foil is significantly reduced and the corresponding Strouhal number decreases.

Chapter 7

Conclusions and recommendations for future work

7.1 Conclusions

Whilst significant research has been conducted in the area of submerged foils for ship efficiency in waves, it is only recently that the focus has shifted towards wave propelled USVs. This thesis has presented numerical and experimental analysis of a free running wave powered vessel, with a particular focus on the dynamic response of foils mounted at the bow and stern.

An important area of research that has not been previously investigated is the ability to predict the free running forward speed of pitch-driven wave propelled vessels. In this thesis, a method for achieving this has been developed by combining the theories of seakeeping and unsteady flapping foils. Whilst each theory is not complex, the coupling of a foil and vessel in waves with consideration of the Doppler effect is a novel approach. Using this method, a numerical model has been developed to predict the forward speed and power generation of a flapping foil wave powered vessel in regular head and following waves, and has been shown, through experimental validation, to achieve reasonable results. A method for predicting the forward speed and power generation in irregular waves has also been proposed.

Experiments proved that the new concept of wave energy recovery is viable, and, although

the efficiency of the experimental setup was low, the analysis has shown that the concept has the potential to provide an effective means of recovering wave energy. Furthermore, if the friction losses are neglected, the numerical predictions show that a reasonable amount of power can be generated by the PMTLG power take off device. The experimental and numerical analysis has also demonstrated the ability to achieve simultaneous wave propulsion and energy recovery, and thus the potential for station keeping by adjusting the balance between thrust generation and power take-off.

Previous work has identified the difference in the effectiveness of the forward and aft foils, but has not considered this observation in detail. The coupled response has been investigated both experimentally and numerically in both head and following waves. The results show a significant increase in the response of the forward foil in contrast to the aft foil in head waves, and vice versa in following waves. This outcome is partly due to the phase difference between the vessel heave and pitch motions, which impacts the Strouhal number of the submerged flapping foils. Furthermore, the interactions of the foil with the local wave profile is shown to be of significant importance, and the optimum wave-phasing parameter is shown to be equal to $\pi/2$, which is when the foil heave velocity is out of phase with the local wave orbital vertical velocity. The analysis in this thesis shows that the location of the foil significantly effects this parameter, and its consideration is important for the design of flapping foil wave powered vessels in order to ensure that the foils are not in phase with the local wave profile at the modal wave frequency. Further analysis that investigates the fluid dynamic interactions between the forward and aft foil, and between the foils and the hull will act to further inform the effect of foil location on the coupled response. This was considered beyond the scope of this research but is highlighted as a key area for future research.

This thesis identifies the key parameters that influence the coupled response of a wave powered vessel. Parameter optimization is particularly difficult for two main reasons; design parameters are numerous; and ocean waves are highly variable. However, an obvious initial design consideration is the length of the vessel, which should be designed to match the optimum wavelength to length ratio for a given sea state. This is due to the frequency dependency of a wave powered system, which is evident for both wave propulsion and energy recovery. For a pitch-driven system, the optimum wavelength to length ratio is shown to be between 1 and 1.25, and for a heave-driven system it is shown to be 5. The proportionality law is not applicable for other parameters such as the foil size and spring constant. For these parameters it is suggested that future designs should incorporate the ability to adapt to a modal wave frequency whilst in operation. This could take the form of telescopic foils that could reduce the size of the foils for higher wave frequencies, and increase their

size for lower wave frequencies. With regard to the design of the hull form for a wave propelled vessel, the numerical results show that a large length to beam ratio, low waterplane area coefficient and light displacement is most beneficial for wave propulsion.

The validation process highlighted differences between simulation and experiment in certain areas, which suggests that additional effects are not represented in the numerical model, such as interactions between the foils and the hull, interactions with the free surface and interactions between the foils. Previous research has shown that these interactions can have positive as well as negative effects on the overall thrust generation (Epps et al. 2016, Bockmann & Steen 2016). Other factors include the dynamic stall of the foil lift due to shed vortices and transient responses in the time domain for both the vessel and foil response. These effects could be an area for future research, but for the purposes of this study, the applied numerical methods are considered acceptable.

7.2 Future work

This thesis has identified a number of areas, which would benefit from further research. Recommendations for future work are as follows:

a) An experimental analysis of the response in irregular waves for both wave propulsion and energy recovery would provide the basis to validate a numerical methodology, such as the one proposed in Chapter 6. Furthermore, to better predict the response in a real sea state, the effect of beam and quartering waves, oblique waves, and short crested waves should be investigated.

b) The concept of a wave energy recovery system utilizing submerged flapping foils has been shown to be viable, but further research is recommended to improve the efficiency and setup for in-situ applications. Also, the use of a PMTLG device may not be the most efficient mechanism and comparisons should be made with alternative methods. To complete this area of research, a full scale trial of the station keeping and recharging capability of a flapping foil wave powered vessel should be undertaken.

c) For following waves, an improved numerical method is recommended for the evaluation of vessel motions and added resistance due to waves.

d) Building on previous research in the area, a detailed fluid dynamic analysis of the interaction between the foils in a wavy flow is recommended, with a particular focus on the interaction between

the vortices shed by the leading foil and the local wave-induced flow field. Also, an investigation into the effect of the presence of the foils on the flow field around the hull is recommended, and vice versa.

e) Investigation of semi-active free running wave propulsion, whereby the foils are independently actuated to increase the thrust generation in waves, and potentially increase the efficiency of the trailing foil with regard to shed vortices.

f) Analysis of foil camber, flexibility, sweep, sectional shape and depth of submergence on the free running propulsive performance of a wave propelled vessel.

7.3 Main contributions

The following scientific contributions have resulted from the work presented in this thesis:

1. A validated hybrid numerical method to predict the free running forward speed of a flapping foil wave powered vessel.
2. Both a numerical and experimental assessment of a novel wave energy recovery concept that utilizes submerged flapping foils.
3. An explanation of the effect of the wave-phasing parameter on the propulsive performance of flapping foil wave powered vessels.
4. An experimental investigation into the effect of foil location, and an analysis of the difference in the response of bow and stern mounted foils.
5. Design guidance for flapping foil wave powered vessels, and proposal of a method to simultaneously control forward speed and recover wave energy.

Publications

The experimental aspects of this research have been partly published in the following conference papers:

1. Bowker, J., Townsend, N., Tan, M., and Shenoi, R. A. (2016) 'Experimental analysis of submerged flapping foils; implications for autonomous surface vehicles (ASVs)', In, OCEANS'16 MTS/IEEE , United States. 19 Sept 2016.

2. Bowker, J., Townsend, N., Tan, M., and Shenoi, R. A. (2015) 'Experimental study of a wave energy scavenging system onboard autonomous surface vessels (ASVs)', In, OCEANS'15 MTS/IEEE OCEANS'15 MTS/IEEE Genova, Italy. 18 - 21 May 2015.

Appendix A

History of wave propulsion; inventors and full scale trials

The first wave propelled boat was the original 'Autonaut' developed by Linden (1895). This was a 13 ft boat with forward and aft flapping fins of flexible plates (Linden 1895). However, the idea had been conceptualised much earlier by Vrooman (1858), who suggested that a series of flapping fins could harness the wave energy for propulsion. Schulve (1911) proposed a different mechanism that utilizes the wave-induced heave motion of floats alongside the hull of the vessel to drive a propeller. Other early developments involved both model and full scale trials that were only reported as interesting ideas rather than academic studies (Anon 1935, Popular Science 1950). A timeline of the early inventors is shown in Figure A.1.

Other than a full scale prototype built by Gause (Mechanix Illustrated 1967), wave propelled boats did not receive significant attention until the 1970s when Einar Jakobsen started a series of model experiments and full scale trials. Jakobsen (1981) installed a spring-loaded flapping foil at the bow of a model and performed experiments in a wave basin. Further developments, led to the first trials onboard a commercial vessel called M/S Kystfangst (Dybdahl 1986). The trials proved the full scale feasibility of submerged foils to reduce the motions of a vessel and generate thrust to augment the main propulsion. A similar full scale trial was conducted on a Russian trawler, which showed that a pair of submerged foils at the bow could significantly contribute to the propulsive thrust and reduce the pitch motion of the vessel by up to 50% (Nikoel et al. 1995).

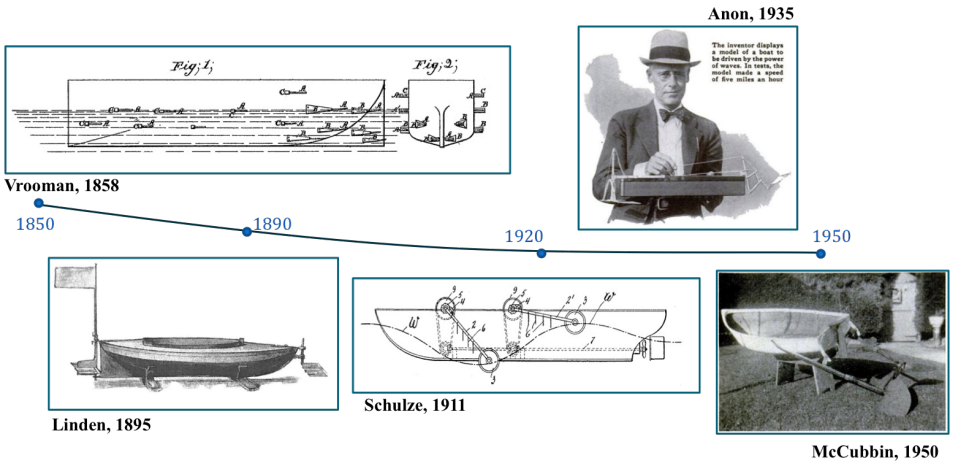

Figure A.1: Early years - inventors

In parallel to the developments in Europe, a similar setup was installed on a fishing boat in Japan by Isshiki (1991). The trials in Japan recorded a reduction in vessel pitch and an overall reduction in resistance as well as a reduction of slamming at the bow (Terao and Isshiki 1991). Terao then designed a specialised wave driven flapping foil propulsion system for a catamaran called the Suntory Mermaid II. In 2008, Suntory Mermaid II spectacularly demonstrated the feasibility of a purely wave propelled vessel by crossing the Pacific Ocean in 110 days, which remains the longest voyage undertaken by a manned wave propelled boat (Popular Science 2008). Figure A.2 shows a timeline of full scale wave propelled boat trials.

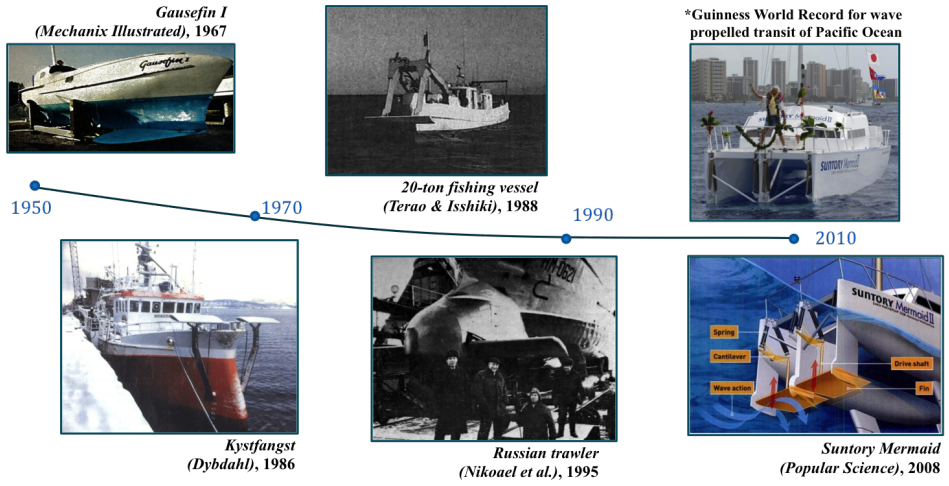

Figure A.2: Post 1950s full scale trials

Appendix B

Surge force empirical correction

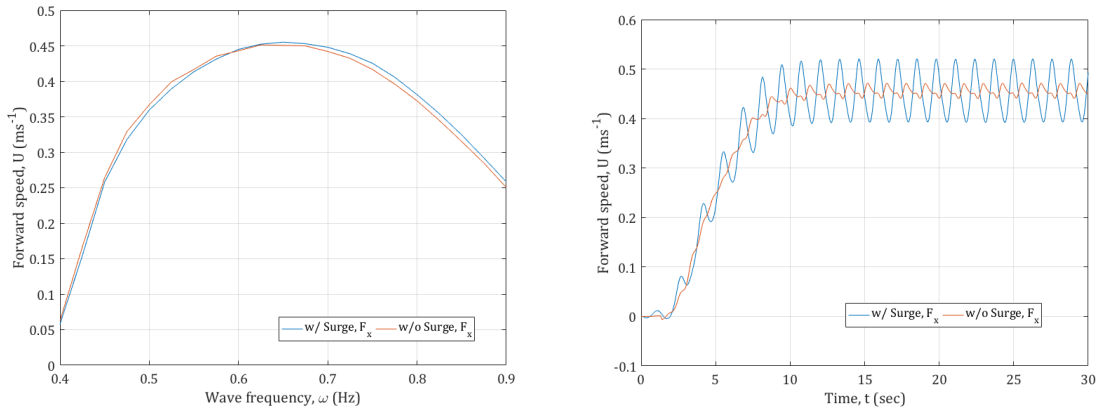

(a) Frequency domain

(b) Time domain

Figure B.1: Forward speed comparison with and without the addition of a wave-induced surge force

Whilst the numerical prediction of the vessel surge force was shown to be inaccurate at high wave frequencies, the overall effect on the average forward speed is shown to be minimal (see Figure B.1. However, for a complete model further analysis is provided in this appendix to investigate the surge force acting on the vessel.

Previous research has shown that the Froude-Krylov assumption can significantly over predict the surge force (Hashimoto 2016). Due to the frequency squared component in the surge force calculation, the force increases significantly with wave frequency. However, experimental data shows

that the surge force of the vessel decreases with an increase in wave frequency. The reason for this is that the Froude-Krylov surge force does not account for diffraction forces or what has been termed the Smith effect. This effect is due to the interaction of the hull form with the surrounding fluid which causes a reduction in the instantaneous pressure field of the incident wave (Korvin-Kroukovsky 1955). An empirical correction for the surge force is shown to be inversely proportional to the wave number:

$$\mu_d = \frac{1}{k^m}$$

where m is a tuning factor and equal to 0 for $k < 1$. From the analysis presented in Figure B.2 a tuning factor of 1.6 is implemened for this particular case.

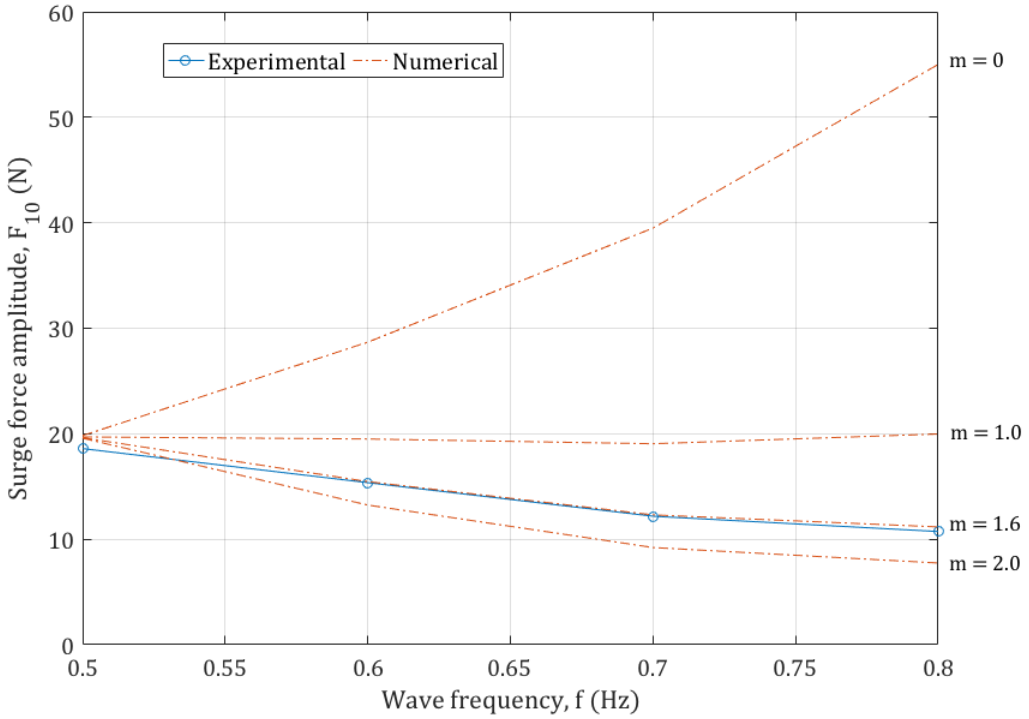

Figure B.2: Effect of the tuning factor on the empirical correction for the surge force

Appendix C

Non-dimensionalised free running results

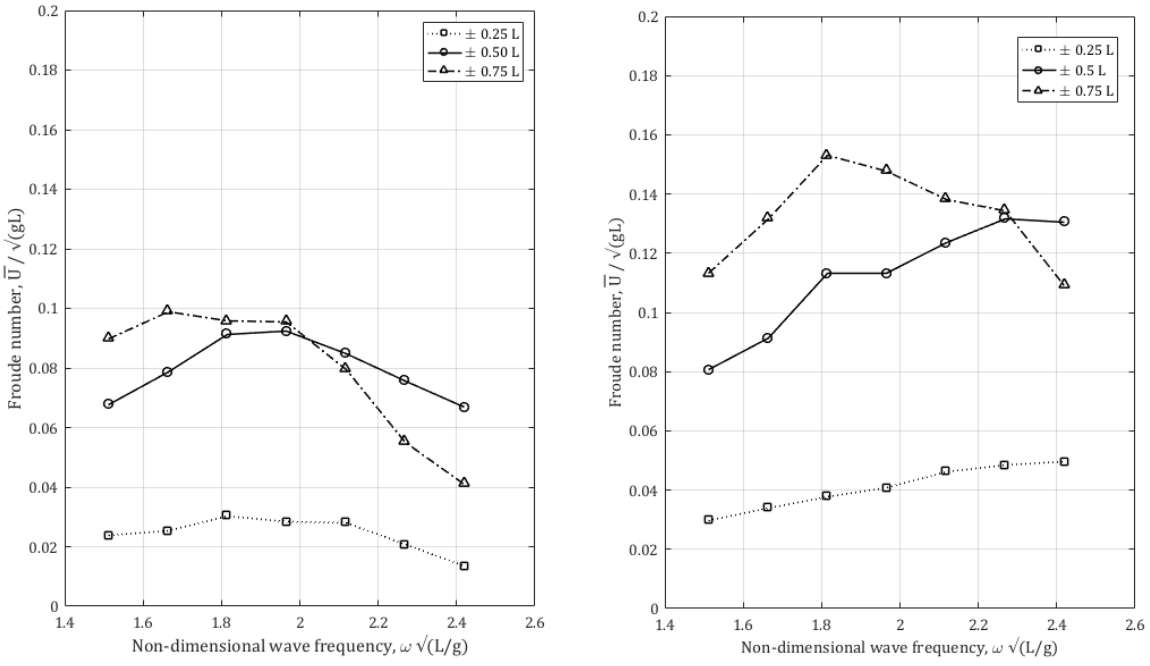

(a) Head waves

(b) Following waves

Figure C.1: Mean non-dimensional free running vessel forward speed for varying foil locations in head and following waves

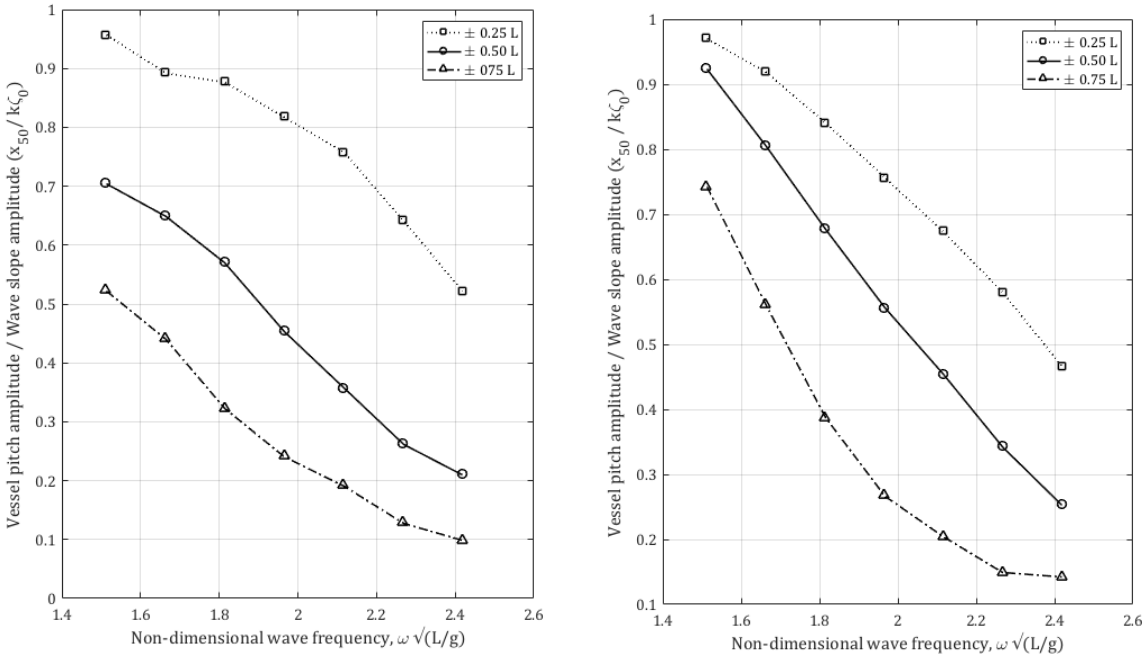

(a) Head waves (b) Following waves

Figure C.2: Free running vessel pitch RAO for varying foil locations in head and following waves

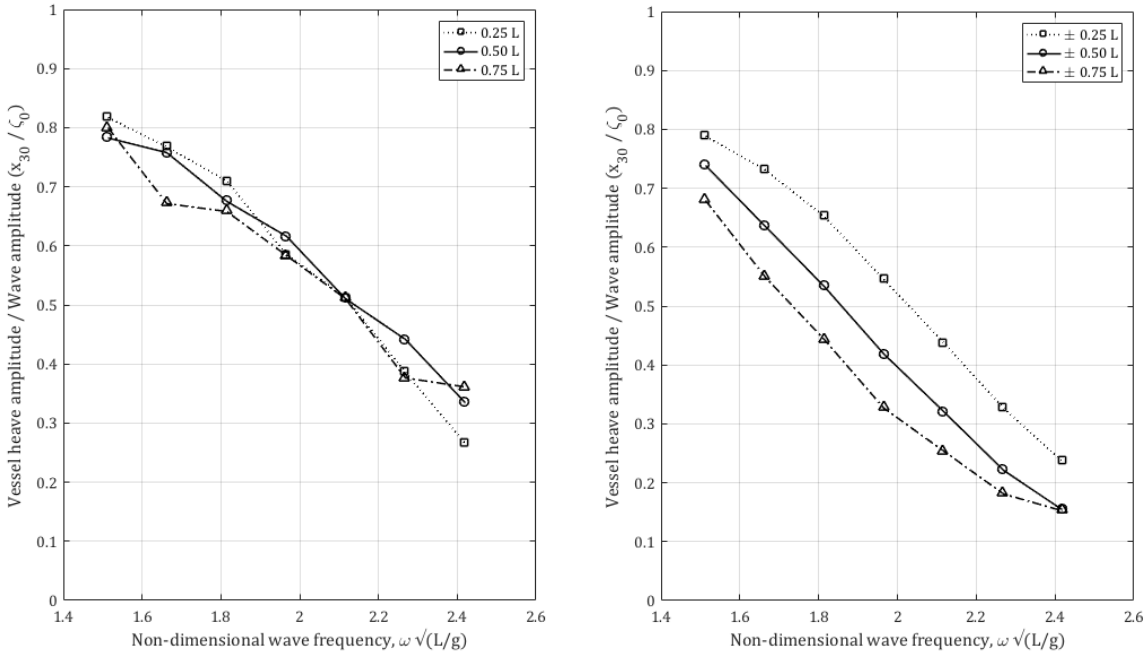

(a) Head waves (b) Following waves

Figure C.3: Free running vessel heave RAO for varying foil locations in head and following waves

References

Anderson, J. M., Streitlien, K., Barrett, D. S. and Triantafyllou, M. S. (1998) 'Oscillating foils of high propulsive efficiency', Journal of Fluid Mechanics, 360, pp. 41-72.

Anon. (1983) 'Wave power for ship propulsion', The Motor Ship, 64(757), pp.67–69.

Arribas, F. (2007) 'Some methods to obtain the added resistance of a ship advancing in waves', Ocean Engineering, 34, pp. 946-955.

Babu, M., Krishnankutty, P. and Mallikarjuna, J. (2014) 'Experimental study of flapping foil propulsion system for ships and underwater vehicles and PIV study of caudal fin propulsors', In, Autonomous Underwater Vehicles (AUV), 2014 IEEE/OES, Oxford, MS. pp.1-7.

Belibassakis, K. A. and Politis, G. K. (2013) 'Hydrodynamic performance of flapping wings for augmenting ship propulsion in waves', Ocean Engineering, 72(0), pp. 227-240.

Belibassakis, K.A. and Filippas, E. (2015) 'Ship propulsion in waves by actively controlled flapping foils', Applied Ocean Research, 52, 1-11.

Belibassakis, K.A. (2015) 'Marine propulsion in waves by flapping-foil systems', In, 8th GRACM International Congress on Computational Mechanics, Volos.

Belibassakis, K., Gerostathis, Th., Filippas, E., Toubal, J. and Rey, V. (2015) 'Oscillating hydrofoils as energy devices operating in waves and currents', 11th European Wave and Tidal Energy Conference (EWTEC2015), 27-30 May, Nantes, France.

Belibassakis, K., Gerostathis, Th., Filippas, E. (2016) 'Biomimetic marine energy devices in waves an sheared currents', 2nd International Conference on Renewable Energies Offshore (RENEW2016),

24-26 October, Lisbon, Portugal.

Bentley Software (2014) Maxsurf Motions Advanced and Maxsurf Resistance [Computer Program], Available at: https://www.bentley.com/en/products/product-line/offshore-struc-tural-analysis-software/-maxsurf

Betz, A. (1912) 'Ein Beitrag zur Erklarung des Segelfluges', Zeitschrift für Flugtechnik und Motorluftschiffahrt, 3, pp. 269-272.

Bockmann, E. (2015) 'Wave propulsion of ships', PhD Thesis, NTNU, Norway.

Bockmann, E., Steen, S. (2016) 'Model test and simulation of a ship with wavefoils'. Applied Ocean Research. vol. 57.

Bockmann, E. and Steen, S. (2013) 'The Effect of a Fixed Foil on Ship Propulsion and Motions', translated by Launceston, Tasmania, Australia.

Bockmann, E. and Steen, S. (2014) 'Experiments with actively pitch-controlled and spring-loaded oscillating foils', Applied Ocean Research, 48, pp. 227-235.

Boschitsch, B.M., Dewey, P.A. and Smits, A.J. (2014)'Propulsive performance of unsteady tandem hydrofoils in an in-line configuration', Physics of Fluids, 26

Bose, N. and Lien, J. (1990) 'Energy Absorption from Ocean Waves: A Free Ride for Cetaceans', Proceedings of the Royal Society of London. Series B, Biological Sciences, 240(1299), pp. 591-605.

Cao, Y., Townsend, N.C. and Tan, M. (2017) 'Hybrid renewable energy system for ocean going platforms', At OCEANS'17 MTS/IEEE OCEANS'17 MTS/IEEE, Aberdeen, United Kingdom. 19 - 22 Jun 2017

Daniel, T., Manley, J. and Trenaman, N. (2011) 'The Wave Glider: enabling a new approach to persistent ocean observation and research', Ocean Dynamics, 61(10), pp. 1509-1520.

De Silva, L. and Yamaguchi, H. (2012) 'Numerical study on active wave devouring propulsion', Journal of Marine Science and Technology, 17(3), pp. 261-275.

Dormand, J. and Prince, P. (1980) 'A family of embedded Runge-Kutta formulae', Journal of Computational and Applied Mathematics, 6(1), pp. 19-26.

Dybdahl, K. (1988). 'Foilpropellen kan revolusjonere skipsfarten', Teknisk Ukeblad/ Teknikk, no. 39, October 1988, pp.10-11.

Ekaterinaris, J.A. and Platzer, M.F. (1997) 'Computational Prediction of Airfoil Dynamic Stall', Progress in Aerospace Sciences, 33, pp. 759-846

Epps, B.P., Muscutt, L.E., Roesler, B.T. and Weymouth, G.D. (2016) 'On the Interfoil Spacing and Phase Lag of Tandem Flapping Foil Propulsors', Journal of Ship Production and Design., pp. 1-39.

Feng, P., Ma, N. and Gu, X. (2014) 'A practical method for predicting the propulsive performance of energy efficient ship with wave devouring hydrofoils at actual seas', Journal of Engineering for the Maritime Environment, 228(4), pp. 348-361

Fenucci, D., Caffaz, A., Costanzi, R., Fontanesi, E., Manzari, V., Sani, L., Stifani, M., Tricarico, D., Turetta, A. and Caiti, A. (2016) 'WAVE: a WAVE energy recovery module for long endurance gliders and AUVs', At OCEANS'16 MTS/IEEE, Moneterey, US

Filippas, E. S. and Belibassakis, K. A. (2014) 'Hydrodynamic analysis of flapping-foil thrusters operating beneath the free surface and in waves', Engineering Analysis with Boundary Elements, 41(0), pp. 47-59.

Filippas, E.S. (2015) 'Augmenting Ship Propulsion in Waves Using Flapping Foils Initially Designed for Roll Stabilization', Procedia Computer Science, Vol. 66, pp. 103-111

Filippas, E. S., Gerostathis, T.P. and Belibassakis, K. A. (2018) 'Semi-activated oscillating hydrofoil as a nearshore biomimetic energy system in waves and currents', Ocean Engineering, 154, pp. 396-415.

Garrick, I. E. (1937) 'Propulsion of a flapping and oscillating airfoil', Report No. 567, Cranfield: NACA.

Grue, J., Mo, A. and Palm, E. (1988) 'Propulsion of a foil moving in water waves', Journal of Fluid Mechanics, 186, pp. 393-417.

Hao, H., Ma, Q., Liao, K. and Zheng, X. (2017) 'Experimental Studies on Hydrodynamics of a Floater-Adjusted Wave Propulsion Device', The 27th International Ocean and Polar Engineering Conference, 25-30 June, San Francisco, California, USA

Harper, K. A., Berkemeier, M. D. and Grace, S. (1998) 'Modeling the dynamics of spring-driven oscillating-foil propulsion', Oceanic Engineering, IEEE Journal of, 23(3), pp. 285-296.

Hashimoto, H., Yoneda, S., Tahara, Y. and Kobayashi, E. (2016) 'CFD-based study on the prediction of wave-induced surge force, Ocean Engineering, Volume 120, pp. 389-397

Hine, R., Willcox, S., Hine, G. and Richardson, T. (2009) 'The Wave Glider: A Wave-Powered autonomous marine vehicle', OCEANS 2009, MTS/IEEE Biloxi - Marine Technology for Our Future: Global and Local Challenges, 1.

Hine, R. (2013) 'Watercraft that harvest both locomotive thrust and electrical power from wave motion', US8808041

Hoener, S.F, "Fluid dynamic drag", published by author, 1965

Hough, G.R. and Moran, S.P. (1969) 'Froude number effects on two-dimensional hydrofoils', Journal of Ship Research, 13, pp. 53-60.

Huang, S., Wu, T., Hsu, Y., Guo, J., Tsai, J. and Chiu, F. (2016) 'Effective energy-saving device of Eco-Ship by using wave propulsion', Techno-Ocean 2016, Kobe, Japan

Isshiki, H. (1982) 'A Theory of Wave Devouring Propulsion : 1st Report : Thrust Generation by a Linear Wells Turbine', Journal of the Society of Naval Architects of Japan, (151), pp. 54-64.

Isshiki, H. and Murakami, M. (1983) 'A Theory of Wave Devouring Propulsion(3rd Report): An Experimental Verification of Thrust Generation by a Passive-type Hydrofoil Propulsor', Journal of the Society of Naval Architects of Japan, (154), pp. 125-135.

Isshiki, H. and Murakami, M. (1984) 'A Theory of Wave Devouring Propulsion(4th Report): A Comparison Between Theory and Experiment in Case of a Passive-Type Hydrofoil Propulsor', Journal of the Society of Naval Architects of Japan, (156), pp. 102-114.

Isshiki, H. (1994) 'Wave energy utilization into ship propulsion by fins attached to a ship', Proceedings of the Fourth International Offshore and Polar Engineering Conference, Osaka, Japan (Apr/1994), pp. 508-521

Isshiki, H. (2015) 'Utilization of Wave Energy to Improve Propulsive and Seekeeping Performances of a Ship in Rough Weather', Asian Journal of Engineering and Technology, 3(6).

ITTC (1957) Proceedings of the 8th ITTC, Canal de Experiencias Hidrodinamicas, El Pardo, Madrid, Spain

ITTC (2005) 'Testing and Extrapolation Methods, Loads and Responses, Seakeeping Experiments', ITTC Recommended Procedures and Guidelines Report

ITTC (2008) 'Guide in the Expression of Uncertainty in Experimental Hydrodynamics', ITTC Procedure 7.5-02- 01-01

ITTC (2017) 'Verification and Validation of Linear and Weakly Nonlinear Seakeeping Computer Codes', ITTC Recommended Procedures and Guidelines Report, Seakeeping Committee of the 28th ITTC

Jakobsen, E. (1981) 'The foilpropeller, wave power for propulsion', In, Second International Symposium on Wave and Tidal Energy, BHRA Fluid Engineering, pp. 363–369.

Jones, K. and Platzer, M.F. (1997) 'Numerical Computation of Flapping-Wing Propulsion and Power Extraction', 35th AIAA Aerospace Sciences Meeting, Reno, Nevada

Jones, K., Dohring, C., and Platzer, M.. (1996) 'Wake structures behind plunging airfoils - A comparison of numerical and experimental results', 34th Aerospace Sciences Meeting and Exhibit, Aerospace Sciences Meetings,

Jones, K., Dohring, C., and Platzer, M.. (1998) 'Experimental and Computational Investigation of the Knoller-Betz Effect', AIAA Journal, 36(7), pp. 1240-1246,

Joosen, W.P.A., (1966) 'Added resistance in waves', In: Proceedings of the Sixth Symposium on Naval Hydrodynamics, Washington

Journee, J.M.J, (1976) 'Motions and Resistance of a Ship in Regular Following Waves', Report 440, Delft Univerity of Technology, Ship Hydrodynamics Laboratory, September 1976.

Katz, J. and Plotkin, A. (2001) 'Low-Speed Aerodynamics', Cambridge University Press.

Katzmayr, R. (1922). 'Effect of periodic changes of angles of attack on behavior of airfoils'.

Kim, M., Hizir, O., Turan, O., Day, S. and Incecik, A. (2017) 'Estimation of added resistance and ship speed loss in a seaway', Ocean Engineering, 141, pp. 465-476.

Kinsey, T. and Dumas, G. (2012) 'Optimal tandem configuration for oscillating foils hydrokinetic turbine', J. Fluids Eng. 134.

Knoller, R. (1909) 'Die Gesetze des Luftwiderstandes', Flug- und Motortechnik, 3, pp. 1-7.

Konstantinov, G. A. and Yakimov, Y. L. (1995) 'Calculation of the thrust of a wave-powered marine propelling device', Fluid Dynamics, 30(3), pp. 453-456

Korvin-Kroukovsky, B.V. (1955). 'Investigation of ship motions in regular waves', Transactions SNAME, 63, pp.386-435.

Lighthill, M.J., (1969) 'Hydromechanics of Aquatic Animal Propulsion' Annual Review of Fluid Mechanics,1, pp.413-446

Lighthill, J. (1975) 'Mathematical Biofluiddynamics', Society for Industrial and Applied Mathematics.

Linden, H. (1895) 'Improved combination with floating bodies, of fins adapted to effect their propulsion', GB Patent 14,630. Filed Aug. 1, 1895. Patented Jul. 18, 1896.

Liquid Robotics, Inc. (2015), accessed 10 October 2015, https://www.liquid-robotics.com/

Liu, P., Li, Y.,Hong, Y. and Zhang, Y. (2011) 'The modelling and analysis of wave powering surface vehicle', at OCEANS '11 IEEE, Waikoloa, HI, USA

Liu, P., Su, Y. and Liao, Y. (2016) 'Numerical and Experimental Studies on the Propulsion Performance of A Wave Glide Propulsor', China Ocean Engineering, Vol. 30(3), pp.393-406

Lloyd, M. (1998) 'Seakeeping; Ship Behaviour in Rough Weather', Book (Revised Edition), Ellis Horwood Ltd.

Manley, J. and Wilcox, S. (2010) 'The wave glider: A persistent platform for ocean science', In, OCEANS 2010 IEEE - Sydney, Sydney, Aus

Mannam, N. P. B., Krishnankutty, P., Vijayakumaran, H. and Sunny, R. C., (2017) 'Experimental and Numerical Study of Penguin Mode Flapping Foil Propulsion System for Ships', Journal of Bionic Engineering, 14, pp. 770-780.

MathWorks Inc (2014), [Computer Software], Version R2014b.

McCormick, M. E. (2007) 'Ocean Wave Energy Conversion', DOVER PUBN Incorporated.

Mechanix Illustrated (1972) 'Mr. Gause's incredible self-propelled boat!', Article, October 1972, pp. 22

MOST (AV) Ltd (2015), accessed 10 October 2015, http://www.autonautusv.com/specificat-ions

Naito, S., Isshiki, H., and Fujimoto, E., (1986) 'Thrust Generation of a Fin Attached to a Ship in Waves', Journal of KSNAJ, 202, pp. 23–29.

Naito, S. and Isshiki, H. (2005) 'Effect of Bow Wings on Ship Propulsion and Motions', Applied Mechanics Reviews, 58

Nikolaev, M. N., Savitskiy, A. I. and Senkin, Y. U. F. (1995) 'Basics of calculation of the efficiency of a ship with propulsor of the wing type', Sudostroenie, 4, pp. 7-10.

Ngo, P., Ogle, J., Das, J., Thomas, J., Anderson, W. and Smith., R.N. (2014) 'Predicting the Speed of a Wave Glider Autonomous Surface Vehicle from Wave Model Data', Intelligent Robots and Systems (IROS 2014), 2014 IEEE/RSJ International Conference on, Chicago, IL USA

Popular Mechanics (1933) 'Fins to Stop Ship's Rolling Governed by Gyro', Article, April 1933, pp. 509

Popular Science (1950) 'Waves serve as boat's engine', Article, February 1950, pp. 224.

Popular Science (2008) 'Wave runner', Article, March 2008

Read, D.A., Hover, F.S. and Triantafyllou, M.S. (2003) 'Forces on oscillating foils for propulsion and maneuvering', Journal of Fluids and Structures, 17, 163-183

Roh, H., Joe, H., Song, S., Sung, M. and Yu, S. (2016) 'Hydrodynamic modeling and optimization of mobile wave energy harvesting system for the robotic buoy', In, OCEANS'16 MTS/IEEE Monterey, California, US

Salvesen, N., Tuck, E. and Faltinsen, O. (1970) 'Ship Motions and Sea Loads', Trans. of SNAME, pp. 78.

Sclavounos P., Borgen H. (2004) 'Seakeeping analysis of a high-speed monohull with a motion control bow hydrofoil' Journal of Ship Research 48(2), pp. 77–117

Silverstein, A. and Joyner, U. T. (1939) 'Experimental Verification of the theory of oscillating airfoils', Report no. 673, National Advisory Committee for Aeronautics (NACA).

Sheldahl, R. and Klimas, P. (1981) 'Aerodynamic Characteristics of Seven Symmetrical Airfoil Sections Through 180-Degree Angle of Attack for Use in Aerodynamic Analysis of Vertical Axis Wind Turbines', Technical Report (SAND80-2114), Sandia National Laboratories.

Schulze, O. (1911) 'Wave motor', US Patent 1,033,476. Filed Jan. 5, 1911. Patented Jul. 23, 1912.

Sun, T., Zhao, J., Yan, X. and Xu, P. (2016) 'A New Flapping-Hydrofoil Wave Power Generating Unmanned Ocean Vehicle', Proceedings of the ASME 2016 35th International Conference on Ocean, Offshore and Arctic Engineering, OMAE2016, June 19-24, Busan, South Korea.

Taghipoura, R., Perez, T. and Moana, T. (2008) 'Hybrid frequency–time domain models for dynamic response analysis of marine structures', Ocean Engineering, 35, pp. 685-705.

Taylor, G.K., Nudds, R.L. and Thomas, A.L.R., (2003) 'Flying and swimming animals cruise at a Strouhal number tuned for high power efficiency', Nature 425, pp. 707-711.

Terao, Y. (1982) 'A floating structure which moves towards the waves (possibility of wave devouring propulsion)' Journal of the Kansai Society of Naval Architects, Japan, 184, pp. 51–54.

Terao, Y. and Isshiki, H. (1991). 'Wave devouring propulsion sea trial', In, Eighteenth Symposium on Naval Hydrodynamics, pp. 287–296.

Terao, Y. and Sakagami, N. (2013) 'Application of a Wave Devouring Propulsion System to Ocean Engineering', ASME 2013 32nd International Conference on Ocean, Offshore and Arctic Engineering, Vol.5: Ocean Engineering, Nantes, France

Terao Y. and Sakagami, N. (2015) 'Design and development of an autonomous wave-powered boat with a wave devouring propulsion system', Advanced Robotics, Vol.29(1), pp.89-102

Thaweewat, N., Phoemsapthawee, S. and Juntasaro, V.,(2018) 'Semi-active flapping foil for marine propulsion', Ocean Engineering, 147, pp. 556-564

Theodorsen, T. (1935) 'General theory of aerodynamic instability and the mechanism of flutter', Report no. 496, National Advisory Committee for Aeronautics (NACA).

Thorburn, K. and Leijon, M. (2007) 'Farm size comparison with analytical model of linear generator

wave energy converters', Ocean Eng. 34, pp. 908–916

Tian, B., Yu, J. and Zhang, A. (2015) 'Dynamic modeling of wave driven unmanned surface vehicle in longitudinal profile based on D-H approach', Journal of Central South University, 22, pp. 4578-4584

Triantafyllou, M. S., Triantafyllou, G. S. and Gopalkrishnan, R. (1991) 'Wake mechanics for thrust generation in oscillating foils', Physics of Fluids A: Fluid Dynamics (1989-1993), 3(12), pp. 2835-2837.

Triantafyllou, G. S., Triantafyllou, M. S. and Grosenbaugh, M. A. (1993) 'Optimal thrust development in oscillating foils with application to fish propulsion', Physics of Fluids A: Fluid Dynamics (1989-1993), 3(12), pp. 2835-2837.

Tuncer, I.H., and Platzer, M.F., (2000) 'Computational Study of Flapping Airfoil Aerodynamics', Journal of Aircraft, 37(3), pp. 514-520.

Villareal, T. and Wilson, C. (2014) 'A Comparison of the Pac-X Trans-Pacific Wave Glider Data and Satellite Data (MODIS, Aquarius, TRMM and VIIRS)', PLoS ONE 9(4).

Von Kármán, T. and Burgers, J. M. (1935) 'Aerodynamic Theory: General aerodynamic theory.' Perfect fluids J. Springer.

Vrooman, D. (1858) 'Vibrating propeller' US Patent 22,097. Patented Nov. 15, 1858.

Wigley, W. C. S. (1934) 'A Comparison of Experiment and Calculated Wave-Profiles and Wave-Resistances for a Form Having Parabolic Waterlines', Proc. R. Soc. Lond. A, 144(851)

Wu, J., Shu, C., Zhao, N. and Tian, F. (2015) 'Numerical study on the power extraction performance of a flapping foil with a flexible tail', Physics of Fluids, 27(1).

Wu, T. Y. (1960) 'Swimming of a Waving Plate', California Institute of Pasadena, Defense Technical Information Center.

Wu, T. Y. (1972) 'Extraction of flow energy by a wing oscillating in waves', Jounral of Ship Research, 14(1), pp. 66-78.

Xie, Y., Lu, K. and Zhang, D. (2014) 'Investigation on energy extraction performance of an oscillating foil with modified flapping motion', Renewable Energy, 63, pp. 550-557.

Xie, H., Wang, D., Lin, Z., Qiu, S. and Ye, J. (2017) 'Hydrodynamic Performance of Tandem Oscillating Foils in Waves', The 27th International Ocean and Polar Engineering Conference, 25-30 June, San Francisco, California, USA

Xu, G.D, Duan, W.Y. and Zhou, B.Z. (2017) 'Propulsion of an active flapping foil in heading waves of deep water', Engineering Analysis with Boundary Elements, 84, pp. 63-76

Yamaguchi, H. and Bose, N. (1994) 'Oscillating Foils for Marine Propulsion', translated by Osaka, Japan, The Internaional Society of Offshore and Polar Engineers.

Yu, Z., Zheng, Z., Yang, X. and Chang, Z. (2016) 'Dynamic Analysis of Propulsion Mechanism Directly Driven by Wave Energy for Marine Mobile Buoy' Chinese Journal of Mechanical Engineering, 29

Zhao, J., Sun, T., Sheng, C. and Yan, X. (2016) 'A concept design of small ocean vehicle with flap-foils to harvest wave energy', In OCEANS MTS/IEEE 2016 - Shanghai, China

Zheng, Z., Huany, P., Gao., D. and Chang, Z. (2015) 'Analysis of electromagnetic force of the linear generator in point absorber wave energy converters', Journal of Marine Science and Technology, Vol. 23, No. 4, pp. 475-480

Zhou, C., Wang, B., Zhou, H., Li, J. and Xiong, R. (2017) 'Dynamic modeling of a wave glider' Frontiers of Information Technology & Electronic Engineering, 18(9), pp. 1295-1304

Zhu, Q., Wolfgang, M. J., Yue, D. K. P., and Triantafyllou, M. S., (2002) 'Three-dimensional flow structures and vorticity control in fish-like swimming', Journal of Fluid Mechanics, 468, pp 1-28

Conference papers

For reference, the following publications are attached:

1. Bowker, J., Townsend, N., Tan, M., and Shenoi, R. A. (2016) 'Experimental analysis of submerged flapping foils; implications for autonomous surface vehicles (ASVs)', In, OCEANS'16 MTS/IEEE , United States. 19 Sept 2016.

2. Bowker, J., Townsend, N., Tan, M., and Shenoi, R. A. (2015) 'Experimental study of a wave energy scavenging system onboard autonomous surface vessels (ASVs)', In, OCEANS'15 MTS/IEEE OCEANS'15 MTS/IEEE Genova, Italy. 18 - 21 May 2015.

Experimental analysis of submerged flapping foils; implications for autonomous surface vehicles (ASVs)

J. A. Bowker, N. C. Townsend, M. Tan, R. A. Shenoi
Fluid Structure Interactions Group, Faculty of Engineering and the Environment
University of Southampton
SO17 1BJ UK
jab1e08@soton.ac.uk

***Abstract*—Autonomous surface vehicles (ASVs) have proven effective as ocean observing platforms for maritime operations. In most cases it is advantageous to operate ASVs for extensive missions in order to maximize their cost effectiveness. Such long endurance missions require ASVs to be capable of scavenging ambient energy from the surrounding ocean environment.**

Submerged flapping foils are currently utilized as an effective mechanism to convert ocean wave energy directly into propulsion. The authors propose a novel setup whereby these foils can heave relative to the surface vehicle and, through the application of a power take off (PTO) system, can recover a proportion of the incoming wave energy.

Experiments were performed to investigate the coupled response between a surface vehicle and submerged flapping foils within the context of generating power and propulsion from incoming waves onboard ASVs. Results show that the response of a surface vehicle with submerged flapping foils is particularly sensitive to design parameters such as the longitudinal location of the foils and the seakeeping characteristics of the surface vehicle. Through optimising the PTO system, this setup could recover a useful proportion of wave energy for ASV platforms.

I. Introduction

Autonomous surface vehicles (ASVs) are constantly exposed to ambient wave energy and efforts towards harnessing this ocean energy have been mostly restricted to wave-propelled boats utilizing the response of submerged flapping foils. The aim of this paper is to analyse the wave induced coupled relationship between a surface vehicle and submerged flapping foils for not just propulsion but also wave energy scavenging onboard ASVs.

Whilst the concept of wave-induced submerged flapping foil propulsion was established almost 120 years ago, the application has not been fully realised until recently with the emergence of ASV technology. Figure 1 shows the cumulative publications relating to wave-propelled boats. An increase in the research area is noted during the 1980s, which is mainly attributable to the research carried out by Isshiki et al. on the principles of flapping foil wave propulsion [1,2,3,4].

MOST (Autonomous Vessels) Ltd have developed a long range endurance wave propelled ASV called AutoNaut, shown in Figure 2 [5]. Through utilizing the wave-induced response of submerged flapping foils at the bow and stern,

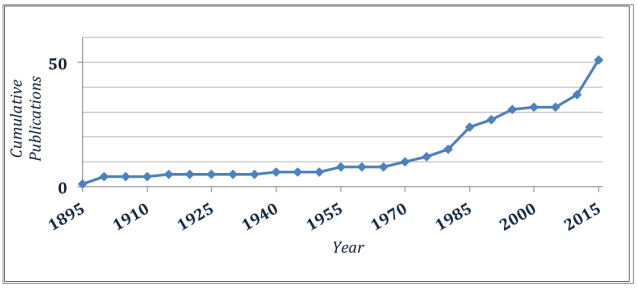

Figure 1: Cumulative publications on flapping foil wave propulsion

AutoNaut propels itself based upon the techniques patented and developed by Linden and Jakobsen respectively [6,7]. The Wave Glider ASV, developed by Liquid Robotics, operates on a similar principle but predominantly harnesses the wave-induced heave motion of a surface float [8]. A series of prototype 'wave devouring' ASVs have also been developed by Terao at the Sakagami Laboratory, which are small catamarans with two submerged foils mounted at the bow [9]. The forward speed of such vehicles is predominantly dictated by the encountered wave energy and current systems follow a circular pattern for station keeping scenarios [8].

The proposed setup, depicted in Figure 3, could alleviate the necessity to follow circular routes for station keeping and, instead, recover wave energy for the powering of onboard systems. If the foils are free to heave relative to the surface vehicle there is minimal induced flow over the foils and the resultant thrust is reduced. In this instance, a proportion of wave energy, which would be converted into propulsion, is absorbed through the relative motion of the foils and harnessed by a PTO system.

A. Wave energy scavenging

The potential to harvest wave energy for onboard power generation on ASVs or AUVs remains relatively unexplored and requires further investigation. Townsend (2015, 2016) has developed a theory and experimental platform to recover wave

energy. The system is based upon the gyroscopic principle, whereby a spinning flywheel reacts to the wave-induced motions and energy can be captured from the resultant precessional torque from the gyroscopic system [10,11]. Brown et al. (2006) carried out an initial analysis on an inertial energy capture system for an autonomous underwater vehicle (AUV) that involves a mass-spring system combined with a backdriven ball screw generator. The study concludes that a linear magnetic system maybe a more suitable and simple power take-off system [12]. A similar mass-spring theory can be applied for the recovery of wave energy using submerged flapping foils. In this case, a linear magnet generator is regarded as a more effective solution due to the absence of inefficient gearing systems.

B. Wave energy propulsion

A comprehensive understanding of the coupled dynamics of a surface vehicle with submerged flapping foils is required to inform the design of vehicles solely powered by waves such as ASVs. Figure 3 schematically shows how the wave energy induces the hull motions which is directly coupled with the response of the submerged flapping foils. The wave induced hull motion creates an incident flow velocity and angle of attack at the leading edge of a submerged flapping foil, which consequently generates a propulsive thrust. It is well established that the pitch motion of a vessel in a seaway is significantly reduced due to the presence of a foil submerged at the bow [13,14]. With respect to this coupled response between a surface vehicle and submerged flapping foils, previous numerical analysis has addressed the foil location and size. Naito and Isshiki (1986), Beblissakas and Filippas (2015) and Bockmann (2015) showed that, for a ship with a fixed speed in waves, the longitudinal location of the foil has a large effect on the thrust generated and reduction in vessel motions [15,16,17]. The experimental analysis of this effect is yet to be carried out and is considered a key aspect in the design of a wave propelled ASV.

II. Coupled response

The vessel heave (η_3) and pitch (η_5) motions in waves are defined by Newtonian equations of motion which combine the inertial, damping, restoring, coupled and forcing terms. The following equations of motion also include the effect of submerged foils by adding terms for the vertical hydrodynamic force (${F_{3_i}}^F$) due to the foils and the associated moment about the LCG (${F_{5_i}}^F$):

Figure 2: MOST (AV) Ltd ASV; AutoNaut [5]

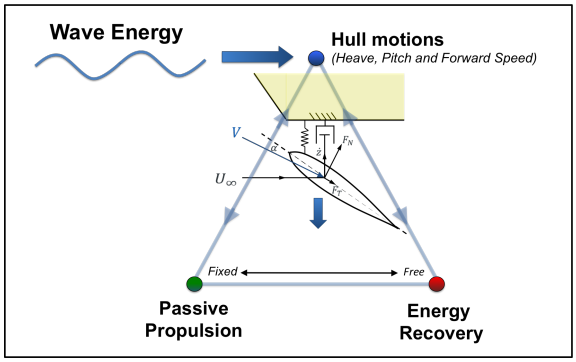

Figure 3: Schematic outlining the research problem

$$\underline{Heave}: \quad \overbrace{(M_B + A_{33})\ddot{\eta}_3}^{Inertial} + \overbrace{B_{33}\dot{\eta}_3}^{Damping} + \overbrace{C_{33}\eta_3}^{Restoring} + \overbrace{A_{35}\ddot{\eta}_5 + B_{35}\dot{\eta}_5 + C_{35}\eta_5}^{Coupled} = \overbrace{{F_3}^B + {F_{3_i}}^F}^{Forcing} \tag{1}$$

$$\underline{Pitch}: \quad \overbrace{(I_5 + A_{55})\ddot{\eta}_5}^{Inertial} + \overbrace{B_{55}\dot{\eta}_5}^{Damping} + \overbrace{C_{55}\eta_5}^{Restoring} + \overbrace{A_{53}\ddot{\eta}_3 + B_{53}\dot{\eta}_3 + C_{53}\eta_3}^{Coupled} = \overbrace{{F_5}^B + {F_{5_i}}^F}^{Forcing} \tag{2}$$

where the terms are defined as follows ($i, j = 3, 5$):

${F_3}^B$ - heave excitation force due to waves
${F_5}^B$ - pitch excitation force due to waves
${F_3}^F$ - heave force due to submerged foils
${F_5}^F$ - pitch force due to submerged foils
M - total mass of the vessel
I_j - moment of inertia for vessel
A_{ij} - added mass coefficient
B_{ij} - damping coefficient
C_{ij} - hydrostatic restoring coefficient for pure heave

These equations describe the coupled motion whereby the resultant hydrodynamic forces acting on the foils have a significant influence on the hull motions. For thrust generation the submerged foils are forced to oscillate in the incoming waves as shown in Figure 4 a). Consequently a hydrodynamic lift force acts on the foil which, when resolved in the forward direction, combines to overcome the foil drag and hull resistance to drive the vessel forward. Alternatively, the hydrodynamic forces acting on the foil can result in a relative foil motion which opposes that of the surface vessel and can drive a PTO device to recover wave energy, shown in Figure 4 b).

The wave induced flapping motion of the submerged foils, combined with the wave orbital particle velocities, generates an incident flow stream at the leading edge of the foil. The magnitude (V) and angle of attack (α_e) of the flow at the leading edge of the submerged foils is resolved as a combination of the vehicle forward speed (U), vessel pitch induced heave velocity ($\dot{\eta}_{35}$), vessel heave velocity ($\dot{\eta}_3$), foil velocity ($\dot{z}$) and the wave horizontal and vertical orbital velocities (u and v respectively):

$$V = \sqrt{\left(U+u\right)^2 + \left(v - \dot{\eta}_3 + \dot{z} + \dot{\eta}_{35}\right)^2} \tag{3}$$

$$\alpha = (\theta + \beta) - tan^{-1}\Big(\frac{v - \dot{\eta}_3 + \dot{z} + \dot{\eta}_{35}}{U+u}\Big) \tag{4}$$

where θ and β are the foil and vessel pitch angles respectively.

The vector velocity of the flow at the leading edge defines the forces and moments that are exerted about the hydrodynamic centre of the foils. The moment about the hydrodynamic centre of the foil is a combination of the hydrodynamic moment and the lift force acting normal to the chord line at a distance from the foil pivot point. The foil pitch is constrained by a rotational spring and influenced by the added mass due to the heave motion of the foil. The foil heave is either fixed or constrained by a PTO mechanism, which in this case is a permanent magnet tubular linear generator (PMTLG). The PMTLG device is capable of converting linear drive into electrical power through electromagnetic induction; a permanent magnet rod is moved within a series of coils.

In the scenario where the foils are free to heave relative to the vessel a hydrodynamic force acts in the vertical direction. The foil is constrained by the damping of the generator and a restoring spring force. The force, F_{gen}, is an opposing electromotive force (emf) exerted on the foil from the generator due to the current induced in the stator coils. For a three phase linear generator the induced voltage at the ith coil is directly proportional to the foil relative heave velocity ($\dot{z}_{rel}$) and the position of the permanent magnet rod (the relative heave of the foil (z_{rel}):

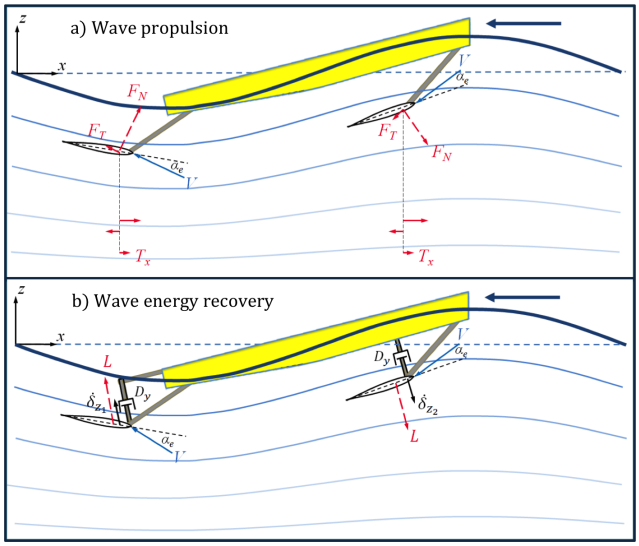

Figure 4: Schematic of wave energy propulsion and energy scavenging

$$V_i(t) = \epsilon_c \dot{z}_{rel}(t) cos\Big(\frac{2\pi}{w_p} z_{rel}(t) - \delta_i\Big) \tag{5}$$

where ϵ_c is the emf constant in V/ms^{-1}, w_p is the length of one electrical cycle i.e. the pole width of the permanent magnet and δ_i is the phase difference between each set of coils. For the simplest electrical circuit the generated electrical power can be equated assuming a constant resistance or load (R_{load}) [18]:

$$P_z(t) = \sum_{i=1}^{3} \frac{V_i(t)^2}{R_{load}} \tag{6}$$

The opposing generator force can, therefore, be estimated with consideration for the generator efficiency (η_{eff}) [18]:

$$F_{gen}(t) = \sum_{i=1}^{3} \frac{P_z(t)}{\dot{z}_{rel}(t)\ \eta_{eff}} \tag{7}$$

III. Towing Tank Experiments

Ideally, the experiments would involve free running (wave propulsion) and station keeping (energy scavenging) tests in waves whereby the response of the flapping foils can be analysed with respect to response of the surface vehicle. The

free running experiments were made possible by using a rudder to control the heading of the experimental model and, through using a remote control package, the vehicle could be steered up and down the tank. However, the rudder is unable to control the heading of the vehicle during the station keeping scenario and it was, therefore, decided to conduct the wave energy scavenging experiments with the model secured to a towing carriage.

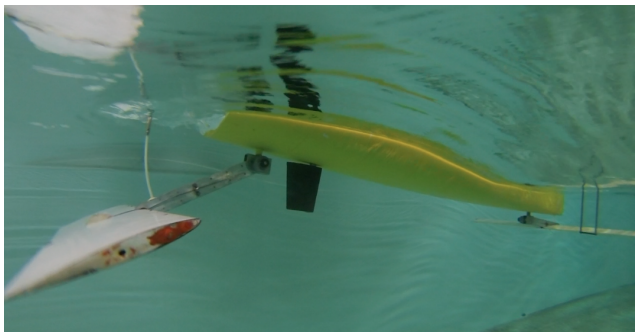

Figure 5: Underwater view of setup with foils free to heave about rotary springs, which are located at the base of the pivot arm beneath the hull

The objective of the free running experiments was to assess the propulsive response of the flapping foil setup in a series of regular waves with an additional aim of capturing the effect of the foil longitudinal locations on the hull motions and corresponding forward speed. The objective of the wave energy scavenging experiments was to also analyse the effect of the foils on the hull motions of the vehicle with a main focus on the power generation response of the submerged foils in waves.

A. Experimental setup

The experimental model used for the towing tank tests was the same platform used in previous experiments conducted by Bowker et al. (2015) with modifications to install a PTO system[19]. The experimental platform has been fitted with PMTLGs at the bow and stern, which are connected to the foils via flexible rods as shown in Figures 6 and 5.

The foils are mounted at the end of pivot arms and spring loaded in pitch through a bending torque applied by piano wire which is located through the rotating shaft. The spring applies a torque about the leading edge of the foil, which has the following inverse relationship with the pitch angle (θ): $\tau = 10 \times \theta^{-0.15}$. The foils can either be fixed or free to heave about the rotating point beneath the hull (see Figure 5), which houses a set of four springs that work together to maintain the foils neutral depth and apply a restoring force to the PTO setup. The model is also fitted with a rudder which is controlled using a servo and remote control package. Due to the added supporting structure and watertight deck, less ballast weight is added than the previous experiments by Bowker et al. (2015) and totals 25 kg. The hull and foil particulars are detailed in Table I.

Table I: Experimetnal Model and Foil Particulars

Parameter	Value	Units
Waterline length, L	2.27	m
Beam, B	0.3	m
Draft, T	0.1	m
Displacement, Δ	55	kg
Foil chord, c	0.23	m
Foil span, s	1	m
Foil type	NACA0012	-
Foil arm (lengths), a	0.35, 0.9	m

B. Methodology; Wave energy scavenging

Experiments were performed at the Southampton Solent University towing tank with the model secured to the carriage, which remained at a constant distance from the wave machine. The tank is 60m in length, 3.7m wide and 1.8m deep. The model was free to heave and pitch at the tow post fixing, which was secured approximately 100mm aft of the model's longitudinal centre of gravity (LCG). The model was contrained in head waves and the flapping foils were free to move relative to the surface vehicle via the PMTLGs mounted above the foils (see Figure 5. The power cables and hall sensor wires were fed back to the carriage where the position and generated power was recorded. During each test the wave height, vessel motions, relative foil positon and induced voltage was recorded. The tests were repeated three times and carried out in a range of regular waves; at two different waves heights (0.12m and 0.18m) and a range of wave frequencies (0.4 - 1.0 Hz) at increments of 0.1 Hz. In order to analyse the effect of submerged foils on the motions of the surface vehicle, further experiments were conducted with the foils fixed.

C. Methodology; Wave energy propulsion

In order to assess the propulsive characteristics of the flapping foil setup, free running experiments were conducted in a controlled environment at the University of Southampton towing tank. The tank is 138m in length, 6m wide and 3.5m deep. The model was tested in head and following regular waves, which were kept at a constant wave height of 0.12m and the wave frequency was increased from 0.5 Hz to 0.8 Hz at increments of 0.1 Hz. Additional repeat tests were made at 0.7 Hz to assess repeatability. The foil longitudinal location was changed by approximately 0.6m to analyse their effect on the hull motions. The tests assessed the setup with the foils situated at two different locations; firstly, with the foils close to the forward and aft perpendiculars and, secondly, with the foils extended as shown in Figure 6. The model was stationed at the carriage approximately 30m from the wave and progressed towards the wave machine in head waves before being turned around and tested in following waves. The approximate period for each run varied from 60 to 180 seconds depending on the

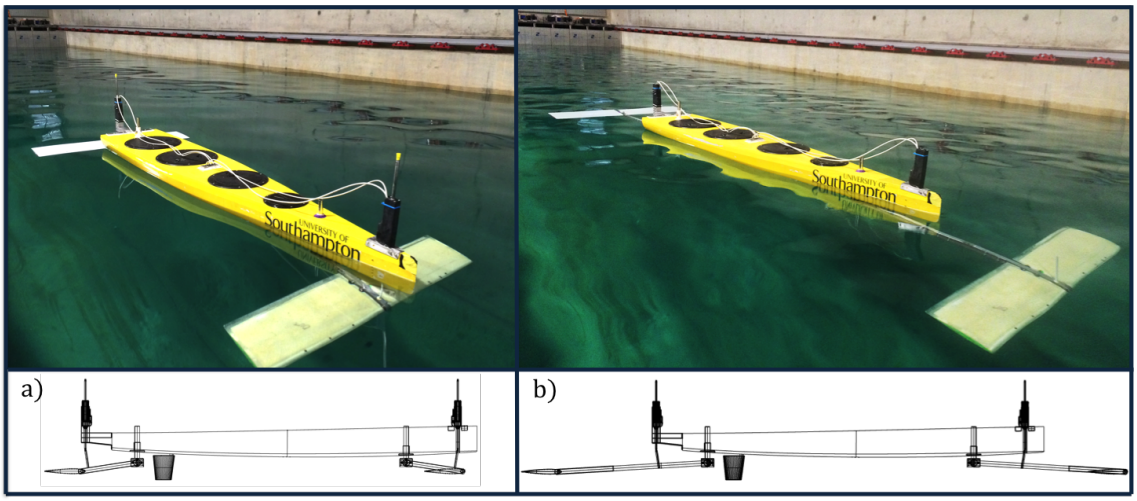

Figure 6: Longitudinal location of foils (at the pivot point from amidships); a) Aft foil = -1.326m, Fwd foil = 1.042m ($L_{LOA} = 2.7m$) b) Aft foil = 1.920m, Fwd foil = 1.646m ($L_{LOA} = 3.8m$)

forward speed of the vehicle and the wave reflection from the opposite end of the tank.

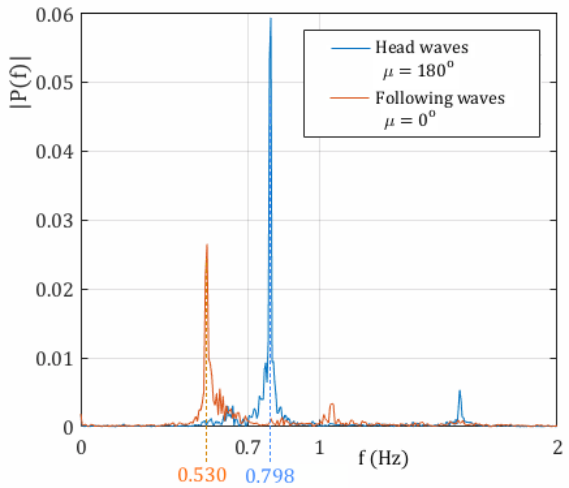

Figure 7: Example fast fourier transfrom analysis of encountered frequency (extended foil condition in a wave of 0.7 Hz)

An inertial sensor was used to acquire the vessel heave and pitch motions. It was also possible to ascertain the forward speed from the encountered frequency. The sensor was situated approximately at the LCG and VCG (vertical centre of gravity) of the model and data was recorded at a rate of 100 Hz onto a computer onboard. The output data was in the form of linear accelerations and rotational velocities. The data was filtered using a Butterworth second order filter with a normalized cutoff frequency of 0.01. However, significant drift errors occurred when converting the surge acceleration data in to forward speed. Performing fast fourier transfrom (FFT) analysis on the data at a specific cut in and out time made it possible to acquire the encountered frequency, as shown in Figure 7. Assuming harmonic hull motions for waves with a wavelength greater than the waterline length of the model, the vehicle forward speed can be calculated from the encountered wave frequency by rearranging the following equation:

$$\omega_e = \omega - kUcos\mu \tag{8}$$

where k is the wave number, ω_e is the encountered frequency and ω is the wave frequency. The heading of the vessel, μ, is given as at 0^o in following waves and 180^o in head waves. Using this technique the forward speed and hull motions could be acquired using a single inertial sensor.

IV. Results

A. Vessel motions

Following the assumption that the hull motions are sinusoidal in small amplitude regular waves, it is possible to estimate the amplitude of the motion response from the root mean square (RMS) of the data. As the RMS of a sine wave with unit amplitude is $\frac{1}{\sqrt{2}}$, the amplitude of the hull motions is obtained by multiplying the RMS of the data set by $\sqrt{2}$. Applying this technique to the data acquired in the constrained condition allows for the calculation of motion transfer functions, which are plotted in Figure 8. For the free running experiments, it was necessary to filter and integrate the inertial data before calculating the amplitude of the linear heave and angular pitch displacements, the results of which are plotted as transfer functions with respect to encountered wave frequency in Figure 9.

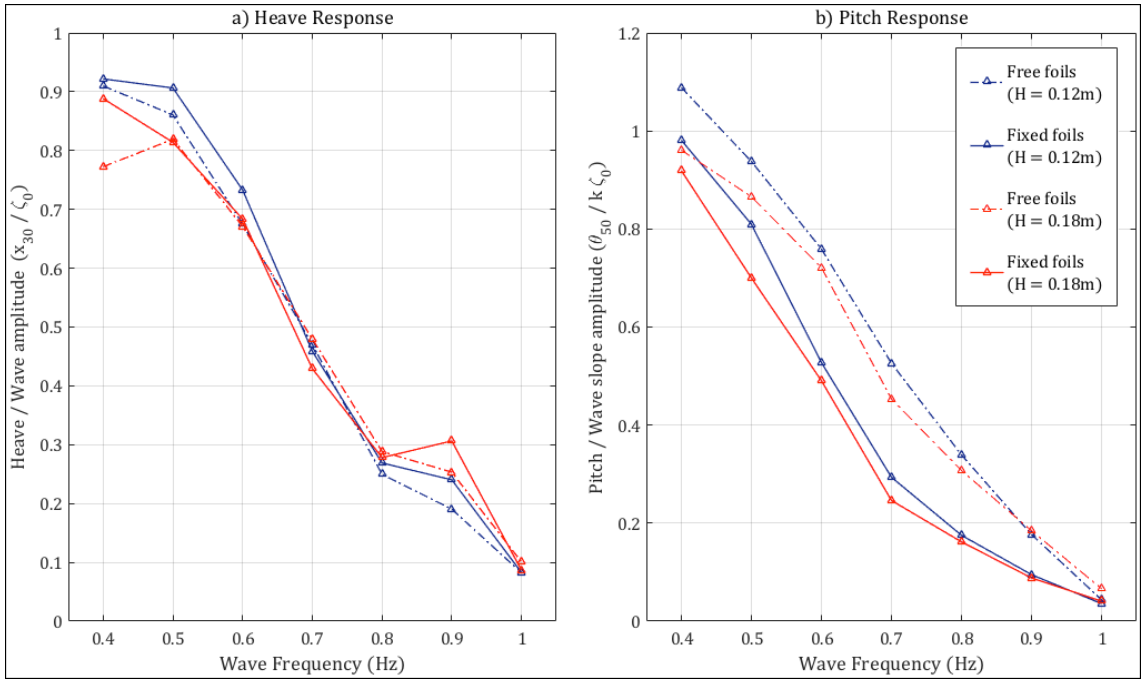

Figure 8: Effect of the foils on the hull motions in the constrained condition (secured to the carriage). Mean heave standard deviation, $\sigma_3 = 0.0013m$ and mean pitch standard deviation, $\sigma_5 = 0.0019rad$

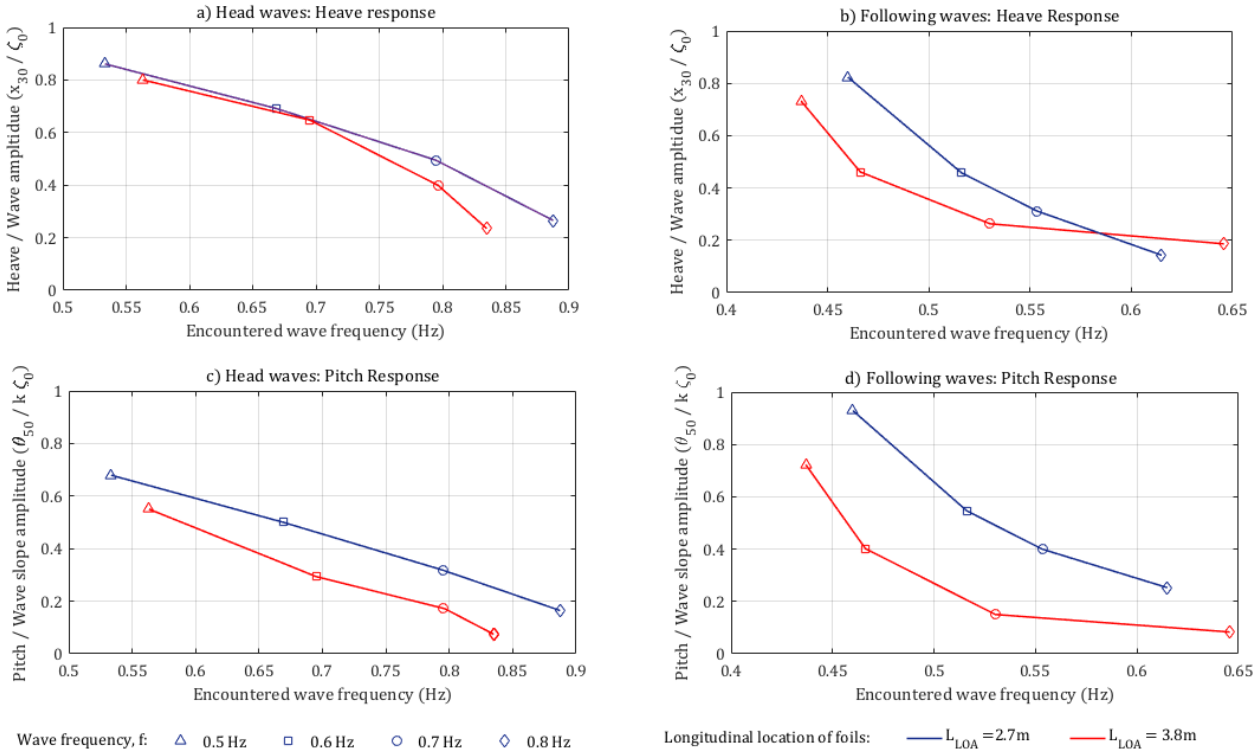

Figure 9: Effect of the location of the foils on the hull motions in head and following waves for the free running experiments Mean heave standard deviation at 0.7 Hz, $\sigma_3 = 0.0052m$ and mean pitch standard deviation at 0.7 Hz, $\sigma_5 = 0.0019rad$

Table II: Percentage reduction in vessel pitch due to extending the location of the foils (relative to initial foil location at the bow and stern)

Wave Frequency, Hz	Head waves	Following waves
0.5	19.0%	22.2%
0.6	41.4%	26.4%
0.7	46.1%	62.4%
0.8	54.9%	67.1%

Figure 8 b) shows the transfer functions for pitch in regular waves of varying height and frequency. There is a reduction of upto 50% in the vessel pitch amplitude due to the presence of the foils when in the fixed foil condition. Figure 8 a) shows that the heave motion of the surface vehicle remains relatively unchanged with or without the foils free to move. The free running results in Figure 9 b) further identify the dominant effect of submerged foils on the pitch motion of the surface vehicle. Increasing the longitudinal location of the foils by a factor of approximately 40% significantly reduces the pitch amplitude in head and following waves, which is summarized in Table II. Figure 9 a) shows that the foil location has a minimal effect on the vessel heave amplitude with respect to wave frequency. However, there is a noticeable shift in the heave motions with respect to the encountered wave frequency, especially for following waves. This indicates that the foils also affect the heave motion of the surface vehicle.

B. Power Generation

The power generated by each foil was calculated from Equation 6 by measuring the induced voltage over a resistance load of 0.47 Ω on each phase and taking the mean generated power ($\bar{P}_z$) for each test case. From applying linear wave theory, the input wave power for each test can be estimated using the following definition for wave power (P_w):

$$P_w = \frac{\rho g H c_g b}{8} \tag{9}$$

where H is the wave height, c_g is the wave group celerity or velocity and b is the breadth of the surface vehicle. The energy recovery efficiency can, therefore, be defined as:

$$\eta_{recovery} = \frac{\bar{P}_z}{P_w} \tag{10}$$

Figures 10 a) and b) show the resulting energy recovery efficiency and peak generated power with respect to wave frequency. Reasonable repeatability is found with the experiment and the same trend with respect to wave frequency is found for both the forward and aft foil. The scavenging of wave energy in this case is shown to be fairly inefficient but this may be due to an suboptimal tuning of the PTO setup. However, the experiments have highlighted several key trends in the application of using submerged flapping foils as wave energy scavenging devices. Most noticeable is the frequency dependent response of the system. Like most wave energy devices there is a significant peak in the generation of power about the resonant motion of the wave energy converter. This is also reflected in the peak power generation but with greater uncertainty due to considering only a single data point for the peak response. For the median wave frequencies (0.5-0.9 Hz), the mean generated power is almost directly proportional to

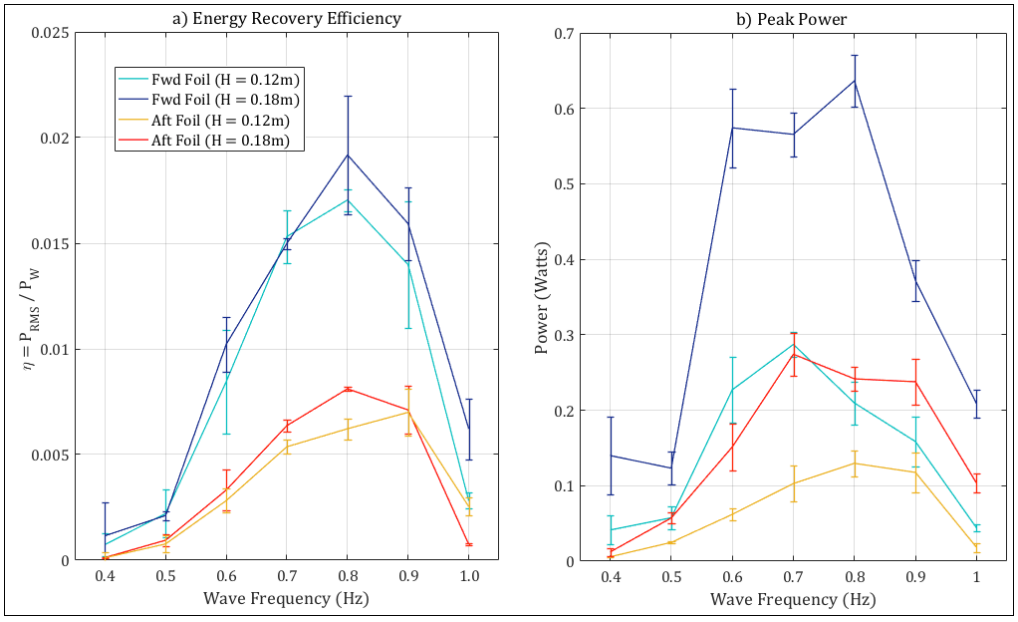

Figure 10: Power generated at waves heights of 0.12 and 0.18m over a range of wave frequencies, interpreted as: a) Energy recovery efficiency and b) Peak power generation

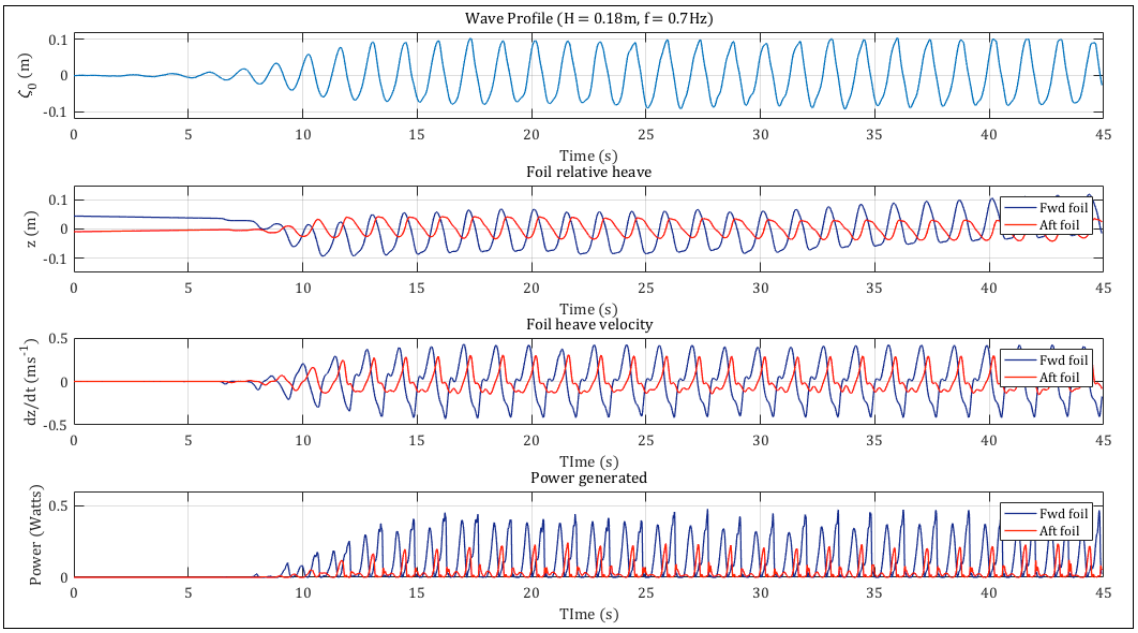

Figure 11: Example time history of wave profile, relative foil motions and corresponding power generation for a regular wave (f = 0.7Hz and H = 0.18m)

the square of the wave height (12 and 18 cm):

$$\text{Fwd foil: } \frac{\bar{P}_{18}}{\bar{P}_{12}} \simeq 1.1 \times \frac{H_{18}}{H_{12}}^2$$

$$\text{Aft foil: } \frac{\bar{P}_{18}}{\bar{P}_{12}} \simeq 0.9 \times \frac{H_{18}}{H_{12}}^2$$

An exemplar time history of the wave amplitude, foil response and power generation is shown in Figure 11. The relative heave velocity of the foil generates the induced voltage in the PMTLG and it can be seen that the forward foil responds at a significantly greater heave velocity compared to the aft foil. It is also interesting to note that the foils operate almost out of phase to one another in this example, but further analysis is required to investigate this with respect to the wave frequency.

C. Propulsion

Figure 12 shows the forward speed of the free running model in head and following waves with two different foil locations. Extending the location of the foils has a significantly positive effect on the forward speed of the surface vehicle but only at lower frequencies. At the higher end of the wave frequency range (> 0.7 Hz) the pitch motion of the vessel is significantly reduced due to the extension of the foils, as shown in Table II. This reduction in vessel pitch has an effect on the induced flapping motions of the submerged foils and, therefore, results in a reduction in forward speed at high wave frequencies for following and head waves. At lower frequencies (< 0.7 Hz), the forward

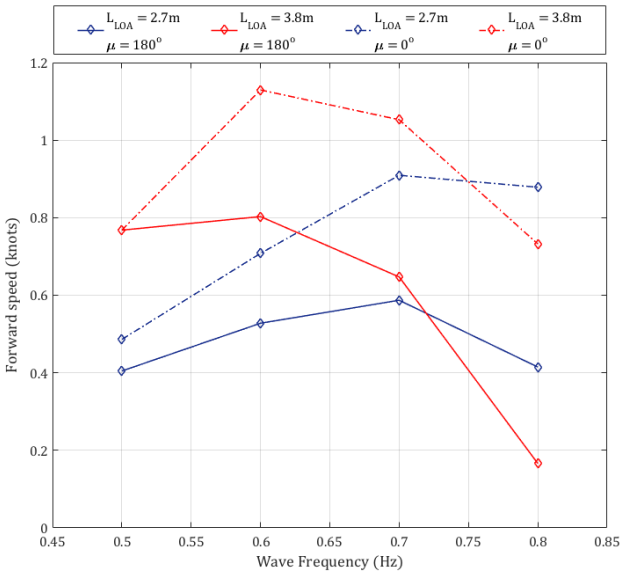

Figure 12: Forward speed comparison between the longitudinal location of the foils in head ($\mu = 180^o$) and following waves($\mu = 0^o$); H = 0.12m

speed is significantly greater with extended foils which suggests that an increase in the wave induced flapping foil motion is due to an increase in the moment arm from the LCG.

The forward speed is also very dependent on the

encountered wave frequency which in turn is a function of the forward speed. As the wave frequency increases there is a substantial increase in the difference between the forward speed for following and head waves. For head waves, at higher wave frequencies ($> 0.6Hz$), the surface vehicle is propelled into the waves which increases the encountered wave frequency away from the resonant pitch frequency of 0.6 Hz. This Doppler effect reduces the pitch motion which consequently reduces the wave induced flapping foil propulsion. For following waves, also at higher wave frequencies, the forward speed has the opposite effect; the surface vehicle is propelled away from the incoming waves towards the resonant frequency.

V. Discussion

The results identify a significant reduction in the vessel pitch due to the effect of the submerged foils. This is in agreement with previous experiments conducted by Bockmann and Steen (2015) in head waves which highlighted a reduction in pitch of upto 60% with one foil mounted at the bow [14]. The study by Bockmann and Steen (2015) also identified a significant reduction in heave, which is contrary to the results presented in Figure 8 a). The difference between these results may be attributed to the fact that, in the current experiments, the foils were only mounted at the bow and also at the aft of the vehicle. Therefore, in pitch motion, the lift force generated by the forward and aft foil within one wave period results in moments that act in the same angular direction about the LCG, as shown in Figure 4 a). However, for heave motion, the resultant vertical forces acting on the forward and aft foils effectively oppose each other within one wave period and, therefore, there is a minimal overall effect on the vessel heave motion, as depicted in Figure 4 a).

The free running experiments confirmed a similar effect on the hull motions in head waves due to the longitudinal location of the forward and aft foils; identifying a significant reduction in pitch whilst there is a minimal effect on heave. However, in following waves Figure 9 a), shows that the extended foils effectively reduces the vessel heave with respect to the encountered wave frequency but not the actual wave frequency. In following waves, the foils are orientated away from the incident wave and this may have an effect on the hydrodynamic forces acting on the foils. Further research is required to investigate this interesting outcome.

Figure 13 shows how the relative motion of the submerged foil at the bow drives the permanent magnet through the PMTLG PTO device. At maximum positive vessel pitch the surface vehicle can be seen to work against the submerged foil where the relative displacement between the bow and the foil is reduced. The opposite effect is observed for maximum negative vessel pitch. Therefore, the generated power is related to the local velocities experienced by the surface vehicle at the forward and aft remote locations of the submerged foils. This explains the difference in power generated by the forward and aft foils, highlighted in Figure 10. For the experiments,

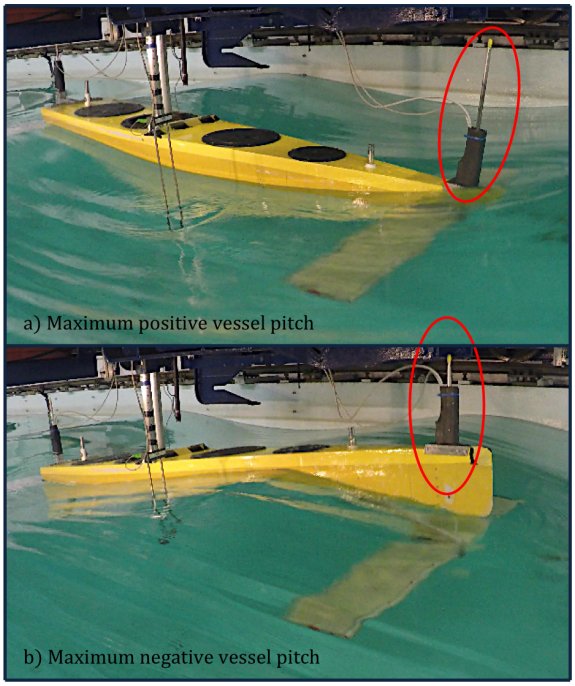

Figure 13: Relative foil and permanent magnet rod heave in regular waves (f = 0.7Hz and H = 0.18m) during; a) Maximum positive vessel pitch and b) Maximum negative vessel pitch

the centre of rotation for vessel pitch was fixed at the location where the tow post is secured which was approximately 0.1m abaft of the LCG (-0.15 from the amidships). As the tow post fixing was located aft of the LCG, the forward and aft foils were not spaced equally from the LCG. The forward and aft foils were located 1.3m and 1.1m from the tow post fixing respectively which resulted in differing local velocities at the remote locations. At the aft foil there is, therefore, less pitch induced heave and this is reflected in the power generated as shown in Figure 11. The reduction in power generated by the aft foil may also be attributed to the effect of the forward foil and the hull on the incoming wave energy.

The power generated was shown to be fairly inefficient with a maximum energy recovery efficiency of approximately 2%. However, the PTO requires optimization and the load in the electrical circuit should be tuned to maximise the efficiency of this device. This is highlighted as an important aspect for future work and a common problem in developing ASV wave energy scavenging devices, especially due to the frequency dependent response of the setup. The experiments for energy recovery were also limited by the maximum wave height that could be generated in the towing tank, which is a height of 0.2m. However, an interesting outcome from the experiments was the proportional relationship between the generated power and wave height. Applying the proportional relationship defined in the previous section, it is possible to extrapolate the power generated in alternative regular waves.

For example, in a wave height of 0.4m and frequency of 0.7Hz, the forward foil is predicted to generate a maximum of 3 watts and mean of 1 watt. This type of wave energy recovery could potentially contribute to the powering of onboard ASV systems and the recharging of batteries during station keeping scenarios.

The free running experiments identified a significant effect of the longitudinal location of the foils on the forward speed of the vehicle. Whether the effect is positive or negative is dependent on the incident wave frequency which has interesting implications for the design of a wave induced flapping foil propulsor for ASVs. For example, it is evident at lower wave frequencies that extending the longitudinal location of the foils will yield an increase in the propulsive thrust which suggests that the length of a pitch induced wave propelled vessel should be optimized for a particular sea area depending on the wave statistics. Also, designing the resonant pitch frequency to produce an optimum response from the flapping foils is regarded as an important development. Ideally, this would need to change with respect to the heading of the surface vehicle.

VI. Conclusions

Within the context of wave energy recovery and propulsion, the experiments described here have highlighted the importance of several factors that influence the response of submerged flapping foils onboard ASVs. Most notable of these, is that the foils have a significant effect on the vessel which, in this case, can be regarded as the main wave energy converter. In terms of implications for ASVs, optimum seakeeping characteristics and foil location should be combined to maximise the conversion of wave energy for propulsion and onboard power generation.

Acknowledgements

This research is supported by the Lloyd's Register Foundation.

References

[1] Isshiki, H., "A theory of wave devouring propulsion (1st Report) - Thrust generation by a linear Wells turbine." J. Soc. Naval Arch. Japan, (151):5464. 1982

[2] Isshiki, H., "A theory of wave devouring propulsion (2nd Report) - Optimized foil motions for a passive-type wave devouring propulsor." J. Soc. Naval Arch. Japan, (152):89100, 1982.

[3] Isshiki, H., and Murakami, M., "A theory of wave devouring propulsion (3rd Report) - An experimental verification of thrust generation by a passive-type hydrofoil propulsor." J. Soc. Naval Arch. Japan, (154):118128, 1983.

[4] Isshiki, H., and Murakami, M., "A theory of wave devouring propulsion (4th Report) - A comparison between theory and experiment in case of a passive-type hydrofoil propulsor." J. Soc. Naval Arch. Japan, (156):102114, 1984.

[5] MOST (AV) Ltd, accessed March 2015, ¡http://www.autonautusv.com/specifications

[6] Linden, H., "Improved combination with floating bodies, of fins adapted to effect their propulsion." GB Patent 14,630. Filed Aug. 1, 1895. Patented Jul. 18, 1896.

[7] Jakobsen, E., "The foilpropeller, wave power for propulsion." In Second International Symposium on Wave and Tidal Energy, BHRA Fluid Engineering, pages 363369. 1981.

[8] Manley, J., and Willcox, S., "The Wave Glider: A persistent platform for ocean science." OCEANS 2010 IEEE - Sydney, 1, 2010.

[9] Terao, Y., and N. Sakagami. "Design and development of an autonomous wave-powered boat with a wave devouring propulsion system." Advanced Robotics, vol. 29(1), pp 89-102, 2015.

[10] Townsend, N.C. and Shenoi, R.A., "Feasibility study of a new energy scavenging system for an autonomous underwater vehicle." Autonomous Robots, 1-13, 2015.

[11] Townsend, N., "Self powered Autonomous Underwater Vehicles (AUVs): Results from a gyroscopic energy scavenging prototype." IET Renewable Power Generation, 1-12. 2016

[12] Brown, P., Hardisty, D., and Molteno, T. C. A.,, "Wave-powered small-scale generation systems for ocean exploration. Proc. Int. Conf. Oceans-Asia Pacific, Singapore, pp.1-6, 2006.

[13] Naito, S., and Isshiki, H., "Effect of Bow Wings on Ship Propulsion and Motions." Applied Mechanics Reviews, vol. 58, pp 253-268, 2005.

[14] Bockmann, E., and Steen, S., "The Effect of a Fixed Foil on Ship Propulsion and Motions." translated by Launceston, Tasmania, Australia. 2015.

[15] Naito, S., Isshiki, H. and Fujimoto, E., "Thrust generation of a Fin Attached to a Ship in Waves." Journal of KSNAJ, vol. 202, pp. 23-29, 1986.

[16] Belibassakis, K.A. and Filippas, E., "Ship propulsion in waves by actively controlled flapping foils." Applied Ocean Research, 52, 1-11, 2015.

[17] Bockmann, E., "Wave propulsion of ships." PhD Thesis, NTNU, Norway, 2015.

[18] Zheng, Z., Huang, P., Gao, D., and Chang, Z., "Analysis of electromagnetic force of the linear generator in point absorber wave energy converters." Journal of Marine Science and Technology, vol. 23(4), pp. 475-480, 2015.

[19] Bowker, J., Townsend, N.C., Tan, M., and Shenoi, R.A., "Experimental study of a wave energy scavenging system onboard autonomous surface vessels (ASVs)." In, OCEANS15 MTS/IEEE Genova, Genova, IT, 2015.

Experimental study of a wave energy scavenging system onboard autonomous surface vessels (ASVs)

J. A. Bowker, N. C. Townsend, M. Tan, R. A. Shenoi
Fluid Structure Interactions Group, Faculty of Engineering and the Environment
University of Southampton
SO17 1BJ UK
jab1e08@soton.ac.uk

***Abstract*—Autonomous Surface Vehicles (ASV) have many potential applications in the maritime industry and ocean science. To subsist in the ocean space, an ASV must have the ability to scavenge energy from the surrounding environment. Waves are an abundant source of energy on the ocean surface and a suitable resource for an ASV to scavenge. Flapping foils have been shown to generate thrust in a wavy flow and power in a uniform flow. The aim of this experimental study is to investigate the relationship between flapping foil propulsion and power generation in the context of ASVs. Initial experiments incorporating fully passive flapping foils submerged at the bow and stern of a surface vessel in head waves were performed in a towing tank. The spring-loaded foils were located at the end of rigid pivot arms protruding at the bow and abaft of the vessel. The pivot arms were free to rotate about a location beneath the keel line and restrained by adjustable rotational dampers. In this free condition, wave energy is recovered in the form of work applied by the flapping foils through the rotary dampers which were used to simulate the damping effects of a power take-off device. Thrust was generated under conditions when the pivot arm was fixed. This system, referred to as the Flapping Energy Utilization and Recovery (FLEUR) system, could serve as a dual-purpose wave energy scavenging propulsor and power generator for long-endurance ASVs.**

I. Introduction

Efforts have been made to increase the longevity of the ASV deployment through the scavenging of marine energy resources. It is well-known that the marine environment is a particularly challenging domain to operate man-made systems in and steps to improve the reliability and energy scavenging capabilities of ASVs is required to achieve their full potential. The spectrum of current ASVs ranges from systems that have a high onboard power capacity for fast speeds and significant onboard capability through to long range endurance ASVs that harvest marine energy for propulsion and limited onboard powering. With the rapid developments in technology and the development of hybrid marine energy scavenging devices, it is expected that the aforementioned spectrum range of ASV capability versus endurance will narrow resulting in the long term deployment of highly capable ASVs [1], see Figure 1. The motivation for this research is to contribute to the attainment of ASV self-sustainability through the development of marine energy scavenging devices.

Wave energy is an abundant source of marine energy on the ocean surface, with 90% of high frequency waves storing an energy density of greater than 2kW/m [2]. This research is, therefore, focused on the utilization and recovery of wave energy for ASV propulsion and onboard energy harvesting.

Numerous autonomous marine vessels have been designed to utilize wave energy for direct propulsion. The Wave Glider, developed by Liquid Robotics, is passively propelled by a submerged set of foils, referred to as the 'glider', attached to a surface float via a tether [3]. As the float heaves in response to the ocean waves, the submerged glider heaved and plunged through the water. The resulting effective flow over the foils generates thrust that drives the float forward over the waves.

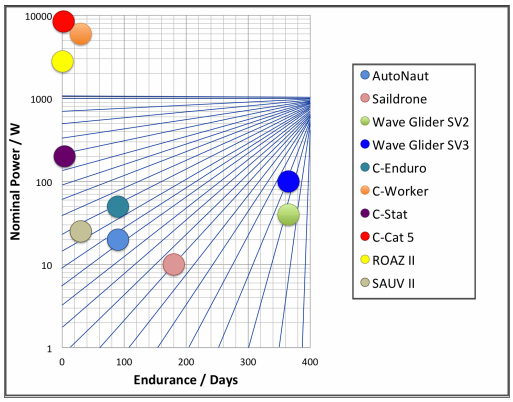

Figure 1: Convergence of ASV endurance and capability [3][4][5][6][7][8]

MOST (Autonomous Vessels) Ltd have also developed a long range endurance wave propelled ASV and have recently launched the commercial version called AutoNaut [7]. AutoNaut propels itself using the same technique patented and developed by Linden and Jakobsen respectively [9][10]. The vessel consists of two flapping foils, one at the bow and one at the stern, and propels itself using the wave induced vessel motions to generate thrust from spring-loaded foils. Using a similar method, Terao and Sakagami have developed a system called the Wave Devouring Propulsion System (WDPS), which is an ASV propelled using vessel induced motions to excite spring-loaded foils [11]. Research carried out by Townsend and Shenoi has investigated the use of a gyroscopic system to harvest wave energy onboard vessels through gyroscopic precession in response to the wave-induced vessel pitch and

roll. The study has been expanded to test the feasibility of using this gyroscopic system for recharging autonomous underwater vehicles (AUVs) at the sea surface [12].

The proposed Flapping Energy Utilization and Recovery (FLEUR) system presented in this paper is an expansion of previous work on spring-loaded wave devouring flapping foils, incorporating the capability of generating onboard power. The advantage of such a system is the ability to alter the mode of a remote ASV to either propulsion or power generation depending on the mission status.

II. Flapping Foil Thrust and Power Generation

Considerable theoretical and experimental studies have been carried out to investigate the characteristics of flapping foils and their suitability for potential applications. Isshiki uses the term 'wave devouring propulsion' to describe the mechanism of submerged flapping foils generating thrust in waves [13]. Wave devouring propulsion suitably describes the field of research from the initial theory presented by Wu and the theory developed by Grue et al. through to recent studies that investigate their application on-board ships [14][15][16]. Power generation from flapping foils is a more recent body of research, which has seen increased levels of interest due to its potential application as a more efficient flow energy harvesters when compared to their rotary counterparts such as tidal turbines[17].

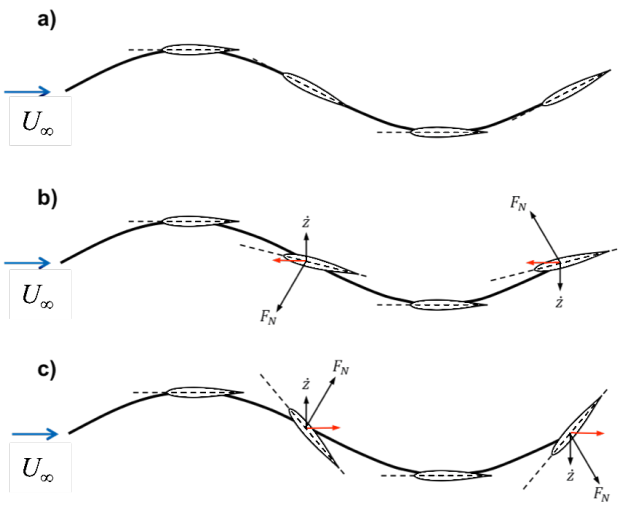

Figure 2: Flapping foil kinematics heaving and pitching in a steady flow; a) Feathering b) Thrust generation c) Power generation

Figure 2 shows the pathline of a flapping foil immersed in a constant flow stream, U_∞, with prescribed pitch and heave motions. The prescribed motion produces a response that is synonymous with either feathering, propulsion or power generation. The foil heave velocity, $\dot{z}$, contributes to the relative flow at the leading edge resulting in an effective angle of attack due to the foil motions, α_e. By defining the foil pitch (θ), the effective angle of attack is evaluated as follows:

$$\alpha_e = \theta - tan^{-1}(\frac{-\dot{z}}{U_\infty})$$

This relationship between the effective angle of attack and the foil motions defines the resultant hydrodynamic force. Depending on the flapping characteristics of the foil, the resultant hydrodynamic force will dictate the function of the system. Power is generated if the lift force in the vertical axis is synchronous with the foil heave velocity. This power provides the impetuous for the foil to heave as well as generating further power that can be harvested during the cycle. However, in this instance, drag develops over the cycle in the form of a Von Karman vortex street in the down-stream flow field [18]. Optimizing the flapping foil parameters for propulsion generates a hydrodynamic force with a horizontal component which exceeds the drag component to produce a net thrust. In this mode, the foil sheds a reverse Von Karman vortex street in the down-stream flow field that is indicative of a jet stream. The thrust can be evaluated by analyzing the change in momentum of the fluid, as depicted by Jones et al. in Figure 3.

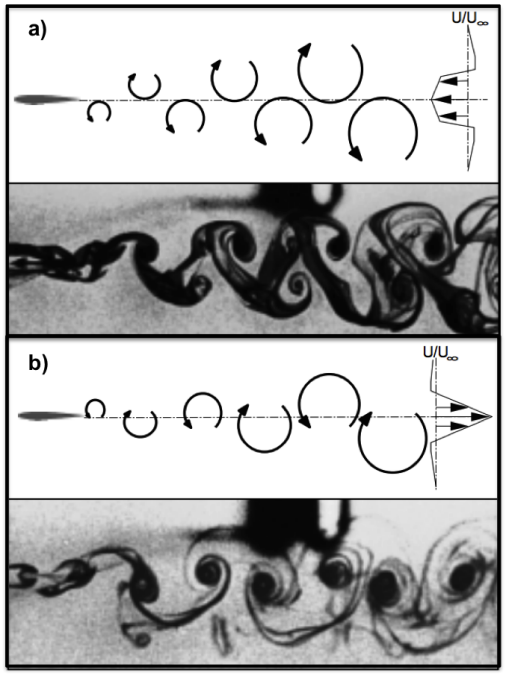

Figure 3: Down-stream flow field; a) Drag b) Thrust [18]

Previous studies have identified that the introduction of waves significantly contributes to the thrust generated by flapping foils. Immersing the flapping foil in a wavy flow introduces another velocity component to the system in the form of orbital particle motions in the fluid stream. In deep water, the profile of a regular wave can be modelled using linear wave theory, from which the velocity potential is differentiated to derive the horizontal and vertical wave orbital

particle velocities, u and v respectively. Further research has incorporated the analysis of fixed foils submerged beneath a surface vessel [16]. Coupling the wave induced vessel motions with that of a spring-loaded foil activates the flapping characteristics required for thrust generation.

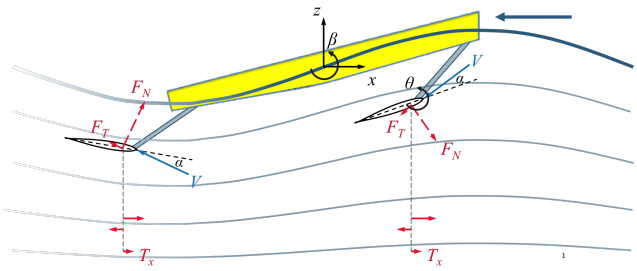

Figure 4: Schematic of the FLEUR system for ASV propulsion

The vessel heave (z_b), pitch (β) and pitch induced heave (z_β) contributes to the global position of a submerged foil and, hence, drives the motion of the foil through the water. A vessel with forward speed, U, in incoming head waves induces an incident flow stream with an equivalent velocity of U_∞ at the leading edge of the foil. Considering a quasi-steady approach, the flow over the foil is a combination of the incoming wave, the resulting vessel motions and the independent foil oscillations. Figure 4 illustrates the global frame of reference for the FLEUR system in the propulsion mode. The magnitude of the flow, V, and the angle of attack, α, are, therefore, evaluated as follows:

$$V = \sqrt{\left(U_\infty + u\right)^2 + \left(v - \dot{z}_b + \dot{z}_f + \dot{z}_\beta\right)^2}$$

$$\alpha = (\theta + \beta) - tan^{-1}\left(\frac{v - \dot{z}_b + \dot{z}_f + \dot{z}_\beta}{U_\infty + u}\right)$$

Through resolving the resultant hydrodynamic forces in the global frame of reference, it can be shown that the flapping foil system is capable of generating thrust. This phenomena has been investigated to improve the propulsive efficiency of ships in waves and applied to passively propel ASVs. In the same way, the FLEUR system takes advantage of wave induced vessel motions to generate propulsion utilizing submerged spring-loaded flapping foils. However, the design also incorporates the capability to recover wave energy for on-board power generation.

The submerged flapping foils are fixed to the hull abaft and beneath the bow via a rigid pivot arm of length, a, shown in Figure 4. In the propulsion mode, the foils are not free to heave independently of the vessel and zero power is recovered. By allowing the pivot arm to rotate about a point located near the keel line, the torque from the foils can apply mechanical work about the pivot point and recover power from the wave energy. In the power recovery mode, the foils are free to heave and pitch; restrained by a rotational viscous damper and rotational spring respectively. Assuming the rotational inertia and mass of the foil is negligible the equations of motion of a flapping foil pivoting about the leading edge and restrained by a rotational spring is simplified as follows:

$$\Sigma M_\theta = M_{c/4} - k_\theta\theta - \cancelto{0}{\xi_\theta\omega_\theta} \longrightarrow M_\theta = k_\theta\theta$$

where $M_{c/4}$ is the hydrodynamic moment about the hydrodynamic centre of the foil, assumed to be at one quarter of the chord from the leading edge. The rotational spring stiffness and damping constants for the leading edge and pivot arm are constant parameters; k and and ξ, respectively. Applying the same assumptions for the pivot arm but regarding it as a damped system the equation of motions can also be simplified as:

$$\Sigma M_\phi = F_\phi a - \cancelto{0}{k_\phi\phi} - \xi_\phi\omega_\phi \longrightarrow F_\phi a = \xi_\phi\omega_\phi$$

where F_ϕ is the resultant hydrodynamic force applied to the pivot arm by the flapping foils. Assuming, that the total loss of mechanical energy via the damper is converted into electrical energy, it is possible to regard the rotational damper as a generator. The power recovered by the system is the work done by the flapping foils over time:

$$P = \tau\omega = F_\phi a\omega_\phi = \xi_\phi{\omega_\phi}^2$$

III. Experimental Setup

An existing towing tank model has been modified for the purpose of the initial experiments. The model hull has been strengthened for testing in waves with the addition of a longitudinal stiffener, which also provides the housing for the flapping foil mounts. The general arrangement of the model is shown below in Figure 5 along with the corresponding model and foil particulars detailed in Table I.

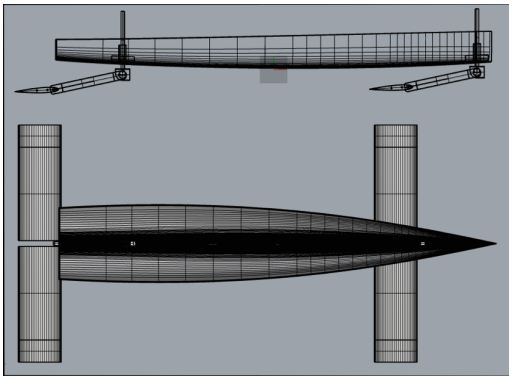

Figure 5: General arrangement of the experimental model

The model has been designed to accommodate the testing of various parameters and limit the added resistance incurred by the addition of appendages. The foils are fixed using vertical stainless steel tubes that protrude through the keel of the hull at the bow and abaft as shown in Figure 6. This setup provides

Table I: FLEUR ASV Particulars

Parameter	Value	Units
Length, L	2.27	m
Beam, B	0.3	m
Draft, T	0.1	m
Displacement, Δ	52	kg
Chord, c	0.23	m
Span, s	1	m
Foil type	NACA0012	-
Foil arm, a	0.4	m

the capability to alter the foil orientation and depth for further tests. The foils are mounted in two halves either side of the pivot arm and fixed via a shaft that rotates through three bearings that are pressed into the pivot arm, as can be seen in Figure 7.

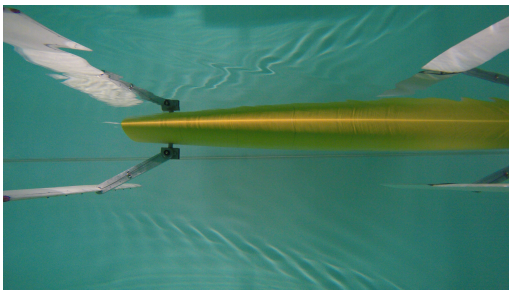

Figure 6: Underwater view of forward and aft foil setup

The spring constant can be altered using the same technique used by Bockmann et al. in their experiments to test the performance of a flapping foil under passive and active pitch conditions [19], illustrated in Figure 8. A length of spring steel is fixed to the foil rotational shaft either side of the bearing mounting, shown in Figure 7. The working length of the spring steel, d, can be adjusted by fixing the rod at different locations on the pivot arm, thus changing the spring constant. The centre of pitch can be set at the leading edge, one-quarter chord and half chord.

Figure 7: Pivot arm and rotational spring setup

For the purposes of the initial experiments the centre of pitch was located at the leading edge and the spring constant remained unaltered at a value of approximately 0.43 Nm/rad.

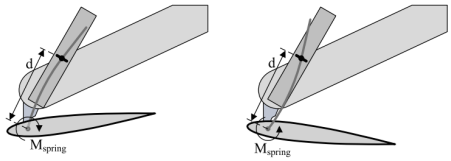

Figure 8: Pitch rotational spring setup used by Bockmann et al. [19]

By adjusting the height of the vertical mounting and setting the neutral pitch angle of the foil to 18^o relative to the pivot arm, shown in Figure 18 a) and Figure 19 a), the foil depth was set to 0.25m below the waterline. The foils are neutrally buoyant to prevent buoyancy forces or weight from applying a torque to the pivot arm. The depth of the foils was, therefore, maintained at 0.25m in the neutral condition.

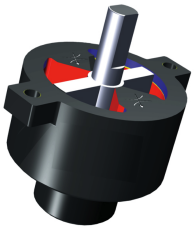

Figure 9: Cross section of the rotary damper

An adjustable rotational damper was used to constrain the rotary motion of the pivot arm. The damper is adjustable using a screw which alters the size of the orifice that the working fluid flows through to pass between the two reservoirs shown in Figure 9. Calibration experiments were conducted to calculate the damping constant values for the various screw settings. The number of turns from the highest damping setting (fully screwed) correlates to the damping constant as shown in Table II.

Table II: Damping constants calibration

No. of Turns	Damping constant, ζ / Nm/rads^{-1}
0	6.76
0.5	4.90
1	4.34
2	4.36

The angular position of the pivot arms were recorded using incremental magnetic rotary encoders rated to 1P68 protection. The signal outputs of the encoders were in the form of two quadrature sinusoidal analogue signals which can be interpolated to acquire the angular position and direction of rotation. The rotary damper and encoder are both mounted to a box section that form the pivot point and shaft connection for the pivot arm. The stainless steel box sections are welded to vertical stainless steel tubes through which the cables for the rotary encoders pass through to connect to the data

acquisition setup.

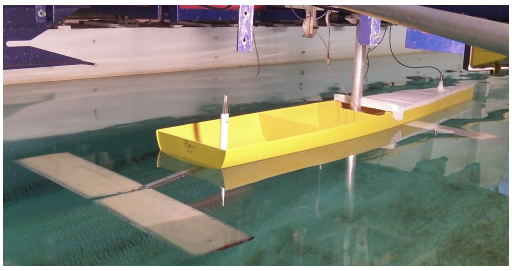

Figure 10: Carriage setup

The experiments were conducted at the Solent University towing tank. The tank is 60 m long, 3.7 m wide, 1.8m deep and has a wave generator capable of generating waves of upto 0.1 m in height at a frequency of upto 1 Hz. The model was fixed to the carriage via a tow post that is free to heave and allows the model to pitch, shown in Figure 10. Data was acquired for the wave height, vessel heave and pitch, drag and the angular position of the pivot arm. The experiments were carried out under three different conditions; bollard pull (zero carriage forward speed), towed condition and free running. For each condition the mode of the foils was altered at the pivot point through either fixing the pivot arm or applying a variable damping force by adjusting the rotary damper. In order to investigate the response of the foils and the vessel motions about the natural wave period in head waves, the system was tested over a series of increasing wave frequencies, from 0.4 to 1 Hz. No scaling laws were applied as the model is considered representative of a full scale ASV. Therefore, the frequency of waves generated in the tank are more representative of wind waves rather than ocean swell. For the majority of tests the wave height was kept constant at 0.08 m to maximise the hull motions whilst minimizing the amount of water ingress over the freeboard of the model.

IV. Results

A. Vessel motions

The pitch and heave motion of the model were interpreted by calculating the root square mean (RMS) of the time history for a range of wave frequencies, the results of which are found in Figures 11 and 12 respectively. The results reflect the expected response of a vessel that is exposed to head on regular waves of varying frequency [20]. The frequency is representative of wavelengths that exceed the length of the vessel (0.4 Hz - 9.8 m) to wavelengths less than that of the vessel length (1 Hz - 1.6 m).

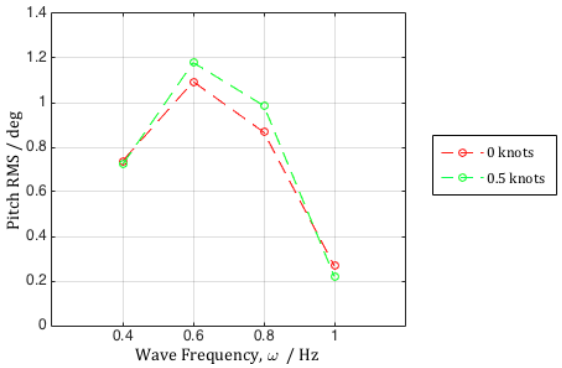

Figure 11: Pitch motion in waves of height, 0.08m.

It can be seen in Figure 11, that the resonant pitch response, in terms of pitch amplitude, is approximately equal to 0.6 Hz and the heave response of the model decreases with increasing wave frequency. With the increase of vessel speed from zero to 0.5 knots, we see that the model pitch motion increases but the heave does not change significantly.

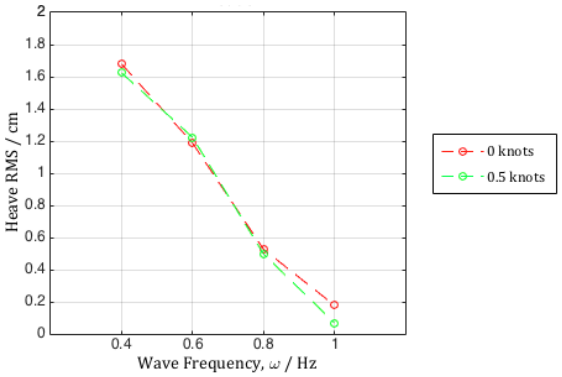

Figure 12: Heave motion in waves of height, 0.08m.

Figure 13 shows the RMS pitch response of the model whilst fixed to the carriage at zero speed under different conditions. Fixed foils mounted at the bow and stern of the vessel significantly reduces the pitch motions when compared to the pitch motion of the model with a bare hull. In the condition where the foils are free to heave the vessel pitch motion decreases with the increase of pivot arm damping.

B. Propulsion

Figure 14 shows the bollard pull of the foils when the carriage was stationary and the reduction of drag when the carriage had a forward speed of 0.5 knots. Both sets of results identify that there is an optimum frequency of approximately 0.8 Hz; at which the foils generate thrust due to the combined vessel motions at this frequency. The flapping mechanism of the foils that leads to the generation of thrust is captured in the underwater snapshots shown in Figures 18 and 19 for the aft and forward foils respectively. In experiments where the foils were free to heave but restrained by a rotary damper, the

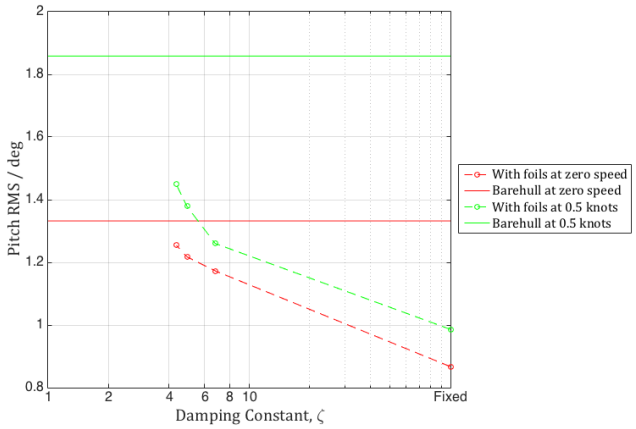

Figure 13: Influence of relative foil motions on the pitch of the model in waves of height, 0.08m, and frequency, 0.8 Hz

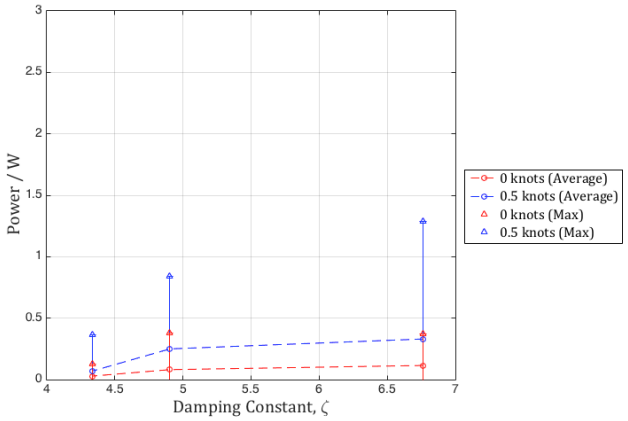

Figure 15: Forward foil maximum and average power with varying damping constant in waves of frequency, 0.8 Hz and height, 0.08m.

flapping foils generated zero thrust. This was also confirmed in the free running tests and is most likely due to the relatively low damping applied to the pivot arm.

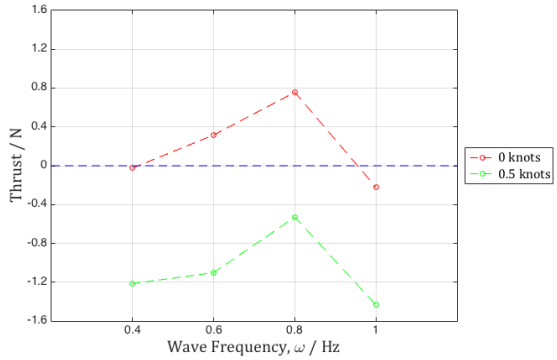

Figure 14: Thrust generation in waves of height 0.08m

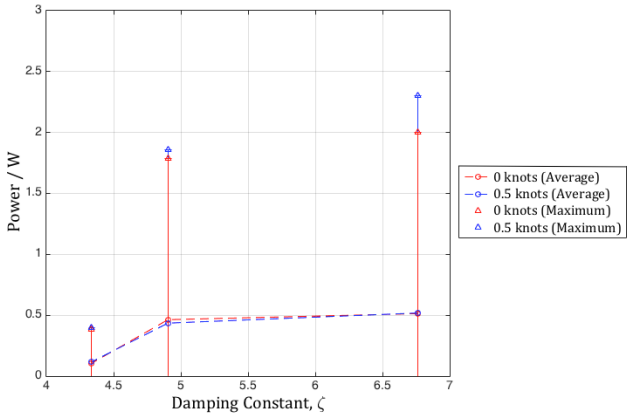

Figure 16: Aft foil maximum and average power with varying damping constant in waves of frequency, 0.8 Hz and height, 0.08m.

C. *Power Generation*

By adjusting the damping settings, detailed in Table II, it was possible to assess the effect of foil heave on the power generated. Figures 15 and 16 show the maximum and average power generated by the forward and aft foil respectively. Both figures present a trend showing the increase of power generation with the increase in damping.

Drawing comparisons between Figures 15 and 16 it is apparent that the forward foil generates less power than the aft foil. The foils are not located equidistant from the longitudinal centre of rotation (the tow post fitting in this case). Consequently, the pitch induced heave is significantly less for the forward foil and, therefore, the rate at which the forward foil heaves relative to the vessel is less than that of the aft foil.

Figure 17 shows the time history of foil heave, pivot arm angular velocity and the equivalent power generated by the aft foil at zero speed in an incoming wave of height, 0.08 m, and frequency, 0.8 Hz with the damping setting at 0. The foil heave was evaluated from the rotational data acquired by the rotary encoder using basic trigonometry. The results show an increase in foil response as the wave height progresses from zero to 0.08 m. The foil is seen to start at an initial depth slightly shallower than its neutral position before settling into a steady oscillation about the neutral position. The cyclic response of the foil is reflected in the power generated at the rotary damper.

The power generated by the aft foil is seen to peak within each cycle at the point where the foil is plunging/heaving at its maximum velocity through the neutral heave position. The peak power is not sustained as the foil is encouraged to oscillate within the same period as the wave induced motions of the model. The results present a promising generation of power, upto a maximum of 2 watts per foil, and proves that it is possible to recover wave energy using flapping foils onboard

ASVs.

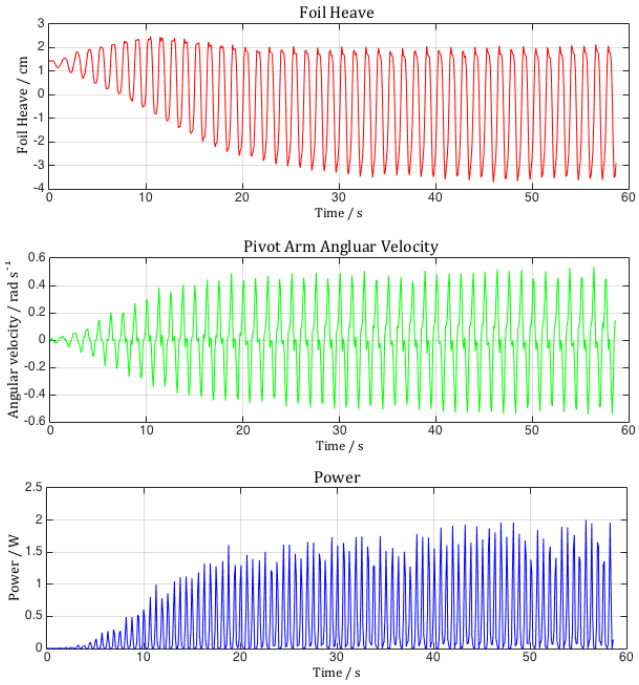

Figure 17: Foil motions and power generation time history at zero speed on damping setting 0 in an incoming waves of height,0.08 m, and frequency, 0.8 Hz.

D. Free running

Free running tests were carried out in the towing tank to assess the performance of the FLEUR system without the constraining effects of fixing the model to the carriage. The model was located in the centre of the tank and exposed to head on regular waves with a frequency of 0.8 Hz and two different heights; 0.1 m and 0.08 m. Posts, which were situated every 3 m along the tank, were used to clock the average speed of the model in 3 m intervals. With the foils fixed, the model achieved a maximum forward speed of approximately 0.43 knots and 0.27 knots for wave heights of 0.1 m and 0.08 m, respectively. The model was also tested with the foils free to heave on the damping setting of 1 turn. In this scenario, the vessel held station in both sets of wave heights and was assumed to be generating power. However, no data was acquired as running cables back to the data acquisition hardware on the carriage was not feasible. Using results acquired on the carriage from previous tests it maybe assumed that the aft foil was generating a maximum of approximately 1.7 W and 0.4 W in waves of 0.1 m and 0.08 m respectively. The damping setting used in this instance was much less than optimal and further experiments are required to optimize this aspect of the FLEUR system.

V. Discussion

In comparison to most seakeeping analysis, large wave induced vessel motions are a desired characteristic for the FLEUR system. Maximising the combined pitch and heave motions drives the foils through the water to generate thrust from the flapping foils. The model was initially tested in wave heights of 0.1 m to maximise the vessel motions. However, there was a risk of water ingress and it was identified that the wave height significantly contributed to the added wave resistance. It was, therefore, concluded that solely maximising the vessel motions will not produce the optimum propulsive performance as the added wave resistance needs to be considered. The coupled foil and vessel added wave resistance was not evaluated in this set of experiments but will be a critical area for future research.

The motions of the entire system are coupled so that the foils absorb energy from the incoming waves and, hence, result in a reduction in the vessel motion. This feedback in the coupled system reduces the propulsive gain made by the flapping foils. It is, therefore, possible to design an optimal foil chord length for a particular vessel where there is a peak in propulsive performance. Evaluating the foil chord length is particularly important for optimizing the performance of the FLEUR system in irregular waves as well as waves in various headings. The initial experiments have been conducted in waves that are assumed to provoke the optimal response from the system and further experiments are required to assess its performance in a variety of different sea states and headings. The effect of fixing the model to the carriage impedes the natural behaviour of coupled system and consequently the results may have underestimated the thrust generated by the foils.

Allowing the foils to independently heave relative to the model significantly reduced their propulsive performance. This may have been due to a slight backlash in the rotary damper that permitted a few degrees of free motion irrespective of the applied damping setting. This slight backlash made it difficult to investigate the possibility of simultaneous thrust and power generation. Further enhancements in propulsive performance may also be made by changing the pitch spring constant as highlighted by Bockmann et al.[19].

The range of damping applied in these experiments did not encompass the optimum damping constant for power generation which indicates that the value of applied damping from the rotary damper was too low. However, the uncertainty associated with backlash is difficult to quantify and improvements to the method for simulating power take-off is necessary.

In the free running tests, the damping setting was set to 1 turn which applies a damping constant that is too low for the system to effectively recover power from the incoming waves. The power generated in this study was not harvested or stored and the development of a power take-off device is required. However, the results indicate that it is possible to gain net power and thrust from the same system. Improving the model to allow for more advanced testing under free running

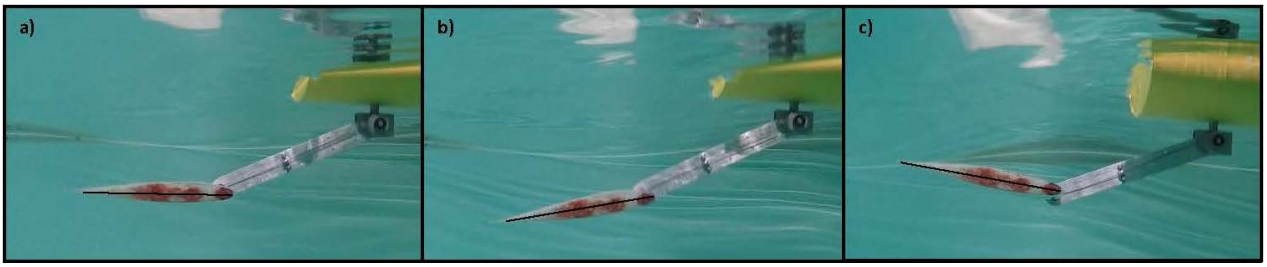

Figure 18: Aft foil spring loaded motion: a) Neutral Angle b) Positive Pitch c) Negative Pitch

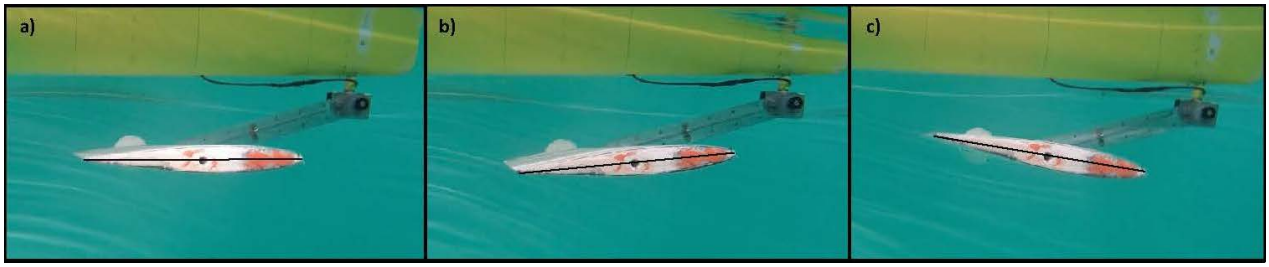

Figure 19: Forward foil spring loaded motion: a) Neutral Angle b) Positive Pitch c) Negative Pitch

conditions is seen as a key objective for future research.

VI. Conclusions

The ability to alter the mode of flapping foils from ASV propulsion to onboard power generation has been outlined and proven from these initial experiments. The mode of the flapping foils was changed from propulsion to power generation by allowing the foils to heave independently from the vessel and, therefore, recover wave energy in the form of work done about the rotary damper. Thrust was generated in the form of bollard pull, forward speed and drag reduction. In the power generation mode, the results showed that a maximum of approximately 4 watts and an average of 1 watt is attainable from two sets of foils. Upon optimization, the FLEUR system could recover a useful amount of power for ASV onboard systems and introduce the flexibility required to remotely control and alter the ASV mission directive such as station holding, charging, transiting and evading.

VII. Further work

Further experiments are required to improve the range of damping required to analyze the simultaneous generation of power and thrust from the system. Linear dampers have been proposed as a more effective means of adjusting and applying damping to the pivot arms. It was also identified that fixing the system to the towing tank carriage may have limited the response and overall performance of the system. Hence, future experiments should be carried out in a free running condition where the model is remotely operated in the towing tank and data is acquired onboard. Ideally, this would also incorporate the ability to remotely change the mode of the flapping foils. Furthermore, the FLEUR system could incorporate the ability to use stored energy to actively drive the flapping foil system and consequently propel itself in circumstances where no wave energy is available or an increase in vessel speed is required.

Acknowledgements

This research was supported by the Lloyd's Register Foundation.

References

[1] Manley, Justin E. "Unmanned surface vehicles, 15 years of development." OCEANS 2008. IEEE, 2008.

[2] Zheng, C., Shao, L., Shi, W., Su, Q., Lin, G., Li, X. and Chen, X.,"An assessment of global ocean wave energy resources over the last 45 a", Acta Oceanologica Sinica, vol. 33(1), pp 92-101, 2014.

[3] Manley, Justin, and Scott Willcox. "The wave glider: A persistent platform for ocean science." OCEANS '10 IEEE-Sydney. IEEE, 2010.

[4] D. Crimmins, C. Patty, M. Beliard, J. Baker, J. Jalbert, R. Komerska, S. Chappell, and D. Blidberg, Long-endurance test results of the solar powered AUV system, OCEANS 06, pp. 15, 2006.

[5] Saildrone Inc, March 2015, accessed March 2015, http://www.saildrone.com/

[6] Martins, Alfredo, et al. "ROAZ and ROAZ II autonomous surface vehicle design and implementation." International Lifesaving Congress. 2007.

[7] MOST (AV) Ltd, accessed March 2015, ¡http://www.autonautusv.com/specifications

[8] ASV Global, accessed March 2015, http://www.asvglobal.com/science-survey

[9] Linden, H. ”Improved combination with floating bodies, of fins adapted to effect their propulsion”. GB Patent 14,630. Filed Aug. 1, 1895. Patented Jul. 18, 1896.

[10] Jakobsen, E., ”The foil propeller, wave power for propulsion”. In Second International Symposium on Wave and Tidal Energy, BHRA Fluid Engineering, pp 363369, 1981.

[11] Terao, Y., and N. Sakagami. ”Design and development of an autonomous wave-powered boat with a wave devouring propulsion system.” Advanced Robotics, vol. 29(1), pp 89-102, 2015.

[12] Townsend, N.C. and Shenoi, R.A., ’Recharging autonomous underwater vehicles from ambient wave induced motions’, OCEANS13, MTS/IEEE, San Diego September 23rd - 26th, 2013.

[13] Isshiki, H. and Murakami, M., ”A Theory of Wave Devouring Propulsion(4th Report) : A Comparison Between Theory and Experiment in Case of a Passive-Type Hydrofoil Propulsor”, Journal of the Society of Naval Architects of Japan, vol. 156, pp. 102-114, 1984.

[14] Wu, T. Y., ’Extraction of flow energy by a wing oscillating in waves’, Journal of Ship Research, vol. 14(1), pp 66-78, 1972

[15] Grue, J., Mo, A. and Palm, E., ”Propulsion of a foil moving in water waves”, Journal of Fluid Mechanics, vol. 186, pp 393-417, 1988

[16] Filippas, E. S. and Belibassakis, K. A., ”Hydrodynamic analysis of flapping-foil thrusters operating beneath the free surface and in waves”, Engineering Analysis with Boundary Elements, vol. 41(0), pp 47-59, 2014.

[17] Young, J., Lai, J. C. S. and Platzer, M. F., ”A review of progress and challenges in flapping foil power generation”, Progress in Aerospace Sciences, vol. 67(0), pp 2-28, 2014.

[18] Jones, K. and Platzer, M., ”Numerical computation of flapping-wing propulsion and power extraction”, In 35th Aerospace Sciences Meeting and Exhibit, American Institute of Aeronautics and Astronautics, 1997.

[19] Bockmann, E and Steen, S, ”Experiments with actively pitch-controlled and spring-loaded oscillating foils”, Applied Ocean Research, vol. 48, pp 227-335, 2014.

[20] A. R. J. M. Lloyd, ”Seakeeping: ship behaviour in rough weather”, Ellis Horwood Series in Marine Technology, Ellis Horwood Limited, Chapter 13, 1989.